

Electronic Thesis and Dissertation Repository

---

2-26-2018 2:30 PM

## Condition Assessment of Concrete Bridge Decks Using Ground and Airborne Infrared Thermography

Tarek Omar, *The University of Western Ontario*

Supervisor: Nehdi Moncef, *The University of Western Ontario*

A thesis submitted in partial fulfillment of the requirements for the Doctor of Philosophy degree in Civil and Environmental Engineering

© Tarek Omar 2018

Follow this and additional works at: <https://ir.lib.uwo.ca/etd>



Part of the [Civil Engineering Commons](#), [Construction Engineering and Management Commons](#), [Structural Engineering Commons](#), and the [Transportation Engineering Commons](#)

---

### Recommended Citation

Omar, Tarek, "Condition Assessment of Concrete Bridge Decks Using Ground and Airborne Infrared Thermography" (2018). *Electronic Thesis and Dissertation Repository*. 5252.  
<https://ir.lib.uwo.ca/etd/5252>

This Dissertation/Thesis is brought to you for free and open access by Scholarship@Western. It has been accepted for inclusion in Electronic Thesis and Dissertation Repository by an authorized administrator of Scholarship@Western. For more information, please contact [wlsadmin@uwo.ca](mailto:wlsadmin@uwo.ca).

## **Abstract**

Applications of nondestructive testing (NDT) technologies have shown promise in assessing the condition of existing concrete bridges. Infrared thermography (IRT) has gradually gained wider acceptance as a NDT and evaluation tool in the civil engineering field. The high capability of IRT in detecting subsurface delamination, commercial availability of infrared cameras, lower cost compared with other technologies, speed of data collection, and remote sensing are some of the expected benefits of applying this technique in bridge deck inspection practices. The research conducted in this thesis aims at developing a rational condition assessment procedure for concrete bridge decks based on IRT technology, and automating its analysis process in order to add this invaluable technique to the bridge inspector's tool box. Ground penetrating radar (GPR) has also been vastly recognized as a NDT technique capable of evaluating the potential of active corrosion. Therefore, integrating IRT and GPR results in this research provides more precise assessments of bridge deck conditions. In addition, the research aims to establish a unique link between NDT technologies and inspector findings by developing a novel bridge deck condition rating index (BDCI). The proposed system captures the integrated results of IRT and GPR techniques, along with visual inspection judgements, thus overcoming the inherent scientific uncertainties of this process. Finally, the research aims to explore the potential application of unmanned aerial vehicle (UAV) infrared thermography for detecting hidden defects in concrete bridge decks.

The NDT work in this thesis was conducted on full-scale deteriorated reinforced concrete bridge decks located in Montreal, Quebec and London, Ontario. The proposed models have been validated through various case studies. IRT, either from the ground or by utilizing a UAV with high-resolution thermal infrared imagery, was found to be an appropriate technology for inspecting and precisely detecting subsurface anomalies in concrete bridge decks. The proposed analysis produced thermal mosaic maps from individual IR images captured from motion. The k-means clustering technique was utilized to segment the mosaics and identify objective thresholds and, hence, to delineate different categories of delamination in the entire bridge decks. The proposed integration methodology of NDT technologies and visual inspection results provided more reliable BDCI. The information that was sought to identify

the parameters affecting the integration process was gathered from bridge engineers with extensive experience and intuition. The analysis process utilized the fuzzy set theory to account for uncertainties and imprecision in the measurements of bridge deck defects detected by IRT and GPR testing along with bridge inspector observations.

The developed analysis procedure should stimulate wider acceptance of IRT as a rapid, systematic and cost-effective evaluation technique for detecting bridge deck delaminations. The proposed combination of IRT and GPR results should expand their correlative use in bridge deck inspection. Integrating the proposed BDCI procedure with existing bridge management systems can provide a detailed and timely picture of bridge health, thus helping transportation agencies in identifying critical deficiencies at various service life stages. Consequently, this can yield sizeable reductions in bridge inspection costs, effective allocation of limited maintenance and repair funds, and promote the safety, mobility, longevity, and reliability of our highway transportation assets.

## **Keywords**

Concrete bridge decks; deterioration; subsurface delamination; NDT; IRT; GPR; condition assessment and rating models; threshold classification; segmentation; integration; thermal mosaic maps; unmanned aerial vehicles; uncertainty; fuzzy modeling.

## Co-Authorship

This thesis has been prepared in accordance with the regulations for an Integrated-Article format thesis stipulated by the Faculty of Graduate Studies at Western University, London, Ontario, Canada. The in-situ bridge non-destructive testing, data analysis, modeling, and writing of draft manuscripts for publication were carried out by the candidate under the close guidance and direct supervision of his thesis advisor, who provided important comments, helped to refine ideas, and provided recommendations for editing the texts. The role of any other co-author, if applicable, was to provide general advice or contribute to the final version of manuscripts. The following publications have been either accepted or submitted to peer-reviewed technical journals and international conferences:

▪ **Refereed Journal Articles:**

1. **Omar, T.**, Nehdi, M., and Zayed, T. “Condition Assessment of Reinforced Concrete Bridges: Current Practice and Research Challenges.” *Canadian Journal of Civil Engineering*. (Chapter 2), **Submitted**.
2. **Omar, T.**, Nehdi, M., and Zayed, T. “Performance of NDT Techniques in Appraising Condition of Reinforced Concrete Bridge Decks.” *J. of Performance of Constructed Facilities*. (Chapter 3), **Published**, DOI: 10.1061/(ASCE)CF.1943-5509.0001098.
3. **Omar, T.**, Nehdi, M., and Zayed, T. “Infrared Thermography Model for Rational Condition Assessment of Concrete Bridge Decks.” *J. of Construction and Building Materials*. (Chapter 4), **Published**, DOI: 10.1016/j.conbuildmat.2018.02.126.
4. **Omar, T.**, Nehdi, M., Zayed, T. “Rational Condition Assessment of Reinforced Concrete Bridge Decks Subjected to Corrosion-Induced Delamination.” *J. of Materials in Civil Engineering*. (Chapter 5), **Published**, DOI: 10.1061/(ASCE)MT.1943-5533.0002114.
5. **Omar, T.**, Nehdi, M., and Zayed, T. “Integrated Condition Rating Model for Reinforced Concrete Bridge Decks.” *J. of Performance of Constructed Facilities*. (Chapter 6), **Published**, DOI: 10.1061/(ASCE)CF.1943-5509.0001084.

6. **Omar, T.**, and Nehdi, M. “Unmanned Aerial Vehicle Infrared Thermography Remote Sensing for Condition Assessment of Concrete Bridge Decks.” *J. of Automation in Construction*. (Chapter 7), **Published**, DOI: 10.1016/j.autcon.2017.06.024.
7. **Omar, T.**, and Nehdi, M. (2015). “Data Acquisition Technologies for Construction Progress Tracking.” *J. of Automation in Construction*. **Published**, DOI: 10.1016/j.autcon.2016.06.016.

▪ **Conference Proceedings:**

1. **Omar, T.**, and Nehdi, M. (2017). “Clustering-Based Threshold Model for Condition Assessment of Concrete Bridge Decks Using Infrared Thermography.” Chapter. In book: “*Facing the Challenges in Structural Engineering, Sustainable Civil Infrastructures*”, pp: 242-253. H. Rodrigues et al. (eds.), Springer International Publishing AG. Switzerland, **Published**, DOI: 10.1007/978-3-319-61914-9\_19.
2. **Omar, T.**, and Nehdi, M. (2017). “Automated Data Collection for Progress Tracking Purposes: A Review of Related Techniques.” Chapter. In book: “*Facing the Challenges in Structural Engineering, Sustainable Civil Infrastructures*”, pp: 391-405. H. Rodrigues et al. (eds.), Springer International Publishing AG. Switzerland, **Published**, DOI: 10.1007/978-3-319-61914-9\_30
3. **Omar, T.**, and Nehdi, M. (2017). “Thermal Detection of Sub-Surface Defects in Concrete Bridge Decks Using Unmanned Ariel Vehicle.” *Special Publication on Durability of Concrete Structures Incorporated with conventional and Advanced Materials*. Kim et al. (eds.), American Concrete Institute Publishing. USA. **In Press**.
4. **Omar, T.**, and Nehdi, M. (2016) “Non-Destructive Testing of Bridge Deck Using Passive Infrared Thermography and Ground Penetrating Radar.” *In Proceedings, Annual Conference of the Transportation Association of Canada (TAC)*, Toronto, Ontario, Canada, Sep 25-28. **Published**.

5. **Omar, T.,** and Nehdi, M. (2016) “Application of Passive Infrared Thermography for the Detection of Defects in Concrete Bridge Elements.” *In Proceedings, Annual Conference of the Transportation Association of Canada (TAC)*, Toronto, Ontario, Canada, Sep 25–28. **Published.**
6. **Omar, T.,** and Nehdi, M. (2016) “Condition Assessment and Deterioration Prediction Tools for Concrete Bridges: A New Look.” *In Proceedings, Annual Conference of CSCE*, London, Ontario, Canada, June 1-4. **Published.**
7. **Omar, T.,** and Nehdi, M. (2016) “Evaluation of NDT Techniques for Concrete Bridge Decks Using Fuzzy Analytical Hierarchy.” *In Proceedings, Annual Conference of CSCE*, London, Ontario, Canada, June 1-4. **Published.**
8. **Omar, T.,** and Nehdi, M. (2015) “Learned Lessons from Adelaide Desalination Project.” *In Proceedings, Annual Conference of CSCE*, Regina, Saskatchewan, Canada, May 27–30. **Published.**

## Acknowledgments

First and foremost, I would like to thank Allah for all his blessings to me. He gave me each day the power to undertake this work and complete it satisfactorily. I could never have done this without his blessings, Almighty.

In completion of this thesis, I would like to express my sincere gratitude to my supervisor, Professor Moncef L. Nehdi, who has been very supportive throughout the completion of this thesis with his patience, valuable knowledge, feedback and guidance, while providing me flexibility to work in my own way. Thank you for your confidence in me and giving me the chance to develop my skills as an independent researcher. I am immensely grateful for studying under your precious guidance throughout this research.

I would also like to express my deepest appreciation and gratitude to Professor Tarek Zayed, Concordia University. He has helped the progression of my research by providing new ideas and constructive suggestions over the years. His curiosity in this research project made me think about different aspects of the research outcome. Thank you for your effective contributions to my publications. This work could not have been done without your support.

I acknowledge the support of Radex Detection Inc, an industrial consultant, and to its president Mr. Alex Tarussov for collaborating with Western University to conduct the full-scale bridge survey. My thanks also go to Dr. Ken Maser, senior principal of Infrasense, an industrial consultant, for providing the raw data of some bridges in Wisconsin, and for his valuable advice. The Ministries of Transportation in Ontario and Quebec are acknowledged for their permissions to survey the bridges in London and Montreal, respectively.

From the depths of my heart, I would like to thank my great parents for their sincere encouragement and prayers. I would like to thank my faithful wife and my lovely children: “Abdelrahman and Hebatallah” for all their endless encouragement while I worked on my thesis. They have made every compromise and sacrifice required throughout this doctoral journey. Without their love, tremendous support and patience, it would not have been possible to accomplish my academic goals.

# Table of Contents

<b>Abstract</b> .....	i
<b>Co-Authorship</b> .....	iii
<b>Acknowledgments</b> .....	vi
<b>Table of Contents</b> .....	vii
<b>List of Tables</b> .....	xiii
<b>List of Figures</b> .....	xv
<b>Chapter 1</b> .....	1
<b>Introduction</b> .....	1
1.1 Background.....	1
1.2 Research Motivation .....	4
1.3 Objectives of Thesis.....	5
1.4 Research Methodology and Organization of Thesis.....	6
1.5 Main Contributions .....	9
1.6 References.....	11
<b>Chapter 2</b> .....	12
<b>Current Practice for Condition Assessment of Reinforced Concrete Bridges</b> .....	12
2.1 Introduction.....	12
2.2 Deterioration of Reinforced Concrete Bridges .....	14
2.2.1 Bridge Performance Indicators .....	18
2.3 Bridge Condition Assessment Approaches.....	20
2.3.1 Visual Inspection .....	22
2.3.2 Load Testing .....	24
2.3.3 Structural Health Monitoring.....	26
2.3.4 Non-Destructive Testing.....	30

2.3.5	Finite Element Modelling .....	36
2.3.6	Advantages and Limitations .....	37
2.4	Bridge Deterioration Prediction Tools.....	39
2.4.1	Deterministic Models.....	39
2.4.2	Stochastic Models .....	40
2.4.3	Mechanistic Models .....	42
2.4.4	Advantages and Limitations .....	43
2.5	Bridge Condition Assessment and Artificial Intelligence .....	44
2.5.1	Artificial Neural Networks .....	44
2.5.2	Fuzzy Set Theory .....	46
2.5.3	Evidential Reasoning .....	48
2.5.4	Advantages and Limitations .....	49
2.6	Challenges Requiring Further Research .....	51
2.6.1	Selection of Appropriate Condition Assessment Technique .....	53
2.7	Conclusions.....	54
2.8	References.....	55
<b>Chapter 3</b>	.....	<b>64</b>
<b>Performance of NDT Techniques in Appraising Condition of Reinforced Concrete Bridge Decks</b>	.....	<b>64</b>
3.1	Introduction.....	64
3.2	Model Development.....	66
3.2.1	Selection of the Performance Measures.....	66
3.2.2	Selection of the NDT Alternatives.....	68
3.2.3	Construction of Fuzzy Analytical Hierarchy Model.....	69
3.2.4	Data Collection .....	71
3.2.5	Data Analysis .....	75

3.3	Model Implementation.....	79
3.4	Evaluation and Ranking of NDT Techniques.....	82
3.4.1	Weights of Main Performance Measures.....	83
3.4.2	Overall Ranking of NDT Techniques.....	88
3.5	Validation of Model Results.....	90
3.6	Evaluation of the Proposed Model.....	93
3.7	Conclusions.....	95
3.8	References.....	96
<b>Chapter 4</b>	.....	<b>99</b>
	<b>Infrared Thermography Model for Rational Condition Assessment of Reinforced Concrete Bridge Decks</b> .....	<b>99</b>
4.1	Introduction.....	99
4.2	Infrared Thermography Technology.....	101
4.2.1	Basic Principles of IRT.....	101
4.2.2	Infrared Cameras.....	105
4.2.3	Application of IRT for Concrete Bridge Inspection.....	107
4.2.4	Interpretation of Passive IRT Data.....	109
4.3	Un-Supervised Machine Learning.....	111
4.3.1	k-Means Clustering.....	112
4.4	IRT Model Development.....	113
4.4.1	Data Collection.....	114
4.4.2	Image Pre-Processing.....	117
4.4.3	Image Registration.....	118
4.4.4	Image Segmentation.....	121
4.4.5	IRT Condition Mapping.....	124
4.5	IRT Model Implementation.....	124

4.5.1	Bridge (A)	127
4.5.2	Bridge (B)	129
4.5.3	Bridge C	130
4.6	Evaluation of the Proposed IRT Model	131
4.7	Validation of IRT Model Results	133
4.7.1	Hammer Sounding Test Results	133
4.7.2	GPR Test Results	135
4.8	Further Research to Improve the Proposed IRT Analysis	138
4.9	Conclusions	139
4.10	References	140
<b>Chapter 5</b>		<b>143</b>
	<b>Condition Assessment of Reinforced Concrete Bridge Decks Using Infrared Thermography and Ground Penetrating Radar</b>	<b>143</b>
5.1	Introduction	143
5.2	Ground Penetrating Radar (GPR)	145
5.2.1	Basic Principle of GPR	145
5.2.2	Application of GPR for Concrete Bridge Inspection	147
5.2.3	Interpretation of GPR Scan Data	148
5.3	IRT/GPR Model Development	150
5.3.1	Data Collection	150
5.3.2	Data Analysis	152
5.3.3	Deterioration Condition Maps	154
5.4	IRT/GPR Model Implementation on a Second Case Study	158
5.5	Evaluation of the Proposed IRT/GPR Model	161
5.6	Conclusions	165
5.7	References	166

<b>Chapter 6</b> .....	168
<b>Integrated Condition Rating Model for Reinforced Concrete Bridge Decks Using NDT and Visual Inspection</b> .....	168
6.1 Introduction.....	168
6.2 Existing Bridge Condition Rating Systems .....	170
6.2.1 Bridge Condition Rating Systems in Canada.....	172
6.2.2 Bridge Condition Assessment Using IRT and GPR .....	172
6.3 Fuzzy Bridge Deck Condition Rating Model Development.....	173
6.3.1 Fuzzy Synthetic Evaluation (FSE).....	173
6.3.2 Weighted Fuzzy Union (WFU) Operation.....	179
6.4 Bridge Deck Condition Rating Model Implementation.....	183
6.4.1 Data Collection and Analysis.....	183
6.4.2 Developing BDCI of Bridge Deck.....	184
6.5 Evaluation of the Proposed BDCI Model .....	186
6.6 Conclusions.....	188
6.7 References.....	189
<b>Chapter 7</b> .....	191
<b>Remote Sensing of Reinforced Concrete Bridge Decks Using Unmanned Aerial Vehicle Infrared Thermography</b> .....	191
7.1 Introduction.....	191
7.2 Unmanned Aerial Vehicle (UAV) .....	193
7.2.1 Basic Principle of UAV .....	193
7.2.2 UAV Applications in Civil Engineering.....	194
7.2.3 Successful Application of UAV-IRT System.....	195
7.3 UAV/IRT Model Development .....	196
7.3.1 Planning and Preparation Phase.....	197
7.3.2 Data Acquisition Phase .....	200

7.3.3	Data Analysis Phase.....	201
7.4	Validation of UAV/IRT Model Results.....	206
7.4.1	Hammer Sounding Test Results.....	206
7.4.2	Half-Cell Potential Test Results.....	207
7.5	Evaluation of the Proposed UAV/IRT Model .....	210
7.6	Further Research to Improve the Proposed System.....	211
7.7	Conclusions.....	212
7.8	References.....	213
<b>Chapter 8</b>	.....	<b>215</b>
<b>Summary, Conclusions and Recommendations</b>	.....	<b>215</b>
8.1	Summary and Conclusions .....	215
8.2	Recommendations for Future Research.....	217
<b>Appendix A (Questionnaire Survey)</b>	.....	<b>220</b>
<b>Appendix B (Copyright Permissions)</b>	.....	<b>224</b>
<b>CURRICULUM VITAE</b>	.....	<b>232</b>

## List of Tables

Table 2-1: Common defects in reinforced concrete bridges .....	16
Table 2-2: Evaluation techniques for RC bridge performance indicators and the related references .....	20
Table 2-3: Requirements of different assessment phases of existing bridges .....	21
Table 2-4: Summary of common structural health monitoring systems of bridges.....	27
Table 2-5: Common NDT methods used to evaluate concrete bridge decks.....	33
Table 2-6: Studies utilized combined NDT techniques approach to evaluate bridges .....	35
Table 2-7: Comparison of condition assessment techniques for RC bridges .....	38
Table 2-8: Comparison of deterioration model techniques for concrete bridges.....	44
Table 2-9: Comparison of AI techniques for concrete bridges evaluation .....	50
Table 2-10: Appropriate investigation methods for some deterioration mechanisms in RC bridges.....	53
Table 3-1: Applicable NDT methods to detect specific deterioration types.....	68
Table 3-2: Organization and experience of participants in the survey questionnaire.....	73
Table 3-3: Results of respondents using NDT techniques.....	73
Table 3-4: Linguistic comparison scales for importance .....	75
Table 3-5: Pairwise comparison matrix of main performance parameters with respect to the selection of NDT technique .....	80
Table 3-6: Performance measures weights and ranking of NDT techniques.....	82
Table 3-7: Comparative studies which utilized several NDT techniques on RC bridge decks .....	92

Table 4-1: Features and specifications of the utilized thermal camera.....	114
Table 4-2: Environmental conditions during IR surveys of Montreal bridge.....	116
Table 4-3: Features and specifications of the utilized thermal camera.....	127
Table 4-4: Environmental conditions during IR surveys of Wisconsin bridges.....	127
Table 4-5: Percentage of defective areas in the investigated bridges .....	138
Table 5-1: Features and specifications of the utilized GPR equipment.....	152
Table 5-2: Percentage of defective areas in the analyzed bridge decks.....	163
Table 6-1: Example for a fuzzy pairwise comparison matrix of a participated expert.....	177
Table 6-2: Final weights of bridge deck defects investigated in this study .....	177
Table 6-3: Experts' replies for boundaries identification of the condition categories.....	180
Table 6-4: Summary of severity and extent of defects in the inspected Montreal's bridge deck .....	184
Table 6-5: Recommended actions for the proposed BDCI in this study .....	187
Table 7-1: Features and specifications of the utilized camera (FLIR Vue Pro).....	197
Table 7-2: Features and specifications of the utilized UAV (Inspire 1 Pro).....	198
Table 7-3: Statistical analysis for the influence of IR threshold on the identified defective areas .....	205
Table 7-4: Percentage of defective areas in the analyzed two bridge decks.....	207

## List of Figures

Figure 1-1: Basic components of a BMS.....	2
Figure 1-2: Schematic diagram of research methodology. ....	9
Figure 2-1: Methodological framework for literature review of BCA technologies. ....	13
Figure 2-2: Corrosion-induced delamination and spalling in concrete bridge decks (Gucunski et al., 2013). ....	17
Figure 2-3: Condition assessment mechanisms of reinforced concrete bridges. ....	22
Figure 2-4: Visual inspection of concrete bridge decks and soffits (Gucunski et al., 2013)..	23
Figure 2-5: Non-destructive testing techniques for reinforced concrete bridges.....	30
Figure 2-6: Deterioration prediction models techniques. ....	39
Figure 2-7: Structure of an artificial neural network. ....	45
Figure 2-8: Basic configuration of fuzzy system with fuzzifier and defuzzifier (Senouci et al., 2014, with permission from ASCE).....	47
Figure 2-9: Conceptual framework to identify challenges that require further research in bridge condition assessment. ....	52
Figure 3-1: Methodology adopted for apprising and ranking NDT techniques.....	66
Figure 3-2: Hierarchy framework for ranking NDT techniques. ....	70
Figure 3-3: Snapshot of a question in the survey questionnaire. ....	74
Figure 3-4: A triangular fuzzy number M.....	76
Figure 3-5: Weights and consistency index of the comparison matrix in Table 3-5. ....	81
Figure 3-6: Evaluation of NDT technologies with respect to their capability of specific defect detection.....	84

Figure 3-7: Evaluation of NDT technologies with respect to their speed.....	85
Figure 3-8: Evaluation of NDT technologies with respect to their simplicity. ....	86
Figure 3-9: Evaluation of NDT technologies with respect to their accuracy. ....	87
Figure 3-10: Evaluation of NDT technologies with respect to their cost. ....	88
Figure 3-11: Overall evaluation of NDT technologies with respect to the main performance criteria. ....	89
Figure 4-1: Methodology adopted in developing IRT model to detect and classify subsurface delamination in RC bridge decks.....	100
Figure 4-2: Infrared region in the electromagnetic spectrum (FLIR Guidebook). ....	101
Figure 4-3: General configuration of a typical IR camera (FLIR Guidebook).....	105
Figure 4-4: Infrared energy emitted from concrete bridge deck during day and night.....	108
Figure 4-5: Illustration of the selected concrete bridge located in Montreal, Quebec.....	113
Figure 4-6: Illustration of the FLIR T650sc IR camera and vehicle mounted setup system utilized to survey Montreal bridge.....	115
Figure 4-7: Delamination at (a) daytime; and (b) nighttime surveys.....	117
Figure 4-8: Developed algorithm for condition assessment of concrete bridge decks. ....	118
Figure 4-9: Flowchart for determining number of condition categories (k). ....	123
Figure 4-10: Condition map of the daytime IRT survey of bridge deck in Montreal indicating the severity of the identified delaminated areas.....	125
Figure 4-11: Condition map of the nighttime IRT survey of bridge deck in Montreal indicating the severity of the identified delaminated areas.....	125
Figure 4-12: Thermal and digital images of potential delaminated areas in the bridge soffit. .....	126

Figure 4-13: Condition map of bridge (A) indicating the identified delaminated areas using the developed IRT system.....	128
Figure 4-14: Condition map of bridge (A) indicating the identified delaminated area as per the record of MOT, Wisconsin (Omar et al., 2018).....	128
Figure 4-15: Condition map of bridge (B) indicating the identified delaminated areas using the developed IRT system.....	129
Figure 4-16: Condition map of bridge (B) indicating the identified delaminated area as per the record of MOT, Wisconsin (Omar et al., 2018).....	130
Figure 4-17: Condition map of bridge (C) indicating the severity of the identified delaminated areas using the developed IRT system. ....	131
Figure 4-18: Condition map indicating the severity of corrosion for the surveyed bridge deck in Montreal (Omar et al., 2018). ....	136
Figure 4-19: Corrosion map of bridge C as per the record of Wisconsin DOT (Omar et al., 2018). ....	136
Figure 5-1: Methodology adopted to evaluate RC bridge deck condition using the integration of IRT and GPR testing results. ....	145
Figure 5-2: Illustration of GPR travel paths and the utilized data acquisition unit. ....	151
Figure 5-3: Picking top reinforcing bars in a B-scan profile. ....	153
Figure 5-4: IRT condition map of Montreal’s bridge deck indicating different severity levels of delaminations.....	155
Figure 5-5: GPR condition map of Montreal’s bridge deck indicating different severity levels of potential active corrosion.....	156
Figure 5-6: GPR corrosion map of Montreal’s bridge deck as per the record of MOT, Quebec (Omar et al., 2018).....	156

Figure 5-7: Integrated condition map of Montreal’s bridge deck based on the IRT and GPR results. ....	158
Figure 5-8: IRT condition map of Wisconsin’s bridge deck indicating different severity levels of delaminations. ....	159
Figure 5-9: GPR condition map of Wisconsin’s bridge deck indicating different severity levels of potential active corrosion. ....	160
Figure 5-10: GPR corrosion map of Wisconsin’s bridge deck as per the record of Wisconsin DOT (Omar et al., 2018). ....	160
Figure 5-11: Integrated condition map of Wisconsin’s bridge deck based on the IRT and GPR results. ....	161
Figure 6-1: Methodology of model development adopted in this study. ....	170
Figure 6-2: Condition category’s map utilized for the construction of defects’ membership functions (Omar et al., 2017). ....	174
Figure 6-3: Triangular fuzzy membership functions for various severity of bridge deck’s defects. ....	175
Figure 6-4: Common bridge deck defects and related investigation techniques utilized in this study. ....	176
Figure 6-5: Conception of the proposed bridge deck condition index (BDCI). ....	179
Figure 6-6: Histogram and normal distribution curve of $k_1$ , $k_2$ , and $k_3$ . ....	180
Figure 6-7: Boundaries of condition categories membership functions using linear regression method. ....	181
Figure 6-8: Condition categories membership functions based on $k_1$ , $k_2$ , and $k_3$ . ....	181
Figure 6-9: Aggregated condition categories of Montreal’s bridge deck based on defects measured using different techniques. ....	185

Figure 6-10: Condition rating index of Montreal’s bridge deck based on the proposed model in this study. ....	185
Figure 7-1: UAV-borne thermal survey methodology adopted in this study. ....	193
Figure 7-2: Illustration of the surveyed concrete bridge (A) and an overview of the deck surface condition. ....	196
Figure 7-3: Illustration of the UAV-borne thermal system utilized to scan two RC bridge decks. ....	199
Figure 7-4: Snapshot of the UAV during the flight to scan bridge (A) and a captured thermal image indicating potential delaminated areas. ....	201
Figure 7-5: Condition map of bridge (A) indicating the severity of the identified delaminated areas for the bridge deck and curbs using UAV-borne thermal imagery system. ....	203
Figure 7-6: Condition map of bridge (B) indicating the severity of the identified delaminated areas for the bridge deck and curbs using UAV-borne thermal imagery system. ....	204
Figure 7-7: Condition map of bridge deck (A) indicating the potential corrosion readings for the bridge deck and curbs using HCP testing (Omar and Nehdi, 2017). ....	208
Figure 7-8: Condition map of bridge deck (B) indicating the potential corrosion readings for the bridge deck and curbs using HCP testing (Omar and Nehdi, 2017). ....	209

# Chapter 1

## 1. Introduction

### 1.1 Background

Bridges represent critical infrastructure components within the transportation network. The average age of bridges keeps going up and many are approaching the end of their design lives. Structural problems created by corrosion, aggressive environments, material defects, construction defaults, and unforeseen mechanical or seismic loads can compromise the serviceability and safety of bridges. According to the Canadian infrastructure report card (2016), 26% of bridges are in fair, poor or very poor condition and \$50 billion needs to be invested in their replacement and maintenance, spending \$2 billion for bridges in poor and (or) very poor condition, \$11 billion for bridges in fair condition, and \$37 billion for bridges in good condition. Likewise, about 40% of the bridges in the USA are 50 years or older, with 25% either structurally deficient or functionally obsolete. The most recent estimate as per the United States' 2017 infrastructure report card indicates that the backlog of bridge rehabilitation needs \$123 billion.

The importance of an effective bridge management system (BMS) cannot be overstated, especially in light of recent collapses of bridges in North America and elsewhere. Bridge failures can be catastrophic, both in terms of human life and economic loss, rendering the task of managing this important asset a complex endeavour that attracts growing attention. The basic components of a BMS are illustrated in **Fig. 1-1**. The architecture of a typical BMS consists of a database, a condition assessment module, a structural assessment module, a deterioration prediction module, a lifecycle cost module, and a maintenance optimization module. The database stores the bridge inventory and appraisal data. The condition assessment module evaluates the existing health condition of the bridge. The structural assessment module determines the bridge load carrying capacity. The deterioration prediction module estimates the future condition of bridge components. The life-cycle cost module calculates agency and user costs for various maintenance alternatives. The optimization module determines the most cost-effective maintenance strategies (Hammad *et al.*, 2007). Therefore, reliable bridge condition assessment has

become vital to predicting future performance and optimizing bridge maintenance, rehabilitation and replacement needs and to mitigating socio-economic impacts associated with bridge failures.

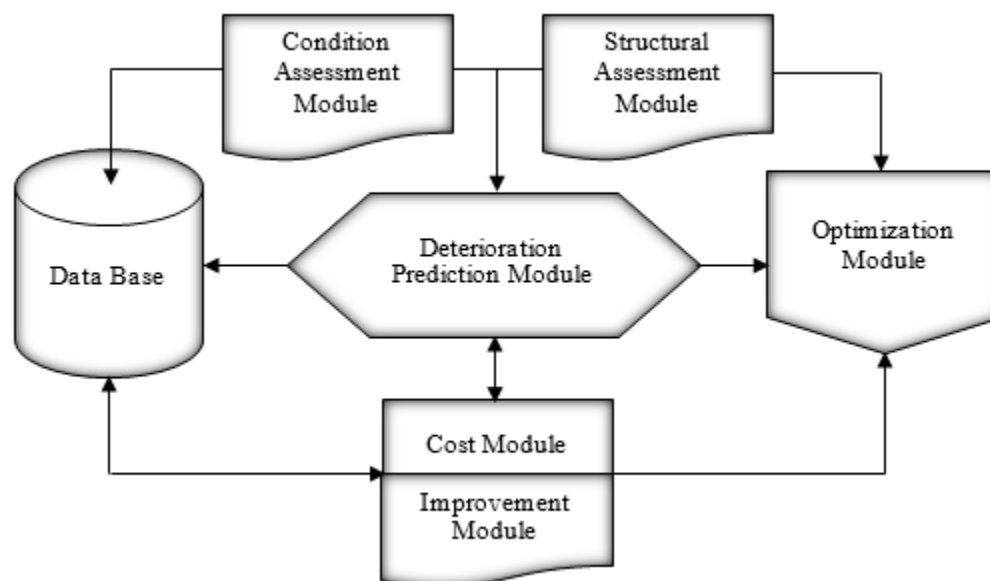


**Figure 1-1: Basic components of a BMS.**

Among all bridge components, the performance of bridge decks was identified as the most important long-term bridge performance issue (Gucunski *et al.*, 2015). While visual inspection is the default bridge deck inspection methodology, it cannot yet detect subsurface flaws such as voids, internal cracks, delamination, or reinforcing steel corrosion. Therefore, there has been growing interest among bridge infrastructure stakeholders in using non-destructive testing (NDT) methods for inspecting and evaluating the condition of bridge decks. Such techniques enable the detection of deterioration processes at their early stages and can be incorporated into the inspection process to provide fast and reliable information about the “under-the-surface” deteriorated conditions. However, NDT techniques have not been widely accepted, either due to unrealistic expectations or improper use (Gucunski *et al.*, 2013). Indeed, most related research efforts still aim at verifying the capability, or comparing the accuracy, of NDT methods in assessing subsurface conditions (Lounis, 2013).

Infrared thermography (IRT) is a remote sensing technology that allows for rapid bridge inspection and visualization of the data in the form of real-time thermal images. Laboratory and field studies of IRT technology for concrete slabs indicate that this NDT technique is capable of detecting subsurface delaminations (Vaghefi *et al.*, 2012). Consequently, it can help bridge inspectors identify areas of unsound concrete before they turn into spalls, which could threaten public safety and eventually reduce the load capacity of bridges. With the advent of newer generations of infrared cameras, IRT is evolving as an accurate, reliable and cost-effective technique that can yield both qualitative and quantitative indicators of a bridge deck condition (Washer *et al.*, 2013). The IRT testing can be broadly classified into two major categories: passive and active. The source of heat is the main difference between these two methods. Solar energy and ambient temperature changes are the main heat sources in conducting a passive IRT test, while active IRT involves generating a temperature gradient using an external source of heat other than the sun (Robert, 1982). Although successful application of the IRT technique has been demonstrated through a number of research projects, most of these efforts have aimed either at verifying the capability of IRT for the detection of subsurface defects in bridge components, or studying the environmental conditions for successful application of the technology.

For instance, Washer *et al.* (2009) studied the effect of environmental conditions on the surface temperature of a concrete block containing subsurface anomalies at different depths. They found that uninterrupted solar loading and low wind speeds provide a better contrast on a thermal IR image and, hence, provide optimum conditions for detecting delaminations in concrete surfaces directly exposed to the sun. High rates of change in ambient temperature were needed to create thermal contrast for the concrete surfaces where no solar loading was present. Clark *et al.* (2003) inspected bridge structures under low ambient temperature and reported that the thermal contrast between the delaminated and sound areas could be about 0.2 to 0.3 °C. In addition, several studies have addressed the effect of delamination depth on thermal contrast during IRT testing. For instance, Manning and Holt (1982) found that the magnitude of thermal contrast correlates with the depth of a delamination where shallower delaminations are associated with larger thermal contrasts than deeper delaminations for the same environmental conditions. However, diurnal temperature and solar loading effects can vary over the course of a day, with certain time

periods having deeper delaminations that present greater contrast than shallower features (Washer *et al.*, 2013). Maser and Roddis (1990) investigated the effects of variable delamination thickness under a certain set of environmental variables using a thermal model. The results revealed that the thickness of the delamination affects the magnitude of the thermal contrast where increasing the delamination thickness increased the maximum thermal contrast. In a study conducted by Washer *et al.* (2009), it was found that the effective time to perform an IRT test depends on the depth of the delamination. The most contrast appears on the IR image approximately four hours after sunrise for a 50 mm deep delamination and seven hours after sunrise for a 75 mm deep delamination.

## 1.2 Research Motivation

The majority of passive IRT testing performed in previous research studies was based on testing specimens prepared in the laboratory environment with simulated defects, then exposing them to solar energy. Hence, several processing algorithms to extract information were developed based on the temperature of the pre-defined defects' locations and sizes with respect to the temperature of the surrounding sound concrete. However, when conducting passive IRT testing in-situ on full-scale bridges, the defects' characteristics are unknown and extracting quantitative measures of subsurface anomalies still relies on the user interpretation of the images. Such qualitative and subjective analyses are rapid, but do not warrant rigorous evaluation of the acquired thermal images. In addition, the severity of delamination is commonly defined based on the pixels associated with temperatures higher than predefined threshold values that are arbitrarily selected. Such a subjective scheme can produce inconsistent results. Currently, limited research is available to automate the thermal detection of subsurface damage: delaminations, internal horizontal cracks or voids on full-scale concrete bridge decks exposed to harsh environments.

In addition, the majority of existing bridge deck condition rating models have been developed based solely on data from visual inspection usually used as a basis for bridge condition assessment. Such models do not take into account the inherent uncertainty associated with inspection results. Consequently, existing BMSs still have shortcomings, especially in the collection of inspection data dominated by subjective judgment, and inaccurate and insufficient quantitative inputs. Indeed, it is critical in bridge condition

ratings to combine the results of several technologies to yield different deterioration mechanisms. For instance, ground penetrating radar (GPR) has been recognized as a sensing technology capable of evaluating deck thickness, concrete cover and rebar configuration, and determining the potential for delamination and corrosive environments in reinforced concrete bridge decks. Currently, there is no bridge condition rating system that has adequately considered the results of NDT technologies. Therefore, there is an essential need for developing an objective bridge condition assessment and rating system based on the integration of commonly employed NDT techniques and taking into consideration the visual inspection findings.

### **1.3 Objectives of Thesis**

The main goal of this research is to develop a rational and scientific assessment and rating process for ageing concrete bridge decks that yields: (1) objective detection of subsurface deficient areas using either ground or aerial IRT technology; and (2) reliable rating index by integrating the achieved IRT results with other NDT testing results and visual inspection observations. To achieve this goal, the following tasks have been undertaken:

1. A critical overview of the state-of-the-art condition assessment and rating techniques for concrete bridges, with emphasis on bridge decks.
2. A comparative analysis to evaluate and rank the most commonly used NDT techniques for detecting defects in concrete bridge decks.
3. Development of an automated defect detection procedure to extract and classify subsurface delaminations in full-scale concrete bridge decks under IRT testing.
4. Development of a procedure for generating an overall condition map for concrete bridge decks by uniting the analysis results of IRT and GPR testing techniques.
5. Development of an integrated condition rating system for concrete bridge decks employing IRT, GPR, and visual inspection techniques.
6. Investigation of the feasibility of applying UAV - IRT technology for detecting subsurface anomalies in concrete bridge decks.

## 1.4 Research Methodology and Organization of Thesis

Although the detailed research methodology of this study will be described in detail in each chapter, the overall methodology is presented in the schematic diagram shown in **Fig. 1-2**.

The thesis has been prepared in an “Integrated-Article” format and contains eight chapters.

This chapter, **Chapter 1**, introduces the overall scope and objectives of the thesis. Then, the methodology and structure of the thesis are outlined. The subsequent six chapters present the thesis objectives.

**Chapter 2** reviews the state of knowledge on bridge condition assessment approaches. Bridge performance indicators and the deterioration mechanisms of concrete bridges are outlined. The strengths, limitations and challenges associated with the application of each bridge condition assessment technique, are discussed. The application of artificial intelligence techniques in bridge assessment are examined and appraised. Bridge deterioration prediction tools are presented and compared. The knowledge gaps for further research are identified and recommendations towards the selection of appropriate assessment techniques so as to identify specific deterioration types are formulated.

**Chapter 3** presents a comparative analysis of the common NDT methods for detecting subsurface defects in concrete bridge decks. The NDT techniques are evaluated and ranked based on a set of flexible multi-attributed performance measures. A fuzzy hierarchical decision-making model is developed. A structured survey questionnaire was conducted to acquire an expert knowledge base through soliciting broad information about the performance of NDT methods which have been implemented by several transportation agencies. The fuzzy preference programme is utilized and a Matlab optimization function is modified and adopted to accommodate the analysis process. The results of the developed model are compared with the findings of a number of previous studies.

**Chapter 4** proposes an objective analysis for detecting and classifying delaminations in concrete bridge decks using passive IRT testing. The basic principles of thermal imaging, application of IRT for concrete bridge inspection, and current analysis and interpretation methods of IR image data are presented. A full-scale deteriorated bridge deck was surveyed

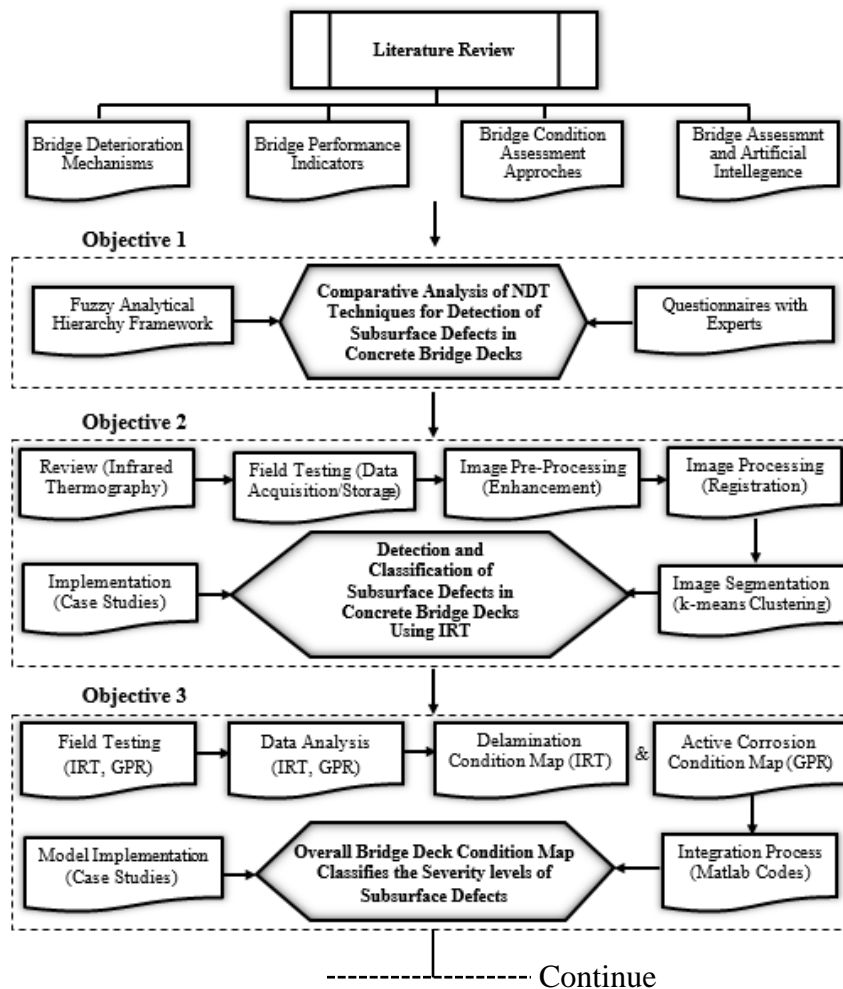
using an advanced thermal camera. The IRT model is developed through several stages of image analysis: pre-processing, registration, and segmentation. A machine learning unsupervised technique is utilized to classify the severity of the detected anomalies. A framework is developed to determine the number of defect condition categories. The developed model is implemented on four case studies and the findings are validated through the results of other testing technologies obtained on the same bridges.

**Chapter 5** integrates the results of two NDT techniques to produce an overall bridge deck condition map, which defines the potential location and severity degree of delamination and active corrosion. The basic principles of GPR, its application for concrete bridge inspection, and current analysis and interpretation methods of GPR scan data are presented. Two full-scale deteriorated bridge decks were surveyed using IR imagery and a GPR data acquisition unit. The analysis of the captured IRT and GPR data is presented. Computational equations to integrate the results are formulated as well as a Matlab code. To validate the proposed integration procedure, the detected defects are quantified and compared with results on the same bridge decks provided by other technologies.

**Chapter 6** establishes a connection between the NDT technologies and the inspector findings by integrating IRT and GPR results with the findings of the routine visual inspections to provide a condition rating system of concrete bridge decks. Thus, the system accounts for both surface and hidden defects in bridge decks. The condition rating systems currently in use in Canada and the United States are discussed and appraised to highlight their drawbacks. In-situ inspections on a full-scale deteriorated bridge deck using IRT, GPR, and visual inspection were conducted. The collected data is analyzed and the detected defects are quantified and converted into condition categories using fuzzy mathematics. The inherent uncertainties in the NDT and visual inspection measurement are considered using the fuzzy synthetic evaluation approach. Interviews with experts having comprehensive bridge experience were carried out to obtain the degree of relative importance for defects as well as the boundaries between the defects' condition categories. The proposed integration methodology is implemented in a case study and the results are compared with the evaluation results obtained by employing each individual technology.

**Chapter 7** investigates the feasibility of using an unmanned aerial vehicle to evaluate the condition of bridge decks utilizing a high resolution thermal sensor. The principles of aerial UAV remote sensing technology are discussed. Two in-service concrete bridge decks were investigated using the proposed system. The planning, flight preparation, and setting up of the proposed UAV-borne thermal system are discussed. The captured thermal data is analyzed using the system developed in Chapter 4. The achieved results are validated using data generated by other NDT technologies on the same bridge decks. Future improvements for the proposed system are recommended.

**Chapter 8** presents the conclusions from this study along with suggestions for further research work. The background information and the related references are included in each chapter.



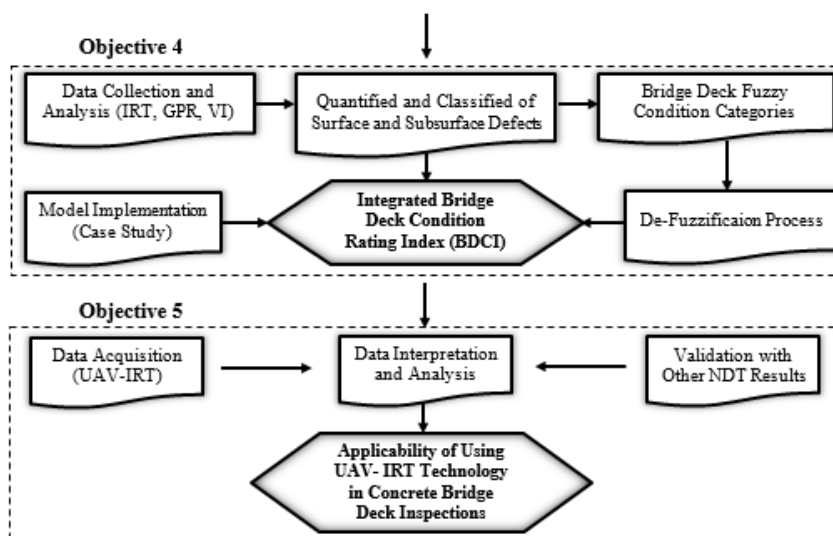


**Figure 1-2: Schematic diagram of research methodology.**

## 1.5 Main Contributions

An innovative bridge deck condition assessment and rating system using a passive IRT technique is proposed in this thesis. The research contributes evidence that supports expanding the use of IRT as a reliable, safe, and rapid condition assessment tool for accurate and consistent evaluation of the sub-surface conditions of reinforced concrete bridge decks. Specific original contributions of this dissertation include:

- Developing a rational decision-making methodology to evaluate the performance of NDT techniques in assessing the conditions of concrete bridge decks. The proposed model guides the bridge stockholders' efforts to incorporate NDT techniques into bridge inspection procedures and can be customized to accommodate different transportation agency policies.
- Developing a robust approach for analyzing IRT data for effective identification of delaminated areas in full-scale reinforced concrete bridge decks. The proposed analysis allows for the detection of subsurface anomalies regardless of the difference in the temperature ranges between various IRT surveys taken at different times and environmental conditions. The Matlab codes, specially written to develop a stitching

algorithm required to create a mosaicked thermogram of the entire bridge deck from a large number of thermal images, were maintained with several input variables to accommodate any other thermal survey data, and thus automate the detection process. In addition, the proposed procedure clearly distinguishes the categories of identified delaminations and presents the findings in terms of condition maps, which provide a quantified basis for informed decision making.

- Developing a rigorous integration procedure of IRT and GPR analysis results to produce an overall bridge deck condition map that classifies the severity levels of detected delaminations and the potential active corrosion areas. Combining the two technologies in inspecting deteriorated concrete bridge decks maximizes the capabilities of each method and compensates for their mutual limitations. Consequently, adopting the proposed approach provides more precise assessments of bridge deck conditions and important information for decision makers.
- Developing an inventive condition rating system that yields both surface and subsurface condition indicators of bridge deck condition. The condition rating models currently in use do not account for subjective information in the assessment process and employ solid linguistic grades that do not take into consideration gradual transitions from one condition category to another. The fuzzy model proposed herein for interpreting a new bridge deck condition index (BDCI) from IRT, GPR and visual inspection techniques is, to the best of the author's knowledge, the first model that simultaneously considers the uncertainties in the NDT along with the visual inspection measurement, thus providing a more reliable rating system. The model could also be extended to accommodate other bridge components, to involve more defect types, and to include the results of any other NDT technologies.
- Developing a novel UAV-IRT system to evaluate the condition of bridge decks without any traffic interruption. Only one previous research, to the best of the author's knowledge, investigated the application of UAV for in-situ assessment of full-scale bridge decks. The proposed system offers a practical and rapid solution for frequent bridge deck inspection and provides quantitative measurements of subsurface defects.

## 1.6 References

- ASCE Infrastructure Report Card (2017), <https://www.infrastructurereportcard.org/category/bridges/> [Accessed 21th February, 2017].
- Canadian Infrastructure Report Card (2016), <https://www.canadainfrastructure.ca>. [Accessed 2nd April, 2016].
- Clark, M., McCann, D., and Forde, M. (2003). "Application of infrared thermography to the non-destructive testing of concrete and masonry bridges." *NDT&E International*, Vol. 36 (4), 265-275.
- Gucunski, N., Kee, S., La, H., Basily, B., Maher, A., and Ghasemi, H. (2015). "Implementation of a Fully Autonomous Platform for Assessment of Concrete Bridge Decks RABIT." *Proc., Structure Congress*, ASCE, Reston, VA, 367-378.
- Gucunski, N., Imani, A., Romero, F., Nazarian, S., Yuan, D., Wiggenhauser, H., Shokouhi, P., Taffe, A., and Kutrubes, D. (2013). "Non-destructive testing to identify concrete bridge deck deterioration." *Proc., 92<sup>nd</sup> Annual Meeting, TRB*, Washington, D.C. SHRP 2 Report, 96 p.
- Hammad, A., Yan, J., and Mostofi, B. (2007). "Recent Development of Bridge Management Systems in Canada." *Proc., Annual Conference of the Transportation Association of Canada*, Saskatchewan, 1-20.
- Lounis, Z. (2013). "Critical concrete infrastructure: extending the life of Canada's bridge network." *Construction Innovation*, NRC, Canada. Vol. 18 (1), 34-49.
- Manning, D., and Holt, F. (1982). "Detecting Delaminations in Concrete Bridge Decks." *Concrete International, ACI*, Vol. 2 (11), 1-8.
- Maser, K., and Roddis, W. (1990). "Principles of Thermography and Radar for Bridge Deck Assessment." *Transportation Engineering*. Vol. 116 (5), 583-601.
- Robert, M. (1982). "Science behind Thermography-Thermal Infrared Sensing for Diagnostics and Control." *Thermosense*, Vol. 371, 2-9.
- Vaghefi, K., Oats, R., Harris, D., Ahlborn, T., Brooks, C., Endsley, K., and Dobson, R. (2012). "Evaluation of commercially available remote sensors for highway bridge condition assessment." *Bridge Engineering*, Vol. 17 (6), 886-895.
- Washer, G., Fenwick, R., and Nelson, S. (2013). "Guidelines for the Thermographic Inspection of Concrete Bridge Components in Shaded Conditions." *Proc., 92<sup>nd</sup> Annual Meeting, TRB*, Washington, D.C. 1-14.
- Washer, G., Fenwick, R., and Harper, J. (2009). "Effects of Environmental Variables on Infrared Imaging of Subsurface Features in Concrete Bridges." *Transportation Research Board*, Vol. No. 2108, 107-114.

## Chapter 2

### 2. Current Practice for Condition Assessment of Reinforced Concrete Bridges

#### 2.1 Introduction

In view of the colossal backlog of ageing reinforced concrete (RC) bridges and the considerable challenge it represents for transportation agencies, reliable bridge condition assessment (BCA) has become essential, especially for creating BMSs required for maintenance decisions and budget allocation. Visual inspection (VI) is the default bridge inspection methodology, yet its results heavily depend on the expertise and judgment of bridge inspectors, yielding primarily qualitative and subjective results. An extensive literature survey indicates that there is a considerable number of studies on specific assessment techniques. For instance, there has been significant focus in using non-destructive testing (NDT) technologies for detecting several deterioration indicators. NDT enables the detection of deterioration processes at their early stages and can be incorporated into the inspection process to evaluate hidden defects such as reinforcing steel corrosion or crack propagation. However, the use of NDT techniques is usually specified for special assessment when severe deficiencies are observed. The term “structural health monitoring” (SHM) encompasses a range of methods and practices designed to assess the condition of a structure based on a combination of measurement, modelling and analysis. However, SHM technology has not been widely adopted as a routine approach for bridge monitoring. In addition, artificial intelligence (AI) techniques deal with intelligent behaviour, learning and adaptation in machines and have been recognized as powerful tools for BCA. Consequently, BCA techniques are evolving rapidly and have reached a certain level of maturity. Therefore, it is important to understand how the assessment techniques, as they pertain to decision-making, have evolved and what is their present state.

In this Chapter, a critical overview of the state of existing BCA, with emphasis on current practices in North America, is presented in a systematic and rigorous manner to determine prospects for improvement. Throughout the chapter sections, the recent research efforts on the available techniques are delineated. The versatility of their potential applications is

discussed and they are compared, highlighting their primary advantages and limitations. The challenges associated with the application of each technique are identified. The AI techniques commonly utilized to develop effective BCA models are also examined and appraised. To assist bridge owners in making informed decisions, this review suggests some recommendations towards the selection of appropriate assessment techniques so as to identify specific deterioration types in order to meet desired service goals. Furthermore, knowledge gaps and needs in this field are outlined in order to motivate further research and development of these technologies, which have been addressed in the present thesis. The methodology adopted to achieve the aforementioned objectives is as follows: (1) developing a structured framework for conducting a comprehensive literature review on BCA based on the vast number of papers published; (2) using this framework to gain an understanding of the current state of the BCA research field; and (3) developing a conceptual framework identifying areas of concern with regard to BCA techniques. **Figure 2-1** illustrates the developed methodological framework for implementing the review.

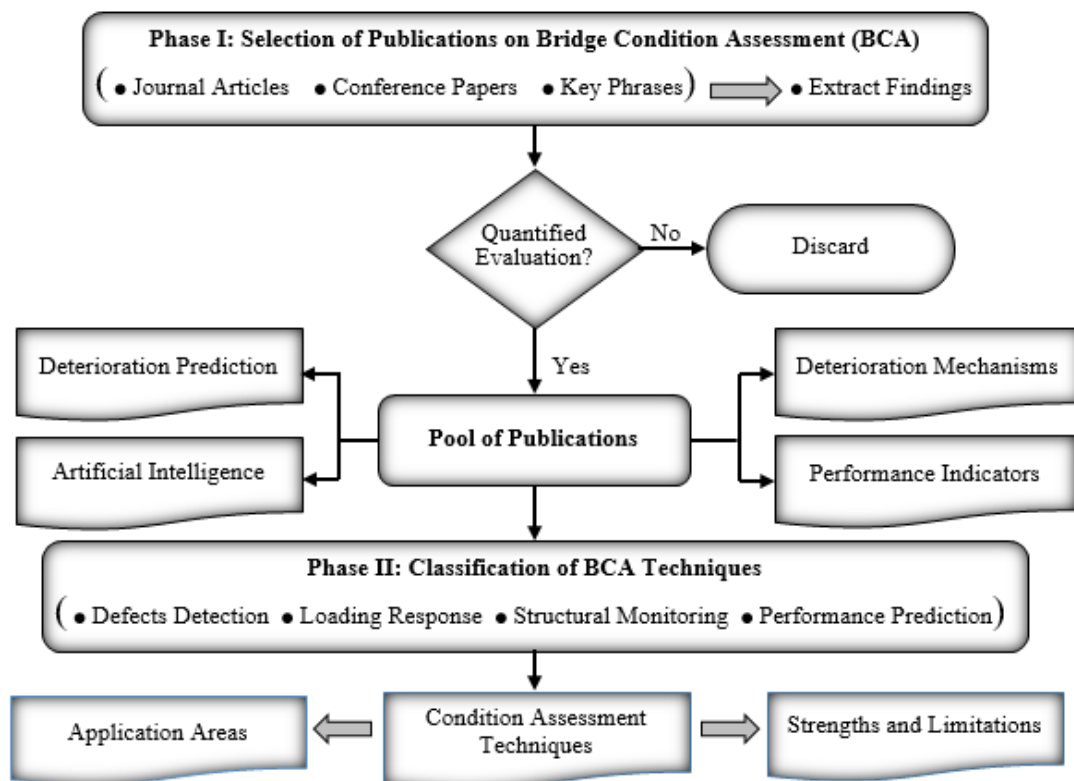


**Figure 2-1: Methodological framework for literature review of BCA technologies.**

It can be observed in this figure that the review consists of two phases in which the first phase is the search for and selection of papers to include in the review and the second phase is the classification of the papers. The first phase started by collecting a comprehensive range of recent research on BCA. The articles were carefully selected from eight diverse academic journals within the domain of bridge construction and management in an attempt to capture recent and relevant developments. Leading research conferences on the topic were also considered in a similar manner. The articles were searched using key phrases, such as “RC bridge assessment” and “RC bridge evaluation”. This process initially identified 197 papers. The retrieved articles were further examined to extract their main findings and emphases. Articles whose primary focus was not based on quantitative evaluation were discarded. Accordingly, the final survey qualitatively aggregates the results of a selected set consisting of 158 research studies, among which 70% were published over the last five years. The second phase started by overviewing the common deterioration mechanisms and common defects occurring in concrete bridges as well as exploring the performance indicators of RC bridges. The BCA techniques were then classified into categories and each article was evaluated so as to be placed into the relevant category. The techniques of each category were discussed to identify their key application areas, principal strengths and limitations. The existing deterioration prediction models were appraised and the achievements of AI technologies in the field of BCA were evaluated. Finally, a conceptual framework was developed to address the challenges and technology gap that need further research and development and to formulate recommendations for the selection of appropriate technologies.

## **2.2 Deterioration of Reinforced Concrete Bridges**

RC bridges are susceptible to various deterioration mechanisms. The distinction among their major causes is purely qualitative since such mechanisms can act in synergy. However, RC bridge deterioration mechanisms can be categorized as physical, chemical, mechanical, and biological processes. Physically-induced deteriorations are caused by factors such as freeze-thaw cycling, crystallization of salts in pores, non-uniform volume changes, temperature gradients, abrasion, erosion and cavitation from water flow. Chemically-induced deteriorations occur because of carbonation, chloride contamination,

sulfate and acid attacks, or alkali-aggregate reactions (Delatte, 2009). Mechanically-induced deteriorations are generally caused by static and/or dynamic loads, or construction faults such as those from premature loading during construction. Biologically-induced deteriorations, such as fungi, moss, and microbials, can cause internal or external concrete damage through physical and chemical interactions (Penttala, 2009). Different deterioration processes lead to different types of defects and will have different effects on the ability of the evaluation techniques to detect and characterize them (Gucunski and Nazarian, 2010).

Damage mechanisms can primarily affect the steel reinforcement or the concrete itself. Corrosion of the reinforcing steel often constitutes the primary deterioration mechanism and major concern for RC bridges and can lead to structural and functional failures. The reinforcing steel becomes susceptible to corrosion when the ingress of chloride ions exceeds a threshold concentration level, which is dependent on factors such as the quality of concrete, relative humidity, temperature and pH of the pore solution. In addition, carbonation of the concrete resulting from the reaction between carbon dioxide and other alkaline constituents of the cement paste reduces the alkalinity of the concrete. Thus, the steel can be de-passivated. As the steel corrodes, rust occupied areas increase in volume, creating internal tensile stresses in the surrounding concrete. Cracking in the concrete surrounding the steel rebar is initiated when such tensile stresses exceed the tensile strength of the concrete. Cracking accelerates the damage mechanisms by providing easy access for chlorides, oxygen and moisture, resulting in subsurface fracture planes (delaminations), which may be localized at the level of steel reinforcement or can extend over a substantial area along different planes beneath the concrete surface (Penttala, 2009). As the deterioration progresses, these fracture planes may become separated from the main structural component, resulting in spalling of the concrete surfaces, which further exposes the embedded steel to the corrosive environment, thus accelerating deterioration, and possibly compromising the bridge's structural integrity, safety and serviceability.

However, the common defects occurring in concrete bridges and their possible causes are briefly described in **Table 2-1**. Such defects represent the main challenge in concrete bridge inspection and repair programmes.

**Table 2-1: Common defects in reinforced concrete bridges**

Defect	Description and Reason
Cracking	<ul style="list-style-type: none"> <li>• <b>Description:</b> partly or completely linear fracture. Classification: geometrically (hairline, narrow, medium and wide) or structurally (shear, and flexural cracks).</li> <li>• <b>Reason:</b> tensile and compressive stresses, shrinkage and expansion, internal or external restraint, differential movements and settlements, rebar corrosion.</li> </ul>
Scaling	<ul style="list-style-type: none"> <li>• <b>Description:</b> local flaking, or loss of surface portions of concrete.</li> <li>• <b>Reason:</b> de-icing chemicals, freeze-thaw cycles, high permeability, non-air entrained, poor concrete consolidation, physical salt attack.</li> </ul>
Disintegration	<ul style="list-style-type: none"> <li>• <b>Description:</b> starts in the form of scaling and progression of severe scaling results in breaking down of concrete into small fragments or particles.</li> <li>• <b>Reason:</b> de-icing chemicals, strong alkalies, sulphate or chloride attack, and/or frost action.</li> </ul>
Abrasion	<ul style="list-style-type: none"> <li>• <b>Description:</b> as the outer paste of concrete wears, the fine and coarse aggregate are exposed and abrasion and impact will cause additional degradation that is related to aggregate-to-paste bond strength.</li> <li>• <b>Reason:</b> inability to resist wear caused by rubbing and friction, and wind-borne particles.</li> </ul>
Corrosion	<ul style="list-style-type: none"> <li>• <b>Description:</b> deterioration of steel bars by electrolysis. Starts with light rust stain on concrete surface, localized pitting, very heavy rusting, and loss of steel section.</li> <li>• <b>Reason:</b> ingress of chloride ions, use of de-icing salts, carbonation, using high w/c ratio, wetting-drying cycles, lack of curing, low thickness of concrete cover.</li> </ul>
Delamination	<ul style="list-style-type: none"> <li>• <b>Description:</b> partial separation areas of the concrete cover at or near the external layer of steel bars where concrete subsequently separates, but not entirely detaches.</li> <li>• <b>Reason:</b> substantial and advanced corrosion in the top steel bars, which swell and develop internal stress, leading to de-ponding between concrete and steel bars.</li> </ul>
Spalling	<ul style="list-style-type: none"> <li>• <b>Description:</b> fragment detached from a larger concrete mass. Common on exposed concrete edges, deck joints or construction joints.</li> <li>• <b>Reason:</b> pressure exerted by corrosion, areas of localized high compressive load concentrations, or by the formation of ice in the delaminated areas.</li> </ul>
Cavitation	<ul style="list-style-type: none"> <li>• <b>Description:</b> irregular concrete surface presented as small holes and pits.</li> <li>• <b>Reason:</b> abrupt change in direction of high-velocity flowing water creates cavities at the concrete surface. When vapor cavities collapse, causing very high instantaneous pressures that impact on the concrete surfaces, causing pitting, noise, and vibration.</li> </ul>

Scour	<ul style="list-style-type: none"> <li>• <b>Description:</b> the removal of material from the stream bed or bank due to the erosive action of moving water in the stream. Measured as the average depth below the original stream bed.</li> <li>• <b>Reason:</b> general scour is caused by the constriction to the natural flow created by the structure, while local scour is caused by an obstruction to the flow by a pier or an abutment.</li> </ul>
Alkali-Aggregate Reaction	<ul style="list-style-type: none"> <li>• <b>Description:</b> expansion occurs under moist conditions, leading to cracking and deterioration of concrete. Has two forms: alkali-silica reaction (ASR) and alkali-carbonate reaction (ACR). ASR is more common than ACR, but ACR tends to be more rapid and severe.</li> <li>• <b>Reason (ASR):</b> some aggregates react adversely with alkalis in concrete to produce a highly expansive gel causing expansion and cracking usually over a period of years,</li> </ul>

The formation of corrosion-induced delamination and spalling in concrete bridge decks is shown in **Fig. 2-2**. Such a deterioration mechanism has been a serious concern for transportation agencies due to the related serviceability and safety considerations.

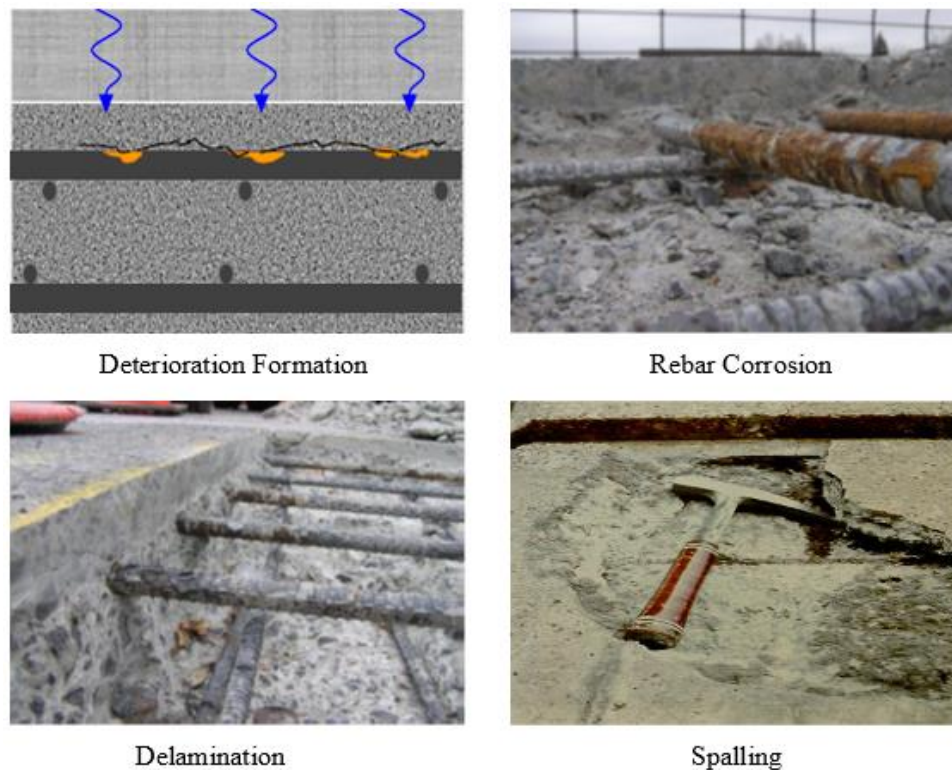


**Figure 2-2: Corrosion-induced delamination and spalling in concrete bridge decks**  
(Gucunski *et al.*, 2013).

## 2.2.1 Bridge Performance Indicators

Bridge performance indicators include scour assessment, fatigue and fracture assessment, seismic assessment, and condition assessment, including load carrying capacity.

### 2.2.1.1 *Scour Assessment*

For a majority of RC bridges spanning watercourses or located in flood plains, failures are attributed to scour damage, which is difficult to detect in real time. Scour is a common soil-structure interaction problem that can occur in three main forms, namely, general scour, contraction scour and local scour. Scour reduces the stiffness of foundation systems and can cause bridge piers to fail without warning. Continuous changes in climate and the increasing frequency of flooding has led to a higher risk of such bridge failures. Several studies investigated scour mechanism and how to predict its depth (e.g. Jannaty *et al.*, 2016; Amini *et al.*, 2014), and various types of instrumentation (e.g. tiltmeters and accelerometers) have been developed to measure bridge response to scour. However, most monitoring regimes are based on underwater instrumentation that requires expensive installation and maintenance, and can often be subjected to damage during times of flooding, when scour risk is at its highest. Consequently, appropriate preventive measures are difficult to apply when scour damage is detected. Therefore, scour monitoring is an important topic for transportation owners, especially during high-flood events and in coastal areas. Currently, there are research efforts investigating scour monitoring using changes in bridge structural dynamic properties to indicate the existence and severity of the scour phenomenon affecting the bridge. Further details on scour assessment and monitoring systems are reported in Prendergast and Gavin, (2014).

### 2.2.1.2 *Fatigue and Fracture Assessment*

Fatigue failure can occur in RC bridges when they are exposed to repetitive loading. Micro-cracks in concrete commonly develop at the aggregate-cement paste transition zone due to different thermal and shrinkage deformations. Repetitive loading extends the length and size of the micro-cracks exacerbating stress concentration, which can lead to a fatigue failure depending on the bridge's geometry, material properties and applied loads. The loads could be caused by short-term traffic, variable long-term loads and wind. Generally,

two types of fatigue loading can result in different failure characteristics: low-cycle fatigue, in which the load is applied at high stress levels for a relatively low number of cycles; and high-cycle fatigue corresponding to a large number of cycles at lower stresses (Saviotti, 2014). Fatigue failure modes could be classified as compression, bending, shear or bonding failure. The fatigue life of a bridge depends as much on the stress levels as on the stress range and the number of loading cycles. Corrosion induced fatigue strength reduction has a large effect on fatigue life. It has been found that the fatigue life of a bridge could be reduced by more than 60% for the low corrosion condition and by more than 70% for the medium and high corrosion conditions (Zhang and Yuan, 2014). Maekawa and Fujiyama (2013) also investigated the crack water interaction and fatigue life assessment of RC bridge decks and concluded that a high loading rate shortens the fatigue life of saturated concrete bridge slabs. However, several models have been developed in the literature for bridge fatigue reliability assessment and the prediction of fatigue life of reinforcing steel rebar based on dynamic analysis, stress wave analysis, and finite element analysis (Newhook and Edalatmanesh, 2013).

### 2.2.1.3 *Seismic Assessment*

The risk associated with the seismic susceptibility of bridges is pertinent to the safety and security of the public and moreover in the case of disasters (Saviotti, 2014). Therefore, bridges located in areas subjected to seismic forces are commonly designed according to specific codes (e.g. performance and displacement-based design) to resist such forces without collapse (Zhang *et al.*, 2016). However, the primary causes of bridge seismic damage include soil liquefaction, bridge age, design or construction modifications, and inelastic deformation during strong earthquakes. There are numerous studies in the literature on the seismic risk assessment of bridges. For instance, Muntasir *et.al.* (2015) presented a review of the different methodologies developed for seismic fragility assessments of highway bridges along with their features, limitations and applications. However, the inherent difficulties of upgrading existing RC bridges to current structural standards highlight the need for more advanced research studies in several areas (e.g. assessment methods, retrofit criteria and intervention techniques) (Saviotti, 2014). **Table 2-2** illustrates some developed techniques and their related references.

**Table 2-2: Evaluation techniques for RC bridge performance indicators and the related references**

Performance Indicator	Evaluation Technique	Reference	Year
Scour Assessment	• Bridge Dynamic Response.	• Elsaid and Seracino	• 2014
	• Sound Wave Devices.	• Fisher et al.	• 2013
	• Driven Rod Devices.	• Zarafshan et al.	• 2012
	• Fibre-Optic Bragg Sensors.	• Zarafshan et al.	• 2012
	• Ultrasonic P-Wave.	• Coe and Brandenburg	• 2011
	• Single-Use Devices.	• Briaud et al.	• 2011
	• Ground Penetrating Radar.	• Anderson et al.	• 2007
Fatigue and Fracture Assessment	• Electrical Conductivity Devices.	• Anderson et al.	• 2007
	• Bridge Dynamic Response.	• Zanjani and Patnaik	• 2014
	• Vehicle-Bridge-Wind Dynamic S.	• Zhang et al.	• 2014
	• Corrosion-Fatigue Strength.	• Zhang and Yuan	• 2014
	• Integrating Reliability and SHM.	• Newhook and Edalatman	• 2013
	• Crack Water Interaction.	• Maekawa and Fujiyama	• 2013
	• Static Ultimate Testing.	• Newhook et al.	• 2011
Seismic Assessment	• Fatigue Damage Accumulation.	• Edalatmanesh Rahman	• 2010
	• Acoustic Survey-Crack Monit.	• Butt et al.	• 2007
	• Seismic Fragility Analysis.	• Muntasir et.al.	• 2015
	• Negative Stiffness Devices.	• Attary et al.	• 2013
	• Probabilistic Time-variant Static.	• Biondini and Frangopol	• 2013
	• Seismic Design of RC Bridges.	• Nogami et al.	• 2013
	• Probabilistic Performance Analy.	• Lau et al.	• 2012
• Target Damage Level.	• Taner and Caner	• 2011	
• Rubber-Based Isolation System.	• Ozbulut and Hurlbaas	• 2011	
• Post Repair Response.	• Do Hyung et al.	• 2010	

### 2.3 Bridge Condition Assessment Approaches

The condition assessment of an existing RC bridge aims at determining whether the bridge will function safely over a specified residual service life. It is based on the results of assessing hazards and load effects to be anticipated in the future. Guidelines for assessment of existing bridges have been developed in many countries. They are commonly separated in phases, starting with a preliminary evaluation, followed by a detailed investigation, expert investigation, and finally an advanced assessment, depending on the structural condition of the investigated bridge (Saviotti, 2014). The preliminary evaluation mainly deals with bridge safety and identifying critical deteriorated bridge members. It should include an intensive study of the original design and as-built documents, the maintenance records, a visual inspection and a photographic survey. The detailed investigation focuses

on those members for which adequate safety was not confirmed by the preliminary evaluation. The fatigue and seismic behaviour of the bridge are also considered in this stage and NDT could be used in order to characterise the basic material properties of the bridge. The final report should establish whether the bridge has sufficient static strength against actual loadings. If a bridge component has major consequences in terms of risk or cost, an expert investigation will be required to check the conclusions and proposals recommended in the detailed investigation report. In-situ assessment using specific testing tools could be adopted to help reach a decision. The advanced assessment determines whether retrofitting interventions could be adopted, and whether large-scale dismantling operations may be required. It could include seismic analysis, material analysis, finite element modeling, and a detailed survey using some of the advanced BCA testing techniques (Saviotti, 2014).

**Table 2-3** summarizes the requirements for each phase of the assessment procedure.

**Table 2-3: Requirements of different assessment phases of existing bridges**

Assessment Procedure	Assessment Requirement
Preliminary Evaluation	<ul style="list-style-type: none"> <li>• Ensure that bridge construction is conforming to the built drawings.</li> <li>• Identify any modification conducted while bridge is in service (e.g. rehabilitation, strengthening, changes to static system.... etc.</li> <li>• Record the presence of any visual degradation evidence (e.g. damaged expansion joints, cracks, scaling, pop-out, spalling.... etc.</li> <li>• The final report should indicate any questionable information.</li> </ul>
Detailed Investigation	<ul style="list-style-type: none"> <li>• Develop FEM numerical model of the entire bridge.</li> <li>• Verify that the structural components and elements are safe.</li> <li>• Concerning specific issues such as fatigue and seismic behaviour.</li> <li>• NDT could be used to characterise the material properties.</li> <li>• The final report should establish whether the bridge has sufficient static strength against actual loadings.</li> </ul>
Expert Investigation	<ul style="list-style-type: none"> <li>• Team of experts will discuss and check the conclusions and proposals recommended in the detailed investigation report.</li> <li>• Further assessment using specific tools can be carried out.</li> <li>• On-site testing could be adopted, if required, in order to provide the dynamic identification of the bridge.</li> </ul>
Advanced Assessment	<ul style="list-style-type: none"> <li>• Determine the global static and cyclic behaviour of the bridge based on detailed on-site survey data, NDT, and FEM analysis.</li> <li>• In some cases, on-site dynamic identification could be performed.</li> <li>• For fatigue assessment, a linear elastic fracture mechanics investigation is required.</li> <li>• The final report should include all the performed analysis and indicate the verification results and any specific retrofit needed.</li> </ul>

The most significant challenge to BCA is the quantification of information on bridge condition (Lounis, 2013). A comprehensive literature survey has shown that BCA techniques can be classified into one (or a combination) of five categories including VI for assessing the apparent condition, load testing (LT) techniques for determining safe loading levels, NDT technologies for detecting deterioration indicators, SHM systems for sensing structural performance, and finite element modelling (FEM) for numerically predicting bridge reliability as shown in **Fig. 2-3**. Each category is investigated subsequently to frame its knowledge gaps and highlight its research needs.

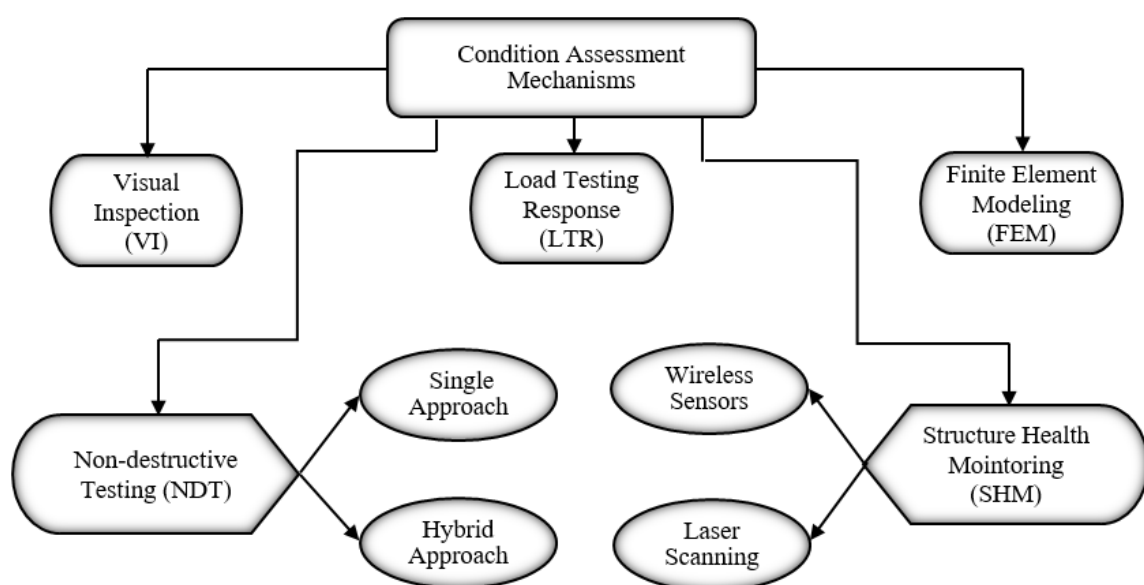


**Figure 2-3: Condition assessment mechanisms of reinforced concrete bridges.**

### 2.3.1 Visual Inspection

Visual Inspection (VI) is the primary component of all existing BMSs. In Canada and the United States, routine VI is often conducted within 24-month intervals depending on the condition of the bridge. Enhanced inspection to access all areas of bridges over 30 years old are typically done with a maximum six years interval, while emergency detailed inspection should be carried out immediately when a component contributing to overall bridge stability has failed, in case of imminent failure, or when public safety is at risk. The use of bridge inspection reporting software has been explored by several asset management

software developers. A bridge inspection software typically consists of interactive forms that retrieve customized inspection guidelines and relevant historic bridge inspection data, capture bridge evaluation data, and automatically associate the captured information with the bridge components, making the bridge inspection records intuitive (Akula *et al.*, 2014). VI can only identify problems once they have progressed to a high level of severity and reached the concrete surface. Furthermore, visual inspection requires lifting tools to gain adequate access to some areas of the bridge as shown in **Fig. 2-4**.



**Figure 2-4: Visual inspection of concrete bridge decks and soffits (Gucunski *et al.*, 2013).**

Research results indicate that assessing a bridge's condition by VI alone is unreliable, as it is unable to identify correctly the repair priorities (Moore *et al.*, 2001). Although the qualifications and experience of those leading bridge inspection are recognized by most inspection standards, the quality and consistency of visual inspection results greatly depend on the motivation and equipment of those conducting such inspections. In spite of the fact that VI is subjective and qualitative, it has been the dominant practice for BCA and for input parameters in deterioration models. An advantage of VI is that it involves a broad evaluation of the entire bridge and is not limited to the detection or assessment of a specific type of damage or a component of the bridge. The VI costs depend on the characteristics of the bridge and are positively correlated to the level of inspection details and frequency. The major components of VI costs belong to traffic management and labour. VI costs

increase, for instance, in cases of underwater inspection to evaluate scour (Agdas *et al.*, 2015). Increased awareness of the shortcomings of visual inspection has motivated advanced BCA approaches. Although more quantitative models of structural deterioration have been developed, they have yet to be incorporated in existing BMSs. Thus, the review reveals the need for unified guidelines and BCA procedures capable of using the accessible data collected during the VI process and accounting for the uncertainty and complexity associated with detailed inspection processes.

### 2.3.2 Load Testing

Condition assessments for the global structure integrity of existing concrete bridges are commonly addressed through structural analysis, load testing, or a combination of methods. For instance, the reliability bridge evaluation rating process described in the AASHTO's (American Association of State Highway and Transportation) manual is based on load testing. Load testing is a procedure to determine the safe loading levels of a bridge, leading to a load rating that indicates the capacity level of a bridge. Through forced static and dynamic load testing in varied load patterns, the maximum response can be detected using strain transducers placed at critical locations on the bridge. Forced vibration testing combined with system identification has been used for many decades to determine the dynamic characteristics of bridges. Load tests are broadly divided into two categories: proving load tests, which are intended as self-supporting alternatives to theoretical assessments, and supplementary load tests, which are intended to be used as an adjunct to theoretical calculations (Zhang *et al.*, 2016). However, the load ratings can be determined by allowable stress, load factors, or load and resistance factor methods. Bridge ratings performed by all three methods follow a similar basic procedure, differing primarily in the load or resistance factors in the rating equation. Although the ratings are determined in both inventory and operating load levels, these three competing rating methods may yield different rated capacities for the same bridge (Wang *et al.*, 2011).

Not only do older bridges deteriorate over time, but they may also not have been designed for increased load demand. Therefore, the required load capacity of an existing bridge should be determined according to the extreme load effects that the bridge will experience from actual traffic during its remaining service life. Extreme vehicle loads have been

researched through methods such as probabilistic vehicle weight models, consecutive traveling vehicle models, and simulation (Zanjani and Patnaik, 2014). Another practical procedure of BCA via load testing is using B-WIM (bridge-weight in motion) monitoring data where the strain measurements can evaluate the bridge condition, especially for bridges under load restriction due to distress (Mosavi *et al.*, 2014). However, it should be noted that this testing is only confined to the elastic range (assuming a heavily overloaded truck represents ultimate load), which gives no information on the non-elastic performance at the ultimate limit state.

Bridge strains, displacements, and accelerations can be measured during load testing. Vertical displacement has been considered the most important among various structural health parameters that could be used for predicting consequent damage or deterioration in RC bridges. For instance, deflection in RC bridges increases with reductions in stiffness when cracking of the concrete occurs. Therefore, service limit states, specified in several design codes and standards, indicate that deflections throughout the entire service life of a bridge must not exceed acceptable limits. Measuring deflections during a load test can be done using linear variable differential transducers-LVDTs, and fibre-optic or similar sensors mounted on a fixed support. While these systems have high rates of data acquisition and reasonable accuracy, it is usually difficult to install them on bridges spanning waterways, bridges with heavy traffic, and when there is need of placing the sensors in contact with an auxiliary frame linked to the ground. (Cruz *et al.*, 2015). Other options include topographical methods, hydraulic methods, and the radar interferometry system. Generally, the topographical methods have low resolution and do not provide high rates of readings, preventing their use in obtaining influence lines and accurate deflection measures. The hydraulic methods have similar drawbacks in addition to the effects of temperature on measurements, while the radar system does not directly measure deflections, which makes it difficult to apply. However, applying the geodetic technique using a robotic total station or a theodolite has been successfully used for bridges characterized by large deflections (Cruz *et al.*, 2015).

Bridge structural integrity can also be assessed by the most probable values of the structural element properties, such as the stiffness obtained using vibration measurements. For

instance, Chen *et al.* (2009) applied image processing methods and utilized the data of vibration measurements and video-based traffic monitoring to update the probability distributions of the elements' stiffness where the most probable values served as reliable indicators of bridge structural integrity. Wang *et al.* (2011) assessed several existing bridge structures and recommended guidelines, established by a coordinated load testing programme and a FEM integrated within a structural reliability framework, to determine practical bridge rating methods. However, loads experienced by bridges are often inferred from limited measurements of external conditions (e.g. ambient temperature, wind speed/direction, wave heights). Therefore, the monitoring of load testing can be combined with other technologies, such as structural health monitoring methods, for improved assessment of concrete bridges.

### 2.3.3 Structural Health Monitoring

Structural Health Monitoring (SHM) is a non-destructive in-situ sensing and evaluation technique that uses multiple sensors embedded in a structure to monitor and analyze the structural response and detect anomalous behaviour in order to estimate deterioration and to evaluate its consequences regarding response, capacity, and service life. A SHM system has the ability to detect damage at any point in time by its real time continuous monitoring. In recent years, several SHM systems have been developed and implemented to provide information for bridge maintenance strategies. Most SHM systems have similar fundamental elements: (1) measurements by sensors and instrumentation, (2) structural assessment (e.g. peak strains or modal analysis), and (3) BCA to support MR&R related decision-making (Alampalli, 2012). The functionality of a SHM system depends on the type and number of sensors used. A monitoring system may rely on single or multiple sensor types, which can be tailored to capture a variety of physical measurements associated with loads, environmental conditions, and bridge responses (Wong, 2007). A SHM system with a variety of sensor types can identify material parameters such as concrete creep, shrinkage and corrosion, environmental effects including temperature gradients, and dynamic responses such as traffic-induced vibrations. **Table 2-4** summarizes some common SHM systems to identify the most important parameters in appraising the overall stiffness and bearing capacity of a bridge structure.

**Table 2-4: Summary of common structural health monitoring systems of bridges**

Monitoring System	Advantages and Limitations
Displacement Sensors (Park <i>et al.</i> , 2005)	<ul style="list-style-type: none"> <li>• Easy to use and can allow rapid collection of data from a large number of points when connected to a data acquisition system.</li> <li>• Reference dependent and time consuming installation.</li> <li>• Cannot be installed under high bridge decks or bridges spanning waterways.</li> </ul>
Acceleration Sensors (Park <i>et al.</i> , 2005)	<ul style="list-style-type: none"> <li>• Have small size and low weight; mainly for vibration monitoring.</li> <li>• Identification effect is poor for low-frequency static displacement</li> <li>• Double integration is required to obtain the displacement. Thus, has low accuracy.</li> </ul>
Strain sensors (Glisic <i>et al.</i> , 2002)	<ul style="list-style-type: none"> <li>• Can measure vertical displacement of a bridge and the deformation of a frame.</li> <li>• Cumbersome to apply and requires a data acquisition system.</li> <li>• Unsuitable for measuring the deformation of long-span bridges.</li> </ul>
Robotic Total Station (Palazzo <i>et al.</i> , 2006)	<ul style="list-style-type: none"> <li>• High precision, automation and can measure the 3D coordinates.</li> <li>• Cannot complete multi-target tasks in a short time.</li> <li>• Due to its low measuring frequency, the requirement of dynamic measurement cannot be satisfied.</li> </ul>
GPS Satellite-Surveying (Cosser <i>et al.</i> , 2014)	<ul style="list-style-type: none"> <li>• Calculate displacement based on measuring the coordinate changes in one, two or three dimensions.</li> <li>• Applicable to all-weather continuous monitoring.</li> <li>• Low measurement rate, high cost, requires skilled professionals.</li> </ul>
Motion detection cameras (Chan <i>et al.</i> , 2009)	<ul style="list-style-type: none"> <li>• Measure bridge displacement through analyzing photo frames.</li> <li>• Require a certain amount of light to achieve accurate results.</li> <li>• Accuracy may be compromised due to susceptibility to vibrations from wind and vehicle loading when mounted on bridge.</li> </ul>
Digital Image Cross-Correlation (Bell <i>et al.</i> , 2012)	<ul style="list-style-type: none"> <li>• Optical measurement technique for collecting displacements.</li> <li>• Rapid testing of in-service bridges through digital photography.</li> <li>• Accuracy of deflection measurement should be verified.</li> </ul>
Radar Sensors (Guan <i>et al.</i> , 2014)	<ul style="list-style-type: none"> <li>• Wireless and mounted sensors with relatively low cost.</li> <li>• Bridge motion can be extracted from the reflected wave signals.</li> <li>• Signal demodulation and data processing are difficult in the presence of noise.</li> </ul>
Laser Doppler Vibrometer (Raghavan, 2007)	<ul style="list-style-type: none"> <li>• Measure the vibration and displacement of bridges.</li> <li>• Provide accurate results but should be placed on the ground underneath the bridge and cannot be left unattended.</li> <li>• Not suitable for long-term continuous monitoring (fixed position)</li> </ul>
Terrestrial Laser Scan (Gordon & Lichti, 2007)	<ul style="list-style-type: none"> <li>• Can rapidly build complex, irregular 3D visualization models.</li> <li>• Low monitoring accuracy; the post-processing is complicated.</li> </ul>
Laser Projection-Sensing (Zhao <i>et al.</i> , 2105)	<ul style="list-style-type: none"> <li>• High image acquisition frequency and able to reflect the variation of structural dynamic displacement completely.</li> <li>• A feasible method to monitor bridge displacement.</li> <li>• Requires long-distance laser devices and high resolution cameras.</li> </ul>

### 2.3.3.1 *Data Acquisition Using Sensors and Laser Scanning*

SHM systems often rely on cables to connect sensors on bridges to a centralized power and data acquisition source. These wired systems are usually very reliable and are capable of high data collection rates. However, data and power cables, along with supporting conduit installation, remain the primary implementation and cost obstacles for cabled monitoring systems (Bao *et al.*, 2013). Fibre-optical sensors (FOS) have been applied for strain, temperature, and vibration measurement. FOS are less susceptible to electrical noise than strain gauges and accelerometers and thus can provide distributed measurements along a bridge but their accuracy is questionable (Higuera *et al.*, 2011). With the increased availability of wireless data networks, sustainable SHM systems have been developed so that pervasive sensor networks allow more efficient monitoring of multiple bridges and bridge segments across large areas. Wireless sensors have alleviated the cost and labour associated with cabled monitoring systems. O'Connor *et al.* (2014) employed a wireless sensor network to measure bridge accelerations, strains and temperatures. However, limitations of using wireless sensors include constraints in power and transmission bandwidth. Solar power supply, vibration, or wind could sustain long-term wireless sensor network operations, while less relevant communication bandwidth constraints could be made by conveying less data. For instance, O'Connor *et al.* (2012) introduced the compressed sensing data acquisition approach to achieve energy efficiency in long-term monitoring applications.

Laser scanning has been used in recent years for several health monitoring and damage detection applications in order to capture the status of structures. The most common application is tracking user-defined key-points on structures over a time period. Laser scanning capabilities, such as texture mapped 3D point clouds, can be used effectively to document quantitative information on present conditions of bridges where individual laser scans of a scene may be captured from different viewpoints to permit the creation of a complete 3D record of a damaged bridge (Olsen *et al.*, 2013). Guldur *et al.* (2015) developed a condition rating system of bridge components using detected and quantified surface damage from texture-mapped laser point clouds. The severity of the detected damage of each structural item was classified and assigned a numerical rating value based

on the AASHTO's condition rating guidelines. The system provides structural evaluation, giving an overall bridge condition based on major deficiencies, including its ability to carry the required loads. Zhao *et al.* (2015) developed a bridge displacement monitoring system based on laser projection-sensing and recommended the use of long-distance laser devices with higher power and good collimation to monitor displacements in large-span bridges.

### 2.3.3.2 *Common Applications of SHM Systems*

SHM applications can be deployed for load rating, short-term assessment of a specific bridge performance aspect (e.g. corrosion or scour) or for long-term monitoring to assess and track a wide range of bridge health conditions. SHM can track previously identified concerns or continuously monitor the bridge performance to detect damage before it reaches critical levels through systems that are deployed pre-emptively during the construction phase. Laory *et al.* (2012) discussed a systematic approach to determine the appropriate number and location of sensors to configure measurement systems in which static measurement data are interpreted for damage detection of continuously monitored bridge structures. Many SHM systems have been deployed on a variety of bridge components, such as long-term monitoring of bridge abutment piles, and remote sensing of corrosion in bridge decks (Huntley and Valsangkar, 2014). Integration of different SHM systems or combinations of them with other techniques can enhance the assessment process. Generally, a monitoring system is designed as an integrated system with all data flowing to a single database and presented through a single user interface.

For instance, Hu and Wang (2013) proposed an integrated SHM system which facilitates the combination of data collection and data analysis. Wireless network sensors, including accelerometers, strain gauges, and temperature sensors, were utilized in a system that can continuously monitor a bridge performance under random loads, where static and dynamic structural response parameters (e.g. vibration acceleration, dynamic displacement, and dynamic strain) can be determined and analyzed. Agdas *et al.* (2015) utilized visual inspection and wireless sensor networks and recommended a hybrid evaluation technique that adopts both approaches for optimal functionality to optimize the efficiency of BCA. Akula *et al.* (2014) introduced an integration BCA system through software called *Toolkit*, which allows inspectors to have access to an intelligent interpretation of SHM obtained

data and to the BCA data corresponding to equivalent components recorded visually by other respondents. However, while the SHM approach is promising as an effective bridge management tool, it still needs further dedicated research to make it a simple, reliable and low-cost option to become a standard aspect in BMSs.

### 2.3.4 Non-Destructive Testing

Non-destructive testing (NDT) techniques enable detection of deterioration processes at their early stages. NDT methods can be incorporated into the bridge inspection process, for example, to evaluate stiffness and strength, moisture content, and subsurface defects such as reinforcing steel corrosion, delamination and crack propagation. NDT is specified in some BMSs through periodical surveys or when visual inspection results indicate irregularities within the bridge structure. Appropriate and effective use of NDT has three requirements: (i) suitable understanding of the underlying phenomenon, (ii) the correct deployment of testing methods, and (iii) the application of appropriate analysis models to quantify the detected defects or variation of properties. The most commonly used NDT methods in onsite assessment and evaluation of RC bridges are illustrated in **Fig. 2-5**.

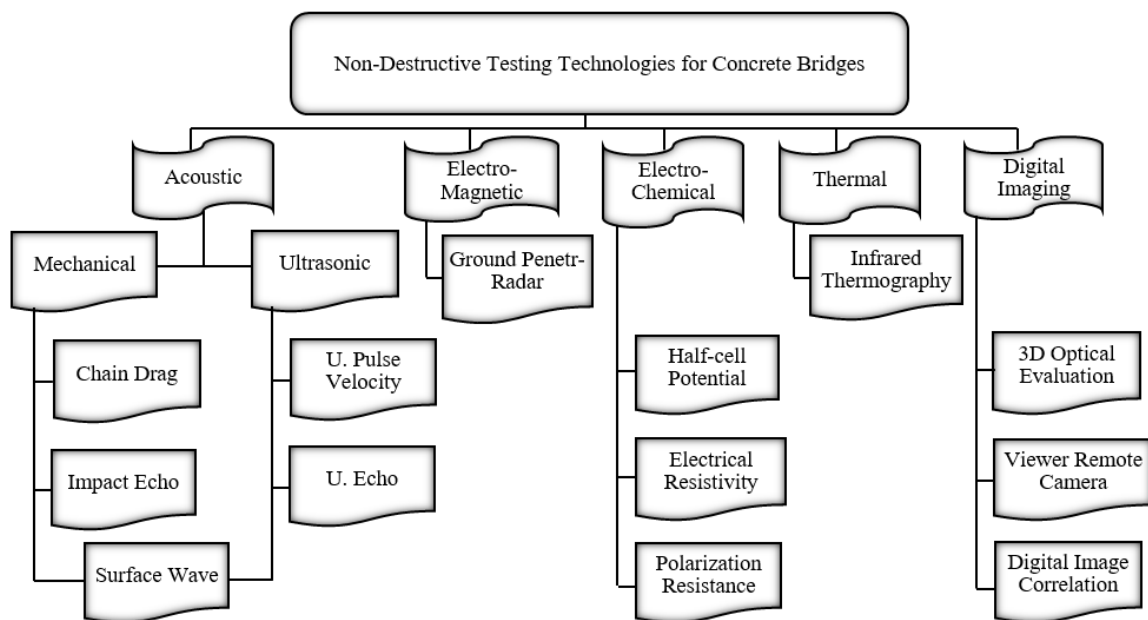


**Figure 2-5: Non-destructive testing techniques for reinforced concrete bridges.**

Among all bridge components, the performance of bridge decks was identified as the most important long-term bridge performance issue. Thus, to perform a practical review of the existing literature on the wide range of NDT techniques, this section will focus only on condition assessment of RC bridge decks.

#### 2.3.4.1 *Conventional NDT techniques*

A number of hand tools, including hammers, steel rods, and chains, have been widely used to detect subsurface anomalies (e.g. delamination, voids and cracks) in concrete bridge decks. Hammer sounding involves tapping the surface of a concrete member with a hammer at multiple locations, while chain dragging involves dragging a chain over the bridge deck surface. In both cases, the user listens to and interprets the distinctive sounds produced. A dull or hollow sound indicates delaminated concrete, and a distinct ringing sound designates non-delaminated concrete. The advantages of these methods include simplicity, portability and low operating cost. However, such techniques require hands-on access and can be labor-intensive and time-consuming for large areas of concrete, while being ineffective for detecting subsurface anomalies in decks having overlays. Traffic control must also be in place so that inspectors can safely access the concrete element. In addition, the interpretation of the sound produced is subject to the operator's judgment and experience. Likewise, initial or incipient delamination often produces oscillations outside the audible range. Hence, delaminations cannot be detected by such methods (Yehia *et al.*, 2007). These limitations have motivated the pursuit of advanced NDT techniques for more effective and reliable bridge inspection.

#### 2.3.4.2 *Advanced NDT Techniques*

A number of NDT techniques that exploit various physical phenomena (acoustic, seismic, electric, thermal, and electromagnetic, etc.), have been explored as a means of improving the reliability of BCA. Generally, such techniques utilize an approach where the objective is to learn about the characteristics of the medium from its response to an applied excitation (Gucunski *et al.*, 2013). For example, probability of active corrosion can be evaluated by half-cell potential (e.g. Pradhan and Bhattacharjee, 2009), electrical resistivity (e.g. Brown, 1980), and ground penetrating radar (e.g. Varnavina *et al.*, 2015), while the corrosion rate

can be identified by the polarization resistance method (e.g. Cady and Gannon, 1992). The presence of vertical cracks leads to a reduced modulus of elasticity of concrete, which can be captured using the ultrasonic surface wave method (e.g. Nazarian *et al.*, 1993). Delamination can be detected using impact echo (e.g. Kee *et al.*, 2012; Parisa *et al.*, 2013), pulse echo (e.g. Krause *et al.*, 2011); and infrared thermography tests (e.g. Washer *et al.*, 2009; Seong *et al.*, 2012). **Table 2-5** compares the advantages and limitations of the most relevant NDT techniques for evaluation of concrete bridge decks. The half-cell potential method will be presented in this section, and IRT and GPR techniques will be presented in Chapters 4 and 5, respectively. However, further details about the theoretical bases, instrumentations, applications, and data analysis of all NDT technologies are provided in a variety of sources such as the AASHTO Manual for Bridge Evaluation (2011), and a report by the American Concrete Institute (ACI 228.2R, 2013).

### ***Half-Cell Potential (HCP)***

Several researchers have applied Half-cell potential (HCP) to identify the potential of steel corrosion in concrete bridge decks. HCP testing is a probabilistic measurement indicating the probability of active corrosion. HCP measurements are conducted by electrically connecting a reference electrode to the steel reinforcement and measuring the potential voltage difference. The magnitude of the measured voltage indicates the corrosion activity. If the potential is more positive than -200 mV, the corrosion activity is highly unlikely at the time of the measurement. If the potential is more negative than -350 mV, there is a high likelihood of active corrosion. Corrosion activity is uncertain when the voltage is in the range of -200 to -350 mV. While the test is easy and inexpensive, it requires a moist concrete cover and uncoated steel bars. Its results could be affected by the concrete resistivity and cover thickness. It is to be noted that an increase in moisture and/or oxygen contents of concrete will cause a negative shift in potential voltage measurement. HCP results also vary with temperature and ion concentrations. Drilled concrete core specimens for chloride ion concentration analysis are usually retrieved from bridge decks being investigated using HCP. The accepted chloride threshold value necessary to de-passivate reinforcement steel and to allow the onset of rebar corrosion (in the presence of oxygen and moisture) is commonly taken as 0.025% by mass of concrete.

**Table 2-5: Common NDT methods used to evaluate concrete bridge decks**

<b>Technique</b>	<b>Physical Phenomena and Description</b>	<b>Applications</b>	<b>Advantages and Limitations</b>
Impact Echo (IE)	<ul style="list-style-type: none"> <li>• Mechanical or seismic stress wave method.</li> <li>• Short-duration stress pulse using mechanical impact.</li> <li>• Compression waves reflect at interfaces of different acoustic impedance.</li> <li>• Monitoring the frequency arrival of reflected waves at a nearby location.</li> </ul>	<ul style="list-style-type: none"> <li>• Detection of cracks and delamination.</li> <li>• Detection of overlay de-bonding.</li> <li>• Evaluate concrete elastic modulus.</li> </ul>	<ul style="list-style-type: none"> <li>• Provides good accuracy on depth and extent of defects.</li> <li>• Impact duration controls size of detected defect.</li> <li>• Less reliable in the presence of overlays.</li> <li>• Requires experienced operator &amp; analyzer.</li> </ul>
Ultrasonic Pulse Echo (UPE)	<ul style="list-style-type: none"> <li>• Ultrasonic stress wave method.</li> <li>• Transducer emits short pulse, high amplitude of ultrasonic waves.</li> <li>• Waves reflection at various acoustic impedance.</li> <li>• Measuring the transit time of the ultrasonic pulse.</li> </ul>	<ul style="list-style-type: none"> <li>• Detection of defects: delamination, cracks &amp; voids.</li> <li>• Deck thickness measurements.</li> <li>• Detection of overlay de-bonding.</li> </ul>	<ul style="list-style-type: none"> <li>• Provides information on the presence and depth of defect.</li> <li>• Time-consuming, less reliable in detecting shallow defects.</li> <li>• Attenuation of transmitted pulses has scattering effect.</li> </ul>
Half-Cell Potential (HCP)	<ul style="list-style-type: none"> <li>• Electrochemical reaction technique.</li> <li>• Measures potential voltage difference between steel reinforcement and standard reference electrode using a voltmeter.</li> </ul>	<ul style="list-style-type: none"> <li>• Identifies probability of active corrosion of steel reinforcement at the time of testing.</li> </ul>	<ul style="list-style-type: none"> <li>• Results affected by concrete resistivity, moisture content and cover thickness.</li> <li>• Cannot be used in presence of overlays or coated rebar.</li> </ul>
Ground Penetrating Radar (GPR)	<ul style="list-style-type: none"> <li>• Electromagnetic (EM) wave propagation method.</li> <li>• EM pulses are emitted via a transmitter antenna.</li> <li>• The higher the frequency of antenna, the better the resolution but the lower the depth of penetration.</li> <li>• Reflection at interface with different electric properties</li> </ul>	<ul style="list-style-type: none"> <li>• Evaluation of deck thickness and concrete cover.</li> <li>• Description of concrete as a corrosive environment</li> <li>• Locating steel reinforcement.</li> </ul>	<ul style="list-style-type: none"> <li>• Rapidly survey with 100% coverage.</li> <li>• Cost-effective method</li> <li>• Not good to detect delamination when no moisture is present.</li> <li>• Cannot provide information about corrosion rates or rebar section loss.</li> </ul>
Infrared Thermography (IRT)	<ul style="list-style-type: none"> <li>• Electromagnetic surface radiation in the IR region.</li> <li>• Utilizes the radiated heat energy to characterize subsurface conditions.</li> <li>• Anomalies interrupt heat transfer and result in surface temperature differentials.</li> </ul>	<ul style="list-style-type: none"> <li>• Detection of defects: delamination, cracks &amp; voids.</li> <li>• Detection of layers and overlay de-bonding.</li> </ul>	<ul style="list-style-type: none"> <li>• Remote sensing technique, allows real time visualization.</li> <li>• Rapid inspection with minimum traffic disruption.</li> <li>• Cost-effective method</li> <li>• Environmental dependence.</li> </ul>

#### 2.3.4.3 *NDT Using Remote Sensing Technologies*

Remote sensing (RS) is gaining popularity for evaluation of bridge condition. The commonly used RS technologies include 3D-optical bridge evaluation (3DOB), bridge viewer remote camera (BVRC), GigaPan, LIDAR, digital image correlation (DIC), and high resolution street view-style digital photography (Adhikari *et al.*, 2012). These technologies do not include emplaced sensors, such as strain gauges or temperature sensors, and can be defined as a form of stand-off SHM and a form of NDT where the device-gathering data are not in contact with the object (Vaghefi *et al.*, 2012). Abudayyeh *et al.* (2004) proposed a framework for automated bridge imaging system based on digital image processing. Their models were capable of storing different surface defects in a structured way and generated automated inspection reports. Ahlborn *et al.* (2012) applied different image technologies in assessing the condition of concrete bridge decks and reported that the 3DOB or BVCR techniques based on close range 3D photogrammetry and the GigaPan technique based on street view-style photography are the best technologies for defect measurement for bridge inspections. The DIC technology uses mathematical algorithms to extract displacement information from a series of photographs and can be used to calculate load rating of BCA throughout the service life of the bridge (Sanayei *et al.*, 2012). Hinzen (2013) demonstrated the feasibility of damage detection and quantification based on Google street view images. However, these technologies should be integrated for complete BCA.

#### 2.3.4.4 *NDT Application Approaches*

NDT methods can be applied alone to evaluate certain defects, or can be combined to cover a wider range of testing capabilities in a complementary manner. Although single NDT approaches have their own merits, there is no single NDT technology that is capable of identifying all of the complex deterioration phenomena that can affect a bridge. Many structural problems will be best studied by a particular NDT method, depending upon which physical properties of the construction materials offer the best scheme of reliable defect detection. However, results of BCA from different NDT techniques do not necessarily agree due to the uncertainty associated in data resulting from these techniques (Yehia *et al.*, 2007; Huston *et al.*, 2011). Therefore, due to the composite nature of concrete

and the many causes of deterioration, a diverse set of NDT technologies could be employed for a more complete conception of a bridge condition. Many case studies exist in which different techniques have been combined. **Table 2-6** illustrates some studies that adopted the NDT combination approach and the objective of these studies. For example, the Federal Highway Administration (FHWA) has recently developed the “RABIT” bridge deck assessment device. RABIT (Robotics Assisted Bridge Inspection Tool) is a fully autonomous robotic system for the condition assessment of concrete bridge decks using the results of multi-model NDT, which utilizes the electrical resistivity, impact echo, ultrasonic surface waves, and ground penetrating radar technologies. The robot’s data visualization platform facilitates an intuitive 3-D presentation of three deterioration types (rebar corrosion, delamination, and concrete degradation) and deck surface features (Gucunski *et al.*, 2015). Pailes (2014) developed a multi-NDT BCA model for concrete bridge decks. He identified the correlations between the utilized methods and developed a statistics-based approach to threshold identification for the utilized methods, which were fused and converted into a deterioration based BCA that identifies locations of active corrosion, delamination, and cracking. Results from multi-NDT surveys indicate a high potential to develop more realistic deterioration models for bridges.

**Table 2-6: Studies utilized combined NDT techniques approach to evaluate bridges**

Techniques Utilized	Objective of the Study	Reference	Year
• IRT, GPR.	• Delamination.	• Alt and Meggers	• 1996
• GPR, Chain Drag, HCP.	• Damage Detection.	• Barnes & Trottier	• 2000
• IE, GPR, Chain Drag.	• Comparative Study.	• Scott et al.	• 2003
• IRT, Chain Drag.	• Delamination.	• Clark et al.	• 2003
• GPR, IE, Dynamic Response.	• Damage Detection.	• Yong and Kee	• 2003
• GPR, UE, Hammer Sounding.	• Comparative Study.	• Wood and Rens	• 2006
• IE, GPR, IRT.	• Comparative Study.	• Yehia et al.	• 2007
• IE, UE.	• Measuring Thickness.	• Algernon et al.	• 2011
• UE, GPR, IRT, HCP.	• Comparative Study.	• Arndt et al.	• 2010
• IE, IRT, Chain Drag.	• Damage Detection.	• Oh et al.	• 2013
• IE, GPR, HCP, IRT, Ultrasonic Surface Waves, Electrical Resistivity, Pulse Echo, Impulse Response.	• Comparative Study.	• Gucunski et al.	• 2013

### 2.3.5 Finite Element Modelling

Another tool that is available for BCA is structural modelling. Finite-element modelling (FEM) is a widely used method for the RC BCA. Research has shown that traditional methods of assessing bridge health are conservative in some cases and that a calibrated bridge FEM can provide a more accurate portrayal of bridge response and structural condition. The construction process, erection methods, material properties, geometric accuracy, and environmental conditions are key factors in the development of robust FE models (Sousa *et al.*, 2014). For instance, Xia *et al.* (2005) developed a FEM for the quantitative condition assessment of a damaged RC bridge deck, including damage location and extent, residual stiffness evaluation, and load-carrying capacity assessment. The model was validated based on dynamically measured data from the undamaged and damaged decks. The damage location and quantification of the damaged deck were then identified, leading to residual stiffness and load-carrying capacity assessment. Wang *et al.* (2011) developed a FEM to assist the design of load tests and the interpretation of their results. The actual bridge test results, in turn, were used to validate the FE analysis. The measured bridge deflections were found in good agreement with those computed by FE analysis. Alani *et al.* (2013) proposed an integrated bridge health mechanism where a FEM was developed using data from visual inspections and calibrated using NDT survey results.

Bell *et al.* (2012) developed a FEM to calculate the load rating and predict the bridge structural performance, which was calibrated via the digital image correlation technique utilized to measure bridge displacements. The system identifies the portion of the bridge that had undergone the greatest amount of deterioration. Ghodoosi *et al.* (2015) evaluated the system reliability of concrete bridges using a FEM and found that the estimated element-level structural conditions degrade faster once corrosion is initiated. FEM can also be used to evaluate the reliability of bridges that use nonconventional materials or structural forms. For example, Ghodoosi *et al.* (2014) developed a FE BCA model for a restrained bridge deck system and calibrated the model with experimental results of static deflection, vibration characteristics, load distribution, and crack patterns. Sousa *et al.* (2014) utilized FEM to assess the long-term performance of concrete bridges and suggested that data collected using permanently installed monitoring systems is the most reliable strategy to

improve such assessments. Subsequently, an integrated framework consisting of both FE modelling and structural monitoring can assist informed decisions.

### 2.3.6 Advantages and Limitations

The advantages and limitations of the commonly used BCA approaches, presented herein, are summarized in **Table 2-7**. Generally, VI, the main tool for evaluating bridge condition, suffers from limitations such as the required time of inspection, the assessment subjectivity, a number of safety risks associated with field inspections, and the need for a clear line of sight. This could affect the efficiency of decision-making and resource allocation. NDT technology can enhance accuracy and yield more efficient BCA. Simultaneously deploying multiple NDT technologies enables accurate detection and characterization of deterioration and provides a better understanding of bridge conditions. This approach also makes the assessment of a large population of bridges feasible. However, the practitioner must deal with substantially larger and more complex data, understand how to properly fuse and interpret the data fusion. Automated data collection and analysis using multiple NDT methods integrated into robotic systems can overcome those obstacles. Integrated remote sensing technologies are also gaining popularity as they provide higher evaluation details.

SHM is becoming common in bridge monitoring. For instance, using wireless SHM to monitor the progression of deficiencies identified during a VI allows for continuous monitoring of identified defects, while maintaining a safe use of the bridge. Yet, SHM systems have some limitations which can hinder their adoption as part of BMSs. These include system complexity, which relies on the desired functionality characteristics, system maintenance to sustain long-term operation, and the requirement of automated data analysis to locate potential damages. However, the use of compressed sensing can simultaneously reduce data sampling rates, on-board storage requirements, and communication data payloads. Using traffic-induced vibration response data has several practical advantages: (i) it does not interrupt traffic; (ii) captures in-situ dynamic behaviour of the bridge undergoing in its normal service; (iii) can be performed continuously, scheduled periodically, or triggered automatically; and (iv) requires no special experimental arrangements. It should be noted that data collected using either NDT or SHM systems is the most reliable strategy to improve and update bridge FEM assessment.

**Table 2-7: Comparison of condition assessment techniques for RC bridges**

Technique	Description, Advantages and Limitations
Visual Inspection (VI)	<p><b>Description:</b> trained engineers recognize, register, and evaluate the physical condition of different bridge elements using inspection manuals and defined codes. The primary and most common interval for inspections is 24 months.</p> <p><b>Advantages:</b> the most cost-effective means for bridge condition evaluation. BMSs rely primarily on VI to record bridge component condition ratings, which are quantified and standardized through a priority-ranking procedure.</p> <p><b>Limitations:</b> subjective evaluation; results greatly depend on the qualifications of those conducting inspections; the findings may not be identical. Consider only the observed physical health of the bridge and cannot detect the hidden defects.</p>
Load Testing (LT)	<p><b>Description:</b> determine the actual load the bridge can carry without distress (load carrying capacity). Condition ratings can be determined by allowable stress, load factor, or load and resistance factor methods.</p> <p><b>Advantages:</b> safe conservative analysis methods. The governing rating is the lesser of the shear capacity of the critical bridge component. Development and updating the load rating software is undertaken by AASHTO.</p> <p><b>Limitations:</b> costly and time consuming. The three rating methods may lead to differently rated capacities and posting limits for the same bridge. No guidance as to which method should be used for specific circumstances.</p>
Structure Health Monitoring (SHM)	<p><b>Description:</b> encompasses a range of methods and practices designed to capture structural response, detect anomalous behaviour, and to assess the bridge condition based on a combination of measurement, modelling and analysis.</p> <p><b>Advantages:</b> reliable and potentially real-time bridge assessment. More meaningful than using load response data. Can be deployed for short-term and long-term assessment. Appropriate for movable bridges than any other method.</p> <p><b>Limitations:</b> wireless sensors rely on battery power. The size and complexity of the bridge could result in complex systems. SHM systems often create liability issues. Require routine, on-site maintenance to sustain long-term operation.</p>
Non-Destructive Testing (NDT)	<p><b>Description:</b> a number of techniques introduced exploit various physical phenomena (acoustic, seismic, electric, electromagnetic, and thermal, etc.) to detect and characterize deterioration processes without damaging the elements.</p> <p><b>Advantages:</b> provide effective, and accurate condition assessment. Objectify the inspection process and make it faster and more reliable. Integration of different techniques is the best approach to identify several different damage states.</p> <p><b>Limitations:</b> applying only one technology provides limited information about the bridge condition. No single technology is capable of identifying all of the deterioration defects. Require trained personnel for data collection and analysis.</p>
Finite Element Modelling (FEM)	<p><b>Description:</b> numerical analysis to investigate the behaviour and response of a bridge structural system. Usually updated or calibrated using results of field inspection supported by NDT or by static and/or dynamic tests on the structure.</p> <p><b>Advantages:</b> allows detailed visualization, can be created using data from visual inspection and then parameterised and calibrated using information from NDT and SHM results. FEMs can satisfactorily capture short-term performance.</p> <p><b>Limitations:</b> FE models typically require calibration. Long-term assessment is a challenge due to advances in structural materials and construction methods.</p>

## 2.4 Bridge Deterioration Prediction Tools

A deterioration prediction model is a link between a measure of existing bridge conditions and a vector of explanatory variables that represent the factors affecting bridge deterioration (Black *et al.*, 2005). Accurate prediction of the deterioration rate is crucial to the success of any BMS. Deterioration models can be categorized according to different mechanisms. For example: (i) linear or nonlinear, (ii) deterministic or stochastic, (iii) aggregate or disaggregate, and (iv) mechanistic or empirical models. Several deterministic, stochastic, and mechanistic models are widely used for predicting the macro and micro responses of bridge components but the degree of efficiency of these models is a matter of debate. These models and their techniques are summarized in **Fig. 2-6**. Each category suffers from some limitations and is briefly discussed in this section.

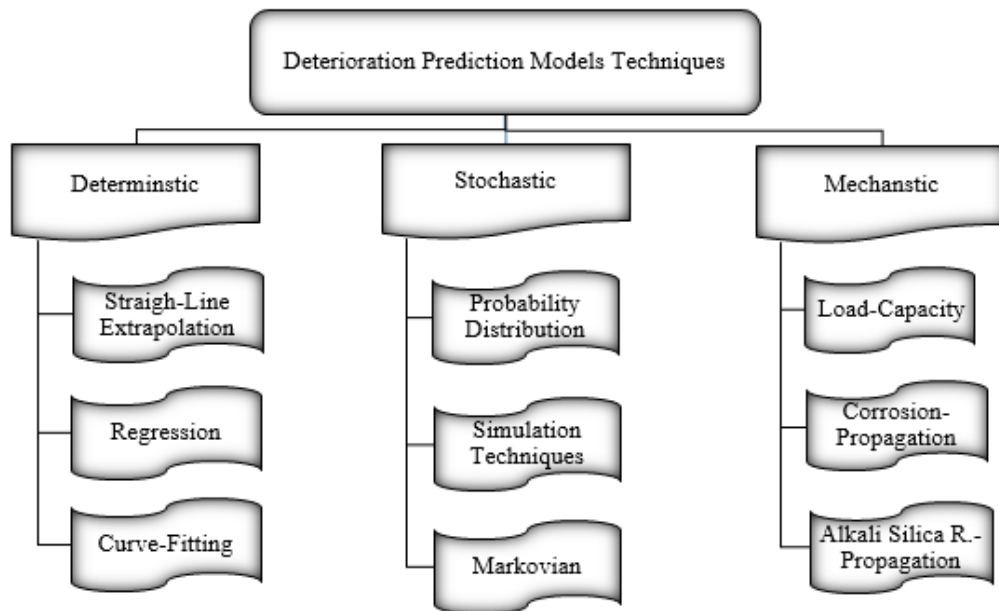


**Figure 2-6: Deterioration prediction models techniques.**

### 2.4.1 Deterministic Models

Deterministic models use a single defined value to describe bridge elements' conditions at a certain given time. They utilize historical data to estimate the deterioration rate using the available statistical techniques. Accordingly, the models can be categorized as straight-line

extrapolation, regression and curve-fitting models. For instance, straight-line extrapolation models can be used to predict the material condition rating of a bridge given the assumption that traffic loading and maintenance history follow a straight line. The models require an initial condition that can be assumed at the time of construction and only one condition measurement after construction at the time of the inspection. Although these models are accurate enough for predicting short-term conditions, they are not appropriate for conditions at long periods of time. They also cannot predict the rate of deterioration of a bridge that has undergone some repair. Regression models depend on developing an empirical relationship between two or more variables that affect the bridge condition: one dependent variable and one or more independent variables. Several forms of regression models are presented in the literature, including linear and non-linear regression. Linear regression models do not provide sufficient accuracy and may underestimate or overestimate the bridge condition at a specific time while the non-linear regression models provide more adequate prediction accuracy (Morcous *et al.*, 2010). Curve-fitting techniques are mathematical methods that depend on constructing a polynomial that best fits bridge condition data. A third order polynomial curve, based on the relationship of bridge component condition rating versus age, was found as an accurate prediction model for several concrete bridges (Elbehairy *et al.*, 2006).

#### **2.4.2 Stochastic Models**

The deterioration process has a stochastic rather than a deterministic nature since several complex mechanisms characterize the variability of a deteriorated element. The use of stochastic models has contributed significantly to the field of modeling bridge deterioration due to the high uncertainty and randomness involved in the deterioration process. Generally, stochastic models can be categorized into probability distribution, simulation and Markov chains models (Morcous *et al.*, 2010). A probability distribution describes the probabilities associated with all values of a random variable. For example, if the random variable is the condition rating of an element in a bridge, then the probabilities associated with all of its values are described by a probability distribution function rather than a deterministic value. The use of probability distribution requires knowledge of the distribution for the variables being predicted, which limits the use of this technique for

individual distress prediction (Abu Dabous *et al.*, 2008). An effective way to deal with uncertainties is through simulation, which can provide more accurate estimates using a large number of “what if” scenarios. The Monte Carlo simulation method takes both sensitivity and input variable probability distribution into consideration and has been widely utilized in concrete bridge deterioration models. The deterioration can be simulated if enough statistics on the transition times required for an element to change its condition are available. The output of the simulation is a probabilistic deterioration profile in terms of the time taken to change from one condition rating to another.

### ***Markovian Models***

A stochastic process is generally defined as the process in which the past behaviour influences the future ones. A Markov process is a conditional stochastic process where the transition probability from a given behaviour to a future behaviour is dependent only on the present behaviour and not on the manner in which the current behaviour was reached (Elbehairy *et al.*, 2006). This assumption was made for simplicity and to facilitate computations but not supported by mechanistic knowledge of material behaviours (Abu Dabous *et al.*, 2008). The Markovian models are the most common example of state-based probabilistic deterioration models and have been employed in many advanced BMSs such as Pontis, and OBMS. State-based probabilistic deterioration models are those used to predict the probability distribution of transition states from one condition to another over multiple discrete time intervals. The Markovian model takes advantage of the discrete condition states identified for inspections, to provide a simple way of describing the likelihood of each possible change in condition at evenly-spaced intervals.

The main challenge in Markovian models is the derivation of the transition probabilities. Several methods have been adopted to estimate the transition probabilities, such as percentage prediction method, expected-value method, ordered probit model, and regression-based optimization methods. Those methods can be used when a statistically significant number of consistent and complete sets of condition data are available, otherwise the Monte Carlo method or expert judgment elicitation procedure may be applied (Black *et al.*, 2005). More improved and realistic models have been recently developed to account for the effect of the time spent between the states on the transition probabilities

(e.g., Semi-Markov, Weibull Survival models, and Hybrid Markov-Weibull models) and to relax the state independence assumption by accounting for the past condition among other explanatory variables (Black *et al.*, 2005). The Bayesian belief network (BBN) models also offer a compact representation of a joint probability distribution, together with a rigorous formalism for the construction of models relying on probabilistic knowledge. The Bayesian procedure has great advantages that cover problems of insufficient data and difficulty in estimating model parameters but it demands careful considerations for the convergence process (Nasrollahi and Washer, 2014). If condition ratings are unavailable, the backwards prediction models (BPM) can produce an estimated rating for the unavailable components or data and use time delay analysis to predict the condition ratings of future components.

### 2.4.3 Mechanistic Models

Mechanistic models describe the specific deterioration mechanisms of particular bridge components where deterioration is described by quantitative performance indicators through knowledge of the physical and chemical processes involved in the deterioration process (Lu and Liu, 2010). Modeling of bridge load-capacity, chloride-induced corrosion, and alkali-silica reaction (ASR) are some examples of research efforts towards the use of mechanistic deterioration models. For instance, Wang *et al.* (2011) used load-carrying capacity to predict bridge deterioration. Ian *et al.* (2015) modeled the deformation of concrete bridges due to the effects of ASR, creep, and shrinkage. Lu and Liu (2010) developed an analytical model that describes the mechanism of damage initiation and accumulation to predict corrosion-induced cracking, spalling, and delamination of reinforced concrete decks and performed numerical simulations, using a FEM, of the condition evolution for different values of model parameters. Morcouc *et al.* (2010) utilized Monte Carlo simulation to generate the probability density function of the time to corrosion initiation and to capture the stochastic nature of the deterioration process. Tarighat and Miyamoto (2010) considered the spatial variability of the deterioration parameters across the bridge components (the materials and geometrical properties) and developed a deterioration model of concrete bridges exposed to corrosion. Shafei *et al.* (2014) calculated the corrosion initiation time through a detailed computational model considering

the most influential parameters, including ambient temperature, relative humidity, chloride binding capacity, and exposure conditions. They also provided a detailed mechanical model that considers the effects of corrosion on decreasing the cross-sectional area of steel, yield strength of steel and the loss of the concrete cover.

#### 2.4.4 Advantages and Limitations

The advantages and limitations of the deterioration prediction models are summarized in **Table 2-8**. Deterministic models are the simplest models where the deterioration rate of one element is generalized to all similar elements. The main limitations of these models are the failing to consider uncertainty and ignoring the effect of unobserved variables and hence, the inherent stochastic nature of demands. The complexity and interaction of the several deterioration mechanisms make it unrealistic to model the deterioration process using a deterministic approach. Several advantages for stochastic models include: (1) represent uncertainty in initial condition, assessment errors and deterioration process, (2) provide an unbiased estimate of needs within any time frame, and (3) do not require long time-series of data. However, they still suffer from several limitations: (1) future deterioration depends only on the current or preceding condition state and does not relate to the historical condition of a bridge or any other attribute (e.g. maintenance) of the bridge elements, (2) assume discrete transition time intervals, a constant bridge population, and stationary transition probabilities, and (3) transition probabilities are estimated in terms of subjective engineering judgement and require frequent updating.

Mechanistic models embrace a reliability-based approach and focus on relevant failure modes of the bridge in determining the reliability of the bridge over time. These models are promising because they relate the qualitative measurement of the condition state to the quantitative physical parameters of the bridge such as material properties, stress conditions, structural behaviors, which are critical data for assessing the structural capacity of the bridge. Although, these models have the ability to predict the deterioration with high accuracy and efficiency, none of the transportation agencies incorporate them in their BMSs as it is difficult to consider the various variables affecting the deterioration process. Another key limitation to this approach is the associated cost to perform detailed condition survey, using NDT techniques, for the network level analysis.

**Table 2-8: Comparison of deterioration model techniques for concrete bridges**

Technique	Description	Advantages & Limitations	
		Advantages	Limitations
Deterministic Models	Use a single condition value of an element at a certain given time. Use historical data to estimate the element deterioration rate.	Simple and easy to understand and develop. Require only one condition rating after construction.	Assume that the environment, structure system, and material properties exhibit the same behaviour. Not accurate for long-term prediction.
Stochastic Models	Consider discrete condition states for inspections. Describe the probabilities of all variables by a probability distribution function.	Consider the inherent uncertainty involved in the deterioration process. Can predict condition within any time frame. Require two inspection cycles.	Condition distribution is independent of the past conditions or any other attribute. Assume discrete transition time intervals. Subjective transition probabilities.
Mechanistic Models	Use quantitative performance indicators through detailed condition surveys and analytical assessments.	Can accurately predict the initiation, propagation, and failure induced by different damage mechanisms.	Difficult to develop when multiple types of deterioration processes are to be modeled together. Costly for data collection, analysis, and modeling.

## 2.5 Bridge Condition Assessment and Artificial Intelligence

Research in artificial intelligence (AI) has focused on using soft computing methods that permit the creation of evaluation and prediction models based on processes found in nature, such as the brain, or natural selection (Flintsch *et al.*, 2004). In comparison with hard computing, which is based on precise, definite, and rigorous data; soft computing techniques allow for imprecise, uncertain, incomplete and subjective data. Because this often describes bridge inventories and condition information, considerable research has been dedicated to using AI techniques in bridge management. Artificial Neural Networks (ANNs), Fuzzy Set Theory (FST), and Evidential Reasoning (ER) are the most common models utilized in evaluating bridge condition and are briefly discussed subsequently.

### 2.5.1 Artificial Neural Networks

Neural networks are based on the principle that a highly interconnected system of simple processing elements can learn complex interrelationships between independent and dependent variables. ANN model is a parallel distributed processing system consisting of

an input layer, an output layer, and hidden layers connected by neurons. Each neuron is a processing element that receives one or more inputs and produces an output, or value, through a transfer function (activation function), which is passed on to the next neuron to determine a final output (Wang and Elhag, 2008). There are several ANN software, which have different scale options. For instance, the Matlab Neural Network toolbox can be used to develop multilayer perceptron ANN models (Lee *et al.*, 2015). **Figure 2-7** illustrates an ANN structure consisting of an input layer, an output layer and hidden layers.

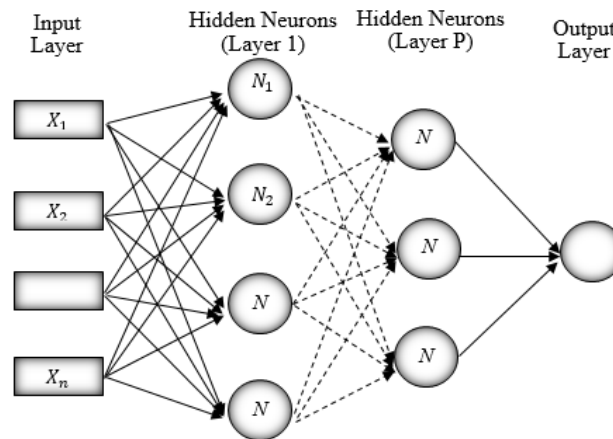


**Figure 2-7: Structure of an artificial neural network.**

Sobanjo (1997) investigated using ANNs in modelling bridge deterioration where a multi-layer ANN was utilized to relate the age of a bridge superstructure to its condition rating. The model yielded 79% of the predicted values matching the actual values with a 15% prediction error. Tokdemir *et al.* (2000) developed a more elaborate model that incorporated additional factors such as highway class, design type, material type, and traffic volume to predict a bridge sufficiency index. The ANN model resulted in 62.5% correct solutions on average percentage with a prediction error of 3%. Huang (2010) developed an ANN condition assessment model for concrete bridges based on statistical analysis of the significant factors affecting the deterioration process. For example, the maintenance history, age of the bridge, previous condition, district where bridge is located, design load, bridge length, average daily traffic, environmental exposure, number of spans, and degree of skew were used as input neurons.

Li and Wang (2011) compared several ANN methods to predict bridge condition ratings based on physical and operational bridge parameters and produced related deterioration curves. Emily (2011) developed two types of ANN, multi-layer perceptrons (MLPs) and ensembles of neural networks (ENNs), to predict the condition ratings of concrete bridge decks using historical condition assessments chronicled in the NBI database. It was reported that ANNs can produce correct responses even in the presence of noise or uncertainty in the training data, and can predict the outcome of complex deteriorations or those with a high degree of nonlinear behaviour. Lee *et al.* (2012) proposed an ANN model for bridge deterioration where a backwards prediction model (BPM) was used to fill in gaps in historical data. The model subsequently uses time delay neural network modelling, similar to the ANN model proposed by Huang (2010) to predict future condition ratings. An advanced integrated model was further developed by Lee *et al.* (2015) that incorporates a time-based model, a state-based model with the Elman neural network and a BPM to predict long-term bridge performance where similar bridge components are grouped together, thereby identifying the common deterioration patterns, achieving 75.4% accuracy with 4% prediction error.

### 2.5.2 Fuzzy Set Theory

To deal with vagueness and uncertainty in modelling bridge condition, probabilistic techniques are usually used, among which the Monte Carlo simulation is the most popular. However, such methods are complex requiring large amounts of data (Kishk and Al-Hajj, 2002). Ross (2010) reported that the deterioration mechanisms and surrounding aggressive environment of concrete cannot be simply identified by separate factors. Fuzzy sets, based on the fuzzy set theory that was first introduced by Zadeh (1965), are developed for handling uncertainties associated with vague, imprecise, qualitative, linguistic, or incomplete data that play an important role in the case of evaluation and predication of bridge conditions (Sasmal *et al.*, 2009).

The vague data are generally represented by fuzzy numbers or fuzzy sets, which can be processed using mathematical operations according to analysis requirements in a fuzzy domain. The main components of building a fuzzy system include: (1) fuzzification: converting input data into partial degrees of one or more membership functions of fuzzy

subsets, (2) inference: computing the true value for the premise of each fuzzy rule and applying it to the conclusion part of each rule, (3) composition: assigning the fuzzy subsets to each output variable and combining them to form a single fuzzy subset for each output variable, and (4) defuzzification: converting the fuzzy output set to a crisp number. Techniques for constructing fuzzy membership functions include pairwise comparison, clustering, direct or reverse rating, polling, neural networks, relative preference, and statistical regression. However, there is no single method that can work for all applications (Sasmal *et al.*, 2009). **Figure 2-8** illustrates the basic configuration of a fuzzy system.

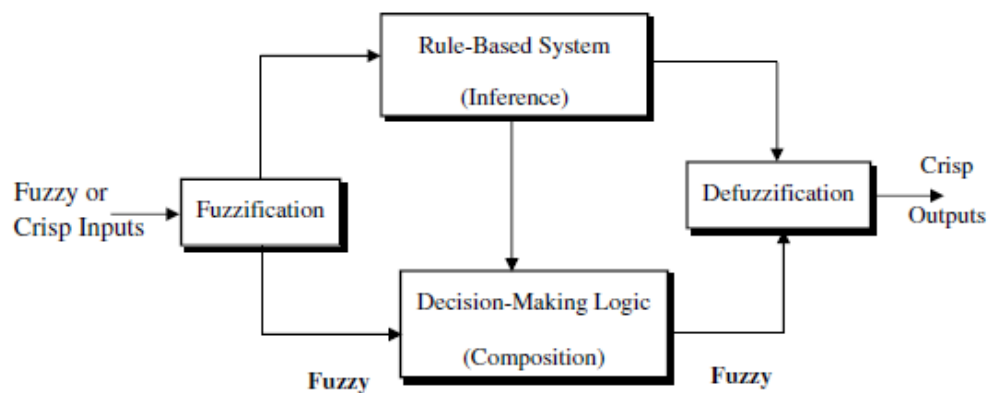


**Figure 2-8: Basic configuration of fuzzy system with fuzzifier and defuzzifier**  
(Senouci *et al.*, 2014, with permission from ASCE).

Extensive studies have been carried out to evaluate the condition of different bridge components using FST as a potential substitute for probabilistic models (Tee *et al.*, 1988; Liang *et al.*, 2002; Sasmal *et al.*, 2009; Tarighat and Miyamoto, 2010; Chen and Fan, 2011; Li and Wang, 2011; Hasan *et al.*, 2013; Moufti *et al.*, 2014). For example, Tee *et al.* (1988) presented a bridge condition assessment model based on resolution identity of fuzzy sets. They presented algorithms for fuzzy weighted average computation. Many bridge condition rating methodologies have since adopted this approach. For instance, Liang *et al.* (2002) used fuzzy mathematics and proposed regression models for predicting the remaining service life of concrete bridges. Sasmal *et al.* (2009) developed a procedure for condition assessment and rating of concrete bridges using fuzzy mathematics where the entire bridge was divided into three major components: deck, superstructure, and

substructure. Each of which is further subdivided into a number of elements, while the defuzzified value of the resultant rating fuzzy set becomes the rating value for the bridge as a whole. Moufti *et al.* (2014) proposed a fuzzy based framework through a detailed bridge condition assessment incorporating a weighted set of possible bridge defects. Li and Wang (2011) developed a fuzzy model to predict the condition rating of concrete bridges where ANN with back-propagation algorithm was applied. The results indicated that the model improved the performance of the knowledge representation system based on enhanced fuzzy inference rules.

### 2.5.3 Evidential Reasoning

Uncertainties can be classified into two main classes: ignorance (incompleteness) and fuzziness (vagueness). The ER approach is characterised by a distributed modelling framework capable of modelling ignorance, whilst fuzziness can be well treated using the fuzzy set theory. The ER approach deals with a wide range of decision problems having precise data, random numbers and subjective judgments with probabilistic uncertainty in a way that is rational, transparent, reliable, systematic and consistent (Yang *et al.*, 2006). The ER approach applies the evidence combination rule of the theory of evidence (D-S), (Dempster, 1967; Shafer, 1976). The theory has the ability of combining pairs of bodies of evidence or belief functions to derive a combining evidence or belief function (Deng *et al.*, 2014). The ER approach for bridge assessment consists of five main parts: (1) identification of bridge condition assessment factors, (2) determination of weights and assessment grades for each factor, (3) distributed modeling framework for the assessment factors, (4) recursive or analytical ER algorithm for aggregating multiple assessment factors, and (5) utility interval based ER ranking, which is required to prioritize bridges in terms of their overall condition assessments (Wang and Elhag, 2008).

ER has been recently used by several researchers to assess and predict bridge condition rating (e.g. Wang and Elhag, 2008; Bolar *et al.*, 2013; Deng *et al.*, 2014; Moufti *et al.*, 2014). For example, Bolar *et al.* (2013) proposed a bridge condition assessment using the hierarchical ER methodology to model the uncertainties inherent in bridge evaluation where bridge data are classified in their respective order of importance into primary, secondary, tertiary and life safety-critical elements to capture both structural importance

and data reliability. The data were combined using D-S evidence theory to obtain respective condition indices and finally grouped to predict the overall bridge condition index. Moufti *et al.* (2014) proposed a fuzzy hierarchical ER approach for condition assessment of concrete bridges under uncertainty based on a multi-level evaluation and aggregation of the detected bridge defect measurement. Deng *et al.* (2014) developed hierarchical ER model for bridge condition assessment, which can handle incomplete basic probability assignment expressing the uncertainty of judgement in the process of assessment. The model extends the D-S evidence theory where the uncertain information was represented and called D-numbers, based on reasonable removal for some of the hypotheses of D-S theory. It is to be noted that the combination of the belief structure generated by the D-S theory and the fuzzy modeling by the fuzzy set theory would be able to handle both fuzzy uncertainty and ignorance concepts.

#### 2.5.4 Advantages and Limitations

The merits and demerits of ANN, FST, and the ER approaches are summarized in **Table 2-9**. The ANN models can learn from existing data and gather knowledge, and perform complex activities. However, ANN have some drawbacks: (i) the individual relations between the input variables and the output variables are not developed by engineering judgment or based on analytical basis; (ii) the conversion to numbers may lead to the loss of information that was contained in the original representation; and (iii) ANNs work well when the input and output variables are numerical values. Fuzzy logic is a means for modelling the uncertainty involved in describing an event/result and is organized as a powerful modelling technique designed to handle natural language and approximate reasoning. Fuzzifying uncertain variables in bridge evaluation has the benefits of enhancing the ability to model real bridge deterioration problems. It is also easier to define fuzzy variables than random variables when no information or limited information is available. Furthermore, mathematical concepts and operations within the framework of the fuzzy set theory are much simpler than those within the probability theory and can easily be updated with new data or modified to accommodate future findings. ER is capable of aggregating both numerical input and qualitative data with uncertainty as evidences towards a comprehensive BCA. The (D-S) evidence theory has an advantage of directly

expressing “uncertainty” by assigning probability that is limited by a lower and an upper bound, which, respectively, measures the total belief for the objects. ER has produced promising results, and thus needs concerted research efforts.

**Table 2-9: Comparison of AI techniques for concrete bridges evaluation**

Technique	Description, Advantages and Limitations
Artificial Neural Networks (ANNs)	<p><b>Description:</b> ANNs are based on: a highly interconnected system of processing elements (neurons); can learn interrelationships between independent and dependent variables. Each neuron receives multiple inputs through weighted connections from previous neurons, performs computations, and transmits the output to other neurons.</p> <p><b>Advantages:</b> can satisfactorily predict nonlinear behaviour even in the presence of uncertainty in the training data. No requirement of predetermining the relationships between inputs and outputs. High capability of self-learning and self-updating. Using optimization algorithms in the learning process reduces error.</p> <p><b>Limitations:</b> relations between the input variables and the output variables are not based on analytical basis. Conversion of input data to numbers may lead to loss of information that was contained in the original representation. Needs training process, which is time consuming and requires large amounts of data.</p>
Fuzzy Set Theory (FST)	<p><b>Description:</b> FST can model vague linguistic variables using the concept of partial membership and approximate reasoning. Involves three steps: fuzzification, aggregation, and defuzzification. Fuzzy sets are processed according to analysis requirements.</p> <p><b>Advantages:</b> most appropriate where human judgment, perception, or decision making are inextricably involved. It is easier to define fuzzy variables than random variables when no information or limited information is available. Allows applying mathematical operations and programming to the fuzzy domain.</p> <p><b>Limitations:</b> cannot provide a full description of the overall assessment of a bridge structure. Triangular fuzzy membership functions give a single value as a full membership function, for each linguistic input variable. A fuzzy set must be adjusted using the normalization operation.</p>
Evidential Reasoning (ER)	<p><b>Description:</b> established on the basis of Dempster-Shafer (D-S) theory of evidence. Assign belief/credibility to the evaluation of the various assessment attributes. Aggregate the multiple attributes based on the distributed assessment and the evidence combination rule.</p> <p><b>Advantages:</b> ER is able to combine both numerical input and qualitative data with uncertainty such as incomplete information, and total ignorance. The final overall assessment of a bridge is a distributed assessment, which offers a panorama of a bridge condition. Can deal with both probabilistic and fuzzy uncertainties.</p> <p><b>Limitations:</b> requires careful identification of all bridge assessment factors. Different sets of assessment grades for bridge elements need to be unified before the implementation of the ER algorithm. Applicable only for bridge condition assessment, not for the prediction of bridge condition ratings.</p>

## 2.6 Challenges Requiring Further Research

The present review highlights some tangible findings including: (1) the existing measurement methods for bridge displacement failed to realize long-term and real-time dynamic monitoring of bridge structures, essentially because of their low degree of automation and insufficient precision (Zhao *et al.*, 2105); (2) there are discrepancies among the different load rating methods where the reasons for these differences should be addressed (Wang *et al.*, 2011); (3) although NDT and SHM systems have become the most effective and significant aids for managing bridge infrastructure, there are a limited number of studies that address uncertainty in their measurements based on quantifiable data (Hesse *et al.*, 2015); (4) further work should be undertaken to demonstrate the accuracy of maturing and emerging sensors for use on SHM of bridge structures (Webb *et al.*, 2015); (5) at present, NDT methods, such as impact echo, radar, ultrasonic, resistivity and infrared are being commonly used for quantitative evaluation of bridge condition to augment visual inspection data (Gucunski *et al.*, 2015); (6) most current research efforts aimed at verifying the capability of integrating NDT techniques to have objective condition assessment systems and determine bridge elements or components condition based on their resilience (Pailes, 2014); (7) the Markovian and regression models have restrictive assumptions implicit in their respective formulations; and (8) AI models can provide more reliable BCA models, but require large bridge information input, while BMS software so far only has very limited NDT and SHM results (Lee *et al.*, 2015).

Bridge engineering is rapidly evolving and much work is ongoing in the specific matter of bridge assessment. **Figure 2-9** illustrates the developed conceptual framework to identify challenges that require further concerted research efforts and development. The prospects for improvement was identified as follows: (1) defining solid criteria for the assessment of general bridge condition based on visual inspection; (2) advancing the use of NDT and SHM in mainstream bridge engineering; (3) developing various fully automated data collection systems based on integrated NDT techniques; (4) developing advanced and simplified data analysis and interpretation; (5) integrating of diverse monitoring systems; (6) developing innovative software for integrating SHM/NDT data and aiding in its interpretation; (7) developing correlations between the bridge damage and internal

deterioration processes; (8) documenting the cost-benefit of the latest applied techniques and augmenting their future study; (9) considering the structural robustness and redundancy concepts in the bridge assessment process; and (10) focusing future research studies on most relevant problems. Indeed, fully automated data collection and interpretation analysis are the primary requirements to improve current BMSs. These will provide rapid and accurate BCA and enable monitoring of deterioration progression through periodical surveys and thus, allow the surveys of hundreds of bridges to become feasible. Consequently, this should yield tremendous reduction in costs associated with the application of NDT technologies and in the frequency and duration of traffic interruptions.

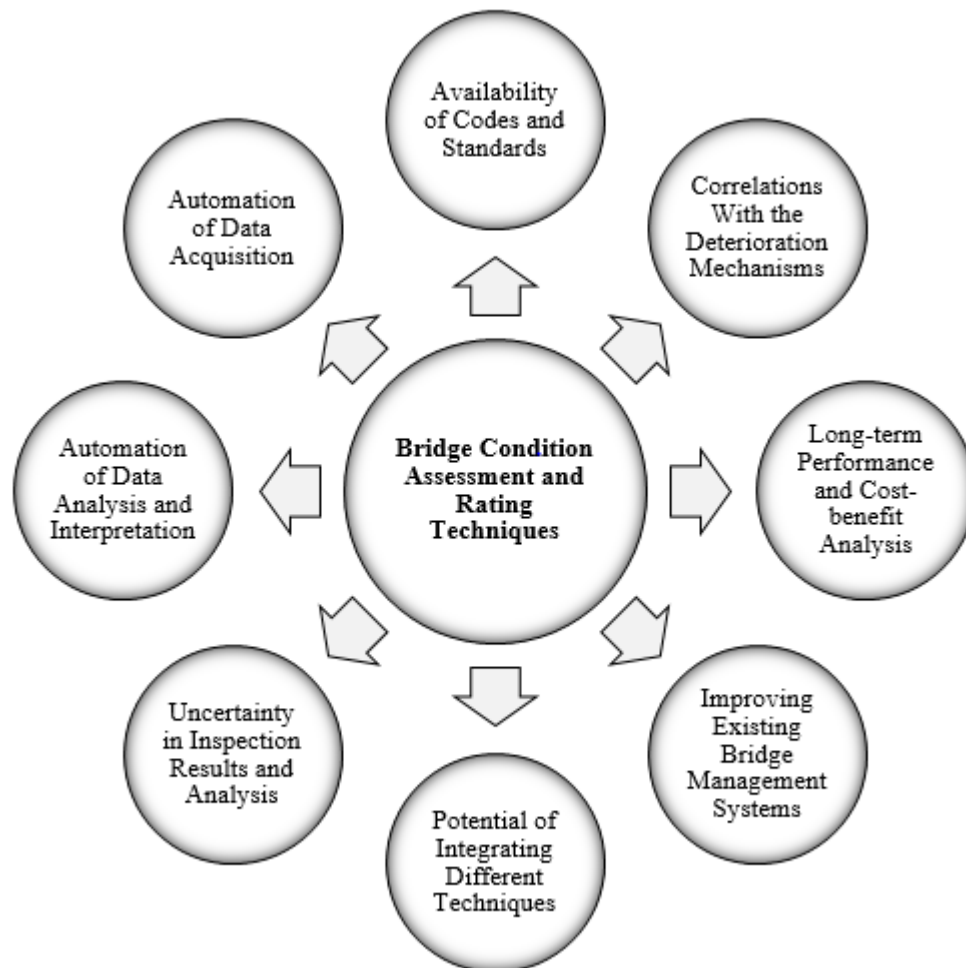


**Figure 2-9: Conceptual framework to identify challenges that require further research in bridge condition assessment.**

### 2.6.1 Selection of Appropriate Condition Assessment Technique

As previously discussed, different deterioration processes lead to different types of bridge component defects, which affect the ability of the evaluation techniques to detect and characterize them. The decision of which technique is more appropriate for BCA is highly dependent on the nature of the available data and is driven by certain factors: (a) the mechanism of deterioration in the bridge being investigated, (b) expected output from the evaluation method, (c) how the assessment data will be used, (d) level of complexity and available time to conduct the evaluation, and (e) the geographic location as well as the traffic density and environmental conditions. For instance, corrosion can be tracked by monitoring the electrical outputs in a cathodic protection system, whereas scour monitoring involves using acoustic, pier-mounted sensors to track scour depth in the regions of bridge piers and abutments. Cameras are useful for displacement monitoring, whereas strain gauges are suitable for deformations. For bridge decks, if delamination is of greatest concern, impact echo or infrared with a higher degree of automation are appropriate, while radar is suitable if corrosion of greatest concern. **Table 2-10** recommends specific BCA methods for some of the common deterioration mechanisms in different bridge structures.

**Table 2-10: Appropriate investigation methods for some deterioration mechanisms in RC bridges**

Concerned Assessment	Recommended Investigation Method
<ul style="list-style-type: none"> <li>• Map patterns of distress such as surface cracks, spalling, scaling, and erosion</li> <li>• Scour damage</li> <li>• Fatigue damage</li> <li>• Breaks in cable-stayed RC bridges.</li> <li>• Corrosion in prestressing strands (in adjacent concrete box-beam bridges).</li> <li>• Damages in long-span suspension RC bridges</li> <li>• Delamination and cracks in RC bridge decks.</li> <li>• Potential of corrosion in concrete bridges</li> <li>• Subsurface defects in superstructure components of RC bridges.</li> <li>• Unknown bridge foundation depth, integrity, type.</li> </ul>	<ul style="list-style-type: none"> <li>• Integrated visual inspection and remote sensing technologies.</li> <li>• Vibration based techniques, scour sensors.</li> <li>• Acoustic emission techniques.</li> <li>• Health monitoring (strain sensors).</li> <li>• Magnetic techniques (magnetic reluctance meters).</li> <li>• Health monitoring techniques (strain sensors &amp; FEM).</li> <li>• Air-coupled impact-echo and infrared thermography.</li> <li>• Half-Cell Potential, electrical resistivity, and ground penetrating radar technologies.</li> <li>• Remote sensing and health monitoring technologies.</li> <li>• Parallel seismic and ultra-seismic techniques.</li> </ul>

## 2.7 Conclusions

Bridge condition assessment procedures have existed for many decades. It was enlightening to realize the extent of ongoing work that is expanding rapidly considering the staggering resources needed to repair ageing bridges, which often exceed the capabilities of bridge owners. BCA is a scientific and technical procedure aimed at producing evidence of bridge health, assessing its structural reliability, and tailoring procedures to prolong its life. According to this framework, this study has provided a much needed review of recent research accomplishments in this field. The reviewed body of knowledge offers recent advances in VI, LT, NDT, SHM, and FEM techniques as well as existing deterioration prediction models and achievements of AI technologies in BCA. The review demonstrates clear need to upgrade existing BMSs to incorporate recent research in this domain.

Future research should consider data that drive the decision making of bridge owners from research planning to implementation, with particular focus on added value. Only then can the use of these technologies in mainstream bridge engineering practice truly be valuable. Innovative design and construction methodologies should be also considered by transportation owners along with improving existing BMSs. For instance, by verifying the accuracy of a bridge FEM with NDT and SHM results, bridge owners can use analysis output for bridge evaluation and decision making. An understanding of the range of capabilities of different NDT techniques and SHM systems will be helpful in directing bridge stakeholders to evaluate the output and, hence, value can actually be delivered. Reliable bridge condition can be effectively achieved using several complementary NDT technologies. Therefore, there is need for more research efforts to develop multi-NDT models. However, caution is recommended before widely using any such methodology. A method should be used only after careful cost-benefit analysis to determine its value in both the short- and long-term. Lastly, the enormous amount of information and knowledge that has already been produced in the BCA field must be integrated into comprehensive decision making systems, which could be used by various participants in the field for quality management and structural assessment purposes of ageing bridges.

## 2.8 References

- AASHTO. (2011). “*Manual for bridge evaluation.*” 2<sup>nd</sup> Ed., Washington, DC.
- Abu Dabous, S., Alkass, S. and Zaki, A. (2008). “A probabilistic methodology for bridge deck condition assessment.” *Bridge Structures*, Vol. 4 (1), 49-56.
- Abudayyeh, O., Al-Bataineh, M., and Abdel-Qader, I. (2004). “An Imaging Data Model for Concrete Bridge Inspection.” *Advances in Engineering Software*, Vol. 35 (8), 473-480.
- American Concrete Institute (2013). “*NDT Methods for Evaluation of Concrete in Structures.*” Report 228.2R-13, 83 p.
- Adhikari, S., Moselhi, O., and Bagchi, A. (2012). “Automated Prediction of Condition State Rating in Bridge Inspection.” *Gerontechnology*, Vol. 11 (2), 81-88.
- Agdas, D., Rice, J., Martinez, J., and Lasar, I. (2015). “Comparison of VI and SHM as Bridge Condition Assessment Methods.” *Performance of Constructed Facilities*, Vol. 30, 1-10.
- Ahlborn, M., Vaghefi, K., and Harris, D. (2012). “Measurement and communication of bridge performance with RS technologies.” *Transportation Research Board*, Vol. 2292 (1), 141-149.
- Akula, M., Zhang, Y., Kamat, V., and Lynch, J. (2014). “Leveraging Structural Health Monitoring for Bridge Condition Assessment.” *Proc., Construction Research Congress*, ASCA, Atlanta, Georgia, 1159-1168.
- Alampalli, S. (2012). “Special Issue on Non-destructive Evaluation and Testing for Bridge Inspection and Evaluation.” *Bridge Engineering*, Vol. (17), 827-828.
- Alani, A., Aboutalebi, M., and Kilic, G. (2013). “Integrated health assessment strategy using NDT for reinforced concrete bridges.” *NDT&E International*, Vol. 61, 80-94.
- Algernon, D., Hiltunen, R., Ferraro, C., and Ishee, C. (2011). “Rebar detection with cover meter and ultrasonic pulse echo combined with automated scanning system.” *Transportation Research Board*, Vol. (2251), 123–131.
- Alt, D., and Meggers, D. (1996). “*Determination of bridge deck subsurface anomalies using IRT and GPR.*” Report FHWA-KS-96-2, Kansas, DOT, 18 p.
- Amini, A., Melville, B., and Ali, T. (2014). “Local scour at piled bridge piers including an examination of the superposition method.” *Canadian J. Civil Engineering*, Vol. 41, 461-471.
- Anderson, N., Ismael, A., and Thitimakorn, T. (2007). “Ground-penetrating radar: a tool for monitoring bridge scour.” *Environmental and Engineering Geoscience*, Vol. 13, 1-10.
- Arndt, R., Jalinoos, F., Cui, J., Huston, D. (2010). “Periodic NDE for bridge maintenance.” *Proc., Structural Faults and Repair Conference*, Edimburgh, 1-9.

- Attary, N., Symans, M., and Nagarajaiah, S., (2013). "Performance Assessment of a Highway Bridge Structure Employing Adaptive Negative Stiffness for Seismic Protection." *Proc. Structures Congress*, ASCE, 1736-46.
- Barnes, C., and Trottier, J. (2000). "Ground-penetrating radar for network-level concrete deck repair management." *Transportation Engineering*, Vol. 126 (3), 257-262.
- Bao, Y., Li, H., Sun, X., Yu, Y., and Ou, J. (2013). "Compressive sampling-based data loss recovery for wireless sensor networks used in civil SHM." *Structural Health Monitoring*, Vol. 12, 78-95.
- Bell, E., Peddle, J., and Goudreau, A. (2012). "Bridge Condition Assessment using Digital Image Correlation and Structural Modeling." *Proc. 6<sup>th</sup> International IABMAS Conference*, Stresa, Lake Maggiore, Italy, 330-338.
- Black, M., Brint, T., and Brailsford, R. (2005). "A Semi-Markov Approach for Modelling Asset Deterioration." *Operational Research Society*, Vol. 56 (11), 1241-1249.
- Biondini, F., and Frangopol, D., (2013). "Time effects on robustness and redundancy of deteriorating concrete structures." *Proc., 11<sup>th</sup> International Conference on Structural Safety and Reliability*, New York, USA, 1-13.
- Bolar, A., Tesfamariam, S., and Sadiq, R. (2013). "Condition assessment for bridges: a hierarchical ER framework." *Structure and Infrastructure Engineering*, Vol. 9 (7), 648-666.
- Briaud, L., Hurlbauss, S., Chang, K., Yao, C., Sharma, H., and Yu, O. (2011). "*Real-time monitoring of bridge scour using remote monitoring technology.*" Project, Texas Department of Transportation, Austin, USA.
- Brown, D. (1980). "Mechanisms of corrosion of steel in concrete in relation to design, inspection, and repair of offshore structures." *ACI, Special Publication*, Vol. 65, 169-204.
- Butt, S., Limaye, V., and Newhook, J., (2007). "Acoustic survey method to map damage in concrete bridge deck slabs." *Acoustic Emission*, Vol. 25, 373-378.
- Cady, P. D., and Gannon, E. J. (1992). "*Condition Evaluation of Concrete Bridges Relative to Corrosion.*" Procedure Manual, Vol. 8, SHRP-S/FR-92-110, NRC, 124 p.
- Chan, T., Ashebo, D., Tam, H., Yu, Y., Chan, T., Lee, P. (2009). "Vertical displacement measurements for bridges using optical fiber sensors and CCD cameras: A preliminary study." *Structure Health Monitoring*, Vol. 8 (3), 243-249.
- Chen, Y., and Fan, P. (2011). "An improved one-dimensional optimization algorithm in non-probabilistic reliability investigation and its application in bridge assessment." *Gong Cheng Li Xue*, Vol. 28 (5), 21-29.
- Chen, Y., Feng, M., and Tan, C. (2009). "Bridge Structural Condition Assessment Based on Vibration and Traffic Monitoring." *Engineering Mechanics*, Vol. 135, 747-758.
- Clark, M. R., McCann, D. M., and Forde, M. C. (2003). "Application of infrared thermography to the non-destructive testing concrete and masonry bridges." *NDT&E International*, Vol. 36 (4), 265-275.

- Coe, T. and Brandenburg, J. (2011). "P-wave Reflection Imaging of a Cast-In-Steel-Shell Bridge Foundation." *Proc., Geo-Frontiers Conference*, Dallas, Texas, 1-9.
- Cosser, E., Roberts, G., Meng, X., and Dodson, A. (2014). "The comparison of single frequency and dual frequency GPS for bridge deflection and vibration monitoring." *Proc., 11<sup>th</sup> International Symposium on Deformation Measure*. Santorini, Greece, 1-8.
- Cruz, J., Roca, J., Escusa, G., and Carvalho, J. (2015). "An alternative system for measuring displacements in bridges by using displacement transducers." *Proc., 3<sup>rd</sup> conference on Smart Monitoring Assess and Rehabilitation of Civil Structures, Antalya, Turkey*, 1-13.
- Delatte, N. (2009). "*Failure, distress and repair of concrete structures.*" Woodhead Publishing, Boca Raton, Fla, 335 p.
- Deng, X., Hu, Y., and Deng, Y. (2014). "Bridge Condition Assessment Using D Numbers" *Scientific World*, Vol. 2014, 1-11.
- Do Hyung, L., Joonam, P., and Kihak, L. (2011). "Nonlinear seismic assessment for the post-repair response of RC bridge piers." *Composites: Part B Engineering*, Vol. 42 (5), 1318-1329.
- Edalatmanesh, R. (2010). "*Structural health monitoring model for fatigue assessment in concrete bridge decks.*" PhD. Thesis. Dalhousie University, Canada. 288 p.
- Elbehairy, H., Hegazy, T., Elbeltagi, E., and Souki, K. (2006). "Comparison of Two Evolutionary Algorithms for LCC Optimization of Bridge Deck Repairs." *Computer-Aided Civil and Infrastructure Engineering*, Vol. 21, 561-572.
- Elsaid, A, and Seracino, R. (2014). "Rapid assessment of foundation scour using the dynamic features of bridge superstructure." *Construction and Building Materials*, Vol. 50, 42-49.
- Emily, W. (2011). "*Artificial Neural Network Models for the Prediction of Bridge Deck Condition Ratings.*" Thesis, Michigan State University, 196 p.
- Fisher, M., Chowdhury, N., Khan, A., and Atamturktur, S. (2013). "An evaluation of scour measurement devices." *Flow Measurement and Instrumentation*, Vol. 33, 55-67.
- Flintsch, W. and Chen, C. (2004). "Soft Computing Applications in Infrastructure Management." *Infrastructure Systems*, Vol. 10 (4), 157-166.
- Ghodoosi, F., Bagchi, A., and Zayed, T. (2015). "System-Level Deterioration Model for Reinforced Concrete Bridge Decks." *Bridge Engineering*, Vol. 20 (5), 1-10.
- Ghodoosi, F., Bagchi, A., and Zayed, T. (2014). "Reliability-Based Condition Assessment of an Externally Restrained Bridge Deck Considering Uncertainties in Key Design Parameters." *Performance of Constructed Facilities*, 1-10.
- Glisic, B., Inaudi, D., and Nan, C. (2002). "Pile monitoring with fiber optic sensors during axial compression, pullout, and flexure tests." *Transportation Research Board*, Vol. (1808), 11-20.

- Gordon, S. J., and Lichti, D. D. (2007). "Modeling Terrestrial Laser Scanner Data for Precise Structural Deformation Measurement." *Surveying Engineering*, Vol. 133, 72–80.
- Guan, S., Rice, J., Li, C., and Wang, G. (2014). "Bridge deflection monitoring using small, low-cost radar sensors." *Proc., Structures Congress*, ASCE, Boston, 2853-2862.
- Gucunski, N., Kee, S., La, H., Basily, B., Maher, A., and Ghasemi, H. (2015). "Implementation of a Fully Autonomous Platform for Assessment of Concrete Bridge Decks RABIT." *Proc., Structure Congress*, ASCE, Reston, VA, 367-378.
- Gucunski, N., Imani, A., Romero, F., Nazarian, S., Yuan, D., Wiggenhauser, H., and Shokouhi, P. (2013). "Non-destructive testing to identify concrete bridge deck deterioration." *Proc., 92<sup>nd</sup> Meeting, TRB. SHRP 2 Report*, 96 p.
- Gucunski, N., and Nazarian, S. (2010). "Material Characterization and Condition Assessment of Reinforced Concrete Bridge Decks by Complementary NDE Technologies." *Proc., Structure Congress*, ASCE, Orlando, Fl., USA, 429-439.
- Guldur, B., Yan, Y., and Hajjar, J. (2015). "Condition Assessment of Bridges Using Terrestrial Laser Scanners." *Proc., Structures Congress*, ASCE, Portland, 355-367.
- Hasan, M., Setunge, S., and Law, D. (2013). "Deterioration prediction of concrete bridges with artificial neural network (ANN) derived from discrete condition data." *Proc., 22<sup>nd</sup> Australian Conference on the Mechanics of Structure, and Materials*, UK, 909-914.
- Hesse, A., Atadero, R., and Ozbek, M. (2015). "Uncertainty in Common NDE Techniques for Use in Risk-Based Bridge Inspection Planning." *Bridge Engineering*, Vol. 20 (11), 1-8.
- Higuera, M., Rodriguez, L., Quintela, A., and Cobo, A. (2011). "Fiber optic sensors in structural health monitoring." *Light wave Technology*, Vol. 29 (4), 587–608.
- Hinzen, G. (2013). "Support of Macroseismic Documentation by Data from Google Street View." *Seismological Research Letters*, Vol. 84 (6), 982-990.
- Hu, X., and Wang, B. (2013). "A Wireless Sensor Network-Based SHM System for Highway Bridges." *Computer-Aided Civil and Infrastructure Engineering*, Vol (28), 193-209.
- Huang, H. (2010). "Artificial neural network model of bridge deterioration." *Performance of Constructed Facilities*, Vol. 24 (6), 597-602.
- Huntley, S. A., and Valsangkar, A. J. (2014). "Behaviour of H-piles supporting an integral abutment bridge." *Canadian Geotechnical J.*, Vol. 51 (7), 713-734.
- Huston, D., Cui, J., and Burns, D. (2011). "Concrete bridge deck condition assessment with automated multi-sensor techniques." *Structure and Infrastructure Engineering*, Vol. 7 (7), 1-11.
- Jannaty, M., Eghbalzadeh, A., and Hosseini, S. (2016). "Using field data to evaluate the complex bridge piers scour methods." *Canadian J. Civil Engineering*, Vol. 43, 218-225.

- Kee, S., Oh, T., Popovics, J., Arndt, R., and Zhu, J. (2012). "Nondestructive Bridge Deck Testing with Air-Coupled IE and IRT." *Bridge Engineering*, Vol. 17, 928-939.
- Kishk, M., and Al-Hajj, A. (2002). "A fuzzy model and algorithm to handle subjectivity in life-cycle costing based decision-making." *Financial Management and Property Construction*, Vol. 5 (1-2), 93-104.
- Krause, M., Mayer, K., Friese, M., Milmann, B., Mielentz, F., Ballier, G. (2011). "Progress in ultrasonic tendon ducts imaging." *European J. of Environmental and Civil Engineering*, Vol. 15 (4), 461-485.
- Laory, I., Hadj, N., Trinh, T., and Smith, I. (2012). "Measurement System Configuration for Damage Identification of CMS" *Bridge Engineering*, Vol. 17, 857-866.
- Lau, T., Waller, L., Vishnukanthan, K., and Sivathayalan, S. (2012). "Fragility relationships for probabilistic performance-based seismic risk assessment of bridge inventories." *Proc., Annual Conference CSCE*, Vol. 4, 2765-2774.
- Lee, J., Bu, G., Guan, H., Loo, Y. (2015). "Prediction of Long-Term Bridge Performance: Integrated Deterioration Approach." *Performance of Constructed Facilities*, Vol. 29 (3), 591-600.
- Lee, J., Guan, H., Loo, Y., and Blumenstein (2012). "Refinement of Backward Prediction Method for Reliable Artificial Intelligence-Based Bridge Deterioration Modelling." *Advances in Structural Engineering*, Vol. 15 (5), 825-836.
- Li, Q., and Wang, K. (2011). "Pavement Smoothness Prediction Based on Fuzzy and Gray Theories." *Computer-Aided Civil and Infrastructure Engineering*, Vol. 26, 69-76.
- Liang, T., Chang, W., and Li, F. (2002). "Grey and regression models predicting the remaining service life of existing RC bridges." *Grey Systems*, Vol. 14 (4), 291-310.
- Lounis, Z. (2013). "Critical concrete infrastructure: extending the life of Canada's bridge network." *Construction Innovation*, NRC, Canada. Vol. 18 (1), 34-49.
- Lu, C., and Liu, R. (2010). "A model for predicting time to corrosion-induced cover cracking in RC structures." *Fracture Mechanics of Concrete*, Vol. 53 (4), 967-976.
- Maekawa, K., and Fujiyama, C. (2013). "Crack Water Interaction and Fatigue Life Assessment of RC Bridge Decks." *Proc., 5<sup>th</sup> Biot Conference on Poromechanics*, ASCE, Vienna, Austria, 2280-2289.
- Moore, M., Phares, B., Graybeal, B., Rolander, D., and Washer, G. (2001). "Reliability of visual inspection for highway bridges." Final Report. No. FHWA-RD-01-020, Vol. 1, Federal Highway Administration (FHWA), 118 p.
- Morcous, G., Lounis, Z., and Cho, Y. (2010). "An Integrated System for Bridge Management Using Probabilistic and Mechanistic Deterioration Models: Application to Bridge Decks." *KSCE J. Civil Engineering*, Vol. 14 (4), 527-537.
- Mosavi, A., Sedarat, H., O'Connor, M., Emami, A., and Lynch, J. (2014). "Calibrating a high-fidelity finite element model of a highway bridge using a multi-variable sensitivity-based optimization approach" *Structure and Infrastructure Engineering*, Vol. 10, 627-42.

- Moufti, S., Zayed, T., and Abu Dabous, S. (2014). "Defect Based Condition Assessment of Concrete Bridges: A Fuzzy Hierarchical Evidential Reasoning Approach." *Proc., Transportation Research Record, 93<sup>rd</sup> Annual Meeting*, 88-96.
- Muntasir, A., Billah, L., and Alam, M. (2015). "Seismic fragility assessment of highway bridges: a state-of-the-art review." *Structure and Infrastructure Engineering*, Vol. 11 (6), 804-832.
- Nasrollahi, M., and Washer, G. (2014). "Estimating Inspection Intervals for Bridges Based on Statistical Analysis of National Bridge Inventory Data." *Bridge Engineering*, Vol. 11, 1-11.
- Nazarian, S., Baker, R., and Crain, K. (1993). "*Development and Testing of a Seismic Pavement Analyzer*." Report SHRP-H- 375, Strategic HRP, NRC, 169 p.
- Newhook, P., and Edalatmanesh, R. (2013). "Integrating reliability and SHM in the fatigue assessment of concrete bridge decks." *Structure and Infrastructure Engineering*, Vol. 9 (7), 619-633.
- Newhook, J., Gaudet, J., and Edalatmanesh, R., (2011). "Investigation of an externally restrained concrete bridge deck slab on a multi-girder bridge model." *Canadian J. Civil Engineering*, Vol. 38 (2), 233–241.
- Nogami, Y., Akiyama, M., and Frangopol, D. (2013). "Seismic design of RC bridge piers to ensure the post-disaster functionality of road network." *Proc., 11<sup>th</sup> International Conference on Structure Safety and Reliability, ICOSSAR*, 3581-3586.
- Oh, T., Kee, S., Arndt, R., and Popovics, J. S. (2013). "Comparison of NDT methods for assessment of a concrete bridge deck." *Engineering Mechanics*, Vol. 139, 305-314.
- Olsen, J., Chen, Z., and Hutchinson, T. (2013). "Optical Techniques for Multiscale Damage Assessment." *Geomatics, Natural Hazards and Risk*, Vol. 4 (1), 49-70.
- Ontario Structure Inspection Manual-OSIM, (2008), *Ontario Ministry of Transp.*, 394 p.
- O'Connor, S., Zhang, Y., Lynch, J., Ettouney, M., and Linden, G. (2014). "Automated Analysis of Long-Term Bridge Behavior and Health using a Cyber-Enabled Wireless Monitoring System." *Proc., SPIE*, Vol. 9063, 1-11.
- O'Connor, S., Lynch, J., and Gilbert, A. (2012). "Compressed sensing embedded in an operational wireless sensor network to achieve energy efficiency in monitoring applications." *Smart Materials and Structure*, Vol. 23, 1-17.
- Ozbulut, E., and Hurlbaas, S. (2011). "Seismic assessment of bridge structures isolated by a shape memory alloy/rubber-based isolation system." *Smart Materials and Structures*, Vol. 20 (1), 1-12.
- Pailes, B. (2014). "*Damage Identification, Progression, and Condition Rating of Bridge Decks Using Multi-Modal Non-Destructive Testing*." Thesis, Rutgers, the State University of New Jersey, 184 p.
- Palazzo, D., Friedmann, R., Nadal, C., Santos, F. M., Veiga, L., and Faggion, P. (2006). "Dynamic monitoring of structures using a robotic total station." *Proc., Shaping the Change XXIII FIG Congress, Munich, Germany*, 1-10.

- Parisa, S., Julia, W., and Herbert, W. (2013). "Detection of Delamination in Concrete Bridge Decks by Joint Amplitude and Phase Analysis of USA Measurements." *Bridge Engineering*, Vol. 19 (3), 1-11.
- Park, K., Kim, S., Park, H., and Lee, K. (2005). "The determination of bridge displacement using measured acceleration." *Engineering Structure*, Vol. 27, 371-378.
- Penttala, V. (2009). "Causes and mechanisms of deterioration in reinforced concrete." In book: Failure, distress and repair of concrete structures, first Edition, Chapter 1, Woodhead Publishing, Editors: Norbert Delatte, 3-31.
- Pradhan, B., and Bhattacharjee, B. (2009). "Half-Cell Potential as an Indicator of Chloride-Induced Corrosion Initiation in RC." *Material in Civil Engineering*, Vol. 21 (10), 543-552.
- Prendergast, L., and Gavin, K. (2014). "A review of bridge scour monitoring techniques" *Rock Mechanics and Geotechnical Engineering*, Vol. 6, 138-149.
- Raghavan, A., and Cesnik, C. E. (2007). "Review of guided-wave structural health monitoring." *Shock and Vibration Digest*, Vol. 39 (2), 91-116.
- Ross, J. (2010). "Fuzzy Logic with Engineering Applications." Book, 3<sup>rd</sup> edition, John Wiley and Sons Ltd, UK, 707 p.
- Sanayei, M., Phelps, J., and Sipple, J. (2012). "Instrumentation NDT & FEM Updating for Bridge Evaluation Using Strain measurements." *Bridge Engineering*, Vol. 17 (1), 130-138.
- Sasmal, S., and Ramanjaneyulu, K. (2009). "Condition evaluation of existing RC bridges using FAH approach." *Expert Systems with Applications*, Vol. 35, 1430-1443.
- Saviotti, A. (2014). "Bridge Assessment, Management & Life Cycle Analysis." *Modern Applied Science*, Vol. 8 (3), 167-183.
- Scott, M., Rezaizadeh, A., Delahaza, A., and Santos, G. (2003). "A comparison of NDE methods for bridge deck assessment." *NDT&E International*, Vol. 36, 245-255.
- Senouci, A., El-Abbasy, M., and Zayed, T. (2014). "Fuzzy-Based Model for Predicting Failure of Oil Pipelines." *J. Infrastructure Systems*, Vol. 20 (4), pp: 4014018 (1-11).
- Seong, K., Taekeum, O., and Popovics, S. (2012). "Non-destructive Bridge Deck Testing with Air-Coupled IE and IR Thermography." *Bridge Engineering*, Vol. 17 (6), 928-939.
- Shafei, B., and Alipour, A. (2014). "Life-Time Risk Assessment of RC Highway Bridges under Deterioration Processes." *Proc., Structure Congress*, No. 249, ASCE, Boston, 1014-1025.
- Sobanjo, J. (1997). "A Neural Network Approach to modeling bridge deterioration." *Proc., 4<sup>th</sup> Congress on computing in Civil Engineering*, Philadelphia, PA, 623- 626.
- Sousa, H., Bento, J., and Figueiras, J. (2014). "Assessment and Management of Concrete Bridges Supported by Monitoring Data-Based FEM." *Bridge Engineering*, Vol. 19, 1-12.

- Taner, Y., and Caner, A. (2011). "Target damage level assessment for seismic performance evaluation of two-column RC bridge bents." *Bridge Structures*, Vol. 8, 135-146.
- Tarighat, A., and Miyamoto, A. (2010). "Fuzzy concrete bridge deck condition rating method for practical bridge management system." *Expert Systems with Applications*, Vol. 36, 12077–12085.
- Tee, B., Bowman, D., and Sinha, C. (1988). "A fuzzy mathematical approach for bridge condition evaluation." *Civil Engineering Systems*, Vol. 5 (1), 17-25.
- Tokdemir, B., Ayvalik, C. and Mohammadi, J. (2000). "Prediction of Highway Bridge Performance by Artificial Neural Networks and Genetic Algorithms." *Proc., 17<sup>th</sup> International Symposium on Automation and Rob in Construction. (ISARC)*, Taipei, Taiwan, 1-8.
- Vaghefi, K., Oats, R., Harris, D., Ahlborn, T., Brooks, C., Endsley, K., Roussi, C., and Shuchman, R. (2012). "Evaluation of Commercially Available Remote Sensors for Highway Bridge Condition Assessment." *Bridge Engineering*. Vol. 17, 886-895.
- Varnavina, A., Khamzin, A., Torgashov, E., Sneed, L., Goodwin, B., and Anderson, N. (2015). "Data acquisition and processing parameters for concrete bridge deck condition assessment using GPR." *Applied Geophysics*, Vol. 114, 123–133.
- Wang, N., Ellingwood, R., and Zureick, H. (2011). "Bridge rating using system reliability assessment." *Bridge Engineering*, Vol. 16 (6), 863–871.
- Wang, Y. and Elhag, T., (2008). "Evidential reasoning approach for bridge condition assessment." *Expert Systems with Applications*, Vol. 34 (1), 689–699.
- Washer, G., Fenwick, R., Bolleni, N., and Harper, J. (2009). "Effects of environmental variable on IR imaging subsurface features of concrete bridges." *Transportation Research Board*, 107-114.
- Webb, G., Vardanega, P., and Middleton, C. (2015). "Categories of SHM deployments: Technologies and capabilities." *Bridge Engineering*, 1-15.
- Wong, K. (2007). "Design of a structural health monitoring system for long-span bridges." *Structural Infrastructure Engineering*, Vol. 3 (2), 169–185.
- Wood, J. C., and Rens, K. L. (2006). "Non-destructive testing of the Lawrence Street Bridge." *Proc., Structures Congress: Structural Engineering and Public Safety*, B. Cross and J. Finke, eds., ASCE, Reston, VA, 1–15.
- Xia, P., and Brownjohn, J. (2005). "Bridge Structural Condition Assessment Using Systematically Validated Finite-Element Model." *Bridge Engineering*, Vol. 9, 418-423.
- Yang, B., Wang, M., and Xu, L. (2006). "Environmental impact assessment using the ER approach." *European J. Operational Research*, Vol. 174 (3), 1885:1913.
- Yehia. S., Abudayyeh, O., and Nabulsi, S. (2007). "Detection of Common Defects in Concrete Bridge Decks Using NDE Techniques." *Bridge Engineering*, Vol. 12, 215-225.

- Yong Hao Z., and Kee Ee Ng. (2003). "Evaluation of concrete structures by advances non-destructive test methods-impact echo, impulse response test and radar survey." *Proc., NDT-CE conference*, Berlin, 1-4.
- Zadeh, L. (1965). "Probability theory and fuzzy logic are complementary rather than competitive." *Technometrics*, Vol. 37 (3), 271–276.
- Zanjani, Z., and Patnaik, A. (2014). "Finite element modeling of the dynamic response of a composite RC bridge for SHM." *International J. Advanced Structure Engineering*, Vol. 6 (55), 1-14.
- Zarafshan, A., Iranmanesh, A., and Ansari, F. (2012). "Vibration-based method and sensor for monitoring of bridge scour." *Bridge Engineering*, Vol.17 (6), 829-38.
- Zhang, L., Zhao, H., OBrien, E., Shao, X., and Tan, C. (2016). "The influence of vehicle–tire contact force area on vehicle–bridge dynamic interaction." *Canadian J. Civil Engineering*, Vol. 43, 769–772.
- Zhang, W., Cai, S., Pan, F., and Zhang, Y. (2014). "Fatigue life estimation of existing bridges under vehicle and non-stationary hurricane wind." *Wind Engineering Industrial Aerodynamic*, Vol. 133 (10), 135-145.
- Zhang, W., and Yuan, H. (2014). "Corrosion fatigue effects on life estimation of deteriorated bridges under vehicle impacts." *Engineering Structures*, Vol. 71, 128-136.
- Zhao, X., Liu, H., Yu, Y., and Xu, X. (2015). "Bridge Displacement Monitoring Method Based on Laser Projection-Sensing Technology." *Sensors*, Vo. 15 (4), 8444-8463.

## Chapter 3

### 3. Performance of NDT Techniques in Appraising Condition of Reinforced Concrete Bridge Decks

#### 3.1 Introduction

As discussed in Chapter 2, the colossal backlog of deteriorated bridges draws attention to the importance of NDT technologies as potential condition assessment tools. Many NDT techniques have been developed and proven to be efficient and effective in enhancing the bridge inspection process and make it faster and reliable. However, the selection of NDT technique(s) to evaluate the current state of bridge(s) is a decision variable. There are several research efforts that have attempted to compare several NDT techniques, relying on physical measures via laboratory or field testing (e.g. Clark *et al.*, 2003; Scott *et al.*, 2003; Wood and Rens, 2006; Yehia *et al.*, 2007; Algernon *et al.*, 2010; Oh *et al.*, 2103; Gucunski *et al.*, 2013). These studies focused mainly on the accuracy and reliability of the employed methods, regardless of other important performance indicators such as simplicity, speed and cost. Furthermore, while the evaluated NDT technologies were comparable in some of those studies, some other findings revealed considerable variation between the NDT quantified results (Hesse *et al.*, 2015).

Therefore, more comprehensive comparative studies need to be conducted to motivate practical evaluation of NDT methods and their wider implementation in bridge inspection. There are two strategies by which to carry out the performance evaluation process. The first strategy is based on quantified data by utilizing the selected techniques and conducting in-situ inspection on full-scale deteriorated bridges. The second strategy is based on qualitative data through the response of competent bridge engineers and NDT experts on an evaluation questionnaire to be formulated for an opinion survey given specific performance indicators. Although the first approach can provide an objective evaluation, there is limited quantifiable data available in the open literature on the NDT techniques for bridges (Hesse *et al.*, 2015). In addition, applying this approach requires substantial field inspection work and the purchase of equipment for each technology, which is not a viable option for many transportation agencies. Conversely, the second approach can benefit from

the knowledge gained by bridge and NDT engineers. Gathering such information from experts with extensive experience in NDT can serve as a tool by which to construct a decision-making procedure. Moreover, expert information cannot be obtained via analysis of limited inspections conducted either in the field or in the laboratory.

In this Chapter, a rational decision-making framework to evaluate and rank the most commonly used NDT techniques for detecting defects in RC bridge decks is developed. The analysis and findings presented herein are accomplished through a literature review and a structural survey questionnaire. The survey acquired an expert knowledge base through soliciting broad information about the performance of NDT methods that have been implemented by several transportation agencies. Although such data is qualitative in nature, it could indicate the overall performance of the technologies based on a range of well-defined performance measures that dominate their profession. Evaluating different technologies in the framework allows for the detection of different types of bridge deck health indicators. In order to make the evaluation more precise, fuzzy logic theory has proved its ability to deal effectively with the inevitable uncertainties and subjectivities inherent in human judgments. Consequently, the Fuzzy Analytical Hierarchy Process (FAHP) is employed. The Fuzzy Preference Programme (FPP) nonlinear based method is adopted to determine the relative weights.

**Figure 3-1** illustrates the adopted systematic methodology by which to achieve the above-mentioned objectives. It can be summarized as follows: (1) define and identify the NDT alternatives to be appraised and ranked; (2) identify a set of flexible multi-attributed performance criteria and sub-criteria required for the evaluation process; (3) develop an analytical hierarchy model consisting of the identified performance criteria and sub-criteria, and the selected NDT alternatives; (4) collect the degree of relative importance for the different elements in the hierarchy using expert judgement; (5) apply a fuzzification scale on the pair-wise comparison matrices using linear triangular fuzzy membership functions; (6) calculate the relative weights of the “fuzzified” pairwise matrices applying the FPP using Matlab software and check for any inconsistencies in the obtained results; (7) rank NDT alternatives based on their calculated weights; and (8) validate the achieved model results with the findings of other comparative studies found in the literature.

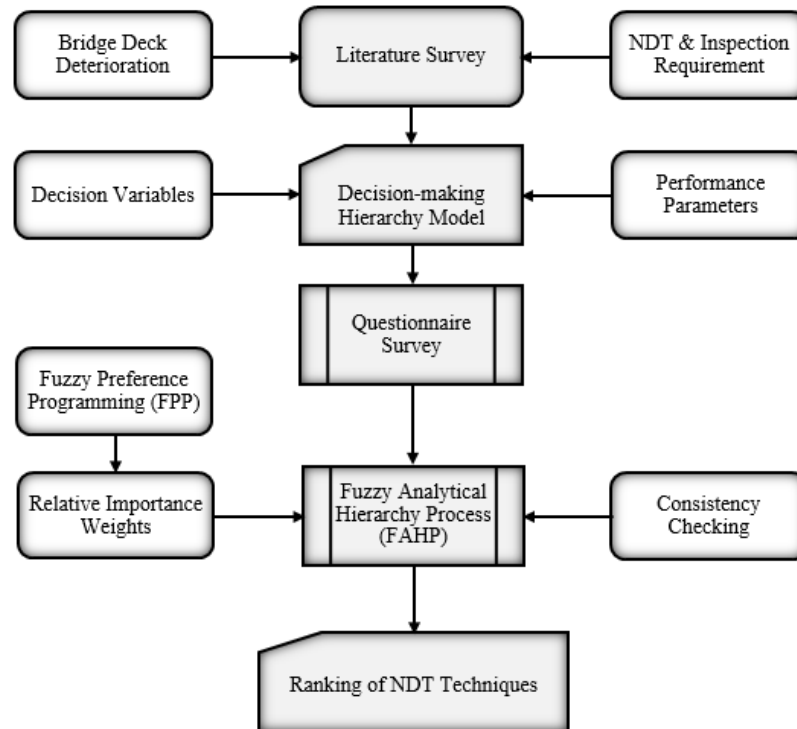


**Figure 3-1: Methodology adopted for appraising and ranking NDT techniques.**

## 3.2 Model Development

### 3.2.1 Selection of the Performance Measures

The performance measures to evaluate various alternatives could significantly influence the ranking result. Thus, it is paramount to identify the most critical parameters in a decision making problem. The five significant performance measures selected for ranking NDT technologies in this study are: (1) capability of each technology based on its exploited physical phenomena to detect at least one of the considered defects; (2) speed of applying each technology; (3) simplicity of applying each technology; (4) accuracy of the obtained results; and (5) the cost associated with applying each technology. Those parameters are similar to those adopted in evaluating the results of nine RC bridge deck NDT methods, in the SHRP2 project. The rationale used for considering only five performance measures is: “although the description of a particular performance provides a more detailed description of that performance in terms of a large number of measures, for most technologies there is either no information regarding a specific performance measure or the measure is not

applicable to that particular technology”. In addition, analyses in terms of a smaller number of performance measures are supposed to be of higher interest and practical value for implementation by transportation agencies and industry (Gucunski *et al.*, 2013).

To proceed with the ranking process against the five major performance criteria in an accurate and feasible manner, they were further subdivided into 15 sub-criteria. For example, the NDT technologies were evaluated against their capabilities for detection of the most serious types of defects. Based on literature surveys, it appears that active corrosion of steel reinforcement, propagation of vertical cracks, and delamination are the most serious types of defects present in RC bridge decks. The rationale behind limiting the deterioration types into only three categories is: “although there are different causes for deterioration, in most cases the reasons cannot be determined by NDT technologies; only their consequences can be determined”. For example, cracking induced by corrosion and shrinkage will result in material degradation, which can be detected through reduced velocity, stiffness, and so forth (Gucunski *et al.*, 2013). In addition, from all the possible deterioration types and mechanisms found in the literature, the three deterioration categories are believed to be of the highest concern to transportation agencies.

The second performance measure (speed) is an important factor for transportation agencies and NDT consultants. Thus, the NDT methods were evaluated against: (i) the speed of data collection; (ii) speed of data analysis; and (iii) importance and potential of the different technologies to be automated. For the third performance measure (simplicity), successful application of these methods requires that those collecting and analyzing data have adequate understanding of the principles of the methods, setting up data acquisition parameters for optimum results, and interpreting the recorded data. Therefore, the NDT methods have been evaluated against: (i) the need for experienced operators; (ii) importance of having an experienced analyzer; and (iii) effects of the environment and traffic on the process of data collection.

The fourth performance parameter (accuracy) of results obtained depends on the ability of each NDT technology to accurately detect a specific defect type. Thus, the accuracy sub-criteria were identified to detect precisely: (i) the extent and severity of delaminations; (ii)

depth and width of vertical cracks; and (iii) presence of active corrosion. Finally, the associated cost of: (i) the required equipment including maintenance costs; (ii) data collection including traffic control cost; and (iii) data analysis were compared among the different NDT methods as sub-criteria of the last performance measure (cost).

### 3.2.2 Selection of the NDT Alternatives

**Table 3-1** describes several applicable NDT methods for detecting the selected three deterioration types. However, based on literature surveys and interviews with bridge experts suggest that the most commonly used NDT methods in onsite assessment and evaluation of RC bridge decks are: Impact Echo (IE), Ultrasonic Pulse Echo (UPE), Half-cell Potential (HCP), Ground Penetrating Radar (GPR), and Infrared Thermography (IRT). Consequently, they were selected as the NDT alternatives for the comparative analysis in this study. Since there is no single technology that has the potential to evaluate all the deterioration mechanisms, the five NDT technologies have been also selected based on their potential for detecting and evaluating the three deterioration types. For instance, HCP has a good potential to identify the probability of active corrosion, while GPR evaluates the conditions for a corrosive environment. UPE and IE have a good potential to detect vertical cracking, while IE, UPE, and IRT have a good potential to detect delamination.

**Table 3-1: Applicable NDT methods to detect specific deterioration types**

Defect	Applicable NDT Method
Cracks and Voids	<ul style="list-style-type: none"> <li>• Acoustic Emission</li> <li>• Impact Echo</li> <li>• Ultrasonic Pulse Echo</li> <li>• Infrared Thermography</li> <li>• Impulse Response</li> <li>• Ultrasonic Surface Waves</li> </ul>
Rebar Corrosion	<ul style="list-style-type: none"> <li>• Half-Cell Potential (corrosion probability)</li> <li>• Ground Penetrating Radar (corrosive environment)</li> <li>• Electrical Resistivity (corrosion probability)</li> <li>• Polarization Resistance (corrosion rate)</li> </ul>
Delamination	<ul style="list-style-type: none"> <li>• Impact Echo</li> <li>• Ultrasonic Pulse Echo</li> <li>• Infrared Thermography</li> <li>• Ultrasonic Surface Waves</li> <li>• Impulse Response</li> </ul>

### 3.2.3 Construction of Fuzzy Analytical Hierarchy Model

Multi-criteria decision-making methods such as analytic hierarchy process, multi-attribute utility theory, and decision trees have the ability to account for multiple decision criteria and address increasing complexity and associated uncertainties by providing clear and easily interpretable results. The analytic hierarchy process (AHP) has been favored in extensive application areas, such as bridge management, and thus gained ground against conventional assessment methods. The AHP, developed by Saaty (1980), is based on modeling decision problems into multiple layers of criteria and sub-criteria to form a hierarchy and provide decision makers a systematic way to evaluate multiple decision alternatives. This is followed by constructing a series of pairwise comparisons among the model variables in the same layer, using the experts' judgments, to decide on their relative importance/influence. The pairwise comparisons are performed using a 9-point fundamental scale of absolute values that represent the strength of judgements. The AHP uses an eigenvalue method to determine the normalized weights of all criteria and sub-criteria in the hierarchy where the intensities of the judgements are assembled in reciprocal matrices. The AHP process has the advantage of allowing the decision maker to perform consistency checks for the provided judgement regarding the relative importance among the decision-making elements. However, the rankings produced by AHP are arbitrary because they are produced by a subjective response. The use of the discrete scale of 1 to 9 does not account for the uncertainty and imprecision associated with judgment during the pairwise comparison process (Sasmal and Ramanjaneyulu, 2008).

The natural top-down approach of the AHP method was utilized to construct the proposed model as illustrated in **Fig. 3-2**. The model was organized into a four-level hierarchy structure, which captures the performance parameters along with the evaluated NDT alternatives. The first level of the hierarchy is the overall goal of the analysis process. The second level contains the main performance measures needed to achieve the overall goal. The third level of the hierarchy holds the sub-criteria to be used for evaluating the NDT alternatives which were added at the bottom level. The model requires relative importance weights to be assigned to the assessment elements, which were collected from bridge and NDT experts and analyzed as described subsequently.

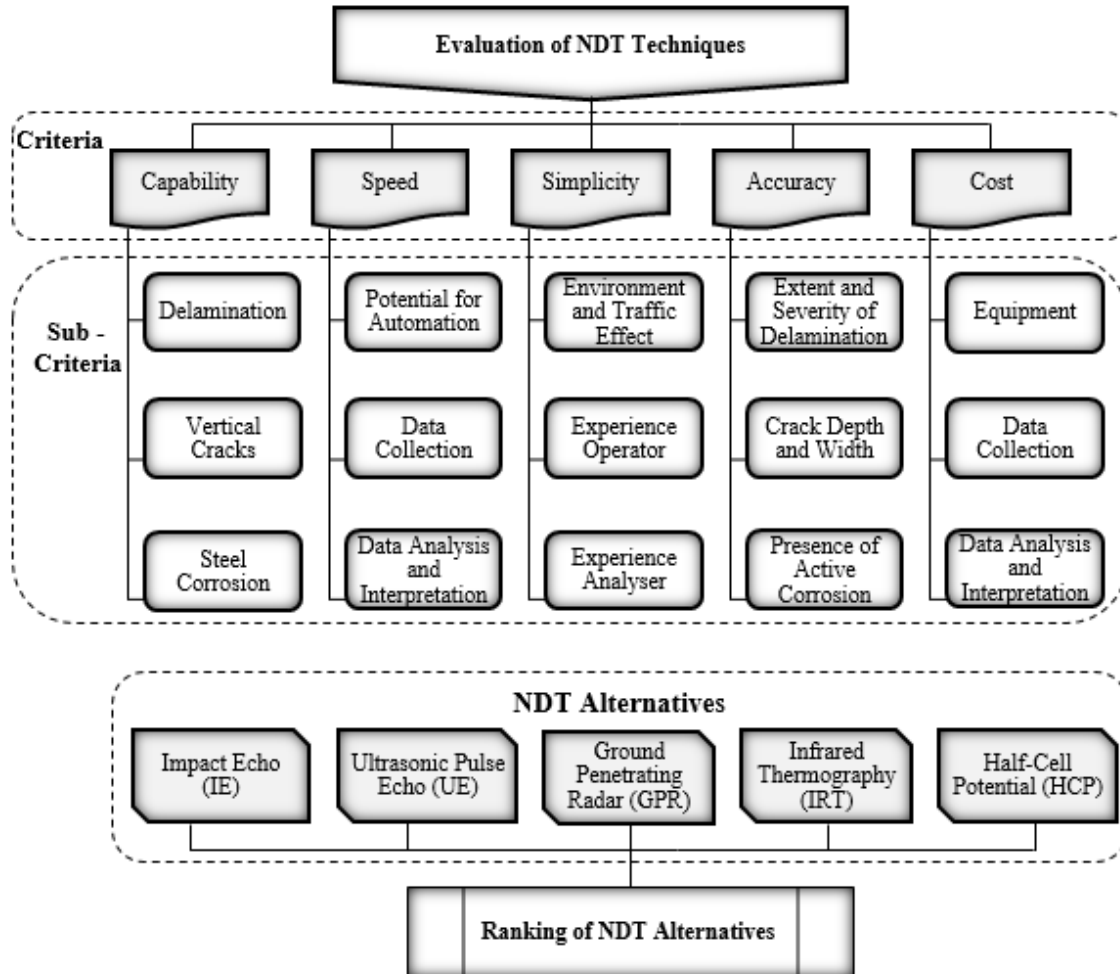


**Figure 3-2: Hierarchy framework for ranking NDT techniques.**

The FST, presented in Chapter 2 is mostly helpful when human judgment is predominant, as is the case with decision making in the evaluation of alternatives. Thus, the FST was introduced for the AHP to make up the deficiency of the conventional AHP modelling, referred to as FAHP, which has been utilized and discussed by several researchers (e.g. Chang, 1996; Huang *et al.*, 2008; Bhattacharyya *et al.*, 2011; Chang and Lee, 2012). The application of FAHP enables taking into account group assessments and can deal effectively with the inherent fuzziness and uncertainty in judgment during the pairwise comparison process. There are various processing techniques based on the source of the fuzziness or uncertainty in the data and analysis requirements (Wang and Elhag, 2008).

Fuzzy numbers can be represented by its membership function ranging between 0 and 1. When comparing two elements, the uncertain numerical ratio is expressed in a fuzzy manner. Membership functions can take various shapes. Linear approximations, such as triangular or trapezoidal fuzzy numbers are frequently used in construction applications (Sasmal and Ramanjaneyulu, 2008). The analysis of the fuzzified comparison matrices that result from the application of the “fuzzification” scale has been the point of interest for many researchers (e.g. Mikhailov, 2004; Sasmal and Ramanjaneyulu, 2008; Huo *et al.*, 2011). For instance, Van Laarhoven and Pedrycz (1983) suggested a fuzzy logarithmic least squares method to obtain the fuzzy weights from a triangular fuzzy comparison matrix. Buckley (1985) utilized the geometric mean method to calculate fuzzy weights. Chang (1996) proposed an extent analysis method, which derives crisp weights for fuzzy comparison matrices. Csutora and Buckley (2001) developed the Lambda-Max method, which is the direct fuzzification of the well-known  $k_{max}$  method. Mikhailov (2004) developed a fuzzy preference programming method, which also derives crisp weights from fuzzy comparison matrices using logarithmic nonlinear programming. Srdjevic (2005) proposed a multicriteria approach for combining prioritization methods within the AHP, including additive normalization, eigenvector, weighted least-squares, logarithmic least-squares, and logarithmic goal programming (Zhou, 2012). These methods have unquestionable potential in fuzzy modelling (Jakiel and Fabianowski, 2015).

### 3.2.4 Data Collection

#### 3.2.4.1 Survey Questionnaire Design

A structured survey questionnaire was constructed to serve the purpose of the evaluation analysis in this study. The survey targeted the participation of a wide spectrum of bridge experts from Canadian ministries and US departments of transportation, NDT consultants, and researchers. The domain includes bridge and NDT professionals from senior engineers and project managers to project engineers and NDT technicians. The process was initiated by soliciting 74 experts to participate in the survey and requesting them to indicate which NDT techniques they were involved with. While 56 experts welcomed receiving the questionnaire, only 35 experts were finally considered and invited. The reason was to ensure that: (1) the experts are working in different departments; and (2) the experts have

experience with at least three of the evaluated techniques. The questionnaire was then distributed using an online survey website service for ease of data collection and to minimize the survey time. Of the 35 experts, a total of 27 responses were completed and received, a 77% response rate. The relatively high response rate is a good indicator of adequate survey design and the respondents' interest in NDT techniques. This response rate also complies with statistical analysis conducted by Baruch (1999), where a reasonable response rate for an academic research was found to be about 60 +/- 20 (%).

The questionnaire consisted of four sections: (1) the first section aimed to obtain general information of the participants' contact information, organization and experience in the bridge and NDT community; (2) the second section aimed to identify the frequency and type of NDT method(s) being used in their bridge schemes; (3) to identify the significance of the factors affecting the successful application of NDT methods, the third section was divided into two parts: part (a) aimed to seek the degree of importance between the five main performance parameters with respect to the selection of the NDT method, while part (b) sensed the degree of importance between the sub-criteria with respect to the related main performance parameter; and (4) the fourth section aimed to seek the degree of importance of employing the selected NDT alternatives with respect to each of the fifteen sub-criteria parameters.

For statistical analysis of the respondents, **Table 3-2** illustrates a summary of information based on the participants' organizations and their experience. Three organization groups were created: the first group included those bridge experts from transportation agencies and represent an overall participation of 44%; the second group included bridge experts from NDT contractors and consultants and represents 41% participation; and the third group includes researchers, who are interested in NDT development, with an overall participation of 15%. The gathered respondents from the three groups agreed on the relative importance of the criteria and sub-criteria. With respect to the participants' experience, the highest participant rate belongs to senior bridge professionals with 41% responses, followed by bridge managers who have 15 to 20 years of experience with 26% responses, while 18% and 15% of the participants have a total of 10 to 15 years and 5 to 10 years of experience, respectively in the bridge and NDT community.

**Table 3-2: Organization and experience of participants in the survey questionnaire**

Organization	Invitation (35 total experts) No (%)	Participation (27 total experts) No (%)	Experience of Participants			
			Over 20 Years No (%)	15 to 20 Years No (%)	10 to 15 Years No (%)	5 to 10 Years No (%)
Transport. Agencies	16 (46%)	12 (44%)	6 (22%)	3 (11%)	2 (7%)	1 (4%)
NDT Consultants	13 (37%)	11 (41%)	4 (15%)	3 (11%)	1 (4%)	3(11%)
Researchers	6 (17%)	4 (15%)	1 (4%)	1 (4%)	2 (7%)	0
		<b>Overall</b>	<b>41 %</b>	<b>26 %</b>	<b>18 %</b>	<b>15 %</b>

**Table 3-3** illustrates a summary regarding the frequency and type of NDT method(s) being used by the participants in their bridge schemes. The HCP was reported as the most utilized method with a percentage of 59% among the participants, followed by the IE method with 48%, and the GPR method with 37%. IRT and UPE methods received relatively low share of utilization, with percentages of 22 and 11, respectively. It should be noted that each participant utilized more than one NDT technique in his/her projects. The responses also indicated that only 14% of the experts are utilizing NDT on a frequent basis, while NDT methods were utilized for detailed investigations and for advanced assessments by 40% and 46%, respectively. According to most of the commonly used bridge inspection procedures, the detailed investigation focuses on those members for which adequate safety was not confirmed by the preliminary evaluation and the advanced assessment only to be conducted when a bridge component has major consequences in terms of risk. These figures indicate the importance of incorporating NDT techniques in existing BMSs and bridge inspection manuals.

**Table 3-3: Results of respondents using NDT techniques**

NDT Technique	Respondents (27 total experts) No (%)	Frequency of Using NDT Technique		
		Frequently Used No (%)	Detailed Investigation No (%)	Advanced Assessment No (%)
Impact Echo (IE)	13 (48%)	2 (7%)	4 (15%)	7 (26%)
Ultrasonic Pulse Echo (UPE)	3 (11%)	0	2 (7%)	1 (4%)
Half-Cell Potential (HCP)	16 (59%)	3 (11%)	6 (22%)	7 (26%)
Ground Penetrating Radar (GPR)	10 (37%)	2 (7%)	3 (11%)	5 (19%)
Infrared Thermography (IRT)	6 (22%)	0	4 (15%)	2 (7%)
	<b>Overall</b>	<b>14 %</b>	<b>40%</b>	<b>46 %</b>

### 3.2.4.2 *Pairwise Comparison Matrices*

The experts were asked to provide the relative importance among the selected performance parameters, which is based on the 9-point Saaty’s linguistic scale for importance (1 being the least favorable and 9 being the most favorable). For example, the experts were asked to provide the degree of importance of accuracy compared with speed, simplicity, and cost when selecting a technology. Another example is to provide the degree of importance for utilizing the IE method if compared with utilizing the IRT method with respect to their capabilities of detecting the extent and severity of delamination, and the degree of importance of utilizing the GPR if compared with utilizing HCP with respect to their potential in detecting the active corrosion. **Figure 3-3** illustrates a snapshot for a survey question to compare the capability performance parameter with the other main performance measures in the evaluation process of NDT methods. The degree of relative importance gathered from the questionnaire responses was utilized to construct a total of 567 pairwise comparison matrices using an Excel worksheet.

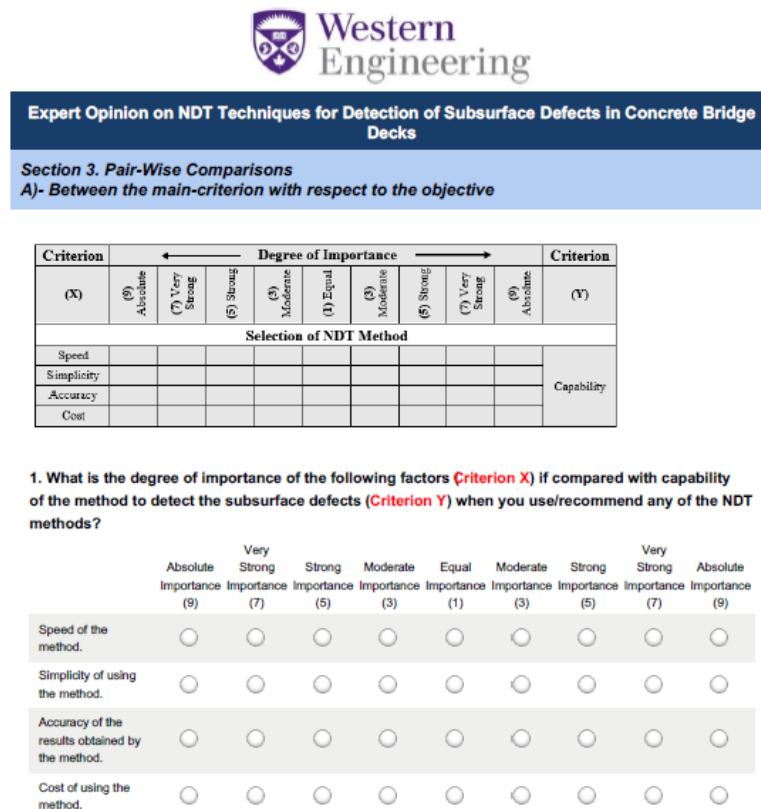


**Figure 3-3: Snapshot of a question in the survey questionnaire.**

### 3.2.5 Data Analysis

#### 3.2.5.1 Fuzzification of Collected Data

A fuzzy set is characterized by a membership function ranging between 0 and 1. A triangular fuzzy number (TFN)  $M$ , as illustrated in **Fig. 3-4** can be represented as  $(l, m, u)$ , which denote the smallest possible value, the most promising value, and the largest possible value, respectively, that describe a fuzzy number. Each TFN has linear representations on its left and right side such that its membership function can be defined as per **Eq. 3-1**.

$$u_M(x) = \begin{cases} (x-l)/(m-l) & l \leq x \leq m \\ (u-x)/(u-m) & m \leq x \leq u \\ 0 & \text{Otherwise} \end{cases} \quad \text{Eq. 3-1}$$

The triangular fuzzy scale, presented in **Table 3-4**, was adopted for the fuzzification process where the difference between most probable (actual response received) with the upper and lower values is equal to one. The fuzzification scale was applied to all of the constructed 567 pairwise comparison matrices. Thus, for a  $(n \times n)$  comparison matrix shown below, there are  $(n + 1)$  variables representing  $n$  weights  $\{x(1), x(2), \dots, x(n)\}$  and a consistency index  $\{\lambda = x(n + 1)\}$ .

$$\left\{ \begin{array}{cccccc} (l_{11}, m_{11}, u_{11}) & (l_{12}, m_{12}, u_{12}) & \cdots & \cdots & \cdots & (l_{1n}, m_{1n}, u_{1n}) \\ (l_{21}, m_{21}, u_{21}) & l_{22}, m_{22}, u_{22} & \cdots & \cdots & \cdots & (l_{2n}, m_{2n}, u_{2n}) \\ \vdots & \vdots & & \vdots & & \vdots \\ (l_{n1}, m_{n1}, u_{n1}) & (l_{n2}, m_{n2}, u_{n2}) & \cdots & \cdots & \cdots & (l_{nn}, m_{nn}, u_{nn}) \end{array} \right\}$$

**Table 3-4: Linguistic comparison scales for importance**

Linguistic scale for importance	Triangular fuzzy scale	Triangular fuzzy reciprocal scale
Equally Important	(1,1,1)	(1,1,1)
Intermediate Level	(1,2,3)	(1/3,1/2,1)
Moderately Important	(2,3,4)	(1/4,1/3,1/2)
Intermediate Level	(3,4,5)	(1/5,1/4,1/3)
Important	(4,5,6)	(1/6,1/5,1/4)
Intermediate Level	(5,6,7)	(1/7,1/6,1/5)
Very Important	(6,7,8)	(1/8,1/7,1/6)
Intermediate Level	(7,8,9)	(1/9,1/8,1/7)
Extremely Important	(8,9,9)	(1/9,1/9,1/8)

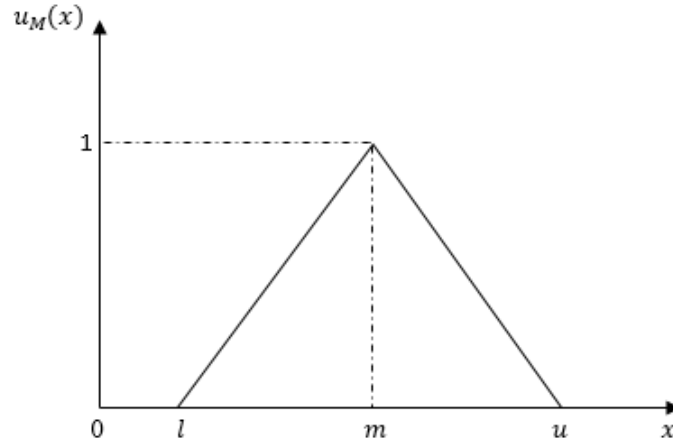


**Figure 3-4: A triangular fuzzy number M.**

### 3.2.5.2 *Relative Importance Weights*

The Fuzzy Preference Programming (FPP), can acquire the consistency values and calculates weights from a triangular fuzzy pairwise comparison matrix using a fuzzy prioritization approach. Therefore, the FPP method was adopted in this study as a reasonable and effective means to calculate the relative weights of the identified performance criteria and sub-criteria and also for the NDT alternatives with respect to each sub-criterion. The Matlab software has excellent performance in matrix operations and data processing and thus, is suitable for solving fuzzy decision-making problems. Zhou (2012) implemented the Mikhailov's fuzzy prioritization approach and proposed a Matlab code to achieve the weights of fuzzy pairwise comparison matrices using the FPP method. The proposed Matlab code was modified and adopted in the analysis process to acquire the weights of fuzzy pairwise comparison matrices as described below.

Considering a set  $F$  of fuzzy comparison judgments represented as triangular fuzzy numbers  $\tilde{a}_{ij}$ , we need to derive a crisp priority vector  $w = (w_1, w_2, \dots, w_n)^T$ , such that the priority ratios  $w_i/w_j$  are approximately within the scopes of the initial fuzzy judgments.

$$F = (\tilde{a}_{ij}) \quad m \leq n(n-1)/2 \quad \tilde{a}_{ij} = (l_{ij}, m_{ij}, u_{ij}) \quad \text{Eq. 3-2}$$

$$l_{ij} \lesssim \frac{w_i}{w_j} \lesssim u_{ij} \quad i = 1, 2, \dots, n-1 \quad j = 2, 3, \dots, n \quad j > i \quad \text{Eq. 3-3}$$

Each crisp priority vector  $w$  satisfies the double-side inequality (**Eq. 3.3**) with some degree, which can be measured by a membership function, linear with respect to the unknown ratio  $w_i/w_j$  as shown in **Eq. 3-4**, and is linearly increasing over the interval  $(-\infty, m_{ij})$  and linearly decreasing over the interval  $(m_{ij}, \infty)$ . The function takes negative values when  $w_i/w_j < l_{ij}$  or  $w_i/w_j > u_{ij}$ , and has a maximum value  $u_{ij} = 1$  at  $w_i/w_j = m_{ij}$ . Over the range  $(l_{ij}, u_{ij})$ , the function coincides with the fuzzy triangular judgment  $(l_{ij}, m_{ij}, u_{ij})$ .

$$u_{ij} \left( \frac{w_i}{w_j} \right) = \begin{cases} \frac{(w_i/w_j) - l_{ij}}{m_{ij} - l_{ij}}, & \frac{w_i}{w_j} \leq m_{ij} \\ \frac{u_{ij} - (w_i/w_j)}{u_{ij} - m_{ij}}, & \frac{w_i}{w_j} \geq m_{ij} \end{cases} \quad \text{Eq. 3-4}$$

The solution to the prioritization problem by the FPP method is based on two main assumptions. The first one requires the existence of non-empty fuzzy feasible area  $P$  on the  $(n - 1)$  dimensional simplex  $Q^{n-1}$ , defined as an intersection of the membership functions, similar to (**Eq. 3-4**) and the simplex hyperplane (**Eq. 3-5**).

$$Q^{n-1} = \{(w_1, w_2, \dots, w_n) | w_i > 0, \sum_{i=1}^n w_i = 1\} \quad \text{Eq. 3-5}$$

The membership function of the fuzzy feasible area is given by  $u_P(w)$ , as shown in **Eq. 3-6**. If the fuzzy judgements are very inconsistent, then  $u_P(w)$  could take negative values for all normalized priority vectors  $w \in Q^{n-1}$ .

$$u_P(w) = \min_{ij} \{u_{ij}(w) | i = 1, 2, \dots, n - 1; j = 2, 3, \dots, n; j > i\} \quad \text{Eq. 3-6}$$

The second assumption of the FPP method specifies a selection rule, which determines a priority vector, having the highest degree of membership in the aggregated membership function (**Eq. 3-6**). It can be noted that  $u_P(w)$  is a convex set, so there is always a priority vector  $w^* \in Q^{n-1}$  that has a maximum degree of membership:

$$\lambda^* = u_p(w^*) = \max_{w \in Q^{n-1}} \min_{ij} \{u_{ij}(w)\} \quad \text{Eq. 3-7}$$

The maximum prioritization problem in **Eq. 3-7** can be represented as:

$$\begin{aligned} & \text{Max } \lambda \\ \lambda & \leq u_{ij}(w), \quad i = 1, 2, \dots, n-1; \quad j = 2, 3, \dots, n; \quad j > i \\ & \sum_{k=1}^n w_k = 1, \quad w_k > 0, \quad k = 1, 2, \dots, n \end{aligned} \quad \text{Eq. 3-8}$$

Taking the specific form of the membership functions (**Eq. 3-4**) into consideration, the problem (**Eq. 3-8**) can be further transformed into a bilinear program of the type:

$$\begin{aligned} & \text{Max } \lambda \\ & (m_{ij} - l_{ij})\lambda w_j - w_i + l_{ij}w_j \leq 0, \\ & (u_{ij} - m_{ij})\lambda w_j + w_i - u_{ij}w_j \leq 0, \\ & \sum_{k=1}^n w_k = 1, \quad w_k > 0, \quad k = 1, 2, \dots, n \\ & i = 1, 2, \dots, n-1; \quad j = 2, 3, \dots, n; \quad j > i \end{aligned} \quad \text{Eq. 3-9}$$

The optimal solution to the non-linear problem above  $(w^*, \lambda^*)$  can be obtained by employing some appropriate numerical method for non-linear optimization. The optimal value  $\lambda^*$ , if it is positive (the maximum value is one), indicates that all solution ratios satisfy the fuzzy judgment completely, which means that the initial set of fuzzy judgments is rather consistent. A negative value of  $\lambda^*$  shows that the solutions' ratios approximately satisfy all double-side inequalities (**Eq. 3-3**). Therefore, the optimal value  $\lambda^*$ , can be used for measuring the consistency of the initial set of fuzzy judgments.

Generally, optimization deals with maximizing or minimizing an objective function and determining the optimum values for a set of variables so that a set of constraints are met. The non-linear optimization problem was solved by employing a numerical method in Matlab software. The optimization function “*fmincon*” is a medium-scale algorithm which attempts to find a constrained minimum of a scalar function of several variables  $x(i)$  starting at an initial estimate, generally referred to as constrained nonlinear optimization.

It was utilized to acquire the weights where the objective function and the constraints have different formats based on the matrices' sizes. The weight for each variable  $x(i)$  takes its value in the range of  $[0, 1]$  and its sum is equal to 1, while the consistency index  $\lambda$  takes its values in the range  $[-\infty, 1]$ . The optimization process was created and when the total constraints of a matrix are satisfied, the algorithm identifies the weights of its variables and considers the results are acceptable if there is consistency.

The full expression of the function is *fmincon* (*networkf*, *X0*, *A*, *B*, *Aeq*, *Beq*, *VLB*, *VUB*, *nonlcon*) where *networkf* represents the objective function and is predefined in the program file as  $f(x) = x(n + 1)$ ; *X0* is the initial estimates of the variables; *A* and *B* are the two coefficients of linear inequality constraint and can be ignored or replaced with two empty arrays  $[\ ]$  in the FPP; *Aeq* and *Beq* are the two coefficients of linear equality constraint  $Aeq \cdot x = Beq$ , as the sum of local weights should be one, they are represented by  $Aeq = [1 \ 1 \dots 1 \ 0]$ , and  $Beq = [1]$ ; *VLB* is the lower bound of the variables and is represented by  $[0; 0; \dots; 0; -\text{inf}]$  because all the local weights have a lower bound of zero, and the lower bound of the consistency index is negative infinity; *VUB* is the upper bound of the variables and is represented by empty array  $[\ ]$  since all the upper bounds are subject to the constraints; and the *nonlcon* is the nonlinear constraints, including non-linear inequality constraint and non-linear equality constraint for the cells above the diagonal as the triangular fuzzy comparison matrix is symmetric, and thus, for a  $(3 \times 3)$  fuzzy comparison matrix, only three elements need to be taken into account, while for a  $(5 \times 5)$  fuzzy comparison matrix, ten elements need to be considered to identify the matrix constraints.

### 3.3 Model Implementation

In order to implement the presented fuzzy analysis model, **Table 3-5** illustrates a fuzzified pairwise comparison sample of one respondent for the main performance parameters with respect to the selection of the NDT method. Each cell in the matrix has three values obtained from the fuzzification process. The matrix has 6 variables in linear equality constraint (5 local weights and a consistency index). According to the FPP method, every triangular fuzzy number  $(l_{ij} \ m_{ij} \ u_{ij})$  was first transformed into nonlinear two double-side inequality constraints as represented in **Equations 3-10 and 3-11**.

$$(m_{ij} - l_{ij}) * x(n + 1) * x(j) - x(i) + (l_{ij}) * x(j) \leq 0; \quad \text{Eq. 3-10}$$

$$(u_{ij} - m_{ij}) * x(n + 1) * x(j) + x(i) - (u_{ij}) * x(j) \leq 0 \quad \text{Eq. 3-11}$$

**Table 3-5: Pairwise comparison matrix of main performance parameters with respect to the selection of NDT technique**

Pairwise Comparison Among The Main Criteria					
Main Criteria	CAP	SP	SIM	ACC	CO
CAP	1,1,1	4,5,6	4,5,6	1/4,1/3,1/2	2,3,4
SP	1/6,1/5,1/4	1,1,1	1,1,1	1/9,1/9,1/8	3/8,3/5,3/2
SIM	1/6,1/5,1/4	1,1,1	1,1,1	1/9,1/9,1/8	3/8,3/5,3/2
ACC	2,3,4	8,9,9	8,9,9	1,1,1	8,9,9
CO	1/4,1/3,1/2	2/3,5/3,8/3	2/3,5/3,8/3	1/9,1/9,1/8	1,1,1

The weights of the matrix were calculated as follows: The below main program “*NDTcriteria.m*” file was constructed in Matlab where the file name was chosen so that it can easily be used when called:

```
[X, fval] = fmincon ('NDTcriteria', X0, [], [], Aeq, Beq, VLB, VUB,
'NDTnonlconcriteria', OPT)
```

$X0 = [0.3; 0.2; 0.2; 0.1; 0.2; 1]; Aeq = [1 \ 1 \ 1 \ 1 \ 1 \ 0]; Beq = [1]; VLB = [0; 0; 0; 0; 0; -inf];$   
and  $VUB = []$ ;

Where  $[X, fval]$  are the optimal solution for the local weights of the matrix and the optimal value of the consistency index, respectively. The corresponding objective function file “*NDTcriteria.m*” and the nonlinear constraint function file “*NDTnonlconcriteria.m*” were predefined by:

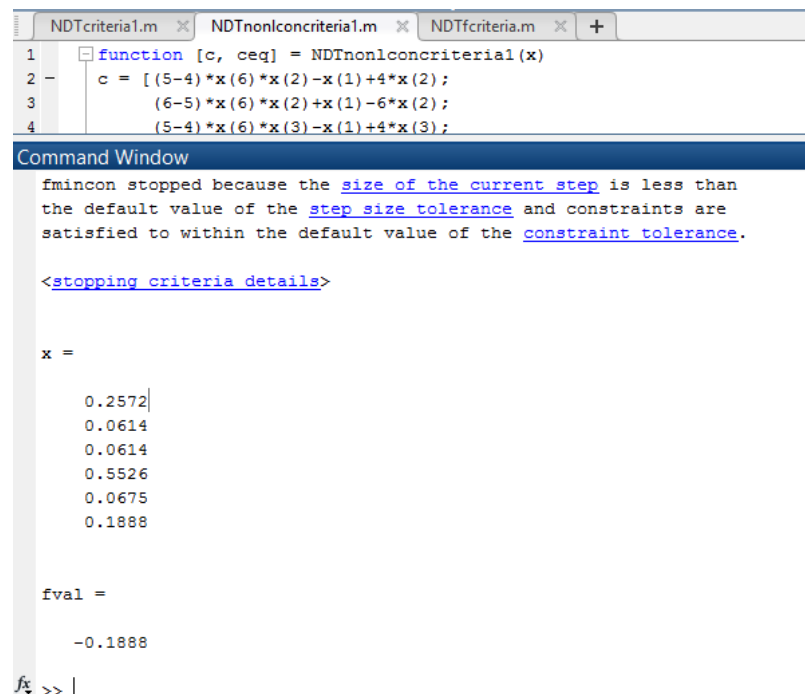
Function  $f = NDTcriteria(x); f = x(6)$ ; Function  $[C, Ceq] = NDTnonlconcriteria(x)$ ;

Where the value of function  $f$  is related to  $n$ , the nonlinear inequality constraint ‘ $C$ ’ is presented as per **Eq. 3-10** and **3-11**, and the nonlinear equality constraint  $Ceq$  is represented by an empty array  $[]$  as there is no nonlinear equality constraint for the FPP method. Thus, the Function  $[C, Ceq]$  was given by:

$$C = [(5-4)*x(6)*x(2) - x(1) + 4*x(2); (6-5)*x(6)*x(2) + x(1) - 6*x(2); (5-4)*x(6)*x(3) - x(1) + 4*x(3); (6-5)*x(6)*x(3) + x(1) - 6*x(3); (1/3-1/4)*x(6)*x(4) - x(1) + 1/4*x(4); (1/2-1/3)*x(6)*x(4) + x(1)1/2*x(4); (3-2)*x(6)*x(5) - x(1) + 2*x(5); (4-3)*x(6)*x(5) + x(1) - 4*x(5); (1-1)*x(6)*x(3) - x(2) + 1*x(3); (1-1)*x(6)*x(3) + x(2) - 1*x(3); (1/9-1/9)*x(6)*x(4) - x(2) + 1/9*x(4); (1/8-1/9)*x(6)*x(4) + x(2) - 1/8*x(4); (3/5-3/8)*x(6)*x(5) - x(2) + 3/8*x(5); (3/2-3/5)*x(6)*x(5) + x(2) - 3/2*x(5); (1/9-1/9)*x(6)*x(4) - x(3) + 1/9*x(4); (1/8-1/9)*x(6)*x(4) + x(3) - 1/8*x(4); (3/5-3/8)*x(6)*x(5) - x(3) + 3/8*x(5); (3/2-3/5)*x(6)*x(5) + x(3) - 3/2*x(5); (9-8)*x(6)*x(5) - x(4) + 8*x(5); (9-9)*x(6)*x(5) + x(4) - 9*x(5)];$$

$$Ceq = [ ];$$

The results after running the program are shown in **Fig. 3-5**, where the local weights  $x(1)$ ,  $x(2)$ ,  $x(3)$ ,  $x(4)$ ,  $x(5)$  are 0.2572, 0.0614, 0.0614, 0.5526, and 0.0675, respectively. The consistency index  $x(6)$  is 0.1888 > 0, which means the fuzzy comparison matrix has a good consistency, and the results are acceptable.



```

NDTcriteria1.m  NDTnonconcriteria1.m  NDTfcriteria.m  +
1  function [c, ceq] = NDTnonconcriteria1(x)
2  -   c = [(5-4)*x(6)*x(2)-x(1)+4*x(2);
3      (6-5)*x(6)*x(2)+x(1)-6*x(2);
4      (5-4)*x(6)*x(3)-x(1)+4*x(3);
Command Window
fmincon stopped because the size of the current step is less than
the default value of the step size tolerance and constraints are
satisfied to within the default value of the constraint tolerance.

<stopping criteria details>

x =

    0.2572
    0.0614
    0.0614
    0.5526
    0.0675
    0.1888

fval =

   -0.1888

fx >> |

```

**Figure 3-5: Weights and consistency index of the comparison matrix in Table 3-5.**

### 3.4 Evaluation and Ranking of NDT Techniques

The local weights were obtained for all participants' fuzzified pairwise comparisons, and then the calculated weights were averaged to obtain the final local weights for the main performance criteria, sub-criteria and NDT alternatives. The obtained weights were analyzed in order to check for inconsistency and unrealistic responses. The percent difference between the relative weights obtained from each of the gathered responses and the average weight was calculated. As a result, two of the questionnaires were discarded due to the high percent difference. The final global weights for the sub-criteria were obtained by multiplying the weights of the main performance criteria by the sub-criteria local weights. The final score for each NDT alternative was then obtained by summing the results of multiplying the weights of each method by the global weights of all sub-criteria. **Table 3-6** illustrates all the achieved weights and will be discussed below.

**Table 3-6: Performance measures weights and ranking of NDT techniques**

Pairwise Comparison Weights		NDT Alternatives						
Main Criteria	Main Criteria Weight	Sub-Criteria	Sub-Criteria Weight	IE	UPE	GPR	IRT	HCP
Capability	0.40	Delamination	0.18	0.40	0.20	0.10	0.30	0
		Vertical Cracks	0.07	0.45	0.55	0	0	0
		Steel Corrosion	0.15	0	0	0.40	0	0.60
Speed	0.09	Data Collection	0.05	0.17	0.15	0.24	0.24	0.20
		Data Analysis	0.03	0.15	0.14	0.21	0.23	0.27
		Potential for Automation	0.01	0.20	0.20	0.20	0.20	0.20
Simplicity	0.06	Experience Operator	0.02	0.15	0.12	0.20	0.28	0.25
		Experience Analyzer	0.03	0.15	0.12	0.20	0.25	0.28
		Environment Effect	0.01	0.23	0.18	0.24	0.15	0.20
Accuracy	0.32	Extent of Delamination	0.13	0.38	0.22	0.13	0.27	0
		Depth/Width of Cracks	0.08	0.45	0.55	0	0	0
		Presence of Corrosion	0.11	0	0	0.40	0	0.60
Cost	0.13	Equipment	0.03	0.18	0.12	0.23	0.21	0.26
		Data Collection	0.06	0.17	0.14	0.21	0.23	0.25
		Data Analysis	0.04	0.13	0.10	0.21	0.26	0.30
SUM	1.00		1.00					
<b>Total Score</b>				<b>0.23</b>	<b>0.18</b>	<b>0.21</b>	<b>0.16</b>	<b>0.22</b>

### 3.4.1 Weights of Main Performance Measures

As discussed above, each performance measure was assigned a weight value based on its importance in ranking the NDT alternatives. It can be observed from **Table 3-6** that the capability of the NDT techniques to detect specific deterioration mechanism(s) attained the highest weight of 40%, among all the five performance measures considered in this study. Indeed, the participants considered “capability” as the most fundamental and important performance measure for the evaluation of any NDT technology. This is because if a certain defect cannot be detected by a given technology, the other four performance measures are meaningless. Since the level of accuracy in the inspection result of any technology can be used to more easily assess changes in the condition of a bridge deck over its service life, the parameter “accuracy” obtained the second weight value of 32%. This emphasizes that, without a high level of accuracy in detecting defects in bridge decks, remediation and rehabilitation cannot be accomplished.

The performance parameter “cost” obtained the third priority after the capability and accuracy parameters with a weight value of 13%. This is because the cost/effectiveness ratio of a technique could directly affect its employment. In addition, a low cost technique may be compelling for its application before more expensive means are employed. The performance parameter “speed” of investigation using a technique is an advantage that could add value for a technique. Thus, it obtained the fourth weight value of 9%. Lastly, the performance parameter “simplicity” of employing a technique obtained a weight value of 6%. Simplicity could be advantageous for a technique as long as it provides comparable information to that achieved by other more sophisticated techniques. For a precise ranking, the NDT methods were evaluated below with the perspective of the sub-criteria’s of the main performance measures.

#### 3.4.1.1 *Evaluation of NDT Techniques from Perspective of Capability*

The NDT techniques were evaluated in perspective of their capability to detect specifically three types of defects: delamination, vertical cracking, and steel corrosion. The participants considered the ability of detecting delamination as the primary significant factor, thus it attained the highest weight value of 45%. The ability of the techniques to evaluate the

corrosive environment was the second significant factor with 38% weight value, while the ability to detect vertical cracks obtained the least weight value of 17%. The achieved weights of the different technologies with respect to these three factors are illustrated in **Fig. 3-6**. Comparing the achieved results confirms that: (i) four technologies have the capability of detecting delamination. The highest weight assigned for the IE method followed by the IRT and UPE methods and lastly the GPR method; (ii) the two methods having capability of detecting vertical cracks were UPE which obtained the highest weight, followed by the IE method; and (iii) two methods have capability to evaluate active corrosion of steel reinforcement: HCP and GPR, respectively. This complies with the physics of these methods, making them attractive in bridge deck evaluation.

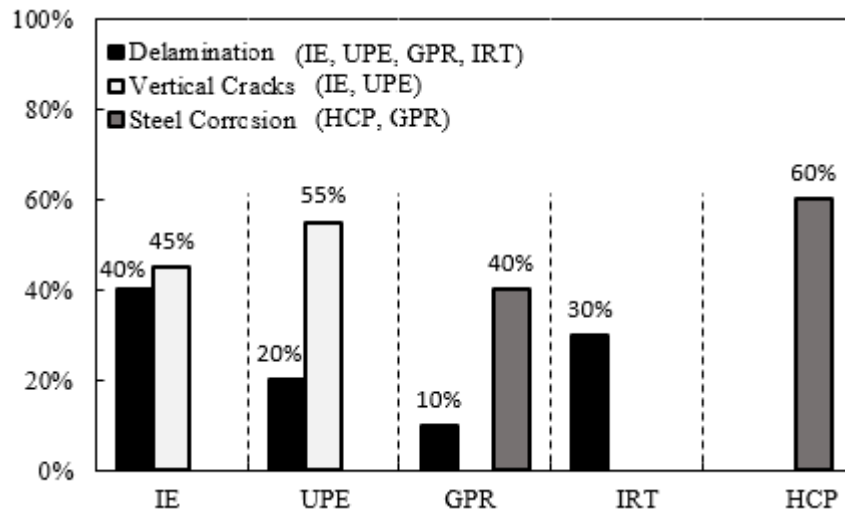


**Figure 3-6: Evaluation of NDT technologies with respect to their capability of specific defect detection.**

#### 3.4.1.2 *Evaluation of NDT Techniques from Perspective of Speed*

The NDT techniques were also evaluated in view of their speed during data collection and processing of the collected raw data, as well towards their potential to have an automation process. The participants considered the speed of data collection as the primary significant factor, which thus attained the highest weight value of 55%. The importance of this factor likely reflects the need to reduce the cost of traffic control and the inconveniences

associated with traffic interruptions during the data acquisition process. The speed of data analysis was the second significant factor with 30% weight value, while the potential of automation obtained the least weight value of 15%. The evaluation results of the five NDT techniques with respect to these three performance factors (**Fig. 3-7**) indicate that: (i) the GPR and IRT methods obtained the highest data collection weight since they are the fastest technologies as they can collect data in a continuous manner, while other technologies depend on spot measurements; (ii) HCP was identified as the technology that provides the highest speed of data analysis and interpretation because it indicates the likelihood of corrosion activity directly at the time of test; and (iii) based on the judgment of the participants; all the technologies have equal potential of automation and hence obtained equal weights.

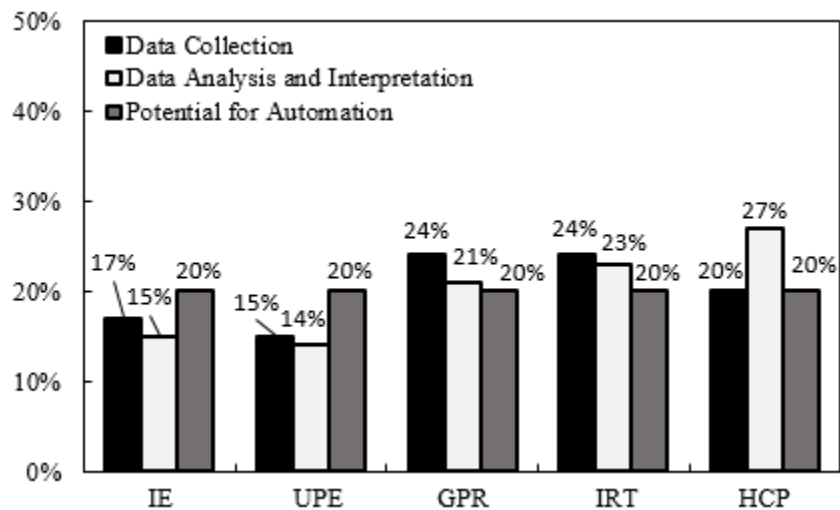


**Figure 3-7: Evaluation of NDT technologies with respect to their speed.**

### 3.4.1.3 *Evaluation of NDT Techniques from Perspective of Simplicity*

The NDT techniques were evaluated in view of the required expertise for data collection and analysis in addition to the effects of environmental conditions and traffic on the data acquisition process. The participants considered the expertise for data analysis as the primary significant factor, thus it attained the highest weight value of 45%. The expertise for data collection was the secondary significant factor with 40% weight value, while the

effect of environmental conditions and traffic obtained the least weight value of 15%. The achieved weights of the different technologies with respect to these three factors are illustrated in **Fig. 3-8**. Comparing the achieved results confirms that: (i) IE and UPE are the most sophisticated technologies that require a high level of expertise in both data collection and data analysis and interpretation. Thus, they obtained the minimum weights among the other technologies; (ii) the environmental conditions have a significant influence on employing the IRT, thus it obtained the lowest weight. In fact IRT testing typically requires clear skies, mild wind, dry concrete surface, and intense solar radiation to achieve the heat-flow conditions needed to detect the presence of delaminations.

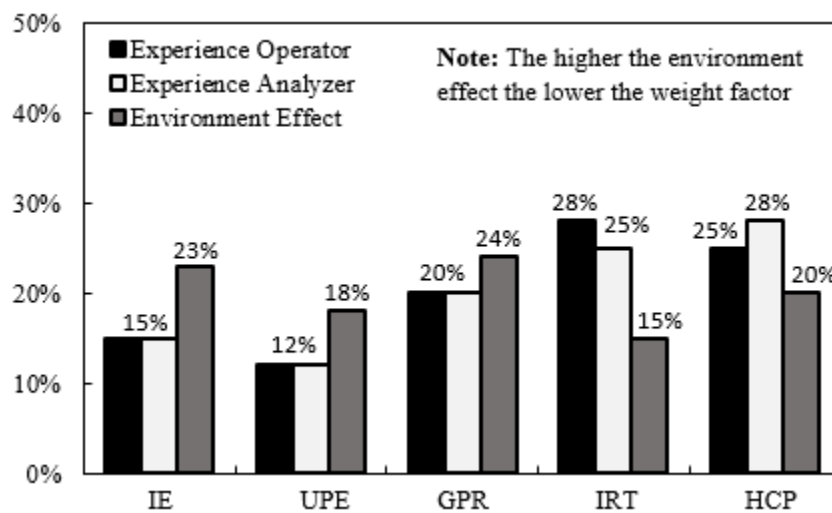


**Figure 3-8: Evaluation of NDT technologies with respect to their simplicity.**

#### 3.4.1.4 *Evaluation of NDT Techniques from Perspective of Accuracy*

The NDT techniques were evaluated in perspective of their ability to accurately locate defects. The participants considered the ability to detect the extent and severity of delamination as the primary significant factor, thus it attained the highest weight value of 40%. The ability of the techniques to evaluate the intensity of active corrosion was the second significant factor with 35% weight value, while the ability to detect the depth and width of vertical cracks obtained the least weight value of 25%. **Figure 3-9** illustrates the evaluation results of the five NDT techniques with respect to these three performance

factors. The results indicate that: (i) IE was identified as the technology that provides the highest accuracy in detecting the extent and severity of delamination, followed by the IRT, UPE, and GPR technologies; (ii) UPE was identified as the technology that provides highest accuracy in detecting crack depth and width, followed by the IE method; and (iii) HCP was identified as the technology that provides highest accuracy in evaluating corrosion activity, followed by the GPR method.

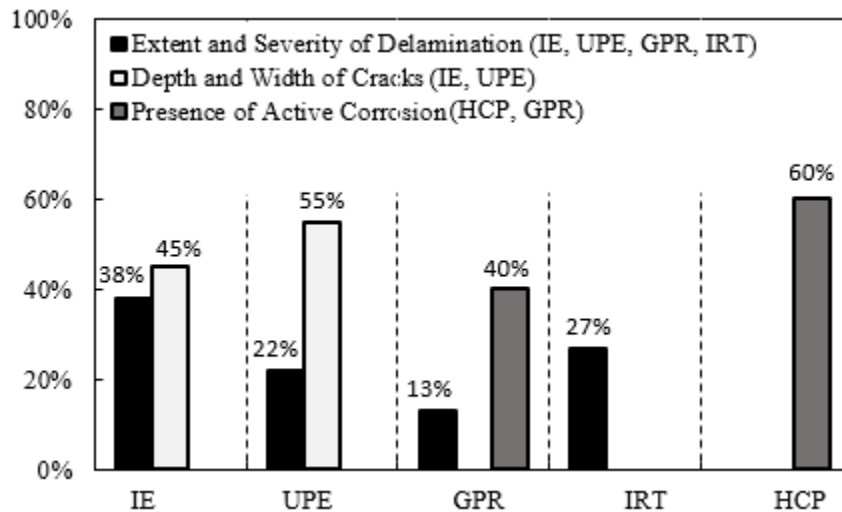


**Figure 3-9: Evaluation of NDT technologies with respect to their accuracy.**

#### 3.4.1.5 *Evaluation of NDT Techniques from Perspective of Cost*

The NDT techniques were evaluated in perspective of the cost of equipment, including maintenance costs; the cost of data collection including the number of operators, expertise level, cost of traffic control, and time needed to collect data; and the cost associated with data analysis and interpretation, including the number of analyzers, expertise level, and time needed to analyze and interpret. The participants considered the cost of data collection as the primary significant factor, thus it attained the highest weight value of 48%. The cost of data analysis and interpretation was the second significant factor with 32% weight value, while the cost of equipment obtained the least weight value of 20%. The achieved weights of the different technologies with respect to these three factors are illustrated in **Fig. 3-10**. Comparing the achieved results indicates that HCP is the lowest cost method with respect

to the three parameters, while IE and UPE are the most expensive methods. Thus, HCP obtained the maximum weight among the other technologies, while IE and UPE obtained the minimum weights.

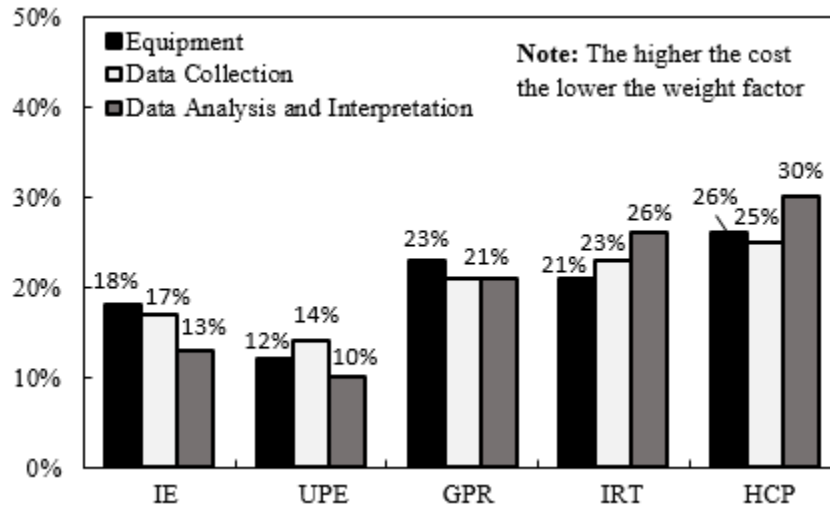


**Figure 3-10: Evaluation of NDT technologies with respect to their cost.**

### 3.4.2 Overall Ranking of NDT Techniques

The overall ranking of the technologies was conducted from high to low. The final score values are presented in **Table 3-6**. The results revealed that IE obtained the maximum score of 23%, the HCP ranked second with 22% and GPR third with 21%, while UPE and IRT received the minimum percentages of 18 and 16, respectively. It should be noted that this overall ranking came from the assigned weights of all parameters and hence was affected by the weights of the significant parameters, such as the capability and accuracy. The score could be changed if the comparison was made only between each group of technologies capable to detect a specific deterioration type. However, the results draw the attention to the fact that, while IE and HCP are currently highly regarded as the most commonly used methods to evaluate delaminations and the likelihood of rebar corrosion, respectively, there is a high potential to increase the use of GPR technology in evaluating the conditions of concrete bridge decks. It also indicates that most participants have concerns regarding IRT results.

For more rational evaluation, **Figure 3-11** illustrates the individual performance of the technologies from the perspectives of the five performance measures considered in this study. The figure indicates that the various NDT technologies are significantly different in terms of a selected performance parameter. For instance, the IE was generally considered by the participants as the most accurate technology. In fact several experts commented in the questionnaire that IE was generally consistent with results from coring when they were carefully performed, but it is also a time consuming method. They further mentioned that GPR could obtain a higher relative importance weight if the delaminated areas under investigation were moist. Evaluating IRT by the experts as the lowest accurate technology could be due to its high sensitivity to the effects of environmental conditions, and thus it is difficult to establish a rule-based criterion to evaluate its raw data. With respect to speed, the figure indicates that the IRT, GPR, and HCP methods were generally considered as the speediest technologies. Although different levels of expertise and experience are needed for the compared technologies, the HCP and IRT were generally considered as the simplest technologies. Similarly, the HCP and IRT were generally considered as the lowest cost technologies followed by the GPR method.

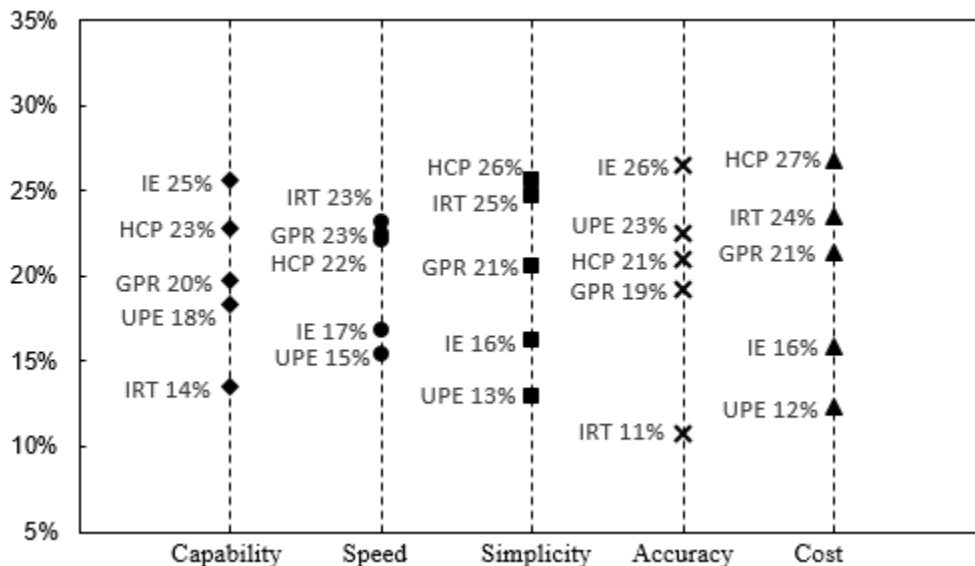


**Figure 3-11: Overall evaluation of NDT technologies with respect to the main performance criteria.**

### 3.5 Validation of Model Results

Indeed, comparing the different NDT techniques based on quantifiable data provides more precise and objective evaluation. Therefore, the achieved results were validated through the findings of some comparative research studies, identified in the open literature that compared various NDT techniques qualitatively and quantitatively. In these comparative studies, each technique has been compared to at least one other technique with respect to different performance parameters. **Table 3-7** summarizes the explored studies and their major findings. For instance, Barnes and Trottier (2000) utilized the HCP and GPR techniques to evaluate nine RC bridge decks and then compared the results with actual recognized and repaired areas. They reported that accurate identification of the defects was indicated by the HCP tests. Good spatial and quantitative correlation was also observed between the GPR-predicted defect locations and the actual deterioration found on the nine decks using the ground-truth survey methods.

Scott *et al.* (2003) applied IE and GPR testing on a full-scale RC bridge deck and reported that all delaminations identified by the IE were validated by the results of core samples extracted from the deck, while the GPR tests provided more rapid inspection, yet were not able to consistently identify delaminations. Yehia *et al.* (2007) conducted a study to determine the reliability of IE, GPR, and IRT technologies on concrete slabs fabricated with three types of flaws (cracks, delaminations, and voids) of known location and dimension. They reported that the IE results identified the extent and depth of all defects efficiently, while the IRT only detected the shallower defects. GPR testing was fairly good at detecting delaminations, but had difficulties with voids and could not detect cracks. Both IRT and GPR testing provided rapid inspections, while the IE was a time-consuming method. Oh *et al.* (2013) utilized air-coupled IE and IRT techniques to evaluate an in-service RC bridge deck. The methods were compared across performance criteria, considering accuracy, testing practicality and cost. They reported that IRT is a very effective approach for rapid detection of shallow defects, although it is hindered by the relatively high capital cost of equipment and high sensitivity to the ambient environment and surface conditions. The air-coupled IE showed good performance and accurate results for bridge decks under active ambient traffic noise and vibration conditions.

Gucunski *et al.* (2013) published a comprehensive study of nine NDT techniques that were utilized in the SHRP2 project to identify typical deterioration mechanisms in RC bridge decks. The evaluated techniques included those adopted in the present research. Ten organizations (NDT service providers, research institutions, and consultants) conducted validation testing in the field and laboratory. After completion of the testing, the data were analyzed and quantitative results were used for the evaluation process in which five performance measures were considered: accuracy, repeatability, ease of use, speed, and cost. Evaluation of the technologies' accuracy was limited by the extent of ground truth information, and hence, was done only through laboratory testing. The report concluded that IE was the most accurate technology in detecting delamination defects, followed by the IRT method. The HCP and electrical resistivity were the two precise technologies to measure the potential of corrosion activity. The surface wave transmission method was the most appropriate for measuring the depth of cracks, whereas the ultra-sonic surface wave method was most successful in quantifying the degradation of concrete. The IE and GPR were the two technologies that had highest potential of repeatability. The IRT testing provided highest inspection speed, followed by the GPR and HCP techniques. In addition, IRT was the easiest technology to use, followed by the HCP method, which was also reported as the least expensive technology. These findings comply to a large extent with the results obtained from the model developed in the present research.

**Table 3-7: Comparative studies which utilized several NDT techniques on RC bridge decks**

Reference	Techniques Utilized	Performance Indicator	Outcomes
• Alt and Meggers (1996)	• IRT, GPR	• Capability, accuracy, repeatability	• Both IRT and GPR were not able to identify all subsurface anomalies due to the concrete and asphalt overlays.
• Barnes and Trottier (2000)	• GPR, HCP, CD	• Accuracy, variability	• GPR provided good spatial and quantitative correlation compared with the HCP and ground-truth results.
• Scott et al. (2003)	• IE, GPR, CD	• Capability, accuracy, speed	• IE results were consistent with coring results, while GPR did not produce consistent responses to delamination.
• Clark et al. (2003)	• IRC,CD	• Accuracy	• IRT successfully identified most delaminations, even though the survey conditions were imperfect.
• Yong and Kee (2003)	• GPR, IE, IR	• Capability	• IE and IR identified hidden anomalies (voids & delamination) having good agreement with ground-truth results.
• Yehia et al. (2007)	• IE, IRT, GPR	• Capability, accuracy, speed, equipment cost	• IE identified all defects, while IRT identified only shallower defects. IRT was the faster method, followed by GPR and IE.
• Gucunski and Nazarian (2010)	• IE, GPR, HCP, USW, ER	• Capability, accuracy	• IE identified delaminations. HCP and ER enabled the assessment of likelihood and severity of corrosion.
• Algernon et al. (2010)	• IE, UPE, Covermeter	• Capability, accuracy	• UPE identified accurate thicknesses of the concrete blocks and IE efficiently located irregularities within the blocks.
• Arndt et al. (2010)	• HCP, GPR, IRT, IE, UPE	• Capability, repeatability	• The HCP/GPR testing monitored the probability of active corrosion. IE identified the defects and the low stiffness areas.
• Oh et al. (2013)	• IE, IRT, CD	• Accuracy, practicality, cost	• IE enabled efficient detecting of delaminations. IRT detected shallow delaminations only.
• Gucunski et al. (2013)	• IE, GPR, HCP, USW, ER, IRT, UPE, IR	• Accuracy, repeatability, ease of use, speed, cost	• IE was the most accurate in detecting delaminations, HCP was accurate in measuring potential of corrosion activity. Tests for all techniques were relatively repeatable. IRT and HCP were the easiest technologies and HCP was the least expensive.

Note: CD (Chain Drag); USW (Ultrasonic Surface Waves); ER (Electrical Resistivity); IR (Impulse Response)

### 3.6 Evaluation of the Proposed Model

This study attempts to provide a rational basis to transportation agencies guiding their efforts to incorporate NDT techniques into bridge inspection procedures through the evaluation of five NDT techniques. Because the data source used in the development of the proposed evaluation methodology came from a survey of bridge owners, consultants and researchers, it was important to only consider expertise with high level of interest in NDT applications. For instance, expertise sourced from a certain network might have a common perception of a particular performance parameter. Thus, including experts from different agencies was considered beneficial to incorporate diversity and ensure representation of different perspectives. It was unlikely that the respondents had experience or were familiar with all the evaluated five NDT technologies. Thus, participation was considered only for experts who had experience with at least three of the NDT of interest. Furthermore, the experts were requested to have their evaluation based solely on evidence used to validate the outcomes of the NDT techniques employed in their schemes (e. g. coring, chloride content...etc). Such a plan was taken into account in order to ensure that the results of the analysis represent the performance of the technologies rather than a popularity contest of NDT alternatives.

The overall ranking of the technologies in this comparative study was, to some extent, influenced by the selected performance measures and the applied weights in the evaluation process. Therefore, some suggestions for improvement were received from the experts. For example, three respondents highlighted that the performance measures should include “commercial availability” since it might influence selection by bridge engineers for a specific project. Another two participants highlighted that the ultrasonic pulse echo method was not used frequently, while choosing surface wave methods could be more appropriate. Another respondent advised that low cost, commercially available remote sensing technologies are an efficient solution to enhancing and monitoring the condition assessment of bridge decks. Although such comments are valuable, it should be noted that the idea here is to propose a methodology rather than apply the exact numbers achieved in the present research. Moreover, the proposed hierarchy structure can be customized to accommodate different transportation agency policies.

However, regardless of the accuracy of results in terms of the applied model and the presented fuzzy analysis, it should be noted that there is no technology that is a "solve-all" solution to assessing the condition of a bridge deck. Each of the evaluated technologies has some drawbacks and is appropriate for a specific type of defect/problem. For instance, IE, the technology which obtained the highest ranking in this study, requires many testing points and inadequate receiver contact can yield inaccurate and false measurements. Furthermore, testing rough concrete surfaces could affect the establishment of the low impulse time necessary to detect small and shallow defects. The HCP testing does not provide quantitative information on the corrosion rate. In addition, it cannot be used in the presence of coated rebar and its measurements can be influenced by numerous material properties. GPR can indirectly assess the potential of rebar corrosion, while the presence of congested reinforcement can prevent GPR signal penetration. In addition, GPR does not provide information on the corrosion rate. The results of the UPE technology could be significantly affected by the attenuation of the transmitted pulses. The IRT as a remote sensing technology could provide real-time results, but is dependent on ambient conditions and its conventional inspection method cannot indicate the depth of delaminations and voids. Recently, Washer (2016) introduced the ultra-time domain IRT technology based on IR continuous monitoring and reported that applying long term measurements using IR camera is capable of detecting the depth of delaminations in RC bridge decks.

The decision on which NDT technology to select or equipment to acquire for a specific project depends primarily on the type of deterioration representing the highest concern to the transportation agency and the degree of deterioration details required. Generally, an optimal selection strategy would seek to minimize the costs of inspection, while still ensuring an adequate accuracy and reliability of the NDT technique to be utilized. However, the decision could be controlled by many other criteria, such as the size and complexity level of the network, geographic location, traffic density, environmental conditions, how the assessment data will be used, and available time to conduct the evaluation. Moreover, the selection process should be accompanied by a comprehensive cost-benefit analysis. It should be noted that, generally, to achieve a reliable evaluation of a bridge deck condition, the selected NDT technique(s) must be suitable for the components of the bridge deck under investigation. The testing must be performed by

qualified personnel with adequate knowledge of the requirements and specifications that are relevant to their applications and limitations.

Indeed, integrating several NDT techniques has emerged to provide more reliable evaluation on the condition of bridge decks. Therefore, research has attempted to integrate two or more NDT techniques to detect all possible defects and improve the assessment process. For example, the FHWA has recently developed the “RABIT” bridge deck assessment device. RABIT (Robotics Assisted Bridge Inspection Tool) is a fully autonomous robotic system for the condition assessment of concrete bridge decks using the results of multi-model NDT, which utilizes the electrical resistivity, impact echo, ultrasonic surface waves, and ground penetrating radar technologies. The robot’s data visualization platform facilitates an intuitive 3-D presentation of three deterioration types (rebar corrosion, delamination, and concrete degradation) and deck surface features (Gucunski *et al.*, 2015). However, because not all the transportation agencies employ fully NDT evaluation due to the associated costs, they should have access to at least two of the five technologies explored herein for a better understanding of a deck’s condition. This will also make the assessment of a large population of bridge decks more feasible.

### **3.7 Conclusions**

Transportation agencies have a great need to evaluate bridge deck conditions using NDT techniques in order to optimize the effective timing, scope, and approaches for preventive maintenance, repair, and replacement. An attempt has been made in the present research to critically analysis the performance of commonly utilized NDT technologies to assess the condition of RC bridge decks. Thus, hierarchical decision modeling was utilized as an effective management tool to evaluate the performance of five NDT technologies. AHP, which is a well-known multivariable decision making methodology, provides a basis for group decision making and can utilize both qualitative and quantitative criteria in the same framework. The proposed model was developed based on a combination of literature review and questionnaire survey with subject matter experts representing different bridge community organizations. The NDT methods were evaluated and ranked based on a set of flexible multi-attributed criteria and sub-criteria, developed to form a hierarchical decision. The different hierarchal elements were assigned pairwise comparisons using a fundamental

scale of absolute values that represent the strength of judgements by the participants. In order to make the evaluation analysis more precise, the fuzzy set theory was adopted to deal with vagueness and uncertainty in the decision making process. The results of the developed model were validated through the findings of multiple research studies retrieved from the open literature, which deployed physical laboratory and field NDT testing. The outcomes revealed that no single technology is capable of recognizing all three primary defect types, and that comprehensive condition assessment could be better conducted using more than one technique to compensate for each single technique limitations. The factors that could affect the selection of a NDT technique were discussed. Applying this management aspect can assist bridge stakeholders in the appraisal and selection of different NDT technologies to detect different types of bridge deck health indicators at both the project and network levels.

### 3.8 References

- Algernon, D., Hiltunen, D., and Ferraro, C. (2010). “*Validation of nondestructive testing equipment for concrete.*” Department of Civil and Coastal Engineering, University of Florida, Final Report, 142 p.
- Alt, D., and Meggers, D. (1996). “*Determination of bridge deck subsurface anomalies using infrared thermography and ground penetrating radar.*” Report FHWA-KS-96-2, Kansas, DOT, 18 p.
- Arndt, R., Jalinoos, F., Cui, J., Huston, D. (2010). “Periodic NDE for bridge maintenance.” *Proc., Structural Faults and Repair Conference*, Edimburgh, 1-10.
- Barnes, C. and Trottier, J. (2000). “Ground-Penetrating Radar for Network-Level Concrete Deck Repair Management.” *Transportation Engineering*, Vol. 126 (3), 257-262.
- Baruch, Y. (1999). “Response rate in academic studies-A comparative analysis.” *Human Relations*, Vol. 52 (4), 421-438.
- Bhattacharyya, R., Kumar, P. and Kar, S. (2011). “Fuzzy R&D portfolio selection of interdependent projects.” *Computers and Mathematics with Applications*, Vol. 62, 3857-3870.
- Buckley, J. (1985). “Fuzzy hierarchical analysis.” *Fuzzy Sets and Systems*, Vol. 17, 233-247.
- Chang, Y., (1996). “Application of the extent analysis method on fuzzy AHP.” *European, Operational Research*, Vol (95), 649–655.
- Chang, T., and Lee, H. (2012). “A fuzzy DEA and knapsack formulation integrated model for project selection.” *Computers and Operations Research*, Vol. 39, 112-125.

- Clark, M. R., McCann, D. M., and Forde, M. C. (2003). "Application of infrared thermography to the non-destructive testing concrete and masonry bridges." *NDT&E International*, Vol. 36 (4), 265-275.
- Csutora, R., and Buckley, J. J. (2001). "Fuzzy hierarchical analysis: The Lamda-Max method." *Fuzzy Sets and Systems*, Vol. 120, 181-195.
- Gucunski, N., Kee, S., La, H., Basily, B., Maher, A., and Ghasemi, H. (2015). "Implementation of a Fully Autonomous Platform for Assessment of Concrete Bridge Decks RABIT." *Proc., Structure Congress*, ASCE, Reston, VA, 367-378.
- Gucunski, N., Imani, A., Romero, F., Nazarian, S., Yuan, D., Wiggenger, H., Shokouhi, P., Taffe, A., and Kutrubes, D. (2013). "NDT to identify concrete bridge deck deterioration." *Proc., 92nd Annual Meeting, TRB*, SHRP 2 Report, 96 p.
- Gucunski, N., and Nazarian, S. (2010). "Material Characterization and Condition Assessment of Reinforced Concrete Bridge Decks by Complementary NDE Technologies." *Proc., Structures Congress*, ASCE, Orlando, FL, 429-439.
- Hesse, A., Atadero, R., and Ozbek, M. (2015). "Uncertainty in Common NDE Techniques for Use in Risk-Based Bridge Inspection Planning: Existing Data." *Bridge Engineering*, Vol. 20 (11), 1-8.
- Huang, C., Chu, P., and Chiang, Y. (2008). "A fuzzy AHP application in government-sponsored R&D project selection." *The International. Management Science*, Vol. 36, 1038-1052.
- Huo, L., Lan, J., and Wang, Z. (2011). "New parametric prioritization methods for an analytical hierarchy process based on a pairwise comparison matrix." *Mathematical and Computer Modelling*, Vol. 54 (11-12), 2736-49.
- Jakiel, P., and Fabianowski, D. (2015). "FAHP model used for assessment of highway RC bridge structural and technological arrangements." *Expert Systems with Applications*, Vol. 42, 4054-4061.
- Mikhailov, L. (2004). "Group prioritization in the AHP by fuzzy preference programming method." *Computers and Operations Research*, Vol. 31 (2), 293-301.
- Oh, T., Kee, S.-H., Arndt, W., Popovics, S., and Zhu, J. (2013). "Comparison of NDT methods for assessment of a concrete bridge deck." *Engineering Mechanics*, Vol. 139 (3), 305-314.
- Saaty. (1980). "*The analytic hierarchy process: Planning, Priority Setting and Resource Allocation*." Book, Publisher: McGraw-Hill, New York, 237 p.
- Sasmal, S., and Ramanjaneyulu, K. (2008). "Condition evaluation of existing reinforced concrete bridges using fuzzy based analytic hierarchy approach." *Expert Systems with Applications*, Vol. 35 (3), 1430-1443.
- Scott, M., Rezaizadeh, A., Delahaza, A., Santos, C., and Moore, M., Graybeal, B., Washer, G. (2003). "A comparison of nondestructive evaluation methods for bridge deck assessment." *NDT&E International*, Vol. 36, 245-255.

- Srdjevic, B. (2005). "Combining different prioritization methods in the-analytic hierarchy process synthesis." *Computers and Operations Research*, Vol. 32, 1897-1919.
- Van Laarhoven, P. J. M. and Pedrycz, W. (1983). "A fuzzy extension of Saaty's priority theory." *Fuzzy Sets and Systems*, Vol. 11 (1/3), 229-241.
- Wang, Y. and Elhag, T., (2008). "Evidential reasoning approach for bridge condition assessment." *Expert Systems with Applications*, Vol. 34 (1), 689–699.
- Washer, G. (2016). "*Infrared Technologies for Bridge Maintenance*." University of Missouri. Report, 35 p.
- Wood, J. C., and Rens, K. L. (2006). "Nondestructive testing of the Lawrence Street Bridge." *Proc., Structures Congress*, ASCE, Reston, VA, 1–15.
- Yehia, S., Abudayyeh, O., Nabulsi, S., and Abdel-Qader, I. (2007). "Detection of Common Defects in Concrete Bridge Decks Using NDE Techniques." *Bridge Engineering*, Vol. 12, 215-225.
- Yong Hao Z., and Kee Ee Ng. (2003). "Evaluation of concrete structures by advances non-destructive test methods-impact echo, impulse response test and radar survey." *Proc., NDT-CE conference*, Berlin, 1-4.
- Zhou, X. (2012). "*Fuzzy Analytical Network Process Implementation with Matlab*." *MATLAB - A Fundamental Tool for Scientific Computing and Engineering Applications – Vol. 3*", Book edited by Vasilios N. Katsikis, Open Access, Chapter 6, 133-160.

## Chapter 4

### 4. Infrared Thermography Model for Rational Condition Assessment of Reinforced Concrete Bridge Decks

#### 4.1 Introduction

Subsurface delaminations are serious and common defects that affect the structural integrity and reduce the service life of RC bridge decks. Delamination could also be indicative of deterioration and potential active corrosion. Therefore, locating and defining the extent of this damage in its initial stages is critical to ensure bridge safety and optimize maintenance and repair needs. Detecting subsurface delaminations in RC bridge decks without physical contact is a considerable advantage of infrared thermography (IRT). Such subsurface anomalies can be detected on the basis of variable concrete properties, such as density, thermal conductivity and specific heat capacity. Data collection using remote sensing technology with thermal IR imagery can reduce traffic disruption and lane closures on and underneath bridge decks, and thus it is less costly than other NDT methods. Generally, IRT testing collects radiant temperature and visualizes the data in the form of real-time thermal infrared images. However, the infrared images can be difficult to interpret, and thus specific data acquisition training is often required (Vaghefi *et al.*, 2012).

There is a dearth of research on the interpretation process of IRT data. In the majority of IRT analyses, the post-processing of IR images depends on the analyzer's personal experience since defective areas are usually identified and calculated based on a visual interpretation approach. Such qualitative and subjective analyses provide quick decisions using the difference in the temperature of the region of interest and a reference region but can lead to inconsistency in the obtained results. Therefore, overcoming the obstacles of IRT data analysis is necessary to tailor this rapid and reliable evaluation technique for RC bridge decks. In this Chapter, a novel procedure to detect and classify subsurface delamination in full-scale RC bridge decks under passive IRT testing is developed. To achieve this goal, the following objectives are pursued throughout the chapter sections: (1) studying the working principles of IRT and the current methods to analyze and interpret the IR thermal data; and (2) developing an automated procedure to: (a) generate a

mosaicked thermogram of the entire bridge deck from individual IR images, (b) identify objective thresholds in order to recognize the sound and defective deck areas and to classify the severity of the defective regions, (c) produce a condition map of the entire bridge deck, delineating the sound and different classes of defects, and (d) quantify the detected delamination defects in each category.

**Figure 4-1** illustrates the adopted systematic methodology to achieve the above-mentioned objectives. It can be summarized as follows: (1) conducting a passive IRT survey in-situ on a full-scale deteriorated concrete bridge deck using an advanced thermal camera; (2) initializing acquisition and storage of the IRT data using the Matlab image acquisition toolbox; (3) enhancing the images' resolution by increasing its dynamic range and reducing the inherent noise using the Flir software; (4) developing a stitching algorithm to create a mosaicked thermogram of the entire bridge deck using especially written Matlab codes; (5) constructing a framework to determine the number of defects' condition categories (clusters) of the subsurface anomalies; (6) segmenting the mosaic to determine the threshold values using the k-means clustering algorithm, a machine learning unsupervised technique, in the Matlab software; (7) creating an IR condition map delineating different categories of the delamination severity using a commercial mapping software; (8) implementing the developed procedure in four full-scale bridge decks; and (9) validating the condition maps with results provided by other technologies on the same bridge decks.

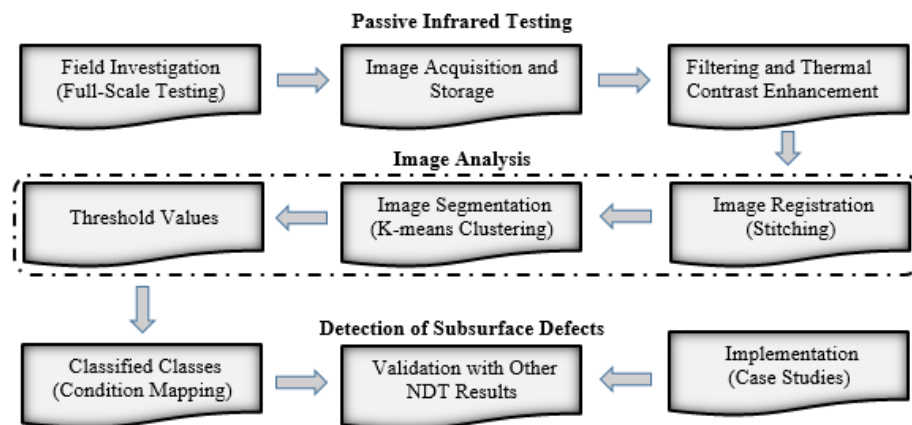


**Figure 4-1: Methodology adopted in developing IRT model to detect and classify subsurface delamination in RC bridge decks.**

## 4.2 Infrared Thermography Technology

This section provides an introduction to the theory of IRT technology along with its application to the in-situ inspection of RC bridges. A brief review of the basic principles of heat transfer and thermal imaging, a review of IR cameras, and application and interpretation of passive IRT testing are presented.

### 4.2.1 Basic Principles of IRT

#### 4.2.1.1 IR Radiation

Any object at a temperature above the absolute zero (-273.15 degrees Celsius or 0 Kelvin) emits infrared radiation (below red). Infrared radiation lies between the visible and microwave portion of the electromagnetic spectrum where the usable part is approximately defined from 0.8 to 14  $\mu\text{m}$ . This range can be further subdivided into near-infrared (0.8-1.5  $\mu\text{m}$ ), short-wavelength infrared (1.5-2.5  $\mu\text{m}$ ), mid-wavelength infrared (2.5-8  $\mu\text{m}$ ), and long-wavelength infrared (8-14  $\mu\text{m}$ ). We experience infrared radiation every day. For instance, the heat that we feel from sunlight, a fire or a radiator is all infrared. Although our eyes cannot see it, the nerves in our skin can feel it as heat. The intensity of the infrared radiation emitted by objects is mainly a function of their temperatures and radiation wavelengths. **Figure 4-2** illustrates the infrared region in the electromagnetic spectrum.

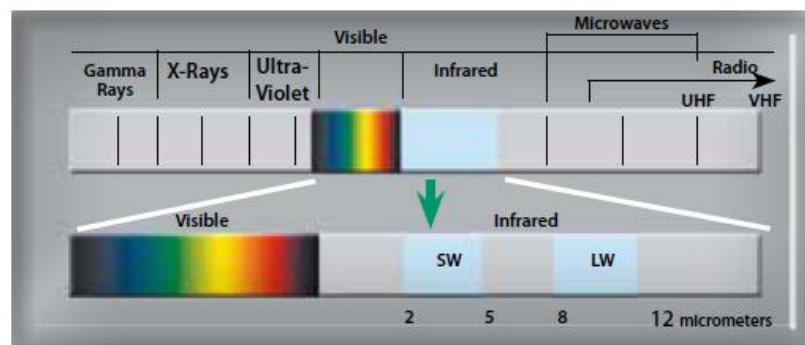


**Figure 4-2: Infrared region in the electromagnetic spectrum (FLIR Guidebook).**

In the thermal radiation theory, there are three ways by which the radiant energy striking an object can be dissipated: absorption, transmission and reflection (Robert, 1982). IRT

employs infrared sensors to detect thermal radiation emitted from materials, and creates an image of surface temperatures based on the emitted radiation. In addition to emitting radiation, an object reacts to incident radiation from its surroundings by absorbing and reflecting a portion of it, or allowing some of it to pass through. From this physical principle, the radiation law is derived as per **Equation 4-1**, which can be simplified as per **Equation 4-2**.

$$E = \alpha E + \beta E + \tau E \quad \text{Eq. 4-1}$$

$$\alpha + \beta + \tau = 1 \quad \text{Eq. 4-2}$$

The coefficients  $\alpha$ ,  $\beta$ , and  $\tau$  describe the object's incident energy absorption ( $\alpha$ ), reflection ( $\beta$ ), and transmission ( $\tau$ ). Each coefficient can have a value from zero to one, depending on how well an object absorbs, reflects, or transmits incident radiation. Stefan-Boltzmann further developed the formula presented in **Equation 4-3**, where the intensity of the infrared radiation emitted by objects was directly proportional to the fourth power of its absolute temperature (Robert, 1982). As per the formula, the amount of radiation increases with temperature. Therefore, the warmer the object the greater the intensity of the emitted infrared radiation.

$$E_{rad} = \varepsilon \sigma T^4 \quad \text{Eq. 4-3}$$

Where:  $E$  is the radiation energy ( $\text{W}\cdot\text{m}^{-2}$ ),  $\sigma$  is Stefan-Boltzmann constant ( $5.67 \times 10^{-8} \text{ W m}^{-2} \text{ K}^{-4}$ ),  $T$  is the surface temperature (Kelvin), and  $\varepsilon$  is the object's emissivity (unit-less value). A material's emissivity is the ability of its surface to emit energy by radiation relative to a black body. In other words it is the ratio of the radiant energy emitted by the body to the radiant energy emitted by a black body at the same temperature. A blackbody is considered as a hypothetical object which absorbs all incident radiations (the transmissivity and the reflectivity are null) and radiates a continuous spectrum. For a perfect blackbody, emissivity is unity, but for real surfaces it is always less than unity. For

concrete, this property is typically greater than 0.92 (Meola, 2012). Emissivity is important in terms of analyzing thermographic images, because different materials may emit radiation at different rates, even though they may be at the same temperature. However, the surface roughness and moisture content of the concrete can influence its emissivity value. The presence of other materials on the surface of the concrete (e.g. staining, water, lane markings, etc.), which have different emissivity properties, can result in apparent temperature variations in the IR image and possibly mask the thermal contrasts created by subsurface anomalies (Clark *et al.*, 2003).

#### 4.2.1.2 *Heat Transfer*

Heat energy moves by conduction, convection and radiation. The thermal energy, received by the concrete surface due to the sun's rays, depends on the concrete absorptivity and the solar radiation on the concrete surface as per **Equation 4-4**. The solar radiation depends on geographical location and the position of the sun relative to the surface of the concrete, whereas absorptivity is a measure of the efficiency of receiving radiated heat.

$$E_s = \alpha_s I_s \quad \text{Eq. 4-4}$$

Where  $\alpha_s$  is the absorptivity of concrete and  $I_s$  is the solar radiation on the concrete surface.

The thermal energy, transfer by convection as a result of temperature differences between the concrete surface and the surrounding air, is given by Newton's law of cooling according to **Equation 4-5**.

$$E_{conv} = h (T_s - T_a) \quad \text{Eq. 4-5}$$

Where  $h$  is a convection coefficient,  $T_a$  is the ambient temperature, and  $T_s$  is the surface temperature of the concrete. The convection coefficient depends on many factors, such as surface roughness and surface area of the concrete, wind velocity, and thermal properties of the air. The convective heat transfer is positive when the ambient temperature is less than the temperature of the concrete, for example, when radiant heating from the sun warms

the concrete above the ambient temperature. In this case, increased wind speed will result in increased energy transfer from the concrete to the surrounding environment. Accordingly, the thermal gradients in the concrete reduces (Washer *et al.*, 2013). In other words convective cooling for solar exposed surfaces may counteract the radiant heating of the sun, and reduce the thermal gradient in the concrete. Conversely, if the ambient temperature is warmer than the concrete, for example, when ambient temperatures are increasing but there is no heating from the sun, then the convective heating transfer is negative. In this case, increased wind speed will accelerate the heat transfer to the concrete, and increase the thermal gradients in the concrete, thereby increase the detectability of a subsurface delamination.

Within the concrete solid, heat transfer via conduction occurs and is affected by its thermal conductivity, which indicates how quickly heat flows through the concrete. It depends on the aggregate types used in the concrete mixture. The thermal diffusivity is the thermal conductivity divided by the volumetric heat capacity. A high thermal diffusivity means that heat transfer through a material will be rapid and the amount of storage will be small. Conversely, low thermal diffusivity indicates a slower rate of heat transfer and a large amount of heat storage (Bagavathiappan *et al.*, 2014). Heat capacity is defined as the amount of heat needed to raise the temperature of a unit mass of a material by one degree and describes its ability to store heat. For the one dimensional plane, the thermal energy transfer by conduction is expressed according to **Equation 4-6**, while the ability of the concrete to conduct and store heat is commonly represented by its thermal inertia, computed as the square root of the product of its thermal conductivity, density, and heat capacity as per **Equation 4-7**.

$$K_{cond} = K \left\{ \frac{T_s - T_a}{L} \right\} \quad \text{Eq. 4-6}$$

$$I = \sqrt{K \sigma C} \quad \text{Eq. 4-7}$$

Where  $K$  is the thermal conductivity,  $L$  is the concrete thickness in the direction of heat flow,  $\sigma$  is the density, and  $C$  is the heat capacity.

### 4.2.2 Infrared Cameras

IR cameras are designed for a specific range of the IR spectrum. An IR camera measures the intensity of emitted infrared radiation from an object and converts it into a visible image. The fact that radiation is a function of object surface temperature makes it possible for the camera to calculate and display this temperature. However, the radiation measured by the camera not only depends on the temperature of the object, but is also a function of the emissivity. Radiation also originates from the surroundings and is reflected in the object. The radiation from the object and the reflected radiation will also be influenced by the absorption of the atmosphere. To measure temperature accurately, it is therefore necessary to compensate for the effects of a number of different radiation sources. The object parameters that must be supplied for the camera include the emissivity of the object, the reflected apparent temperature, the distance between the object and the camera, the relative humidity, and the temperature of the atmosphere.

The main components of IR cameras are a lens that focuses IR onto a detector, plus electronics and software for processing and displaying the signals and images. The configuration of a typical IR camera is shown in **Fig. 4-3**. Infrared energy (A) coming from an object is focused by the optics (B) onto an infrared detector (C). The detector sends the information to sensor electronics (D) for image processing. The electronics translate the data coming from the detector into an image (E) that can be viewed in the viewfinder or on a standard video monitor or LCD screen.

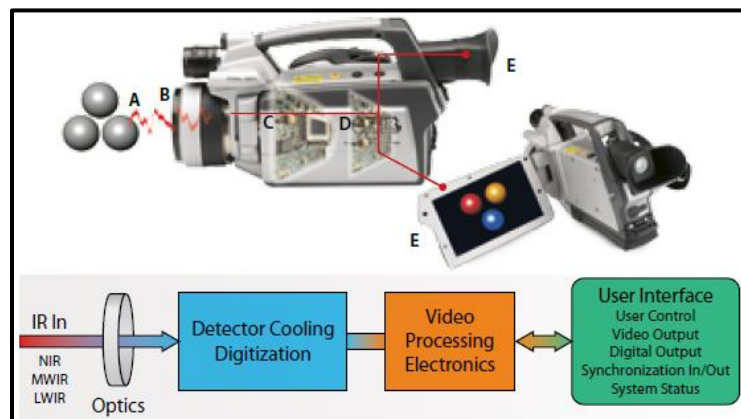


**Figure 4-3: General configuration of a typical IR camera (FLIR Guidebook).**

IRT is the art of transforming an infrared image into a radiometric one, which allows temperature values to be read from the image. So every pixel in the radiometric image is in fact a temperature measurement. In order to do this, complex algorithms are incorporated into the thermal imaging camera. However, the optics and detectors are the heart of IRT systems and must be selected for the desired range (Rinaldi, 2012). Because IR has the same properties as visible light regarding reflection, absorption, and transmission, the optics for thermal cameras are designed in a fashion similar to those of a visual wavelength camera. However, the types of glass used in optics for visible light cameras cannot be used for optics in an infrared camera, as they do not transmit IR wavelengths well enough. Conversely, materials that are transparent to IR are often opaque to visible light. IR camera lenses typically use silicon and germanium materials. Normally silicon is used for medium wavelength IR camera systems, whereas germanium is used in long wavelength cameras. Both materials have good mechanical properties, e.g., they do not break easily, they are non-hygroscopic, and they can be formed into lenses with modern turning methods. As in visible light cameras, IR camera lenses have antireflective coatings. With proper design, IR camera lenses can transmit close to 100% of incident radiation.

The IR camera detector is a focal plane array (FPA) of micrometer-sized pixels made of various materials sensitive to IR wavelengths. FPA resolution can range from about  $160 \times 120$  pixels up to  $1024 \times 1024$  pixels. Some IR cameras have built-in software that allows the user to focus on specific areas of the FPA and calculate the temperature. Other systems utilize a computer or data system with specialized software that provides temperature analysis. Both methods can supply temperature analysis with better than  $\pm 1^\circ \text{C}$  precision. However, the FPA technologies are broken down into two categories: thermal detectors (uncooled microbolometers) and quantum detectors, which are generally faster and more sensitive than thermal detectors. On the other hand, thermal detectors have a lower cost and broader IR spectral response than that of quantum detectors, which also require a cooling system using either liquid nitrogen or a small stirling cycle refrigerator unit (Vladimir, 2014). However, advances in the field of solid state technology have paved the way for the development of newer types of uncooled infrared detectors with better resolution and accuracy. Nowadays, the thermal sensitivity of the uncooled cameras is about  $0.03^\circ \text{C}$  compared to  $0.01^\circ \text{C}$  of the cooled ones (Bagavathiappan *et al.*, 2014).

The most important parameters that must be considered before choosing an IR camera include the spectral range, spatial resolution, temperature range and frame rate. For observing objects at ambient temperature, long wave length band (8–14  $\mu\text{m}$ ) is preferable to detect small thermal contrast and reduce the effects of direct solar radiation during daytime testing. The spatial resolution of an IR camera primarily depends on the object-to-camera distance, lens system and detector size. The spatial resolution decreases with increasing object-to-camera distance, while lens systems with a small field of view (FOV) have higher spatial resolution (Usamentiaga *et al.*, 2014).

#### 4.2.3 Application of IRT for Concrete Bridge Inspection

IRT has been applied for several decades to detect corrosion-induced delaminations in RC bridges (Manning and Holt, 1982). Previous studies highlighted that the immense difference between the volumetric heat capacity of solid concrete and that of the air voids within the concrete element results in warmer delaminated areas than the sound concrete when exposed to solar heating. They further suggested that more severely delaminated regions have stronger thermal contrast values. There are two testing approaches for IRT based on the heat source. The active approach uses an external thermal stimulus to induce the required heat flow condition in the concrete being tested. The passive approach uses natural heat sources, such as solar heating and ambient temperature changes (Robert, 1982). Based on the external stimulus, different methods of active IRT have been developed, such as pulse thermography, step heating, lock-in thermography, and vibro-thermography.

The application of passive IRT testing in full-scale bridge decks relies on detecting characteristic thermal signatures associated with subsurface anomalies since solar loading can provide a strong radiant heating source. When the ambient air temperature is higher than the concrete temperature, heat is transferred into the concrete to bring it toward thermal equilibrium with its surroundings through a thermal gradient. Subsurface defects, such as delaminations, disrupt the heat transfer through the concrete. If a sufficient thermal gradient exists, defects can be detected by measuring the difference in surface temperature that exist between a region of sound concrete and a defected region of concrete under certain environmental conditions (Manning and Holt, 1982). For instance, when the

temperature of the concrete increases, such as during daytime when the sun and ambient environment are heating the concrete, the area above a subsurface delamination warms up at a faster rate than that of surface areas where the concrete is intact. Delaminations can then be detected as “hot spots” on the surface of the material, relative to the intact concrete. Conversely, during nighttime, the air temperature usually decreases and the material cools. Thus, the surface area above delaminations cools at a faster rate than that of the intact concrete and appears as “cold spots” relative to the intact concrete. **Figure 4-4** illustrates the IR emitted from a concrete bridge deck during the day and night.

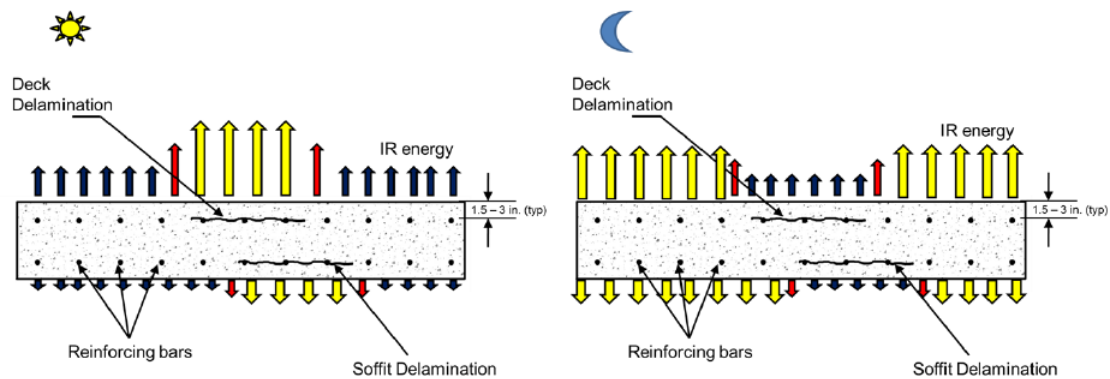


**Figure 4-4: Infrared energy emitted from concrete bridge deck during day and night.**

However, there has been limited application of the IRT technology to inspect full-scale deteriorated RC bridge decks outside the laboratory environment. This could be due to the fact that the technology must be used in controlled environmental conditions to obtain precise evaluations. Environmental conditions such as solar loading, ambient temperature, relative humidity and wind speed affect the accuracy of passive IRT measurements. The effects of these environmental factors can be difficult to characterized and vary over time, such that it can be difficult to determine if the existing environmental conditions at a given point in time are adequate to produce a high quality image. Favorable environmental conditions include sufficient solar loading or changes in ambient temperature to produce a thermal gradient in the concrete, where the concrete surface heats up at a much higher rate than the concrete core. ASTM D4788-03 (Standard Test Method for Detecting

Delaminations in Bridge Decks Using IRT) describes the appropriate environmental conditions necessary for conducting passive IRT inspections. For instance, a minimum of 3-hr direct sunshine is required to create a temperature difference of at least 0.5°C. In addition, IRT testing shall not be carried out when ambient air temperatures are less than 0°C (32°F) and when the wind velocity exceeds 50 km/hr (30 mph).

In addition, characteristics of the subsurface defect (e.g. delamination depth, delamination thickness, materials present in delamination, concrete properties, and asphalt overlays) also affect the test response. In a study by Hiasa *et al.* (2017), they reported that the area of delamination was found to be the most critical factor that directly affects the thermal contrast measures during IRT testing. Kee *et al.* (2012) reported that overnight cooling effect can be used to detect both shallow and deep delaminations, providing clearer images than using the morning heating effect. Watase *et al.* (2015) recommended to predict the thermal contrast first based on actual sensor readings in order to determine the suitable time window for conducting IRT bridge inspections. Maser and Roddis (1990) reported that detection of defects in the presence of an asphalt overlay is difficult because the overlay dampened the thermal contrasts achieved due to the thermal mass above a potential delamination, and the thicker the overlay, the greater the damping effect. A major concern for the reliability of IRT through asphalt overlay is the possible presence of a debonded area which could mislead interpretation. The debonded area could appear as a flaw in the IR image, in addition to the actual delaminations in the concrete. To distinguish debonding for delaminations, Maser and Roddis (1990) suggested that the delaminated areas appear as circular and uniform while the debonded areas present as large, non-circular, and non-uniform.

#### 4.2.4 Interpretation of Passive IRT Data

A main challenge in IRT is how to recognize delaminations in IR images since it can be rather subjective to judge whether color contrast of the image is an indication of damage or not. The location of subsurface delaminations can be identified by analyzing the surface temperature variations. The measured thermal contrasts, defined in **Equation 4-8**, are commonly examined to perform qualitative assessment of the thermographic images in an attempt to identify subsurface deterioration.

$$\Delta t = T_{\text{defective concrete}} - T_{\text{sound concrete}} \quad \text{Eq. 4-8}$$

Where:  $T_{\text{defective concrete}}$  is the surface temperature above a delaminated area and  $T_{\text{sound concrete}}$  is the surface temperature in the intact area of the concrete. Manning and Holt (1982) pointed out that thermal contrast could occur at any ambient temperature, but is greatest during a period of rapid heating and cooling. They also reported that the maximum thermal contrast occurs at a distinct time over the course of a typical day. It should be noted that the thickness of concrete cover may affect the inspection capability of IRT due to the increased weakness of thermal contrasts with increased target depths. In addition, Maldaque (2000) correlated the depth of a defect with observation time and proposed that the deeper defects will be detected at a later time with a reduced contrast, where observation time is a function of the square of the depth as indicated in **Equation 4-9**. He further suggested a relationship between the loss of contrast and increasing depth, where the loss of thermal contrast is proportional to the cube of the target depth, as per **Equation 4-10**.

$$t \sim \frac{z^2}{\delta} \quad \text{Eq. 4-9}$$

$$C \sim \frac{1}{z^3} \quad \text{Eq. 4-10}$$

Where  $t$  is the observation time,  $z$  is the depth of the target,  $\delta$  is the thermal diffusivity, and  $C$  is the thermal contrast loss due to defect depth.

Preprocessing of IR images may include pixel enhancement and noise smoothing, while image processing is commonly conducted using a variety of image segmentation techniques (Qianqian and Youna, 2003). IR image mosaics are commonly used to obtain a global view of a bridge deck through stitching individual images. There are several commercially available stitching software tools that can be utilized for creating this mosaic view of a bridge deck. The majority of their algorithms rely on capturing images from a fixed location in order to stitch them together. This allows projection onto the image plane

to go through the same focal point in all of the images. However, parallax and geometric distortions, which often occur when an image is captured while the IR camera is moving, make the creation of such a mosaic from the large numbers of images a problem because the background appears to shift and automated feature detection methods could stitch the background instead of the foreground (Brown and Lowe, 2007).

Displaying field deployment IR images into a geospatial format is another approach that has been widely adopted by several researchers (e.g. Jiang and Li, 2008; Wu *et al.*, 2012; Vaghefi *et al.*, 2015). For instance, *ArcGIS* (geographic information system) and the *GE* (Google Earth) software can register images to produce GIS thermal IR maps, which allow the analyst to explore data and make measurements. Although this procedure is useful in detecting and calculating delaminated and spall areas present in bridge decks, it usually requires manual editing and relies on the user interpretation, often resulting in undesired subjectivity.

### 4.3 Un-Supervised Machine Learning

Machine learning is a predictive modeling analysis that constructs algorithms capable of learning from and making prediction of data. The algorithms operate by building a model from example inputs to predict data or decisions, rather than strictly following static programme instructions (Melhem and Cheng, 2003). It can be classified based on the nature of input and feedback signals as supervised learning, where the goal is to learn general rules to map inputs and known desired outputs, and un-supervised learning, where no output labels are given and the data are left on its own to find structure in its inputs (Jain, 2010). It can be also statistically categorized as classification, regression and clustering techniques. Clustering methods partition a set of objects into clusters such that objects in the same cluster are more similar to each other than objects in different clusters according to some defined criteria (Huang, 2010). Therefore, clustering analysis can be defined as a statistical technique for discovering whether the individuals of a population fall into different groups by making quantitative comparisons of multiple characteristics (Melhem and Cheng, 2003). The k-means clustering, which is employed in the present research, is briefly described below.

### 4.3.1 k-Means Clustering

k-means clustering is a partitioning technique that was independently discovered in various scientific fields (Dinh *et al.*, 2014). In spite of the fact that k-means was proposed over 50 years ago and thousands of clustering algorithms have been published since then, k-means algorithm is well known for its efficiency in clustering large data sets. As the most commonly used method for statistical data analysis, the k-means procedure divides N-dimensional population into k sets clusters such that the squared error between the empirical mean of a cluster and the points in the cluster is minimized. According to Jain (2010), data clustering has been used for three main purposes: (i) to gain insight into data, generate hypotheses and identify salient features; (ii) to identify the degree of similarity among forms or organisms; and (iii) as a method for organizing the data and summarizing it through cluster prototypes. With respect to the computation algorithm, k-means clustering proceeds by randomly selecting k initial cluster centers ( $c_i$ ), and then iteratively refining them according to two steps: (i) each data point is assigned to the data set associated with the nearest centroid, where the Euclidean distance between the data point  $x_r$  and the centroid  $c_i$  of cluster  $c$  is calculated using **Equation 4-11**; (ii) each cluster center  $c_i$  is updated to be the mean of its constituent data points. The two steps are repeated until the centroids and data points no longer move and the clustering process stops (Wagstaff *et al.*, 2011).

$$d(x_r, c_i) = (\sum_{u=1}^U |x_{ru} - c_{iu}|)^{0.5} \quad \text{Eq. 4-11}$$

Where  $U$  is the dimension of data needed to be categorized. The number of clusters ( $k$ ) is the user defined parameter to perform k-means clustering for a data set.

However, this technique has some inherent shortcomings. For example, the number of clusters must be set in advance; different initializations can lead to different final clustering; the data must be numerical and comparable via Euclidean distance and thus, the algorithm works best on data containing spherical clusters; and is sensitive to points that do not belong to any cluster. Thus, it could distort the centroid positions and a cluster with

empty or few objects may occur in the final result. The k-means algorithm has been extended in many different ways to improve its performance. Some of these extensions deal with additional heuristics involving the minimum cluster size and merging and splitting clusters (Jain, 2010). For instance, in the fuzzy c-means, each data point can be a member of multiple clusters with a membership value. Replacing the means of clusters with modes or medians of the data, by introducing some additional algorithmic parameters, are some of other modifications that have been made by several researchers. The k-modes algorithm enables the clustering of categorical data in a fashion similar to k-means. The k-prototypes algorithm, through the definition of a combined dissimilarity measure, further integrates the k-means and k-modes algorithms to allow for clustering objects described by mixed numeric and categorical attributes.

#### 4.4 IRT Model Development

IRT testing was conducted onsite in a real-world application. An in-service RC bridge deck in Quebec, Canada was scheduled, by the Quebec Ministry of Transportation (MTQ) for rehabilitation. Delaminations, extent of corrosion and high chloride ions content in the bridge were recently outlined by a condition survey. Thus, the bridge was considered as a good candidate and selected for the IRT survey. The bridge was constructed in 1969. Its deck is connected directly to the supporting abutments with no provision in the form of bearings. The critical deck characteristics include a total length of 44.8 m with a transverse width of 9.1 m, which translates into 8 m of drivable surface (supports one lane of traffic in each direction) with one side shoulder. The deck exhibited scaling and pop-outs throughout, with presence of numerous transverse, longitudinal and diagonal cracks. **Figure 4-5** illustrates the location of the surveyed bridge.

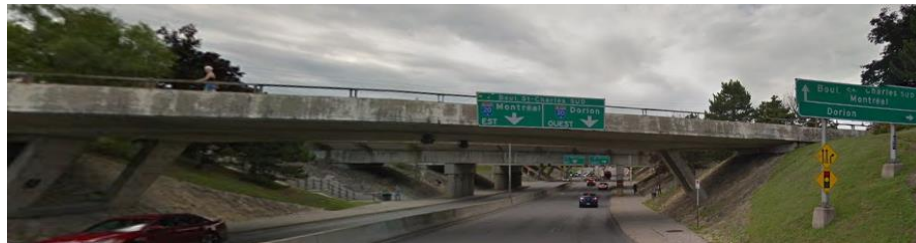


**Figure 4-5:** Illustration of the selected concrete bridge located in Montreal, Quebec.

#### 4.4.1 Data Collection

The IRT survey was carried out according to ASTM D4788-03 using a vehicle-based IRT system. The utilized thermal IR camera was FLIR T650sc. The camera is equipped with an uncooled microbolometer detector capable of detecting the IR radiation in the spectral range of 7.5-14  $\mu\text{m}$ , with thermal sensitivity of 0.03°C at 30° C. It displays thermal images with a resolution of 640 x 480 pixels and has a built-in dual 5 Mpixel digital camera and GPS system. The camera is accommodated with a 25° x 19° FOV. Its features and specifications are summarized in **Table 4-1**.

**Table 4-1: Features and specifications of the utilized thermal camera**

Characteristic	Specification
Detector Type	Uncooled Microbolometer
Spectral Range	7.5 $\mu\text{m}$ – 13 $\mu\text{m}$
Thermal Resolution	640 x 480
Thermal Sensitivity	0.03° C at 30° C
Frame Rate	30 Hz
Field of View	25° x 19°
Temperature Range	-40°C to 2000°C
Focus	Automatic
Accuracy	+/- 1° C, +/- 1% of reading
Built-in Digital Camera	5 MP

Collecting thermal IR images over the entire bridge deck area is highly dependent on the camera's FOV and lens. The ideal option for data collection is to scan one lane on each pass. However, obtaining such horizontal FOV is not always achievable in the field. Therefore, to reduce the number of survey passes, a calibrated 13.1 mm focal lens was utilized. Using this lens means that this camera needed to be located 5.2 m above the concrete bridge deck to cover an entire lane width of 4 m in a single image, which was not a practical solution. Subsequently, for this field deployment, the IR camera was mounted at a height of 2.6 m and oriented facing straight-down to the concrete deck surface to reduce distortion along the image edges. Thus, the angle of the images would be consistent from one image to the next. This allows a 2.13 m x 1.62 m FOV for each image and to survey each single lane with only two passes. **Figure 4-6** illustrates the vehicle mounted setup. The survey was carried out according to ASTM D 4788-03 (2013), where the vehicle

mounted thermal IR camera was driven at a low driving speed of 20 km/hr. over the center of each pass assisted by traffic control. The IR camera was triggered to acquire data every 0.91 m (3 ft.) over the entire deck length. Hence, a total of 392 thermal and digital images were collected, which cover the entire bridge deck. The survey of the deck top surface was conducted twice: The first survey was done on October 23<sup>rd</sup>, 2015 at 9 PM, two hours after sunset. The second survey was conducted on October 27<sup>th</sup>, 2015 at 1 PM, six hours after sunrise. In addition, the bridge soffit was surveyed on October 24<sup>th</sup>, 2015 at 2 PM, seven hours after sunrise, to maximize contrast on the images. IR images were captured for the bridge soffit from the ground level, without need for a bridge access vehicle or controlling traffic under the bridge. The images were taken as snapshots using the available 13.1 mm focal lens. This allowed a 6.4 m x 5.18 m FOV and hence, a total of 28 thermal and digital images were collected, which covers the entire bridge soffit.



**Figure 4-6: Illustration of the FLIR T650sc IR camera and vehicle mounted setup system utilized to survey Montreal bridge.**

The concrete emissivity of 0.95, distance between the front lens of the camera and the concrete deck, actual ambient temperature, reflected temperature, and humidity at the beginning of the data collection were input into the camera software to calibrate the temperature measurements and compensate for the radiation being absorbed in the

atmosphere. Bridge deck dryness was considered during data collection since surface moisture can reduce the thermal contrast on the IR images. Sun direction was also considered during the second data collection survey to avoid shadows on images. The total time of data collection for each survey was approximately two hours. **Table 4-2** summarizes the environmental conditions during both surveys, as well as the ambient temperature variation over the time period the images were captured. The Matlab image acquisition toolbox was utilized to initialize acquisition and storage of the IR and digital images. The digital images were used to separate patches and surface defects from subsurface anomalies.

**Table 4-2:** Environmental conditions during IR surveys of Montreal bridge

Bridge Element	Survey Date	Time of Data Collection	Ambient Temperature (° F)	Ambient Temperature Variation (° F)	Wind Speed (mph)	Humidity (%)
Deck	23/10/2015	9.00 PM	39	- 6	11.3	37
	27/10/2015	1.00 PM	56	- 5	8.1	26
Soffit	24/10/2015	2.00 PM	60	- 7	6	32

Data on thermal cameras appears as a color-coded image in which a color palette is assigned to temperatures at a certain “level” and across a certain “span” determined by the user. The span of the image is the difference between the minimum and maximum temperature displayed in the image, and the “level” is the center of the span. **Figure 4-7** shows two typical thermal images taken during the conducted survey at two different times. Based on the visual interpretation, which is a subjective technique, the defective area can be identified and quantified. For example, the image on the left shows a delamination after several hours of exposure to sunlight being much warmer than the surrounding concrete. The image on the right was taken two hours after sunset and shows a delamination cooling faster than the surrounding solid concrete. It should be noted that it is important to take optical images of the bridge deck during IRT surveys in order to provide a preliminary assessment of the surface deck condition. Consequently, the visual interpretation of the captured thermal images could highlight and separate patches and surface defects from actual subsurface anomalies.

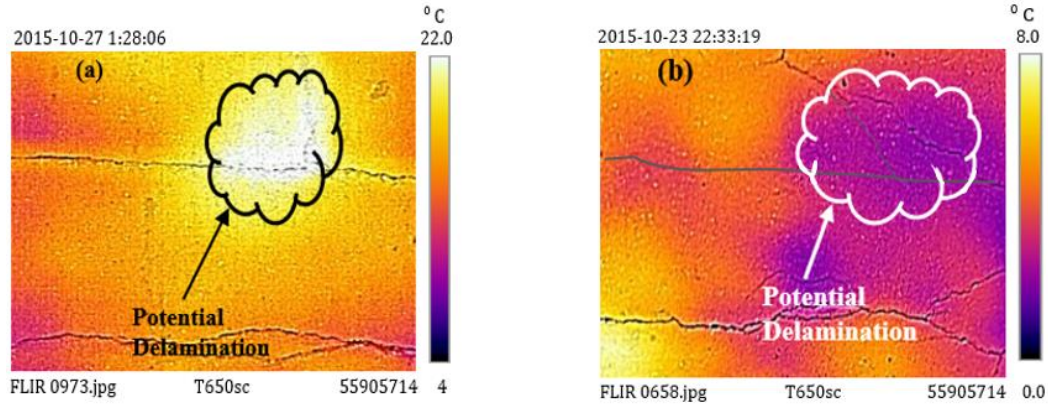


**Figure 4-7: Delamination at (a) daytime; and (b) nighttime surveys.**

Extracting quantitative information, such as size and location of defective areas from a set of IR images, is one of the critical components of thermal data analysis. The challenge here is to develop an automated procedure capable of detecting subsurface defects regardless of the difference in the temperature ranges between various IRT surveys taken at different times and environmental conditions. The developed procedure to achieve this goal consists of several steps as described below.

#### 4.4.2 Image Pre-Processing

In this step, the quality of the thermal images was improved. Three functions in The *FLIR Tools+* and *ResearchIR* software were utilized to enhance the images. For instance, the Gaussian smoothing filter was used to reduce the level of images' background noise where the software selects the size of the filter automatically. Thus, improving the images' resolution, which facilitated the view of small objects. The histogram equalization function was used to distribute the intensities on the histogram, which in turn increased the dynamic range and enhanced the image's thermal contrast. The multi-spectral dynamic imaging function was also utilized. It is a fusion algorithm that embosses visible spectrum details (from the digital camera) onto the infrared image, enabling sharper-looking and quicker target orientation. This phase is useful to differentiate delaminated areas from surface features appearing in the infrared image (e.g. discoloration, oil stains and rust deposits, etc.), yet are unrelated to subsurface conditions. The temperature data of each image was then saved in a separate Excel file using the *ResearchIR* software.

### 4.4.3 Image Registration

The purpose of this step is not to transform the images into one coordinate system, as commonly processed, but to combine the enhanced IR images together to create a plan-view mosaic of the entire bridge deck (mosaicked thermogram). The stitching algorithm to be applied depends on comparing the pixels' features in the images to be grouped and requires exact overlap. However, parallax and geometric distortions, which often occur when an image is captured while the vehicle is moving, makes the creation of such a mosaic from the large numbers of images a difficult task. In addition, commercial software capable of stitching images produce non-radiometric mosaic images, which could lose its dynamic range. To overcome this problem, an algorithm was developed as illustrated in **Fig. 4-8**.

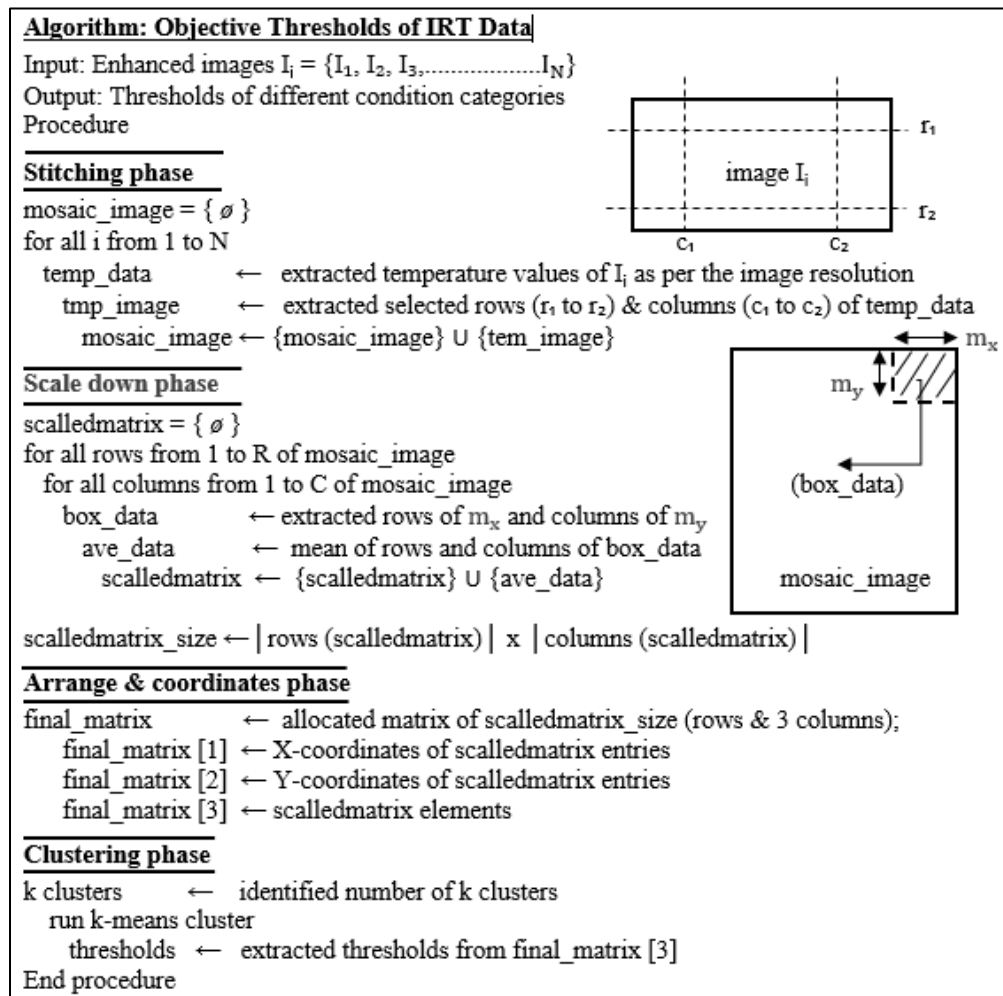


**Figure 4-8: Developed algorithm for condition assessment of concrete bridge decks.**

The analysis process starts by extracting a selected window from each image and stitching it together with the extracted window from the next image and so on as per **Equation 4-12**. This procedure requires the collection of IR images with sufficient overlap and at known traveled spacing based on the camera's FOV. However, the height of each stitched window was the number of pixels that are equivalent to the images' spacing. Hence, this appending process produced continuous data for each survey pass. The dimension in pixels of each window depends on the resolution of the camera and the image spacing. A special Matlab code was written to extract and stitch the selected pixels from each image where the number of the first image, the last image, and the selected pixels were maintained as variable to automate the selection process with any other survey data.

$$\left. \begin{array}{l} \text{for } i = 1 \rightarrow N \\ \alpha_1 = (N - 1) (r_2 - r_1) + r_1 \\ \alpha_2 = (N - 1) (r_2 - r_1) + r_2 \\ \beta_1 = (N - 1) (c_2 - c_1) + c_1 \\ \beta_2 = (N - 1) (c_2 - c_1) + c_2 \end{array} \right\} \quad \text{Eq. 4-12}$$

$$E_i (R, C)_{\substack{R=r_1 \rightarrow r_2 \\ C=c_1 \rightarrow c_2}} \in O_i (I, J)_{\substack{I=1 \rightarrow m \\ J=1 \rightarrow n}} \quad \text{and} \quad M (\alpha, \beta)_{\substack{\alpha=\alpha_1 \rightarrow \alpha_2 \\ \beta=\beta_1 \rightarrow \beta_2}}$$

Where:

$O_i$ : Original matrix of enhanced image  $i \quad i \in (1, 2, 3 \dots N)$

$N$ : number of images

$E_i$ : Extracted matrix from original matrix  $O_i$

$r_1, r_2$ : Start and end rows of an extracted matrix  $E_i$

$c_1, c_2$ : Start and end columns of an extracted matrix  $E_i$

$M$ : Mosaic matrix of the entire bridge deck

For visualization and to facilitate further processing, it was necessary to scale-down the data dimension of the mosaic. This was achieved by assuming that the entire deck was

divided into small ( $m_x * m_y$ ) area boxes, with temperature unable to change within each box. Then, computing the average of pixels, which represents the resolution within the selected box area. To automate this process, the mean function in Matlab was modified and a new code was written to calculate the mean for a specified dimension of input data. The user needs to enter the dimension of the pixels to be averaged based on the deck dimension and the assumed box area. A box area of 10 cm resolution is recommended, but could be considered as 15 cm for a very large mosaic data file (e.g. more than hundred million pixels). **Equation 4-13** represents the mathematical formula of the scale down process of the mosaic data.

$$\left\{ \begin{array}{l} \text{for } ii = 1 \rightarrow i_x \quad \& \quad jj = 1 \rightarrow i_y \\ i_x = C * m_x / W \quad i_y = R * m_y / L \\ S(ii, jj) = \text{Mean} [A(\delta_1, \delta_2) : A(\delta_3, \delta_4)] \\ \delta_1 = (ii - 1)m_x + 1 \\ \delta_2 = (jj - 1)m_y + 1 \\ \delta_3 = ii * m_x \\ \delta_4 = jj * m_y \end{array} \right. \quad \text{Eq. 4-13}$$

Where:

*C and R: Number of columns and rows, respectively, of the mosaic matrix*

*m<sub>x</sub> and m<sub>y</sub> : Dimension of the box area to be averaged*

*W and L: Width and length of the bridge deck*

*S: Scale – down matrix of the entire bridge deck*

To facilitate mapping the mosaic, the coordinates of each pixel in the temperature data file was identified. The origin point (0, 0) was assigned at the corner of the bridge deck and then the coordinates of all other pixels in the file was computed based on the deck dimensions as per **Equation 4-14**. Thus, another Matlab code was written to identify the coordinates of each pixel of the scale-down matrix *S*, and arrange the data in a column order with (x, y, temperature) values of each pixel. To automate this process, the number

of rows and columns of the data file and the dimension of the deck were maintained as variables in the code to accommodate any other survey data. The final output was an excel file containing pixel information (coordinates and temperature) with no change in the thermal contrast values over the entire deck.

$$\left\{ \begin{array}{l} \text{for } I = 1 : C \\ \quad J = 1 : R \\ \quad x = \left(\frac{W}{C}\right) X (I - 1) \\ \quad y = L - \left(\frac{L}{R}\right) X (J - 1) \end{array} \right\} \quad \text{Eq. 4-14}$$

Where:

*C and R: Number of columns and rows, respectively, of the scal – down matrix*

*W and L: Width and length of the bridge deck*

#### 4.4.4 Image Segmentation

The output file from the stitching step can be uploaded in image software, such as *ImageJ* or *AutoPano*, to produce a composed mosaic thermogram for the entire deck. However, further analysis depends on the segmentation technique to be used. Many image segmentation algorithms have been widely used in the image processing field. The purpose of the segmentation process is to partition the image into regions of constituent objects based on the concept of point-based segmentation (e.g. value-based technique), object-based segmentation (e.g. region growing technique), or edge-based segmentation (e.g. edge detection technique). Subjective selection of threshold values remains a limitation in applying point-based segmentation, while the simplest type of region growing technique is to specify some “seed” points as initial regions, and then to aggregate pixels around these regions into bigger and bigger connected regions based on similarity of defined properties. However, thresholding classification is adopted herein.

The un-supervised thresholding classification using the k-means clustering function in Matlab was implemented in the present research to determine objective thresholds. As previously introduced, the k-means clustering algorithm arbitrarily specifies an initial

mean vector for each  $k$  cluster. Each pixel is then assigned to the class whose mean vector is closest to the pixel vector, thus forming the first set of decision boundaries. The new set of cluster mean vectors is then calculated from this classification and the pixels are rearranged. The iterations are continued until there is no significant change in pixel assignments from one iteration to the next or a maximum number of iterations is achieved. It should be noted that there is no established mathematical criterion to identify significant change in data point assignment or the maximum number of iterations. Data was characterized in this study based on one feature vector, which is the pixel numerical temperature values.

#### 4.4.4.1 *Identifying the Number of Clusters (Categories)*

The  $k$ -means clustering requires defining the number of clusters before the algorithm starts. **Figure 4-9** illustrates a rational approach to determine the appropriate number of condition categories (clusters). The flowchart is based on the age of the bridge deck, the thermal contrast values obtained from the thermal images, and the existing deterioration condition of the bridge deck, which can be determined from digital images and visual inspection of the deck. Newly constructed bridges typically experience few problems during their first decade of service, and thus, it is unlikely that deterioration initiates in bridge decks under 10 years of age. This can justify the selected 10-year decision point in the flowchart. ASTM D4788-03 indicates that a temperature difference between the delaminated or debonded area and the adjacent solid concrete of at least  $0.5^{\circ}\text{C}$  must exist to identify delamination by an imaging infrared scanner. This value was adopted herein to differentiate between the sound and deteriorated concrete in order to determine the number of clusters as illustrated in the flowchart. With respect to the deterioration criteria, delamination is defined as a discontinuity of the surface concrete, which is substantially separated but not completely detached from the concrete below or above it and hence, it is invisible. Spalling was chosen from the defects commonly occurring in concrete bridge defects because it is often the continuation of the delamination process, which represents distressed areas. The pressure exerted by corrosion of reinforcement or by the formation of ice in the delaminated area results in the breaking off of the delaminated concrete. Spalling may also occur due to continued deterioration of the old concrete. The Ontario Structure Inspection Manual

(OSIM, 2008) differentiates between light, medium and severe spalling based on defined measures of the spalling areas. These measures were used in the flowchart to determine the number of clusters.

Consequently, the k-means clustering algorithm in Matlab was applied and objective thresholds were identified. It should be noted that the flowchart was developed for concrete bridges with bare decks, while for paved bridge decks the thermal contrast of  $0.5^{\circ}\text{C}$  could be due to the effect of pavement thickness. In addition, spalling could be hidden under the asphalt layer. Therefore, a higher thermal contrast value and visual condition of the deck should be considered in such cases, which requires further research involving scanning of paved bridge decks.

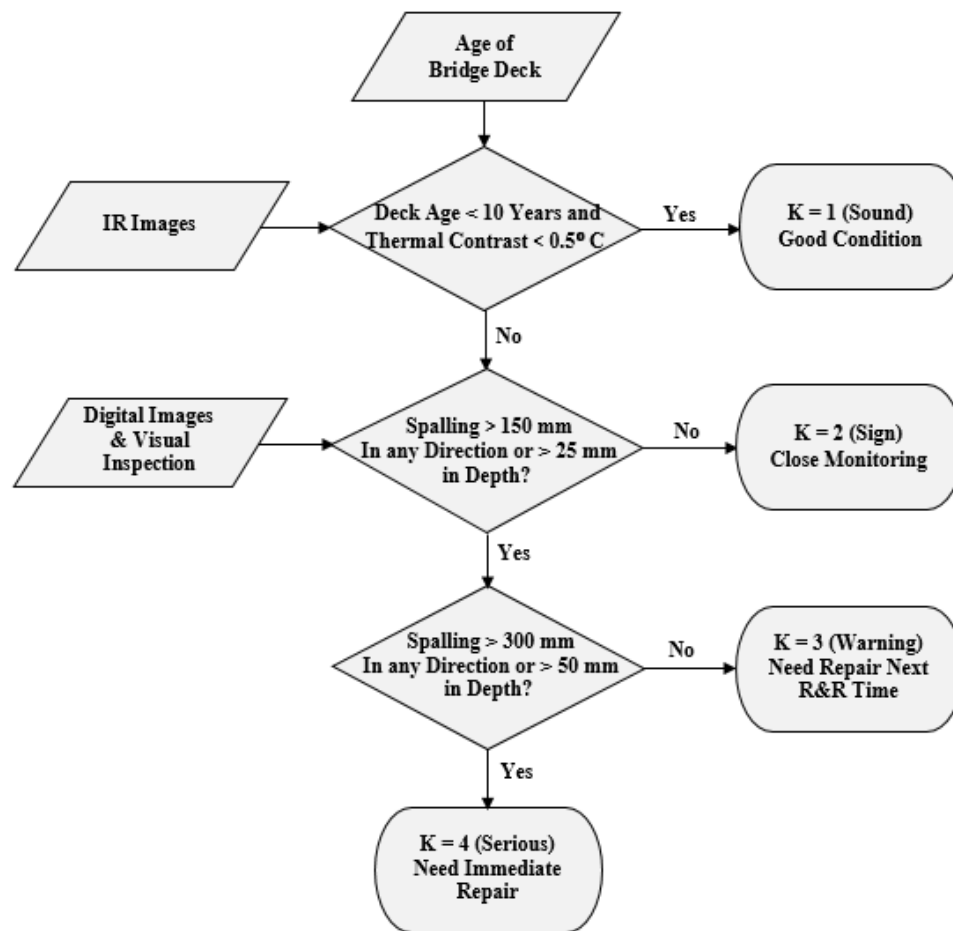


**Figure 4-9: Flowchart for determining number of condition categories (k).**

#### 4.4.5 IRT Condition Mapping

Based on the threshold value of each condition category, the temperature values were grouped into the same number of clusters. Accordingly, a condition map was plotted using a commercial mapping software to reconstruct a high contrast composite image accurately delineating the severity of subsurface defects. Such a delamination map created from the output of IRT bridge inspection can be used to determine the total percentage area of delamination in each category over the entire bridge deck.

### 4.5 IRT Model Implementation

The procedure proposed in the present research was implemented on the surveyed deck and can be summarized as follows: (i) the images were enhanced using *FLIR+* and *ResearchIR* software and the data was then saved as .csv files; (ii) a selected window of 600 x 270 pixels, which represents 0.91m spacing of the images, was extracted from each image and stitched with the extracted window from the next image using an especially developed Matlab code. For a 44.8 m long bridge, the dimension of the stitched strip was 600 x 13,230 pixels and 2400 x 13,230 = 31.75 million pixels for the entire two lane deck; (iii) the data dimension was scaled-down using the Matlab code assuming that the entire deck was divided into small 10x10 cm area boxes, with temperature unable to change within each box, and thus, this resulted in a reduced file with 80 x 450 = 36,000 pixels; (iv) the coordinates of each pixel were identified, and the pixels were arranged in a column order with (x, y, temperature) values of each pixel, using the Matlab code; and (v) the k-means clustering algorithm in Matlab was run to identify the thresholds.

The number of clusters (k) for this bridge was determined as three, considering the developed flowchart, where the bridge deck being considered is about 47 years old, its recorded thermal contrast was higher than 0.5<sup>0</sup> C, and maximum spalling of 225 mm was measured. The condition maps of the deck were plotted and illustrated in **Fig. 4-10** and **Fig. 4-11**, delineating the severity of the subsurface defects at the daytime and nighttime surveys, respectively.

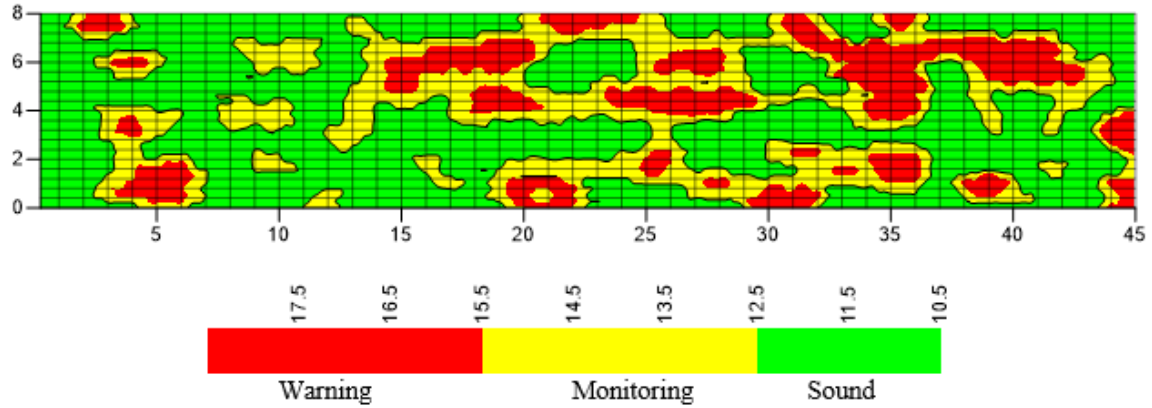


**Figure 4-10: Condition map of the daytime IRT survey of bridge deck in Montreal indicating the severity of the identified delaminated areas.**

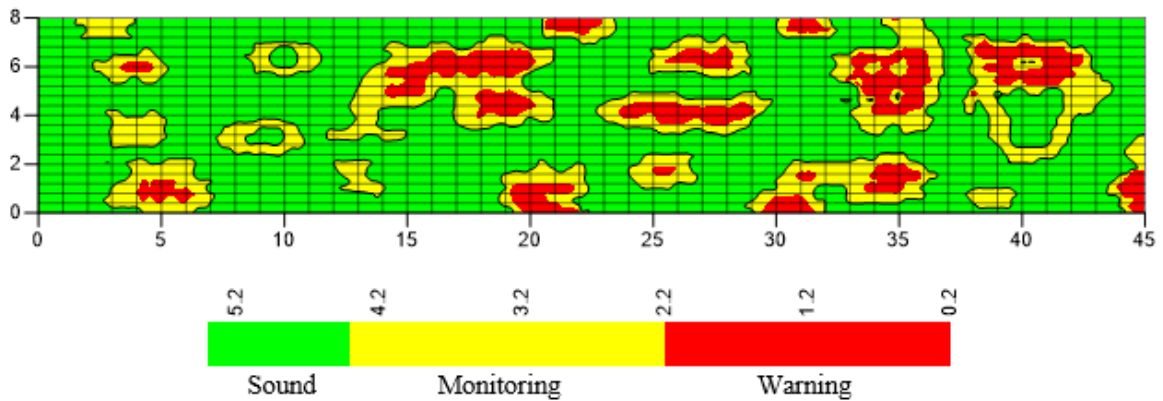


**Figure 4-11: Condition map of the nighttime IRT survey of bridge deck in Montreal indicating the severity of the identified delaminated areas.**

As previously discussed, the thermal energy transferred via conduction is affected by the thermal properties of the concrete, while the thermal conductivity of concrete is dependent on the type of aggregate used in the concrete mixture. However, for concrete bridge components outdoors, convective heat transfer can play a significant role.

The developed procedure for producing a mosaic plan of the bridge deck was not applicable for the soffit case as the images were taken at different angles. Therefore, the images of the bridge soffit were processed individually to identify the delaminated areas in each image.

Having a camera with a larger field of view can solve this issue to some extent, and having less images on the overall bridge soffit can make the data procedure faster and more practical. However, caution must be taken in using the wide-angle lens for the thermal IR camera as the edges of the thermal IR images may be distorted and become not viable for calculating the number of pixels and area of delamination. **Figure 4-12** displays a subset of thermal and related digital images, which were captured by the infrared camera on the bridge soffit, delineating the potential of delaminated areas. Vladimir (2014) reported that the temperature contrasts in soffits are smaller than those for solar exposed surfaces. This was confirmed via the thermal images of the bridge soffit in **Fig. 4-12**.

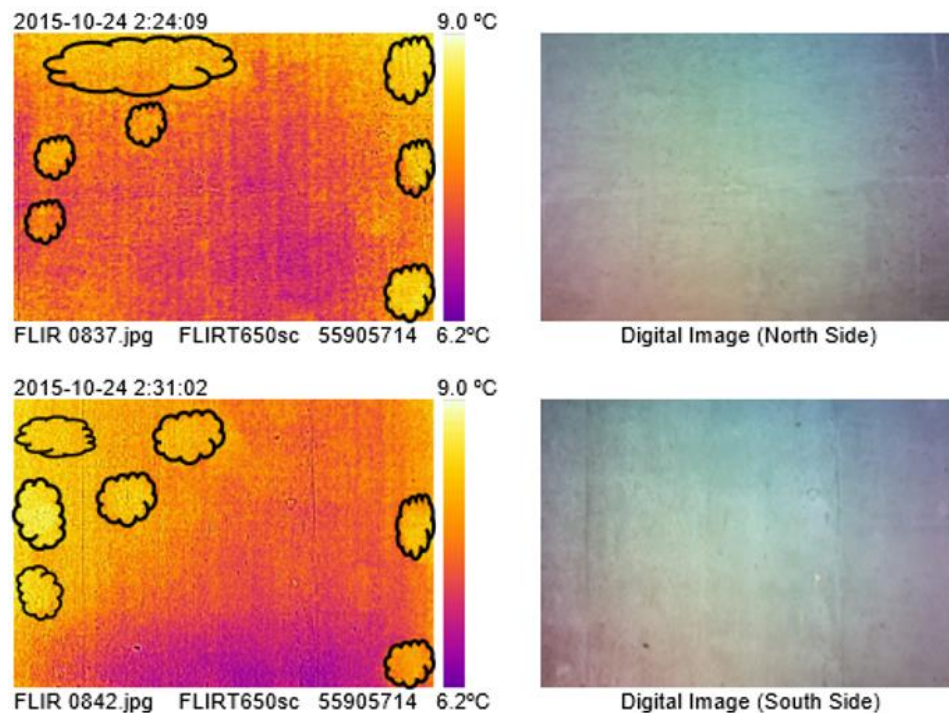


**Figure 4-12: Thermal and digital images of potential delaminated areas in the bridge soffit.**

In order to validate the model thus developed in the present research, the analysis procedure was implemented on three bridge decks located in the state of Wisconsin, USA. The bridges' description, IRT data collection methodology, adopted analysis procedure and results are briefly discussed below.

#### 4.5.1 Bridge (A)

The bridge was constructed in 1963, and consists of seven spans of continuous concrete box girders with a 367.5 mm RC slab deck. The bridge was scanned on July 15, 2010 using IRT. The critical deck characteristics include a total length of 296.9 m with a transverse width of 10.7 m, which translates into 9 m of drivable surface with two side shoulders. The IRT survey was conducted by Infrasense, a *consulting firm specializing in NDT of bridge decks*. The infrared data was collected with corresponding high resolution video at a low driving speed of 20 km/hr. using a vehicle-based system. The IR camera model used was FLIR A41 (M). The camera displays thermal images with a resolution of 320 x 240 pixels. Its features and specifications are summarized in **Table 4-3**. The camera was fixed at 45° to have a FOV that covers one lane per driving pass. The images were taken every 0.305-m (1 ft.) over the 296.9 m of the deck length, hence a total of 1,948 images were collected, which cover the entire two-lane bridge deck. The environmental conditions during the survey are shown in **Table 4-4**.

**Table 4-3: Features and specifications of the utilized thermal camera**

Characteristic	FLIR A40(M)
Detector Type	Uncooled Microbolometer
Spectral Range	7.5 $\mu$ m – 13 $\mu$ m
Thermal Resolution	320 x 240
Thermal Sensitivity	0.08° C at 30° C
Frame Rate	60 Hz
Field of View	24° x 18°
Temperature Range	-40°C to 200°C
Focus	Automatic
Accuracy	+/- 2° C, +/- 2% of reading
Built-in Digital Camera	N/A

**Table 4-4: Environmental conditions during IR surveys of Wisconsin bridges**

Bridge	Survey Date	Time of Data Collection	Ambient Temperature (° F)	Ambient Temperature Variation (° F)	Wind Speed (km/h)	Humidity (%)
Br. (A)	15/07/2010	2.00 PM	84	- 9	12.9	38
Br. (B)	31/05/2011	1.30 PM	80	- 10	16.1	51
Br. (C)	02/07/2015	12.45 PM	76	- 8	9.7	43

The developed analysis procedure was implemented as follows: (i) the images were enhanced using FLIR software and the temperature data was then saved as .csv files of all images; (ii) a selected window of 320 x 25 pixels, which represents one foot image spacing was extracted from each image and stitched with the extracted window from the next image. The dimension of the final stitched file was 640 x 24350 = 15.584 million pixels for the entire two lane deck; (iii) the data dimension was scaled-down and resulted in a reduced file with 60 x 1980 = 118,800 pixels; (iv) since the deck is too long compared with its width, the data was divided into three sections, where each section represents one third of the bridge length; (v) the co-ordinates of each pixel were identified and then arranged in a column order with (x, y, temperature) values of each pixel; (vi) the k-means clustering algorithm in Matlab was applied to identify the thresholds. The number of clusters (k) for this bridge was determined as three, based on the developed flowchart in **Fig. 4-9**; and (vii) the condition map was plotted. **Figure 4-13** illustrates the condition map of the first bridge deck section (dimensions in meter) delineating the severity of the subsurface defects based on the developed system. **Figure 4-14** illustrates the IRT delamination map of the same section (dimensions in feet) as per the record of the Wisconsin DOT.

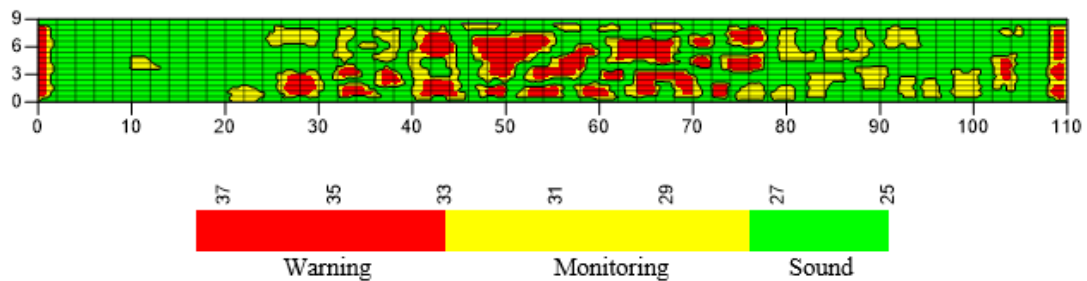


**Figure 4-13: Condition map of bridge (A) indicating the identified delaminated areas using the developed IRT system.**

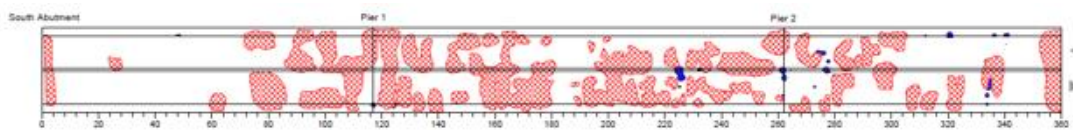


**Figure 4-14: Condition map of bridge (A) indicating the identified delaminated area as per the record of MOT, Wisconsin (Omar *et al.*, 2018).**

#### 4.5.2 Bridge (B)

The bridge was constructed in 1965. It consists of three spans of continuous concrete box girders with a 350.2 mm RC slab deck. The bridge was scanned on May 31, 2011 by Infrasense using IRT, as part of a condition survey. The critical deck characteristics include a total length of 26.3 m with a transverse width of 9.15 m, which translates into 8.36 m of drivable surface (supports a lane of traffic in each direction) with one side shoulder. The IRT survey methodology was carried out similarly to bridge (A) where the same IR camera was utilized. The survey conducted in three passes to include the side shoulder. The images were taken every 0.305 m (1 ft.) over the deck length, hence a total of 261 images were collected, which cover the entire two lanes and the shoulder of the bridge deck. The environmental conditions during the survey are shown in **Table 4-4**. The data was analyzed similar to the previous cases. The dimensions of the final mosaic were  $960 \times 2175 = 2.08$  million pixels and was scaled down to  $90 \times 260 = 23,400$  pixels. The clustering process resulted in thresholds, which represent three condition categories. The condition map was plotted delineating the severity of the subsurface defects as illustrated in **Fig. 4-15** (dimensions in meter). **Figure 4-16** exhibits the IRT delamination map of the deck as per the record of the Wisconsin DOT (dimensions in feet).

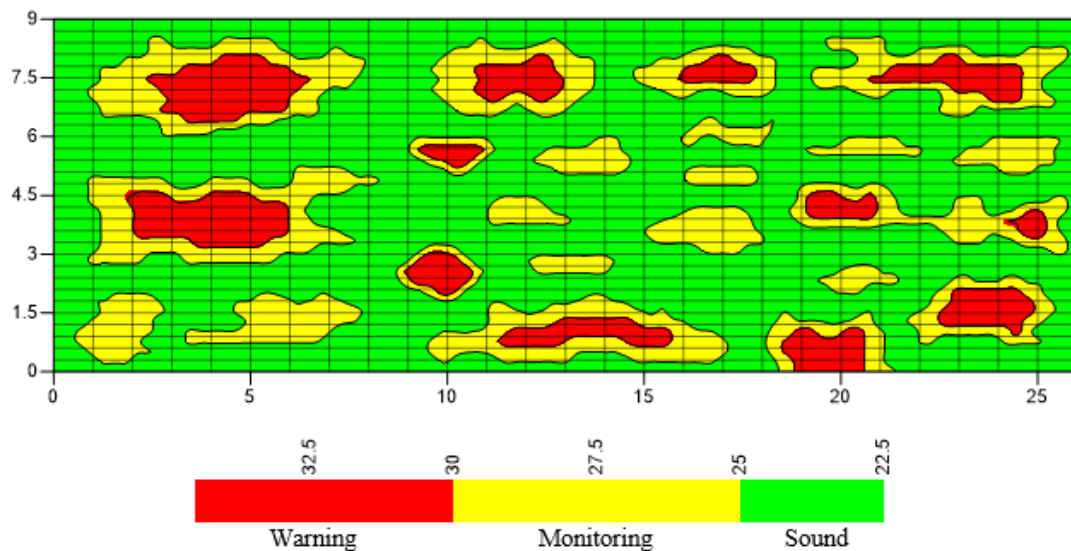


**Figure 4-15: Condition map of bridge (B) indicating the identified delaminated areas using the developed IRT system.**

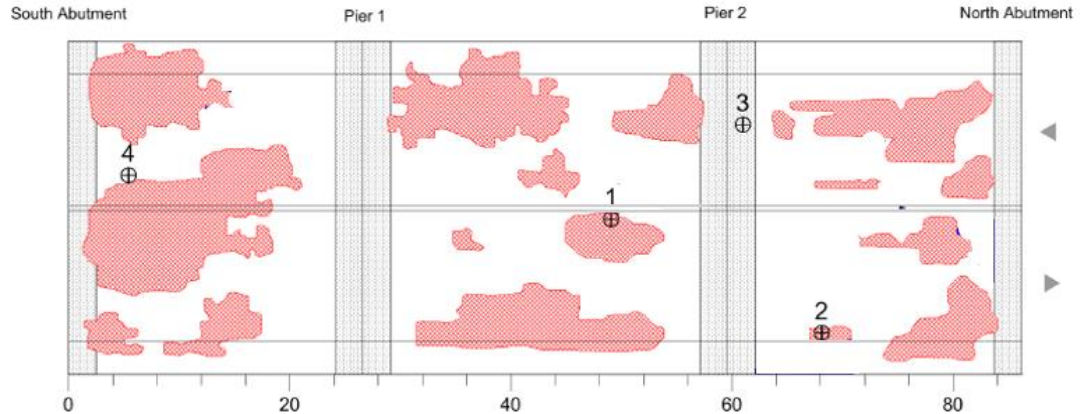


**Figure 4-16: Condition map of bridge (B) indicating the identified delaminated area as per the record of MOT, Wisconsin (Omar *et al.*, 2018).**

### 4.5.3 Bridge C

This bridge was constructed in 1967. It consists of four spans of continuous prestressed girders with a 362.9 mm RC slab deck. The south and north abutments, as well as the bridge piers are supported by driven treated temper piles. The bridge was scanned on July 02, 2015 by Infrasense using IRT and GPR as part of a condition survey. The critical deck characteristics include a total length of 94.5 m with a transverse width of 12.8 m, which translates into 8.6 m of drivable surface (supports a lane of traffic in each direction) with two side shoulders. The IRT survey methodology was carried out similarly to bridges (A) and (B) where the same IR camera was utilized. For this bridge deck with two lanes and left and right shoulders, the survey was carried out in four passes: one in each lane and one in each shoulder. The IRT survey produced a series of infrared images across the length of the deck. The images were taken every 0.305 m (1 ft.) over the deck length, thus a total of 1,240 images were collected. The environmental conditions during the survey are shown in **Table 4-4**. The data was analyzed similar to the previous cases. The dimension of the final stitched file was  $1280 \times 7750 = 9.92$  million pixels and was scaled down to  $128 \times 945 = 120,960$  pixels. The clustering process resulted in thresholds, which represent three condition categories. The condition map was plotted delineating the severity of the subsurface defects as illustrated in **Fig. 4-17**.

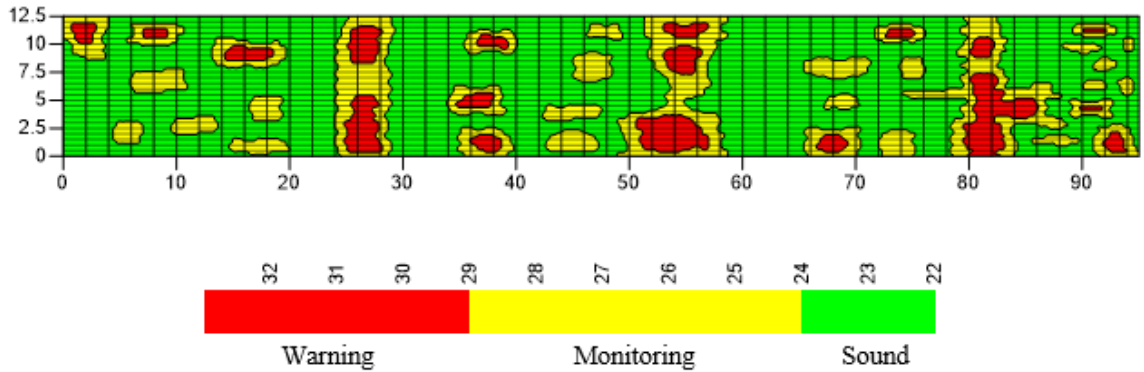


**Figure 4-17: Condition map of bridge C indicating the severity of the identified delaminated areas using the developed IRT system.**

## 4.6 Evaluation of the Proposed IRT Model

Transportation agencies need more conclusive information as to which exact part of a structure should be left intact, repaired, or demolished and replaced during the rehabilitation decision making process. Therefore, creating an accurate condition map with highlighted delamination categories from thermal IRT data is useful to the bridge management team and bridge inspectors responsible for ratings. The classification process adopted for the four bridge cases presented herein resulted in a segmented map for each deck of the surveyed bridges, clearly distinguishing the severity of identified delaminations. Sound concrete areas were represented by a green color, concrete areas that require close monitoring were represented by a yellow color, and warning concrete areas that require repair were represented by a red color. The thresholds between the three condition categories were determined based on the developed clustering process without analyst interference and, thus providing objective classification.

For the surveyed bridge deck in Montreal, the temperature differential between the sound and unsound areas of the concrete deck in the daytime survey was about 8 °C, as shown in in **Fig. 4-10**. During the nighttime survey of the same deck, the image temperature range was reduced to about 5.2° C, as shown in **Fig. 4-11**. The sound concrete areas had the lowest temperature values and the warning concrete areas had the highest temperature values during the daytime survey. Conversely, the sound concrete areas had the highest

temperature values and the warning concrete areas had the lowest temperature values during the nighttime survey. The reason for this is that, during the day, a warming trend existed such that the targets had positive thermal contrasts, which meant that the delaminated regions were at a temperature higher than that of the sound concrete. Conversely, during the night, a cooling trend existed resulting in the targets having a negative thermal contrast, which meant that the delaminated regions were at a temperature lower than that of the sound concrete. In other words, the defective regions warmed at a faster rate in the daytime survey and cooled at a faster rate in the nighttime survey than sound concrete. This is the anticipated behavior based on the fundamental heat transfer theories and complies with previous results reported by Washer *et al.* (2013) and Chase *et al.* (2015). It is also interesting to observe that both daytime and nighttime surveys identified considerably similar locations and geometries of subsurface defected regions. However, some defects were not revealed in the nighttime survey. This is most likely due to the transition between heating and cooling, where there may have been situations where a defect was not detected due to changes in the heat flow regime. In addition, the ambient temperature differential during the conducted nighttime survey was only  $-6^{\circ}$  F, while negative thermal contrast takes a much longer time to develop at the targets (Washer *et al.*, 2009). Hence, conducting the survey at midnight could produce similar results to the daytime survey. Yet the veracity of this assumption has not yet been proven. Nonetheless, it is more common to inspect bridge decks during the day, since the thermal contrast for defects would be much greater.

For bridges (A), (B), and (C), the temperature differentials between the sound and unsound regions of the concrete decks were  $12.5^{\circ}$  C,  $11.9^{\circ}$  C, and  $10.8^{\circ}$  C, respectively, as shown in **Figs. 4-13, 4-15, and 4-17**, respectively. Regardless of the various thermal contrasts and the environmental conditions during each survey time, the severity of the delamination was classified in each case. Again, the sound concrete areas had the lowest temperature values, while the warning concrete areas had the highest temperature values, since all surveys were conducted between 1 to 2 PM to ensure maximum thermal contrast. The produced delamination maps in **Figs. 4-13 and 4-15** generally follow the same trend as the delamination maps in **Figs. 4-14 and 4-16**, respectively, which were produced by

Infrasense using their proprietary software. The location and geometry of subsurface defected regions were identified with considerably comparable results.

It should be noted that it is common for the identified thresholds in the presented cases to differ because the IR images were taken at different times and environmental conditions, especially given the difference in the temperature range over the data collection period. This variety did not affect the condition categories that identify the severity of delaminations. However, it was observed that the threshold values, obtained for the four analyzed data, indicated that sound concrete as it stands for thermal contrast varies from 1 to 2.5<sup>0</sup> C. These results reinforce the fact that, for outdoor surveys, many factors alter the concrete surface temperature of the deck under investigation. Consequently, it is suggested that the ASTM standard should reconsider the specified thermal contrast value (0.5<sup>0</sup> C) to differentiate between sound and delaminated areas in a passive IRT testing. It should also be noted that the developed analysis procedure is capable to identify and classify delaminated areas at any environmental condition provided that the testing meets the minimum environmental conditions' requirements to conduct IRT surveys as specified in ASTM D4788-03. However, the quantified delaminated area in each condition category could be influenced to some extent by the recorded thermal contrast at the time of survey. Further surveys at different times of the year could validate such impact and also evaluate the accuracy of the achieved results. It is recommended to measure the environmental variables, such as wind speed, ambient temperature, solar loading and rainfall on site before the start of each survey.

## **4.7 Validation of IRT Model Results**

### **4.7.1 Hammer Sounding Test Results**

Hammer sounding was conducted on the surveyed bridge deck in Montreal by a bridge inspector from MTQ, before the IR survey. The created IR delamination map of the bridge deck was compared with the hammer sounding results and it was found that the two methods provided very similar sizes and shapes of deck defects. Similarly, the location of the detected delaminated areas revealed by the IRT result for bridges (A), (B), and (C) were confirmed by hammer sounding, which was conducted by the inspection team from

Infrasense. In addition, the delaminated areas, which were not detected by sounding, were subsequently clarified through impact echo testing. The non-detected defects over the piers in bridge (B), were due to the congested steel as indicated in the structural drawings.

Calculating the total delaminated areas in different categories from the mosaicked thermograms provides a quantified basis for powerful decision making and hence, can be paramount in prioritizing alternatives for bridge deck repair. The percentage of delaminated areas in each condition category was calculated by computing the total pixels in the same category over the total pixels in the entire deck area. **Table 4-5** summarizes the results for the surveyed bridge in Montreal and for bridges (A), (B), and (C). The IRT delamination maps for bridges (A) and (B), as per the record of the Wisconsin DOT, does not differentiate the severity of the delaminated areas. Hence, the total percentage of delaminated areas in the entire bridge decks was indicated. Similarly, the total percentage of delaminated areas resulting from hammer sounding tests for all bridges were indicated. The total percentage of delaminated areas in the Montreal bridge soffit was also presented. It was computed for each image, similar to the procedure adopted for the bridge deck.

The daytime condition map of the Montreal bridge deck showed 42% total delaminated areas, whereas the total delaminated areas calculated from the nighttime survey was 36%. Indeed, the concrete mass, thermal inertia and conductivity affect the rate of the transition process. Thus, some delaminated areas in the daytime survey appeared as sound areas in the nighttime survey. The hammer sounding results showed 38% total delaminated areas on the bridge deck and thus, 36% of the total delaminations is common between these two surveys. Similarly, 32% and 28% total delaminated areas on the bridge soffit were identified by the hammer sounding and IRT, respectively. However, it should be noted that it was very hard to locate delaminations at the intersection of the bridge soffit and the abutments. The delaminations in these areas had very small temperature differences from the sound concrete. A reason for this is the amount of concrete present in these areas acts as a large heat sink. Hence, a large temperature change is required to sufficiently affect the temperature of the concrete and allow easy detection of delaminations using IR cameras.

The analysis of IRT data of bridges (A), (B), and (C) showed 39%, 37%, and 28% respectively, of total delaminated areas on the bridge decks, whereas the total delaminated areas for Bridges (A) and (B) as per the records of Wisconsin DOT, were 41% and 40%, respectively from the IR survey and were 37% and 35%, respectively from the hammer sounding tests. Thus, the developed analysis procedure in this research can define the location and extent of delaminations in RC bridge decks with considerably high accuracy.

#### 4.7.2 GPR Test Results

The Montreal bridge investigated by IRT in the present research was surveyed using GPR scanning in September, 2015 (one month before the IR survey) by Radex Detection Inc., a consulting firm specializing in concrete structure scanning, as part of a condition survey program. GPR evaluates the condition of concrete bridge decks based on the difference between reflection amplitudes of the top rebar layer, where strong reflection indicates sound concrete, while the area with high amplitude attenuation is commonly associated with the corrosion of steel reinforcement. Details on the utilized equipment and data acquisition are presented in Chapter 5. The GPR profiles were analyzed based on a line scan (B-scan) visual image analysis technique. The analyst scrolls through each GPR profile and marks visible anomalies based on known criteria of deterioration. The processed profiles are then combined by a proprietary software to create a corrosion map delineating the corrosion severity as illustrated in **Fig. 4-18**. In addition, three core drilling concrete samples for visual and chloride ion concentration analysis were taken from the bridge deck where two cores were taken at corrosion areas and one core was taken at a sound concrete area. For the two cores located at corrosion areas, the chloride ion concentrations were detrimental to the concrete when they were 0.04% by concrete mass, while the commonly accepted chloride threshold that facilitates rebar corrosion in ordinary portland cement concrete is 0.025%. This result could validate corrosion identified by the analysis of GPR scan data. It should be noted that the chloride threshold value could change in blended cements owing to its enhanced corrosion resistance properties (e.g. lower chloride and oxygen diffusion coefficients, lower water penetration, etc.).

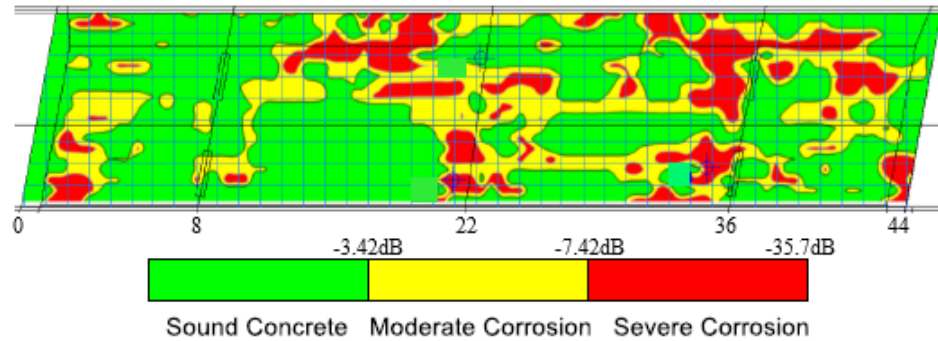


**Figure 4-18: Condition map indicating the severity of corrosion for the surveyed bridge deck in Montreal (Omar *et al.*, 2018).**

The GPR scan for bridge C was carried out by Infrasense at the driving speed using a GPR vehicle-based system for data collection. Details on the utilized equipment and data acquisition are presented in Chapter 5. The corrosion map as per the records of the Wisconsin DOT is illustrated in **Fig. 4-19**. This map was produced by Infrasense proprietary software after analyzing the GPR scan data. It indicates the location and geometry of the corroded areas without differentiating their severity.

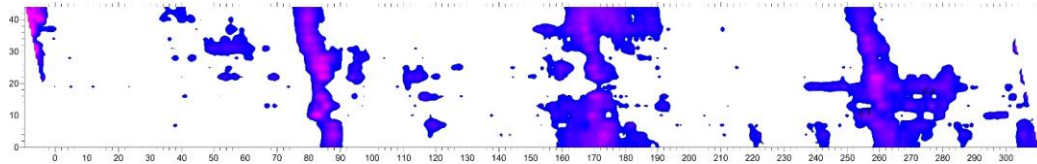


**Figure 4-19: Corrosion map of bridge C as per the record of Wisconsin DOT (Omar *et al.*, 2018).**

In spite of the different mechanisms of both IRT and GPR techniques and their capabilities of detecting different deterioration types, the IRT delamination map achieved by the developed analysis in **Fig. 4-10** was compared with the corrosion map provided by the GPR scanning in **Fig. 4-18**. Though the shapes (geometry) of the two analyses do not match exactly, the areas in which delaminations/corrosion were detected are mostly the same. The percentages of the delaminated and corroded areas in both maps were computed and are presented in **Table 4-5**. The GPR results showed 38% total corroded areas on the bridge

deck, whereas the total delaminated area calculated from the IRT results was 42% (about 10% difference in total defects between the IRT and GPR surveys). This complies with the results of previous studies. For instance, Maser (2009) reported that in most bridge structures, areas of corrosion are associated with delamination even if cracks are not detected directly. Washer *et al.* (2013) reported that not all delamination can be observed in GPR images and both GPR and IRT can be used together for accurate identification of anomalies in highway bridges.

For further verification, the IRT delamination map achieved from the thermal analysis of bridge C in **Fig. 4-17** was compared with the corrosion map provided by the GPR scanning in **Fig. 4-19** since both surveys were conducted on the same day. It can be observed that all corrosion areas identified by the GPR scan were also indicated by the IRT result. Conversely, not all the IRT identified delaminated areas were indicated by the GPR result. The percentages of the delaminated and corroded areas in both maps were computed and are presented in **Table 4-5**. The total defected areas in the bridge deck identified by the GPR and IRT are 23% and 28%, respectively (about 22% difference in total defects between GPR and IRT surveys). This variance could be due to the identification of only highly advanced corrosion areas by GPR scanning. It should be noted that while corrosion is the primary reason leading to delamination in RC bridge decks, there are other possible causes, such as freezing and thawing cycles and poor quality concrete. Thus, this could be another reason for obtaining potential corrosion areas smaller than the detected delaminated areas. However, further evidence from sounding, IE testing and/or core drilling of concrete samples is required to confirm the detected defects in this case study before final conclusions can be made.

Generally, any measurement is susceptible to error. Therefore, the results of IRT and GPR testing presented in **Table 4-5** could have some uncertainties in the quantified defective percentages. For instance, while the utilized camera has a thermal sensitivity of 0.03°C, which is a benefit when temperature differences are low, it has a margin of temperature measurement error up to  $\pm 1^{\circ}\text{C}$ . This could affect the maximum thermal contrast recorded during the survey. Therefore, it is more appropriate to evaluate the achieved results in terms of their precision rather than their accuracy where precision often refers to the closeness of

two or more measurements to each other. However, to verify the actual size and shape of the delamination identified by the proposed analysis procedure, the performance of the thermal camera could be firstly tested in laboratory validation experiments, to assess how well it could detect and map delaminations under controlled conditions. Then, error analysis should be conducted to evaluate the magnitude of variations between the in-situ scanning and experimental test results. This calibration process should give an overall measurement accuracy and thus evaluate the accuracy of the proposed analysis procedure.

**Table 4-5: Percentage of defective areas in the investigated bridges**

Bridge	NDT Survey Type	Survey Result	Concrete Condition		
			Sound	Monitoring	Warning
Montreal Surveyed Bridge	IRT	Nighttime (Deck)	64%	15%	21%
		Daytime (Deck)	58%	17%	25%
		Daytime (Soffit)	28% Total Delaminated Areas		
	Hammer Sounding	MTQ Record (Deck)	38% Total Delaminated Areas		
		MTQ Record (Soffit)	32% Total Delaminated Areas		
		GPR	MTQ Record	62%	16%
Bridge Deck (A)	IRT	Present Research	61%	16%	23%
		DOT Record	41% Total Delaminated Areas		
	Hammer Sounding	DOT Record	37% Total Delaminated Areas		
Bridge Deck (B)	IRT	Present Research	63%	19%	18%
		DOT Record	40% Total Delaminated Areas		
	Hammer Sounding	DOT Record	35% Total Delaminated Areas		
Bridge Deck (C)	IRT	Present Research	72%	12%	16%
		Hammer Sounding	DOT Record	25% Total Delaminated Areas	
	GPR	DOT Record	23% Total Corroded Areas		

#### 4.8 Further Research to Improve the Proposed IRT Analysis

The IRT analysis procedure developed in this study has some drawbacks that need further research. For instance, the magnitude of thermal contrast for a set of IR images could be affected by several factors, such as the thickness of the delamination, the spatial extent of the delamination and its depth. The presented methodology only considered the spatial extent of the delamination. While this factor was found to have the most direct and

significant effect on the thermal contrast values (Hiasa *et al.*, 2017), the other two factors need further consideration. In addition, the thermal data was characterized based on one feature vector (using the pixel numerical values in the IRT images). Other features, such as the shape and texture were not utilized. Hence, applying other image segmentation techniques could improve the classification process. Likewise, the k-means technique employed to identify the threshold values has inherent shortcomings. For instance, it neglects the stochastic nature of the threshold values. Therefore, some recommendations to overcome these limitations include: (i) utilizing the ultra-time domain IRT technique introduced by Washer (2016) through continuous monitoring for detecting the depth and thickness of delaminations in full-scale RC bridge decks; (ii) applying the region growing segmentation technique based on similarity of defined pixel properties to provide more objective classification; (iii) integrating the k-means and k-modes algorithms to allow for clustering pixels described by mixed numeric and categorical attributes; and (iv) employing fuzzy c-means technique to consider the uncertainty in pixel assignment where each data point can be a member of multiple clusters with a membership value.

## 4.9 Conclusions

The detection of concealed subsurface fracture planes is necessary to determine repair priorities of bridge decks. IRT enables recording dynamical variations of temperature in real-time and has been evolved as an effective and well-established non-destructive tool with the ability to provide meaningful condition information in a non-contact manner for bridge inspectors and management teams. The present study developed an easily deployable procedure and a less subjective IRT image analysis to classify the subsurface defects in concrete bridge decks and present the findings in terms of condition maps delineating the identified delaminations in different categories. The results obtained on four full-scale bridge decks demonstrated that temperature differences between delaminations in the same environment can be detected and categorized using the utilized clustering technique. Once the IRT images become available, the developed automated procedure can analyze and determine whether a defect exists with minimum human interference. The subsurface defected regions identified by the developed analysis provided satisfactory and

acceptable results and were confirmed by other NDT techniques including hammer sounding and GPR scans.

A key finding is that the applied methodology allows for the detection of subsurface anomalies at different survey times and environmental conditions. The attention herein has been mainly devoted to the condition evaluation of concrete bridge decks, while an infrared camera can be advantageously exploited with other bridge components. In future work, the authors plan to explore the applicability of the developed analysis to bridge soffit areas. While the developed procedure accurately identified the location and geometry of the subsurface defects, it did not indicate the depth or thickness of such defects. This could be another objective of future research. In addition, the application of further developed image processing tools on the acquired infrared thermal images, along with artificial intelligence-based approaches, can augment the decision making process to make it faster and fully automated without human interference. The present study confirms previous findings and contributes additional evidence, which suggests expanding the use of IRT as a reliable and rapid condition assessment tool for bridge inspections on both bridge and network levels. This will help transportation authorities in optimizing resources for bridge inspection, in prioritizing maintenance needs, and in improving the safety and serviceability of bridges.

#### 4.10 References

- ASTM. *D4788-03* (2013). “Standard Test Method for Detecting Delaminations in Bridge Decks Using Infrared Thermography.” ASTM International, West Conshohocken, PA. [www.astm.org](http://www.astm.org).
- Bagavathiappan, B., Lahiri, T., Philip, J. and Jayakumar, T. (2014). “Infrared thermography for condition monitoring – A review.” *J. Infrared Physics and Technology*. Vol. 60, pp: 35–55.
- Brown, M., and Lowe, D. (2007). “Automatic panoramic image stitching using invariant features.” *International J. Computer Vision*. Vol. 74 (1), 59-73.
- Chase, S., Adu-Gyamfi, Y., and Tunuguntla, P. (2015). “Bridge Deck Sub-Surface Defect Detection using Time-lapse Thermography.” *Proc., 94<sup>th</sup> Annual Meeting, TRB*, Washington, D.C. pp: 1-22.
- Clark, M., McCann, D., and Forde, M. (2003). “Application of infrared thermography to the non-destructive testing of concrete and masonry bridges.” *NDT&E International*, Vol. 36, 265-275.

- Dinh, K., Zayed, T., Moufti, S., Shami, A., Jabri, A., Abouhamad, M., and Dawood, T. (2014). "Clustering-based Threshold Model for Condition Assessment of Concrete Bridge Decks using Ground Penetrating Radar." *Proc., 93<sup>rd</sup> Annual Meeting, TRB*, Washington, DC, Vol. No. 2522, 1-11.
- Hiasa, S., Birgul, R., and Catbas, F. (2017). "Investigation of effective utilization of infrared thermography (IRT) through advanced finite element modeling." *Construction and Building Materials*, Vol. 150, 295-309.
- Huang, H. (2010). "Artificial neural network model of bridge deterioration." *Performance of Constructed Facilities*, Vol. 24 (6), 597-602.
- Jain, K. (2010). "Data clustering: 50 years beyond K-means." *Pattern Recognition Letters*, Vol. 31 (8), 651-666.
- Jiang, M., and Li, L. (2008). "Split-window algorithm for land surface temperature estimation from MSG1-SEVIRI data." *International Journal of Remote Sensing*, Vol. 29 (20), 6067-6074.
- Kee, S., Oh, T., Popovics, J., Arndt, R., and Zhu, J. (2012). "Nondestructive Bridge Deck Testing with Air-Coupled Impact-Echo and Infrared Thermography." *Bridge Engineering*, Vol. 17 (6), 928-939.
- Maldague, X. (2000). "Applications of Infrared Thermography in Nondestructive Evaluation". *Trends in Optical Nondestructive Testing*, 591-609.
- Manning, D., and Holt, F. (1982). "Detecting Delaminations in Concrete Bridge Decks." *Concrete International, ACI*, Vol. 2 (11), 1-8.
- Maser, K. (2009). "Integration of Ground Penetrating Radar and Infrared Thermography for Bridge Deck Condition Testing." *Materials Evaluation*. Vol. 66, 1130-1136.
- Maser, K., and Roddis, W. (1990). "Principles of Thermography and Radar for Bridge Deck Assessment." *Transportation Engineering*. Vol. 116 (5), 583-601.
- Melhem, H. and Cheng, Y. (2003). "Prediction of Remaining Service Life of Bridge Decks Using Machine Learning." *Computing in Civil Engineering*, Vol. 17 (1), 1-9.
- Meola, C., (2012). "*Origin and theory of infrared thermography.*" Published by Bentham eBooks: Infrared Thermography Recent Advances and Future Trends, C. Meola (Ed.), 3-28.
- Omar, T., Nehdi, M., and Zayed, T. (2018). "Infrared Thermography Model for Rational Condition Assessment of Concrete Bridge Decks." *J. of Construction and Building Materials*. Vol. 168, pp: 313-327. DOI: 10.1016/j.conbuildmat.2018.02.126.
- Qianqian, W., jinghai, L., Youna, L. (2002). "Segmentation of infrared image using adaptive thresholding." *Proc. SPIE*, Vol. 4925: Electronic Imaging and Multimedia Technology III, 265-269.
- Rinaldi, R. (2012). "*Infrared devices: short history and new trends.*" Published by Bentham eBooks: Infrared Thermography Recent Advances and Future Trends, R. Rinaldi (Ed.), 29-59.

- Robert, M. (1982). "Science behind Thermography-Thermal Infrared Sensing for Diagnostics and Control." *Thermosense*, Vol. 371, 2-9.
- Usamentiaga, R., Venegas, P., Guerediaga, J., Vega, L., and Molleda, J. (2014). "Infrared Thermography for Temperature Measurement and Non-Destructive Testing." *Sensors*, Vol. (14), 305-348.
- Vaghefi, K., Ahlborn, T., Harris, D., and Brooks, C. (2015). Combined imaging technologies for concrete bridge deck condition assessment." *Performance of Constructed Facilities*, Vol. 29 (4), 1-8.
- Vaghefi, K., Oats, R., Harris, D., Ahlborn, T., Brooks, C., Endsley, K., Roussi, C., and Shuchman, R. (2012). "Evaluation of Commercially Available Remote Sensors for Highway Bridge Condition Assessment." *Bridge Engineering*, Vol. 17, 886-895.
- Vladimir V. (2014). "Thermal NDT: historical milestones, state-of-the-art and trends." *Quantitative Infrared Thermography*. Vol. 11 (1), 66-83.
- Wagstaff, K., Cardie, C., Rogers, S., and Schrödl, S. (2011). "Constrained k-means clustering with background knowledge." *Proc., 18th International Conference on Machine Learning*, Vol. 1, 577-584.
- Washer, G., Fenwick, R., and Nelson, S. (2013). "Guidelines for the Thermographic Inspection of Concrete Bridge Components in Shaded Conditions." *Proc., 92<sup>nd</sup> Annual Meeting, TRB*, Washington, D.C., 1-14.
- Washer, G., Fenwick, R., and Harper, J. (2009). "Effects of Environmental Variables on Infrared Imaging of Subsurface Features in Concrete Bridges." *Transportation Research Board*, Vol. No. 2108, 107-114.
- Watase, A., Birgul, R., Hiasa, S., Matsumoto, M., and Catbas, N. (2015). "Practical identification of favorable time windows for infrared thermography for concrete bridge evaluation." *Construction and Building Materials*, Vol. 101, 1016-1030.
- Wu, X., Yao, H., Xie, D., and Xu, Z. (2012). "Developing of management information system of road and bridge infrastructure based on ArcGIS engine." *Proc., 2<sup>nd</sup> International Conference, Remote Sensing Environment and Transportation Engineering (RSETE)*, IEEE, 1-3.

## Chapter 5

### 5. Condition Assessment of Reinforced Concrete Bridge Decks Using Infrared Thermography and Ground Penetrating Radar

#### 5.1 Introduction

Corrosion of reinforcing steel has been identified as a significant contributor to RC bridge deck deterioration that can affect bridge deck integrity, and thus is one of the greatest concerns in bridge engineering. Precise evaluation of the condition of RC bridge decks, particularly for corrosion induced delaminations, is essential for ensuring bridge performance and safety. Ground penetrating radar (GPR) is one of the most appropriate NDT technologies for inspecting concrete bridge decks subjected to this deterioration mechanism. GPR testing has many advantages, such as its capability to evaluate the conditions for a corrosive environment, its inspection process, which does not require expertise, its relatively inexpensive cost compared with other NDT technologies, its high ability to rapidly survey large areas with full coverage, and its ability to achieve rapid data analysis. GPR uses electromagnetic (EM) signals for subsurface imagery. Several researchers investigated the materials characteristics recognized by EM signals either in the laboratory or in-service bridge decks. The raw GPR data is commonly represented as images that can be processed using several methods to obtain condition maps of the entire bridge decks that indicate the potential of active corrosion areas.

A new approach to NDT has been made in that it is recognized that making use of a combination of NDT methods will give the best possible harvest of information. Alani *et al.* (2013) reported that extra financial implications of using a combination of NDT techniques is acceptable if the evaluation outcome can be seen to have been enhanced. Indeed, GPR and IRT represent two technologies that can provide the needed information. Each technology has been developed and enhanced by improvements in hardware, software, and understanding of the interpretation of data. However, cogent procedures for deciphering their data have yet to be developed. In addition, little effort has been devoted to integrating the two technologies into a system that benefits from the strengths of both

(Maser, 2009). For instance, Maser and Roddis (1990) presented results of field studies using GPR and IRT on asphalt overlaid bridge decks and reported that the combined techniques were able to predict the total area of deterioration to within 5% of what was actually measured. Currently, there is limited research work describing the combined use of the results of these two methods.

In Chapter 4, an objective analysis for detecting and classifying delaminations in full-scale concrete bridge decks using passive IRT testing was developed and demonstrated through several case studies. In this Chapter, a robust procedure for uniting the IRT and GPR test results is developed. To achieve this goal, the following objectives are pursued throughout the chapter sections: (1) studying the working principles of GPR and its application for concrete bridge inspection as well as current analysis and interpretation methods of GPR scan data; (2) analyzing GPR data and identifying objective thresholds to produce a condition map that defines the severity levels of potential active corrosion in RC bridge decks; (3) analyzing IRT data and identifying objective thresholds for creating a condition map that designates the severity levels of delaminations in RC bridge decks; and (4) combining IRT and GPR results to produce an integrated condition map for aging RC bridge decks which classifies the severity levels of detected subsurface defects.

**Figure 5-1** illustrates the adopted systematic methodology to achieve the above-mentioned objectives. It can be summarized as follows: (1) conducting GPR scanning and passive IRT testing on two deteriorated full-scale concrete bridge decks; (2) analyzing the GPR data to extract the amplitude of the reflected waves using the conventional numerical amplitude method; (3) analyzing the IRT data to produce a thermal thermogram for the entire bridge deck from the IR images using the developed automated procedure presented in Chapter 4; (4) applying the k-means classification technique to determine objective thresholds for both GPR and IRT test results; (5) producing bridge deck condition maps identifying the severity levels of delaminations and the potential active corrosion areas from the IRT and GPR testing, respectively; and (6) integrating the analyzed GPR and IRT data using a specially written Matlab code to produce a condition map of the entire bridge deck. To verify the results, the detected defects were quantified and compared with results on the same bridge decks provided by other technologies.

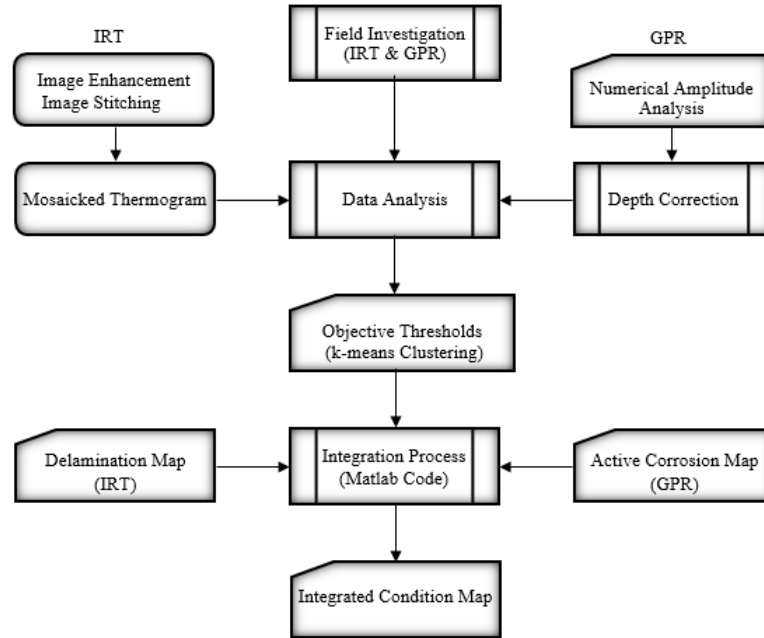


**Figure 5-1: Methodology adopted to evaluate RC bridge deck condition using the integration of IRT and GPR testing results.**

## 5.2 Ground Penetrating Radar (GPR)

### 5.2.1 Basic Principle of GPR

GPR emits short pulses of EM waves for subsurface imagery to detect anomalies in concrete bridge components. Electric conductivity, permittivity and permeability of the concrete are properties that have the greatest effect on the penetration depth of GPR signals and its resolution (Barnes *et al.*, 2008). The electric conductivity of a material is its ability to conduct the electric portion of an EM wave and is affected by the moisture content of the concrete. The higher the moisture content, the higher the conductivity, resulting in shallower GPR signal penetration depth. Dielectric permittivity is the ability of a material to store and transmit an electric charge induced by an EM field. Permeability is the ability of the material to become magnetized in the presence of an EM field. However, when EM energy goes through an interface between two materials of different dielectric properties, the intensity of reflection is determined by the change in the dielectric permittivity and conductivity of materials, where strong reflections indicate higher change in the electrical

properties at interfaces. The relationships between the received signal and the dielectric permittivity and conductivity of materials are described in **Equations 5-1** and **5-2**.

$$R = \frac{\sqrt{\varepsilon_1} - \sqrt{\varepsilon_2}}{\sqrt{\varepsilon_2} + \sqrt{\varepsilon_1}} \quad \text{Eq. 5 - 1}$$

$$\alpha = 1.69 \times 10^3 \frac{\sigma}{\sqrt{\varepsilon}} \quad \text{Eq. 5 - 2}$$

Where:  $R$  is the reflection coefficient;  $\varepsilon_1$  and  $\varepsilon_2$  are the dielectric constant of the first and second material, respectively;  $\alpha$  is the signal attenuation; and  $\sigma$  is the conductivity of the material. When the dielectric constant of the first material is smaller than the dielectric constant of the second material, the result of **Equation 5-1** will be negative. Although the shape of reflection waveform looks the same as the original pulse, their directions (or polarity) are different. This effect, in radar theory, is called change in polarity or phase reversal and should be considered when analyzing GPR signals. It should also be noted that the conductivity of concrete increases with the increasing frequency. Thus, the EM wave of a lower frequency can penetrate deeper inside the structure than that of a higher frequency (Halabe *et al.*, 1993).

Generally, a GPR system includes data collection units and antennas, of which there are two types: mono-static and bi-static. Mono-static antennas consist of one antenna that performs both transmitting and receiving functions, while bi-static antennas include separate antennas for transmitting pulses and receiving those that are reflected (Belli *et al.*, 2011). However, a transmitter antenna emits EM pulses from the surface of the concrete member being investigated at a desired frequency, and then these pulses propagate through the member. The receiving antenna collects the reflected pulses and records their properties, such as wavelength, two-way travel time and amplitude, to analyze and interpret the potential of subsurface corrosion (Gucunski *et al.*, 2013). The changes between transmitted and reflected pulses indicate a change in the materials' properties. Typically, the corroded rebar area in concrete structures has a low dielectric constant, producing

weaker reflected pulses. Therefore, the amplitude of reflection and attenuation are measured as an indication of potential rebar corrosion (Alani *et al.*, 2013).

The evaluation of GPR system performance depends on the ability of the EM signals to propagate to the required depth and the resolution of the resulting “images”. Therefore, the frequency of the antenna is a critical parameter that should be carefully selected to suit the survey’s objective. The propagation depth and resolution are both based on the wavelength of the transmitted signal because the frequency is inversely related to the wavelength. Higher frequency will have shorter wavelengths that produce a narrow cone of transmitted waves, which can focus on smaller areas. To obtain high-quality images, the wavelength should be short, which means that the frequency will be high. In other words, the higher the frequency, the better the resolution, and the shallower will be the propagation depth.

### 5.2.2 Application of GPR for Concrete Bridge Inspection

GPR scanning has been applied for several decades to evaluate the corrosive environment in RC bridge decks with and without overlays. Based on the operation methods, there are two types of GPR systems: air-coupled and ground-coupled. An air-coupled system is connected to a moving vehicle for rapid survey of highways with minimum traffic interruption. Yet, this scheme reduces the quality of the scanned images. Conversely, a ground-coupled system is dragged manually on a pushing cart and requires direct contact with the concrete bridge surface under investigation, usually providing better quality scans. GPR images can be divided into three types: A scan, a one-dimensional plot represents amplitude vs. time; B scan, a two-dimensional image created from a gathering of A-scans. The horizontal axis represents the position of the scan, while the vertical axis represents the two-way travel time; and C scan, a three-dimensional presentation of GPR data formed from a collection of B-scans. C-scans provide a block view for GPR data and are helpful for providing a good image for specific targets. For bridge decks, GPR data is usually analysed based on interpretation of many B-scans (Bostanudin, 2013).

Maser and Rawson (1993) scanned 72 bridge decks after removal of the asphalt overlay using a 1 GHz air coupled GPR acquisition unit, and reported that a correlation of 0.83 was found between the predicted deterioration and the known conditions, with a standard error

of  $\pm 4.1\%$  of the total deck area. Barnes and Trottier (2000) conducted a GPR survey on 24 asphalt covered bridge decks using a 1 GHz air coupled horn antenna and verified the obtained results using half-cell potential testing that was conducted after the asphalt pavement was removed from each deck. They reported that significant agreement was found between the two methods where the average difference between their results was 2.2 %. They also found that the decks which had less than 10% or more than 50% deterioration lacked contrast in between the regions which were perceived as deteriorated or sound, making it difficult to obtain accurate results with GPR. Cardimona *et al.* (2000) investigated 11 bridge decks using a 1.5 GHz ground coupled antenna and presented the results in terms of contour plots. Their results indicated that GPR has a good correlation with several ground truth methods and can accurately estimate the total deteriorated area of bridge decks. Gucunski and Nazarian (2010) evaluated 9 bridge decks with various NDT technologies, including GPR and half-cell potentials, and found very good correlation in zones of the highest deterioration. However, several other authors (e.g. Hong *et al.*, (2012); Lai *et al.*, (2013); and Dinh *et al.*, (2014)) evaluated the condition of RC bridge decks using GPR technology and achieved reasonable results.

### 5.2.3 Interpretation of GPR Scan Data

The ASTM D6087-08 (Standard Test Method for Evaluating Concrete Bridge Decks Using GPR) has evolved from a recommended practice for assessing asphalt-overlaid decks to a specification referenced regardless of the type of deck surface being evaluated. It describes the standard procedure for conducting GPR testing as well as data processing methodologies. The most common analysis method, the numerical amplitude method, depends on the value of the amplitude of the reflected waves from the top layer of reinforcing bars. The rationale behind this analysis method is based on known effects of moisture, chloride content and rust on the recorded GPR signals. The signal reflections at the rebar level are dominant and produce clear hyperbolic shapes. The shape is a hyperbola because the farther the antenna is away from the rebar, the longer it takes for the signal to travel to and from the rebar. Therefore, if the antenna is located directly over the rebar, it will have the shortest travel path. Data in regions with high corrosion will result in very “blurry” hyperbolas. Conversely, the higher the amplitudes of the reflected waves, the

better the condition of the bar. Because the reflection amplitude at each rebar depends on the distance (depth) from concrete surface to the rebar, depth correction through amplitude reduction should be considered in the analysis process (Barnes *et al.*, 2008).

Considering a GPR scan output as an image rather than an amplitude measuring tool, several research efforts have aimed to implement image processing methods. These methods include edge detection, or thresholding an image based on local extrema of intensity, to preprocess the image and isolate potential hyperbola regions. The presence of noise and image blurring can affect the edge detection results, while thresholding requires manually selected parameters that must be tuned to a given dataset. Another approach is template matching to identify hyperbolic regions based on predefined templates stored in a library. The type of concrete, rebar depth and noise are some obstacles to obtaining sound matching of templates with a GPR image.

Visual interpretation is another widely used technique to process GPR data. An experienced analyst scrolls through GPR data profiles and marks attenuated areas and thus, the boundaries of damaged zones can be located (Tarussov *et al.*, 2013). Such an approach is time-consuming and provides qualitative analysis depending on the analyzer's experience. For instance, it may be difficult for the analyzers to clearly define the border between sound and deteriorated regions or to maintain consistent judgement when they switch between profiles. This subjectivity effect is not desired. In addition, thresholds are commonly utilized to identify the boundaries of different levels of deterioration severity. In many instances, these thresholds are defined based on the personal judgment of the analyst, and thus, the subjective selection of threshold values is another limitation in interpreting GPR data (Dinh *et al.*, 2014).

Currently, the analysis and evaluation of GPR data for bridge deck condition assessment is mostly done after data collection. There has been interest by many researchers in developing automated GPR data acquisition and analysis. Indeed, an automated system can help improve the efficiency, reliability and repeatability of GPR data interpretation. For instance, an arc segment finding algorithm was suggested by Krause *et al.* (2007), which successfully finds the rebars and classifies them as good (true-positives) and good-minus

(false-positives). However, their method requires manual computation of threshold parameters to reject low quality rebar signatures and does not interpret the condition of bridges from the rebar detection results. Although, this approach has been successful on simulated defects in the laboratory, it has not yet been employed in full-scale bridge decks.

### **5.3 IRT/GPR Model Development**

Field testing in a real-world application was conducted on two in-service RC bridge decks using both IRT and GPR techniques. The bridges are located in Montreal, Canada and Wisconsin, USA, respectively. The developed IRT/GPR model will be introduced first for the Montreal bridge, and then will be implemented on the Wisconsin bridge.

#### **5.3.1 Data Collection**

The IRT survey was carried out for the Montreal bridge using a vehicle-based system with mounted thermal camera. The bridge characteristics, the features of the utilized thermal camera, the vehicle mounted set-up, and the data acquisition procedure have been presented in detail in Chapter 4. As previously discussed, there are several factors affecting the accuracy of passive IRT testing that can be classified into three principal categories: procedural (e.g. thermographer experience), technical (e.g. camera-to-object distance, depth and thickness of the delaminated areas), and environmental conditions (e.g. solar loading, ambient temperature and wind speed). However, all these factors were addressed in the conducted survey and the Matlab image acquisition toolbox was utilized to initialize acquisition and storage of high resolution thermal data. The same bridge deck was previously GPR scanned, one month before the IRT survey, by Radex Detection Inc., a consultant firm specializing in concrete structure scanning, as part of a condition survey program and the procedure adopted for the GPR scan is discussed below.

As per ASTM D6087-08 (2010), it is required for the GPR scan to form an orthogonal grid along the entire length of the bridge deck, with less than 0.91 m (3 ft.) spacing. The direction of scan paths depends on the direction of the primary steel in the deck. For bridge decks with primary steel in the transverse direction, the scan can be done along the lanes of travel. Conversely, for bridge decks with primary steel in the longitudinal direction, the deck would need to be scanned transverse to the travel lanes. A few settings must initially

be adjusted on the data acquisition unit, such as applying a gain at particular points, usually at the location of the rebar, in order to force subtle variations in weaker data to be more visible, and deciding whether the user wants to collect data according to time or distance. The pushing cart for a ground-coupled GPR system is commonly equipped with a calibrated distance wheel, enabling the distance option during the survey of bridge decks. Thus, it allows data to be mapped out spatially with respect to the actual coordinates of the deck (Tarussov *et al.*, 2013). This can also help the analyzer identifying which part of the bridge deck must be repaired or rehabilitated.

The bridge deck was scanned with a ground-coupled radar system using a pushing cart. After studying the bridge deck plan, a grid of scanning paths with 50 cm spacing and 25 cm offset from the curb was established using water soluble paint dots. For each path, its two ending points were determined by a survey tape, measuring from curb to curb. Then, these points were marked. To move the machine in accurate straight lines by an operator, a survey string was used between the points of each path. The scan was conducted using a GSSI-SIR3000 GPR data acquisition unit with 1600 MHz antenna frequency. **Figure 5-2** illustrates the data acquisition unit and grid pattern used. The GPR unit was calibrated before scanning the bridge deck to ensure accurate measurements. Data collection was made longitudinally on the deck and hence, a total of 16 profiles were collected for the entire bridge deck (8 profiles for each direction) where each profile represented a width of 500 mm. The pass direction was selected so that the antenna crosses over the primary top layer of reinforcing steel at a 90° angle. The first scan path was done in one direction and the second in the reverse direction and so on. The profiles conducted in the reverse direction were reversed during the analysis. Road closure was performed, giving adequate access to the bridge deck.



**Figure 5-2: Illustration of GPR travel paths and the utilized data acquisition unit.**

Detailed information regarding the equipment used and data settings are summarized in **Table 5-1**.

**Table 5-1: Features and specifications of the utilized GPR equipment**

<b>Characteristic</b>	<b>Specification</b>
SIR System	SIR - 3000
Antenna Frequency	1600 MHz
Scans / m	100
Samples / Scan	256
Bits / Sample	16
Gain (No of Point)	1
Gain Value	- 5 dB
High Pass Filter	470 MHz
Low Pass Filter	1930 MHz

### 5.3.2 Data Analysis

The developed automated procedure to analyze the thermal images was presented in Chapter 4. As previously discussed, the methodology includes image preprocessing to enhance the captured images by reducing noise and improving the images' thermal contrasts, image registration that involves a developed stitching algorithm. All the customized Matlab codes that were developed to extract and stitch the selected pixels from each image, to scale-down the mosaic dimension, and to identify the coordinates of each pixel in the mosaic were written with variables to automate the analysis process. Hence, the developed procedure was implemented on the captured thermal images and produced a mosaic thermogram of the entire bridge deck as presented in Chapter 4. However, the procedure adopted to analyze the GPR data of the same bridge deck is presented below.

The conventional numerical amplitude analysis method is based on the effects of moisture, chloride ions content and rust on the recorded GPR signals. This method was utilized in the present research. The scanning profiles were post-processed using the commercial software RADAN 7 (a GPR data analysis software developed by GSSI) to extract important information for further analysis. First, each profile was cut down to ensure that it only includes the bridge deck length. Next, the top reinforcing steel bars were selected (peak of the parabolic shapes). When the entire bars were selected, the software generated an Excel

sheet containing the scan number, amplitude, and two-way travel time for each point (bar). This step was repeated for the entire bridge deck's profiles. **Figure 5-3** illustrates the picked top reinforcing bars, represented as red points, in a B-scan GPR profile.

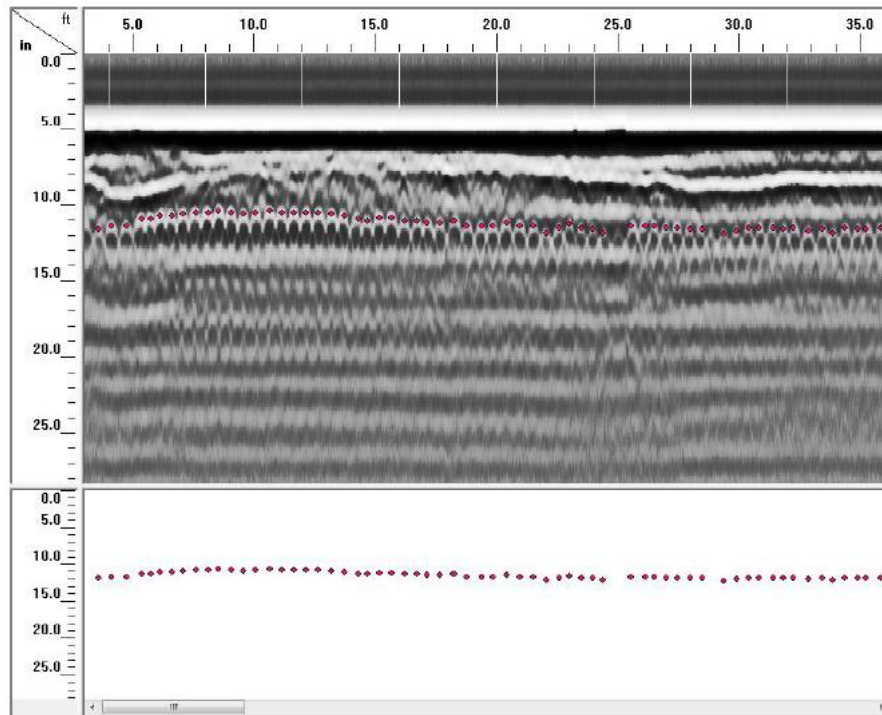


**Figure 5-3: Picking top reinforcing bars in a B-scan profile.**

Reinforcing steel is not always placed at an exact depth throughout the deck during construction. It also may not be located at a constant depth due to defects, variable surface milling depth or due to surface wearing. Thus, the thickness of the concrete cover to the reinforcing steel may vary across the deck and this can lead to variance in the amplitude of the reflected waves because the GPR signal attenuates with depth. Accordingly, deeper rebar has lower amplitudes than rebar located at shallower depths due to the dissipation of energy as the signal travels through concrete. Therefore, to relate deterioration of concrete using the attenuation of the signal at the rebar level, the varying depths of rebar must be accounted for using an analytical approach. Depth correction for GPR data has been a point of interest for many researchers. For instance, Barnes *et al.* (2008) normalized the depth of all reinforcing bars based on the relation between the amplitudes of the reflected waves

and the corresponding two-way travel time. They proposed to plot the recorded amplitude versus two-way travel time values to determine a best-fit linear trend and then remove it from the plot by altering the amplitude, thereby assigning all reflections to a constant depth. Consequently, after the processing of all profiles and generating of Excel sheets were completed, the saved data were imported to a commercial software where a quantile linear regression fitting was performed at 90<sup>th</sup> percentile, and then subtracted from the depth-dependent amplitude in order to perform a depth correction for the reinforcing bars. After normalization was completed, variations in reflection amplitudes were expected to correspond to the deterioration only. The final output was an Excel file containing the coordinates and amplitude of the selected reinforcing bars.

### **5.3.3 Deterioration Condition Maps**

#### **5.3.3.1 *Thresholding Classification***

Thresholding classification was adopted in the proposed methodology to identify objective thresholds for both IRT and GPR data. As previously discussed, classification is the task of organizing data into categories. The k-means clustering function in Matlab that was introduced in Chapter 4 was implemented in the developed model to perform this task. The number of clusters is the user defined parameter to perform k-means clustering for a data set. A developed framework was presented in Chapter 4 to determine the number of clusters for IRT data. However, the AASHTO guide manual for bridge element inspection implements four categories (good, fair, poor, and severe) to represent the condition of each bridge element, all of which have been introduced into the AASHTOWare™ bridge management software BrM, which is currently the primary bridge management software used by transportation agencies across the USA. Similarly, in the Ontario Bridge Management System (OBMS), defects are recorded in four condition categories (excellent, good, fair, and poor) for each bridge component and performance deficiencies for each component where a bridge element will remain in each condition category a period of time during its service life. The severity degrees of a defect in the material condition rating index for the Quebec Ministry of Transportation are defined as light, medium, severe, and very severe. Consequently, the number of clusters herein was considered four to represent the severity levels of potential deterioration identified by the IRT and GPR testing.

### 5.3.3.2 *Delamination Condition Map*

The k-means clustering algorithm in Matlab was first applied to identify the thresholds of the IRT data. For the bridge deck being considered and based on the identified thresholds, the temperature values in each severity level were grouped and uploaded into a commercial mapping software to construct a high contrast composite condition map accurately delineating the different severity levels of subsurface delaminations, as illustrated in **Fig. 5-4**. The area of very severe delamination was very small and, hence, has been combined with the areas of severe delaminations for visualization. This will also ensure an identical degree of attention with respect to the preservation or maintenance actions to be taken for these areas.

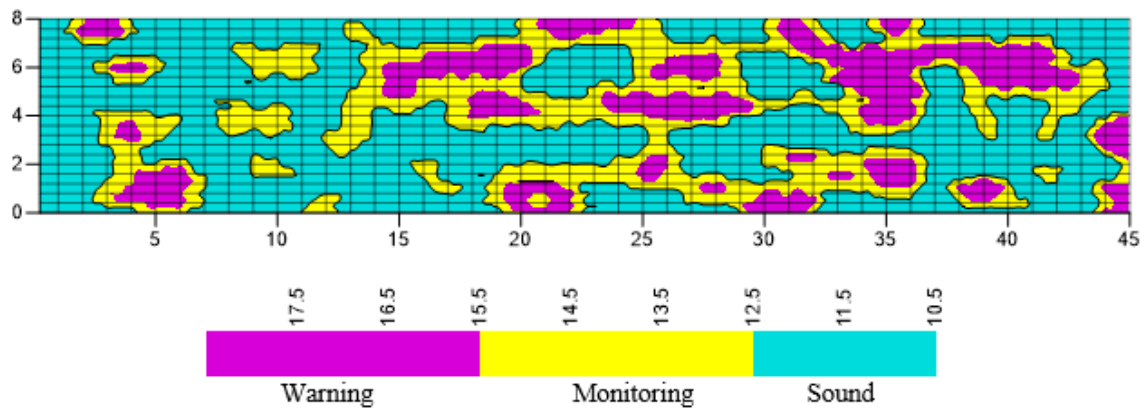


**Figure 5-4: IRT condition map of Montreal's bridge deck indicating different severity levels of delaminations.**

### 5.3.3.3 *Corroded Corrosion Map*

Similarly, for the GPR data and upon completion of the numerical amplitude analysis and the depth correction process, the k-means clustering algorithm in Matlab was applied to identify the thresholds. Based on the identified thresholds, the amplitude values in each severity level were grouped and uploaded in a commercial mapping software to construct a high contrast composite condition map accurately delineating the different severity levels of potential active corrosion, as illustrated in **Fig. 5-5**.

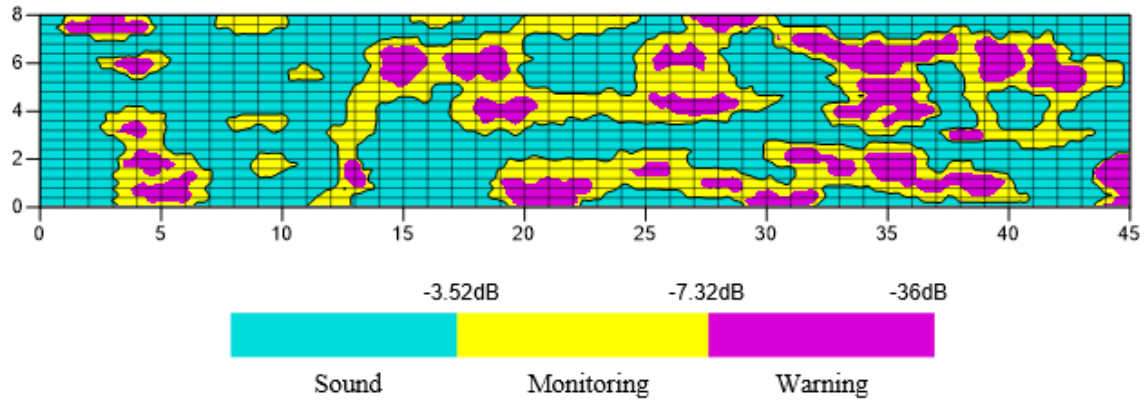


**Figure 5-5: GPR condition map of Montreal's bridge deck indicating different severity levels of potential active corrosion.**

The GPR profiles were also analyzed by Radex Detection Inc., the firm who collected the data based on the line scan (B-scan) visual image analysis technique. The experienced analyst scrolls through each GPR profile and marks the attenuated areas manually while considering some factors, such as the presence of beams or tightly spaced steel reinforcement. The boundaries of damaged zones are located in each profile and then combined by the firm's proprietary software to create a condition map delineating the different severity levels of potential active corrosion, as illustrated in **Fig. 5-6**.

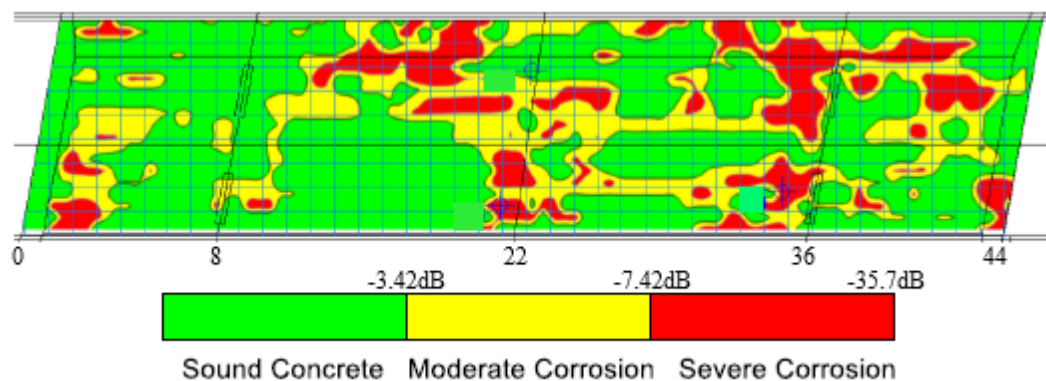


**Figure 5-6: GPR corrosion map of Montreal's bridge deck as per the record of MOT, Quebec (Omar *et al.*, 2018).**

### 5.3.3.4 Combined Condition Map

To obtain a precise evaluation of the bridge deck condition, the results of the deployed NDT techniques were combined. The Excel sheets, resulting from the analysis of the IRT and GPR data, are two matrices  $A$  ( $a \times b$ ) and  $B$  ( $c \times d$ ), respectively where matrix ( $A$ ) represents the temperature values, and matrix ( $B$ ) represents the reflected amplitude values after applying the depth correction. The integration process consists of two steps. First, the largest matrix ( $A$ ) was scaled-down to have a size similar to that of the smallest matrix ( $B$ ) as per **Equation 5-3**, and then both matrices were combined as per **Equation 5-4** using a consistency factor, which accounts for the difference in their data range. A Matlab code was written for this purpose where the code can accommodate any other survey data, and thus, automate the combination process. The integrated data was uploaded into a commercial mapping software to produce a final condition map of the entire bridge deck, as illustrated in **Fig. 5-7**.

$$S_{kl} = \frac{\sum_{i=1}^I \sum_{j=1}^J A_{ij}}{[I \times J]} \quad \text{Eq. 5 - 3}$$

Where:

$S_{kl}$  are the elements of the scaled – down matrix  $S = (c \times d)$

$k = 1 \rightarrow c \quad l = 1 \rightarrow d$

$A_{ij}$  are the elements of matrix  $A \quad i = 1 \rightarrow a \quad j = 1 \rightarrow b \quad [A > B]$

$[I \times J]$  is the window in matrix  $A$  to be averaged  $I = a/c \quad J = b/d$

$$D_{kl} = C_{kl} + \left(\frac{\alpha}{\beta}\right) \times B_{kl} \quad \text{Eq. 5 - 4}$$

Where:

$D_{kl}$  are the elements of the combined matrix  $D = (c \times d)$

$\left(\frac{\alpha}{\beta}\right)$  is a consistency factor

$$\alpha = \text{average of matrix } A_{ij} = \frac{\sum A_{ij}}{(a \times b)}$$

$$\beta = \text{average of matrix } B_{kl} = \frac{\sum B_{kl}}{(c \times d)}$$

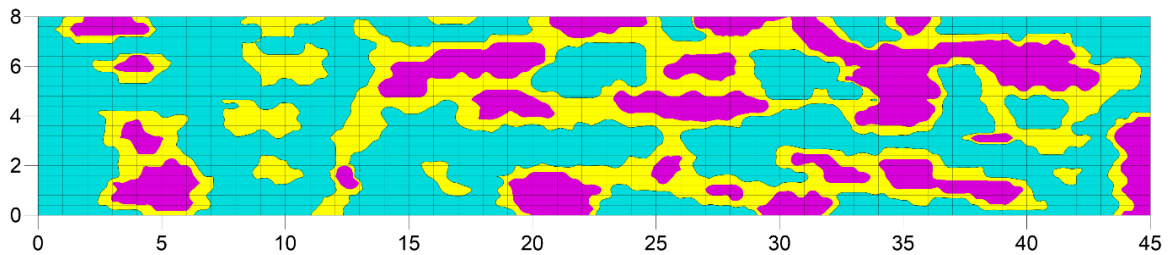


**Figure 5-7: Integrated condition map of Montreal's bridge deck based on the IRT and GPR results.**

#### 5.4 IRT/GPR Model Implementation on a Second Case Study

The integration procedure outlined above was also implemented on the Wisconsin bridge. The IRT survey and GPR scanning were conducted on July 02, 2015 by Infrasense, a consultant firm specializing in concrete structure scanning, as part of a condition survey program. The IRT survey was carried out using a vehicle-based system with mounted thermal camera. The bridge characteristics, the features of the utilized thermal camera, the vehicle mounted set-up, the environmental conditions during the survey, and the data acquisition procedure have been presented in details for the case study of bridge C in Chapter 4. The GPR scan was carried out at driving speed using a GSSI vehicle-based system. Hence, no road closure was required and traffic flow was not disrupted. The GPR data was collected longitudinally on the deck with 0.91 m (3 ft.) spacing between the GPR profiles and hence, a total of 14 profiles were collected for the entire bridge deck (7 profiles for each traffic direction). The data was collected with a combination of a 1-GHz horn and a 1600-MHz ground-coupled antenna.

The developed automated procedure to analyze the thermal images was adopted as follows: (i) the images were enhanced and the temperature data was saved as .csv files for all images; (ii) a selected window of 320 x 25 pixels, which represents 0.305 m (1 ft.) image spacing, was extracted from each image and stitched with the extracted window from the next image. The dimension of the final stitched file was 1280 x 7750 = 9.92 million pixels for the entire two lane deck and two shoulders; (iii) the data dimension was scaled-down resulting in a reduced file with 128 x 945 = 120,960 pixels; (iv) the co-ordinates of each pixel were identified and then arranged in a column order with (x, y, temperature) values of each pixel; (v) the k-means clustering algorithm in Matlab was applied to identify the thresholds; and (vi) the condition map was plotted delineating the different severity levels of the subsurface delaminations, as illustrated in **Fig. 5-8**.

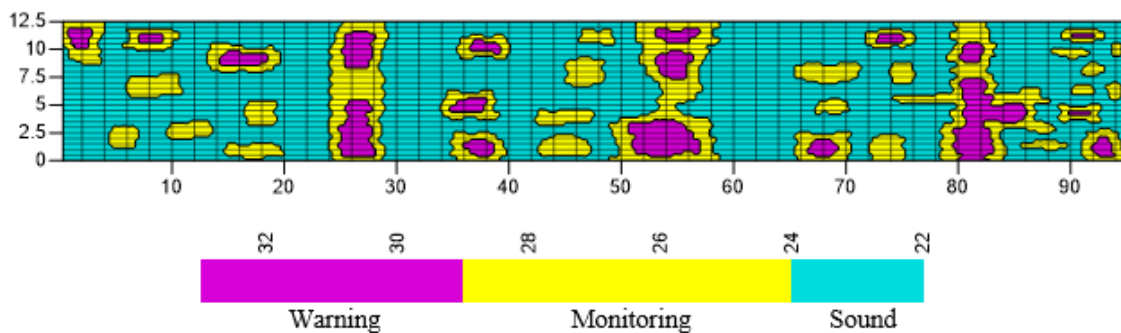


**Figure 5-8: IRT condition map of Wisconsin's bridge deck indicating different severity levels of delaminations.**

The GPR data was analyzed based on the conventional numerical amplitude analysis method and the applied clustering technique. The scanned profiles were post-processed using the commercial radar software RADAN (a GPR data analysis software developed by GSSI), where the top reinforcing steel bars were selected and an Excel sheet containing the scan number, amplitude, and two-way travel time for each bar was generated. This step was repeated for the entire bridge deck's profiles. Depth correction for the reinforcing bars was then applied using a commercial software. The final output was an Excel file containing the coordinates and amplitude of the selected reinforcing bars. The k-means

clustering algorithm was applied to identify the thresholds. Accordingly, the condition map was plotted delineating the different severity levels of potential active corrosion, as illustrated in **Fig. 5-9**. The corrosion map as per the records of the Wisconsin DOT is illustrated in **Fig. 5-10**. This map was produced by the Infrasense proprietary software (dimensions in feet).

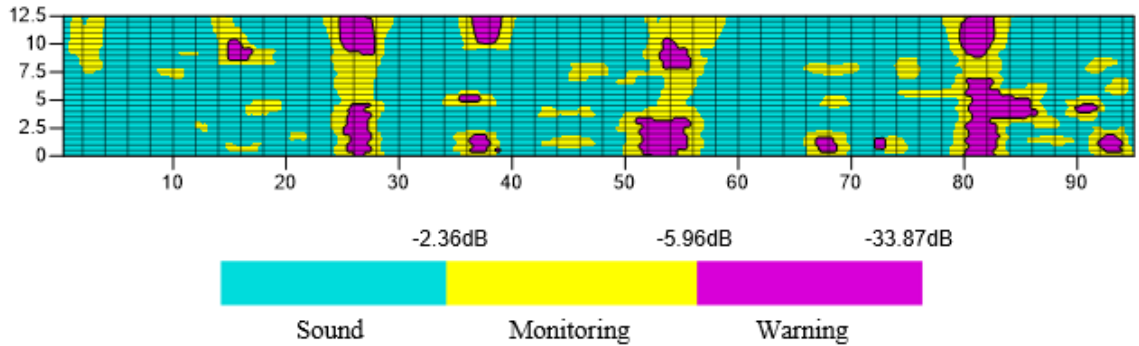


**Figure 5-9: GPR condition map of Wisconsin's bridge deck indicating different severity levels of potential active corrosion.**

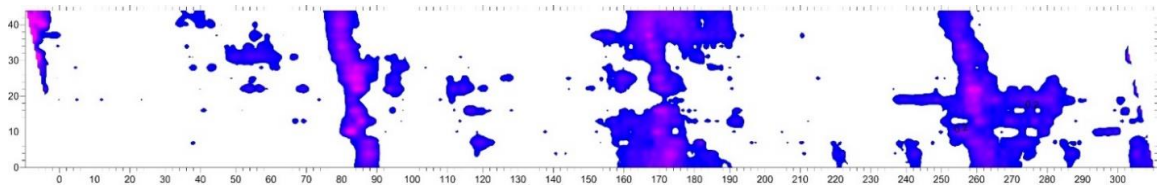


**Figure 5-10: GPR corrosion map of Wisconsin's bridge deck as per the record of Wisconsin DOT (Omar *et al.*, 2018).**

The integration process was then carried out using the written Matlab code. The temperature matrix was first scaled-down to have a size similar to the amplitude matrix, then both matrices were combined. The k-means clustering algorithm was subsequently applied to identify the thresholds. The final condition map of the bridge deck was plotted delineating the integration of the detected delaminations and potential active corrosion areas in different severity levels, as illustrated in **Fig. 5-11**.

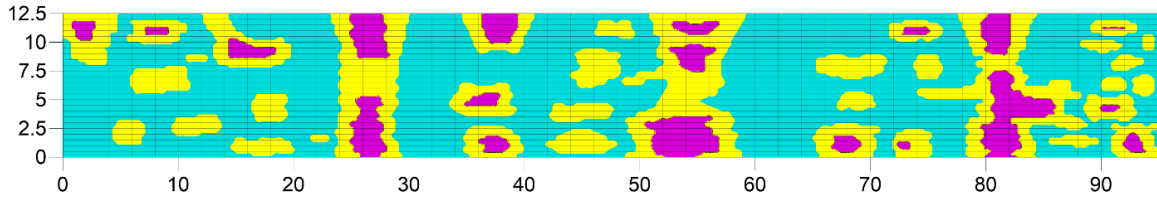


**Figure 5-11: Integrated condition map of Wisconsin's bridge deck based on the IRT and GPR results.**

## 5.5 Evaluation of the Proposed IRT/GPR Model

The presented integration analysis of IRT and GPR data aims to rationalize their use as reliable NDT tools for bridge deck inspection. IRT can highlight overlay and rebar-level delamination, while GPR can delineate areas where corrosion could be active as explained earlier. When testing full-scale bridges, extracting quantitative measures of subsurface defective areas in different severity levels using both techniques remains a challenge. Creating a plan view mosaic of the entire bridge deck from the individual IR images facilitated the application of thresholding classification to identify and categorize subsurface delaminated areas. The thermal contrast developed from the concrete subsurface provided numerical values for the color contrasts that were used to process data more effectively than simply comparing multiple images. This procedure was useful in detecting and calculating delaminated areas present in the bridge decks.

On the other hand, when conducting GPR testing, the relationship between GPR measurements and the real condition of decks is still not well understood. Although the amplitude analysis provides an objective and detailed decibel scale, subjective selection of threshold values remains a limitation. The corrosion maps created in this study categorized the potential corroded areas based on the relative difference between the amplitude values of the reinforcing bars. Maser *et al.* (2012) developed a model to find a threshold for determining whether the concrete is sound or deteriorated by making a correlation between GPR and half-cell potential. Martino *et al.* (2014) developed another model, which is also based on a correlation between GPR and half-cell potential records. Both models determine one threshold to differentiate only between sound and corroded areas. Dinh *et al.* (2014)

developed a threshold model to classify the corroded areas in RC bridge decks based on a GPR scan. Their applied methodology in identifying the number of condition categories was based on visual interpretation of the GPR images, which is rather subjective.

The IRT delamination map achieved from the thermal analysis in **Fig. 5-4** was compared with the corrosion map provided by the GPR analysis in **Fig. 5-5** and also with the GPR map as per the records of the Quebec MOT in **Fig. 5-6**. The three condition categories, which distinguish the severity of delaminations and corrosion, are presented in the three figures as: sound concrete, concrete areas with moderate defects that require close monitoring, and concrete areas with severe defects that give a warning to consider a repair action. The sound concrete areas had the lower temperature values and higher amplitude measures, while the warning concrete areas had the higher temperature values and amplitude attenuation measures. In spite of the different mechanisms of the IRT and GPR techniques and their capabilities of detecting different deterioration types, their bridge deck condition maps established in this case study are comparable. Though the locations and geometry of the defects do not match exactly, the areas in which potential delaminations and corrosion were identified have reasonable correlation. In addition, hammer sounding was conducted on the bridge deck by an MTQ bridge inspector before the IRT survey. The created IRT delamination map of the bridge deck was compared with the hammer sounding results. It was found that the two methods provided similar sizes and shapes of deck defects. The quantified defective areas by the three techniques are discussed below.

Similarly, the IRT delamination map achieved from the thermal analysis of the Wisconsin bridge in **Fig. 5-8** was compared with both the corrosion map provided by the GPR analysis in **Fig. 5-9** and the Wisconsin DOT GPR map in **Fig. 5-10**. It can be observed that all corrosion areas identified by the GPR scan were again indicated by the IRT result. Conversely, not all the identified delaminated areas were indicated by the GPR result. This indicates that only highly advanced corrosion areas were identified by GPR scanning. For more verification, the produced IRT delamination map was compared with the hammer sounding results as per the record of Wisconsin DOT and generally followed similar trend. However, the threshold classification technique adopted in the present research, not only resolves the subjectivity problem in selecting threshold values, but also facilitates the

calculation of area percentage for each condition category. Calculating the total delaminated and corroded areas in different categories from these thermal and corrosion maps provides a quantitative basis for powerful decision making. Thus, prioritizing alternatives in bridge deck rehabilitation plans is facilitated. The percentage of the delaminated and corroded areas in both bridge deck cases were computed and presented in **Table 5-2**. The total percentage of delaminated areas resulting from hammer sounding tests were also indicated.

**Table 5-2: Percentage of defective areas in the analyzed bridge decks**

Bridge Deck	NDT Survey Type	Survey Result	Concrete Condition		
			Sound	Monitoring	Warning
Montreal's Bridge	IRT	Present Research	58%	17%	25%
	GPR		64%	15%	21%
	Combined (IRT & GPR)		53%	19%	28%
	Hammer Sounding	MTQ Record	38% Total Delaminated Areas		
	GPR		37% Total Corroded Areas		
	-----				
Wisconsin's Bridge	IRT	Present Research	72%	12%	16%
	GPR		76%	10%	14%
	Combined (IRT & GPR)		68%	14%	18%
	Hammer Sounding	DOT Record	25% Total Delaminated Areas		
	GPR		23% Total Corroded Areas		
	-----				

For the Montreal bridge, the analysis of the IRT data indicated 42% total delaminated areas in the bridge deck, while the hammer sounding results showed 38% total delaminated areas. Hence, the difference between the findings of the two methods is in the range of about 10%. The GPR analysis showed 36% total areas of potential active corrosion, whereas this percentage as per the records of MOT Quebec, is 37%. For the Wisconsin bridge, the analysis of the IRT data indicated 28% total delaminated areas in the bridge deck, whereas the total delaminated areas identified by hammer sounding as per the records of Wisconsin DOT, were 25%. The GPR analysis showed 24% total areas of potential active corrosion, while as per the DOT Wisconsin records, the corroded areas represent 23%. Thus, the analysis procedure developed herein can precisely define the extent of delamination and the potential locations of active corrosion in concrete bridge decks.

Combining the results of various inspection techniques could provide more reliable evaluation and prevent overestimating or underestimating a bridge deck condition. Thus, relevant research efforts have recently attempted to integrate multiple NDT technologies to assess the overall bridge structural capacity as well as automate the data collection and analysis processes (Gucunski *et al.*, 2013). Adopting this approach during a real field deployment is vital to achieving an efficient bridge condition. **Figures 5-7 and 5-11** demonstrate the importance of the integration concept. For instance, the integrated IRT and GPR results indicated that 53% of the Montreal bridge deck area was sound, while the IRT and GPR separate evaluations were 58% and 64% of the deck's area, respectively, as presented in Table 3. Thus, evaluating the bridge deck condition based solely on IRT or GPR could overestimate the sound area by about 11% and 23%, respectively. Similarly, for the Wisconsin bridge deck, the integrated IRT and GPR results indicated that 68% of the deck's area was sound, while the IRT and GPR separately evaluated the sound deck's area as 72% and 76%, respectively. These results could significantly affect any maintenance actions to be taken and should draw attention to the importance of integrating IRT and GPR results.

However, it is important to highlight that the reliability of the integrated IRT and GPR results depends on the accuracy of data collection and analysis. Indeed, each technique has its own strengths and limitations. For example, IRT has several advantages over other NDT techniques, such as being able to scan a large area in a non-contact manner. It is much faster than conventional methods and has a potential to be applied at near highway speed over a bridge deck, thus mitigating traffic disruption. In addition, the IRT testing can be conducted during both day and night time. Conversely, IRT is dependent upon environmental conditions and can become ineffective if such conditions are unfavorable to produce a thermal gradient in the concrete. For instance, clouds reduce the intensity of incident solar radiation during the day and reflect infrared radiation at night, thus slowing heat transfer at the concrete surface. Rain could lead to concrete surface cooling, thus masking thermal effects from the surface. For decks with a concrete overlay, IRT can clearly reveal the overlay de-bonding, but may have limitations in detecting deeper rebar-level delamination. In addition, factors such as moisture, oil spills, surface texture and staining on the concrete surface can create high noise level in the thermal images.

Similarly, GPR scan of RC bridge decks can cover large areas in a short time and easily penetrate through asphalt layers. Despite its valuable advantages, GPR has limitations, such as its incapability to provide information on corrosion rates or mechanical properties of the tested concrete. GPR cannot directly detect thin or in contact cracks and delaminations. Extreme cold weather can negatively influence GPR results because frozen water is relatively transparent to electromagnetic waves in the frequency range typically used for bridge scans. In addition, de-icing agents can limit the ability for GPR signal to penetrate the deck, and electromagnetic waves from mobile phones can cause noise in GPR results. Therefore, combining the two technologies in inspecting deteriorated bridge decks is very powerful, allowing to maximize the capabilities of each method and compensate for mutual limitations.

## 5.6 Conclusions

An accurate condition assessment of the extent and severity of bridge deck deterioration is essential for transportation agencies in prioritizing preventive maintenance and rehabilitation to preserve and extend the deck life and reduce its life cycle costs. IRT and GPR represent two NDT technologies that can provide reliable, rapid and cost-effective bridge deck evaluation. Hence, they were employed in the present research on two full-scale bridge decks. Both methods require post-processing analysis of the acquired data to reveal subsurface anomalies. A simple analysis procedure of IRT and GPR data was developed herein to detect and classify the severity of subsurface defects in RC bridge decks and integrate IRT and GPR data. The findings are presented in terms of condition maps delineating the different severity levels of subsurface delaminations and potential active corrosion. The boundaries between the condition categories were determined based on the threshold clustering technique applied on the recorded concrete surface temperature, the reflected amplitudes of reinforcing rebar, and the integrated data, thus providing objective thresholds and accurate classification. Accordingly, the percentages of delaminated and potential corroded areas in the bridge decks were quantified in the different categories.

As a surface temperature method, the detection capability of delamination using IRT testing is depth limited. While it is very effective for non-overlaid decks, the IRT

effectiveness can decrease in the presence of overlays. Also, IRT data requires adequate solar radiation and weather conditions to produce the required temperature differentials. The sensitivity of GPR to the presence of chlorides and concrete corrosion makes the technology an ideal tool to identify the potential of corroded areas in RC bridge decks. However, GPR is not as strong at precisely locating delaminated areas. In addition to rebar depth variation, there are several other factors that can jeopardize the efficiency of analyzing GPR reflection amplitudes, including variation of rebar spacing, surface properties, structural variation and construction quality. Currently, rebar depth variation is the only factor that has been taken into account. GPR surveys require dry pavement conditions, but are not temperature or weather dependent.

While both IRT and GPR testing have strengths and limitations, the findings of this study demonstrate that combining the results of the two technologies is effective in evaluating the condition of deteriorated RC bridge decks. Accordingly, integrating the defective areas identified by both methods could provide important information for maintenance decision makers. The methodology proposed herein provides rapid and reliable analysis and hence, could enable the monitoring of deterioration progression through periodical surveys, thus, enabling the effective, rapid and economical surveying of hundreds of bridges.

## 5.7 References

- Alani, A., Aboutalebi, M., and Kilic, G. (2013). "Applications of ground penetrating radar (GPR) in bridge deck monitoring and assessment." *Application Geophysics*, Vol. 97, 45-54.
- Barnes, C., Trottier, J., and Forgeron, D. (2008). "Improved Concrete Bridge Deck Evaluation Using GPR by Accounting for Signal Depth-Amplitude Effects." *NDT & E International*, Vol. 41 (6), 427-433.
- Barnes, C. and Trottier, J. (2000). "Ground-Penetrating Radar for Network-Level Concrete Deck Repair Management." *Transportation Engineering*, Vol. 126 (3), 257-262.
- Belli, K., Wadia, S., and Rappaport, C. (2011). "Integrated Sensor and Media Modeling Environment Developed and Applied to Ground-Penetrating Radar Investigation of Bridge Decks." *Computing in Civil Engineering*, Vol. 25 (1), 10-20.
- Bostanudin, N. (2013). "*Computational methods for processing ground penetrating radar data*". PhD Thesis. University of Portsmouth, England, 288 p.
- Dinh, K., Zayed, T., Moufti, S., Shami, A., Jabri, A., Abouhamad, M., and Dawood, T. (2014). "Clustering-based Threshold Model for Condition Assessment of Concrete

- Bridge Decks using Ground Penetrating Radar." *Proc., 93<sup>rd</sup> Annual Meeting, TRB*, Washington, DC, Vol. No. 2522, 1-11.
- Gucunski, N., Imani, A., Romero, F., Nazarian, S., Yuan, D., Wiggenhauser, H., Shokouhi, P., Taffe, A., and Kutrubes, D. (2013). "Non-destructive testing to identify concrete bridge deck deterioration." *Proc., 92<sup>nd</sup> Annual Meeting, TRB*, Washington, DC, SHRP 2 Report, 96 p.
- Gucunski, N., and Nazarian, S. (2010). "Material Characterization and Condition Assessment of Reinforced Concrete Bridge Decks by Complementary NDE Technologies." *Proc., Structure Congress, ASCE*, Orlando, Fl., USA, 429-439.
- Halabe, U., Sotoodehnia, A., Maser, K. and Kausel, E. (1993). "Modeling the Electromagnetic Properties of Concrete." *ACI Materials Journal*, Vol. 90, 552-63.
- Hong, S., Lai, W. and Helmerich, R. (2012). "Monitoring Accelerated Corrosion in Chloride Contaminated Concrete with Ground Penetrating Radar." *Proc. IEEE 14<sup>th</sup> International Conference on Ground Penetrating Radar*, Shanghai, China, 1-9.
- Krause, V., Abdel-Qader, I., Abudayyeh, O., and Yehia, S. (2007). "An image segmentation algorithm for the detection of rebar in bridge decks from GPR scans." *Proc. IEEE International Conference in Electro/Information Technology*, Chicago, IL, USA, 114-119.
- Lai, W., Kind, T., Stoppel, M., and Wiggenhauser, H. (2013). "Measurement of Accelerated Steel Corrosion in Concrete Using Ground-Penetrating Radar and a Modified Half- Cell Potential Method." *Infrastructure Systems*, Vol. 19, 205-220.
- Maser, K., Martino, N., Doughty, J. and Birken, R. (2012). "Understanding and Detecting Bridge Deck Deterioration Using Ground Penetrating Radar." *Transportation Research Record No. 2313, TRB*, 116-123.
- Maser, K. (2009). "Integration of Ground Penetrating Radar and Infrared Thermography for Bridge Deck Condition Testing." *Materials Evaluation*, Vol. 66, 1130-1136.
- Maser, K., and Rawson, A. (1993). "Network Bridge Deck Surveys Using High Speed Radar: Case Studies of 44 Decks," *Transportation Research Board No. 1347, TRB*, 1018-1025.
- Maser, K., and Roddis, W. (1990). "Principles of Thermography and Radar for Bridge Deck Assessment." *Transportation Engineering*, Vol. 116 (5), 583-601.
- Martino, N., Birken, R., Maser, K., and Wang, M. (2014). "Developing a deterioration threshold model for assessment of concrete bridge decks using ground penetrating radar." *Proc., 93<sup>rd</sup> Annual Meeting, TRB*, No. (14-3861), 1-10.
- Omar, T., Nehdi, M., and Zayed, T. (2018). "Infrared Thermography Model for Rational Condition Assessment of Concrete Bridge Decks." *J. of Construction and Building Materials*. Vol. 168, pp: 313-327. DOI: 10.1016/j.conbuildmat.2018.02.126.
- Tarussov, A., Vandry, M. and De La Haza, A (2013). "Condition assessment of concrete structures using a new analysis method: GPR computer-assisted visual interpretation." *Construction and Building Materials*, Vol. 38, 1246-1254.

## Chapter 6

### 6. Integrated Condition Rating Model for Reinforced Concrete Bridge Decks Using NDT and Visual Inspection

#### 6.1 Introduction

Developing reliable evaluation and condition rating methodologies is paramount for efficient BMSs. For instance, combining various inspection techniques could prevent underestimating or overestimating a bridge deck condition. However, most commonly used bridge condition rating systems utilize data emanating from visual inspection reports inevitably associated with considerable uncertainty. This could possibly lead to unnecessary repair actions or overlooking critical problems. Although the advent of NDT technologies has significantly aided more precise assessment of bridge decks, such techniques have not received due attention in the bridge rating process. Thus, relevant research efforts have recently attempted to integrate multiple NDT technologies to assess the overall bridge structural capacity as well as automate the data collection and analysis processes (Gucunski *et al.*, 2015). Adopting this approach during a real field deployment is vital to achieving an efficient health indicator of bridge condition.

A review of current bridge condition rating systems reveals several drawbacks. For instance, they do not account for subjective information in the assessment process. Indeed, a considerable amount of uncertainty in the current bridge assessment practice stems from ignorance, lack of data, or inability to precisely assess bridge elements with subsurface deterioration. There exists little or no direct incorporation of structural defects' measurements in the overall bridge condition rating process. Common rating practices do not account for the structural role and relative importance of different bridge components and deterioration mechanisms towards the overall evaluation (Wang and Elhag, 2008). In addition, they employ solid linguistic grades that do not take into consideration gradual transition from one condition category to another. Therefore, a superior rational condition rating procedure is needed to capture the results of commonly employed NDT techniques, along with the relative importance of bridge deck different defects. Uncertainty in the evaluation process could be remediated via a set of elaborated fuzzy linguistic variables.

In this Chapter, a systematic integrated condition rating procedure for concrete bridge decks using fuzzy mathematics is developed. To achieve this goal, the following objectives are pursued throughout the chapter sections: (1) study the current bridge condition rating practices, (2) identify and quantify the extent of severity for delaminated and potential corroded areas in RC bridge decks based on IR thermal imaging and GPR scanning, and (3) develop an integrated condition rating model using the fuzzy approach to consider the uncertainty in the IRT, GPR, and visual inspection measurements. **Figure 6-1** illustrates the adopted systematic methodology to achieve the above-mentioned objectives, which consists of four phases. The goal of the first phase is to identify and quantify the severity degrees of defects. This is achieved by conducting in-situ inspection on full-scale deteriorated RC bridge decks using IRT, GPR, and visual inspection. Visual inspection will evaluate the extent and severity of surface defects, while IRT and GPR data will be analyzed to identify the extent and severity of potential subsurface defects. The goal of the second phase is to pursue bridge experts' judgement to provide: (i) degree of relative importance for defects, and (ii) numerical values to identify the boundaries of bridge deck condition categories. This will be acquired through interviews with experts having comprehensive bridge experience.

The goal of the third phase is to convert the identified and quantified defects into bridge deck condition categories. This is achieved by employing the fuzzy synthetic evaluation (FSE) approach to: (i) construct defect linear triangular fuzzy membership functions, (ii) calculate the relative importance weights of defects using the fuzzy preference programme (FPP), (iii) translate the fuzzy defects to fuzzy condition categories, and (iv) integrate the condition categories belonging to each defect type into overall condition categories of the bridge deck. The goal of the last phase is to develop a bridge deck condition index (BDCI) as follows: (i) construct fuzzy membership functions for the condition categories using linear regression analysis; (ii) utilize the area percentage in each condition category to aggregate their membership functions using a fuzzy union operation; and (ii) utilize a defuzzification method to obtain a final crisp value. Then, the developed rating procedure and its application will be demonstrated through a case study on a full-scale reinforced concrete bridge deck. A brief description of the current practices of bridge condition rating, as well as their main drawbacks, will be presented first.

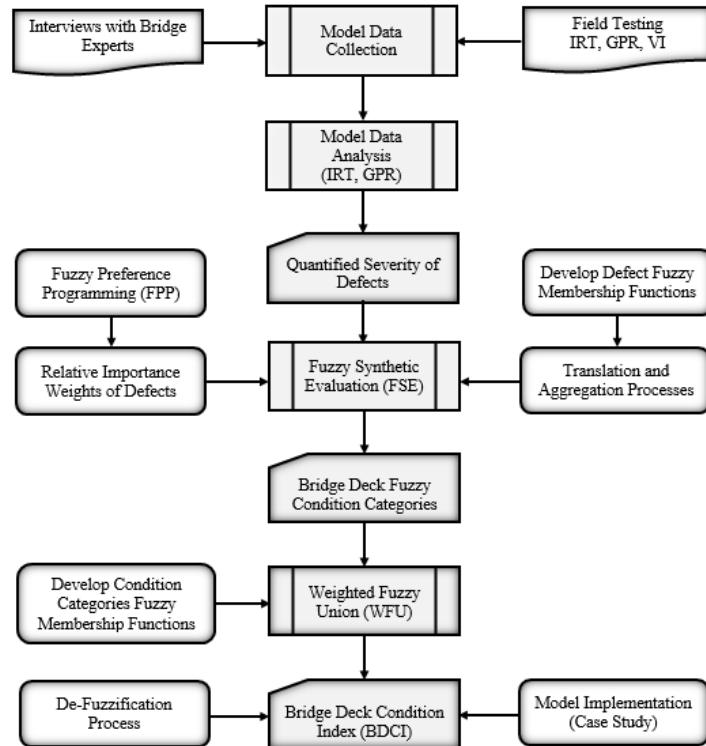


**Figure 6-1: Methodology of model development adopted in this study.**

## 6.2 Existing Bridge Condition Rating Systems

Bridge condition data are generally categorized into condition ratings and condition categories. Condition ratings are codes describing the in-place versus the as-built bridge. Condition categories describe the condition of bridge elements (Nasrollahi and Washer, 2014). The national bridge inventory (NBI) rating system requires condition ratings for three major bridge structural components: (i) deck; (ii) superstructure; and (iii) substructure using a 0 to 9 point scale (9 being excellent condition and 0 implies absolute failure). The FHWA (1995) classifies deficient bridges into two categories: structurally deficient and functionally obsolete. One of the conditions to consider a bridge as structurally deficient is having at least one of its components with a condition rating value of 4 or less. The scale of this condition rating system indicates the urgency of an impending loss of structural integrity, but does not consider a detailed inspection of bridge elements, and thus provides little information about the type and location of possible failure. Hence, it is insufficient to formulate repair strategies, or to estimate costs (Bektas *et al.*, 2013).

The bridge sufficiency rating (BSR) system evaluates bridge data by calculating four rating factors. It starts with a value of 100, then deductions are made for bridge deficiencies down to a potential lowest value of 0. The four rating components are comprised of structural adequacy and safety (S1) which has a value of 55%, serviceability and functional obsolescence (S2) accounting for a value of 30%, essentiality for public use (S3) that receives a value of 15%, and finally special reductions (S4) with a value of 13% (FHWA, 1995). Bridge rehabilitation is determined when  $BSR \leq 80$ , whereas eligibility for replacement is indicated by  $BSR < 50$  and structural deficiency or functional obsolescence. The main problem associated with the BSR system is that it is based on NBI condition ratings. To overcome some of the drawbacks of the NBI condition rating, the commonly recognized (CoRe) element condition rating system was developed. It consists of more than one hundred standardized element-level conditions. The ratings of all the elements can be integrated through a weighted aggregation process to compute the overall bridge health index (BHI) that represents the health of the entire bridge structure (Thompson and Shepard, 2000). The BHI ranges from 0 to 100, where 100 indicates the best state, whereas 0 indicates failure condition. BHI is calculated as the ratio of the sum of the current element value to the sum of the total element value. It can be calculated for an element, a single bridge, or a group of bridges. Although the BHI has been considered by the bridge community as an excellent performance measure, it does not take into consideration inherent uncertainties during the inspection process and its calculation method makes it a deterministic process.

However, to improve the CoRe system of bridge elements, a detailed bridge element inspection system called the AASHTO Guide Manual for Bridge Element Inspection (MBEI) was developed in 2011. The manual was built on the concept of element-level condition rating and further improvement was implemented in 2013 to include National Bridge Elements (NBEs), Bridge Management Elements (BMEs), and Agency-Developed Elements (ADEs). All elements are assigned a standard number representing one of four condition states: good, fair, poor, and severe. NBEs represent the primary structural components of bridges (decks and slabs, superstructure, substructure, railings, bearings, and culverts) necessary to determine the overall condition and safety of the primary load carrying members. BMEs include components of bridges such as joints, wearing surfaces,

protective coating systems and deck/slab protection systems that are typically managed by agencies utilizing BMS. ADEs provide the ability to define custom sub-elements in accordance with the NBEs or BMEs. The new elements contained within the MBEI have been introduced into AASHTOWare™ Bridge Management software BrM, formerly known as Pontis, which is currently the primary bridge management software used by transportation agencies across the USA (Reardon and Chase, 2016).

### **6.2.1 Bridge Condition Rating Systems in Canada**

Each Canadian provincial bridge inspection manual has its own condition rating system. For example, in the Ontario Bridge Management System (OBMS), defects are recorded in each of 4 condition states (excellent, good, fair, and poor) for each bridge component and performance deficiencies for each component (OSIM, 2008). The British Columbia bridge condition index (BCI) is a weighted average of the condition state distribution for various elements where the element replacement cost is used as the weighting factor. BCI is calculated for various strategies as well as for each budget scenario so that bridge network performance can be compared for different funding levels (Reed *et al.*, 2008). Similarly in Quebec, element, bridge, and network levels are considered where the material condition of a bridge element is assessed based on the severity and extent of the detected defects according to a 4-level grading system (A, B, C, and D). Similar to the condition rating systems developed in the USA, the Canadian bridge condition rating systems do not account for fuzzy information in the evaluation process.

### **6.2.2 Bridge Condition Assessment Using IRT and GPR**

IRT and GPR are widely accepted to augment visual inspection data from bridge decks. Consequently, several researchers proposed objective bridge condition assessment systems utilizing these technologies (e.g. Yehia *et al.*, 2007; Maser, 2009; Gucunski *et al.*, 2013; Matsumoto and Mitaini 2013; Dinh *et al.*, 2015). For instance, Maser (2009) employed both IRT and GPR and proposed a two-level bridge deck condition assessment system. Matsumoto and Mitaini (2013) utilized IRT to determine the AASHTO element level condition state for bridge decks, railings and beams, where distressed areas were presented into three classification categories. Dinh *et al.* (2015) utilized GPR to evaluate the

condition of RC bridge decks and proposed a condition rating index based on GPR results. Their proposed rating index only considers corrosion defects and does not consider uncertainty in GPR measurements.

### **6.3 Fuzzy Bridge Deck Condition Rating Model Development**

In this section, a novel fuzzy condition rating model is proposed based on the integration of NDT and visual inspection results to identify an overall condition index for existing RC bridge decks (BDCI). The rationale behind using a fuzzy approach is that: “Assessment of a bridge deck’s defects using visual inspection involves subjectivity and uncertainty. Although assessing bridge decks using NDT techniques provides objective defect measurements with less ambiguity, many factors can also influence the accuracy of the results for the applied technique, such as the experience of the operator and data analyzer. Thus, uncertainty in the severity and extent of measured defects has utmost importance in both visual inspection and NDT”. Therefore, a valid approach to consider uncertainty and integrate both techniques is to establish a uniform fuzzy defect and condition category scheme to achieve the proposed BDCI as elaborated below.

#### **6.3.1 Fuzzy Synthetic Evaluation (FSE)**

The Fuzzy Synthetic Evaluation (FSE) approach is capable of dealing with uncertainties in data sampling and can synthesize the evaluation of defects. The FSE was utilized in this study for fuzzifying and translating each detected defect to an order of descending condition categories and then integrating the condition categories of all defects to obtain overall fuzzy condition categories for a bridge deck. The integration process requires relative importance weights of the various defects based on their effect on the health of a bridge deck. The Fuzzy Preference Programming (FPP) was adopted for this task based on a fuzzy prioritization approach. The applied procedure is described in the following steps.

##### **6.3.1.1 Construction of Defect Fuzzy Membership Functions**

Inaccurate evaluation of the extent and severity degree of a defect will influence the final rating and thus, the measured defects should be treated. Fuzzification of the measured defects requires the construction of defect membership functions. Therefore, each

measured defect was assumed to be associated with an underlying fuzzy set  $F$ , defined by four fuzzy linguistic condition categories ranging over the defect extent. The four condition categories were represented as excellent ( $E$ ), good ( $G$ ), fair ( $F$ ), and poor ( $P$ ), similar to the Ontario bridge condition states, where a RC bridge deck will remain in each condition category a period of time during its service life. Thus, the fuzzy set can be recognized as  $F = [E, G, F, P]$ . The 2012 MTQ (Ministry of Transportation of Quebec) material condition rating index for bridge primary elements (**Fig. 6-2**) implements the extent values for each of the four condition categories based on the severity degree of a defect. Consequently, linear triangular fuzzy membership functions have been constructed for each severity degree (light, medium, severe, and very severe) based on the defect extent (% of deck area affected by the related severity degree). **Figure 6-3** illustrates the constructed membership functions that assisted in handling the fuzzy overlapping nature of the four linguistic condition categories. Reasonable interval values of the specified boundaries of the affected area were considered to determine zones related to each condition category. A membership function of a severity degree represents the extent of a measured defect over the interval  $[0, 1]$ , indicating its degree of belonging to each of the four condition categories.

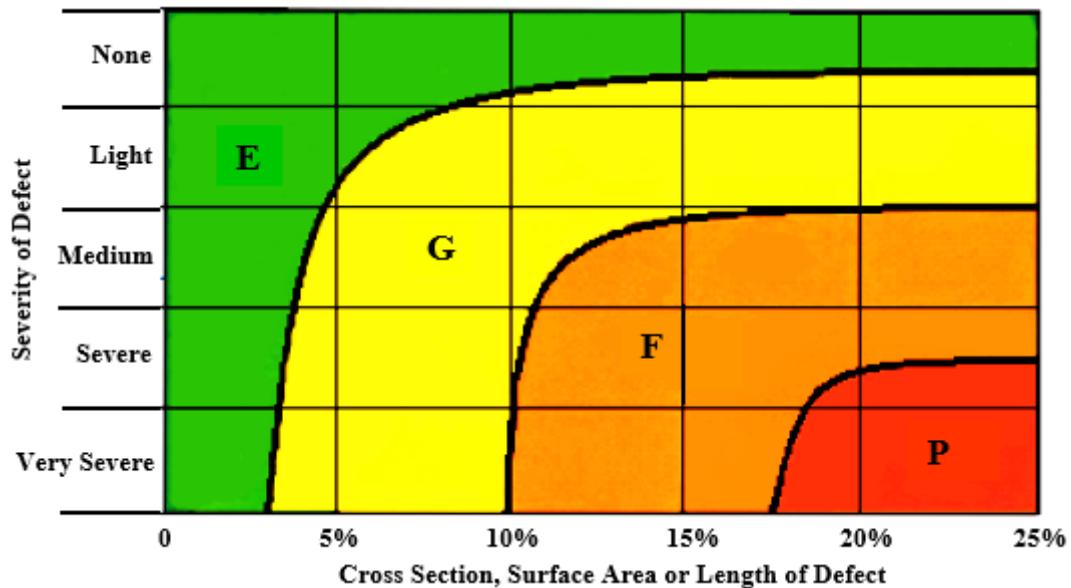


**Figure 6-2: Condition category's map utilized for the construction of defects' membership functions (Omar *et al.*, 2017).**

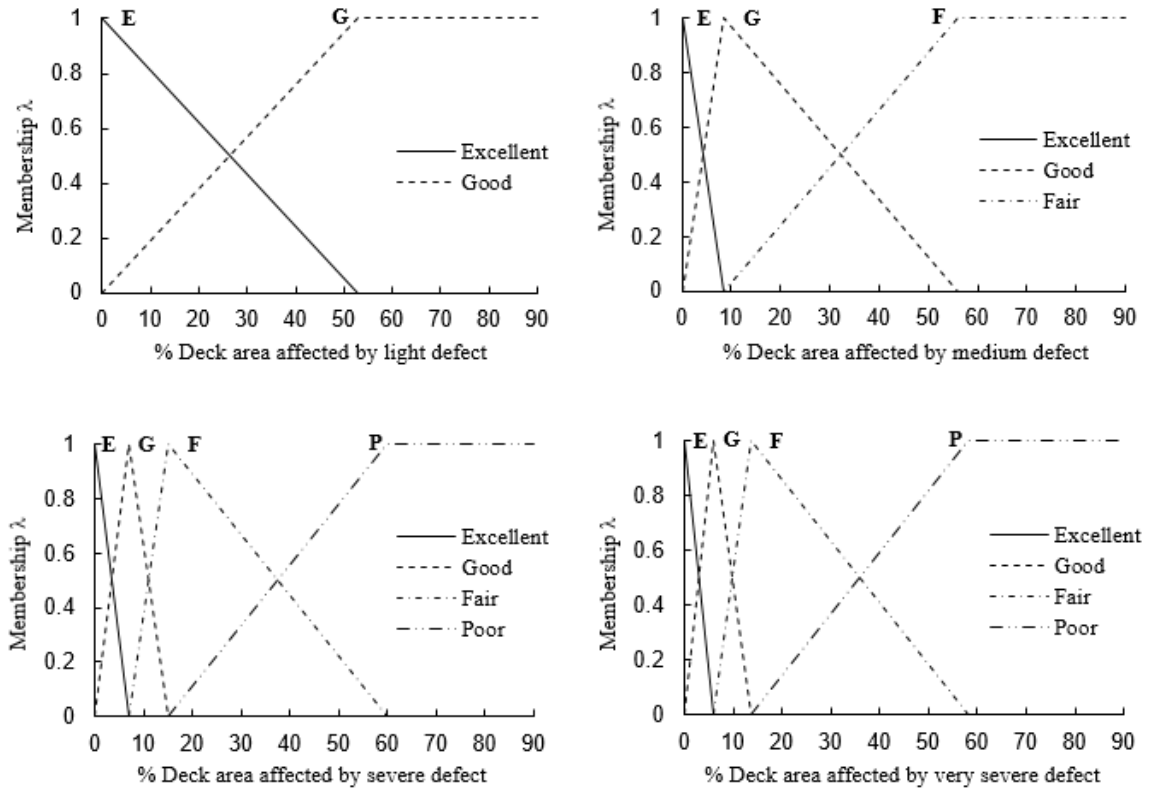


**Figure 6-3: Triangular fuzzy membership functions for various severity of bridge deck's defects.**

### 6.3.1.2 Determination of Defect Relative Importance Weights

**Figure 6-4** illustrates a simple hierarchy of the common defects occurring in RC bridge decks. Relative importance weights representing the effect of these defects on the health of RC bridge decks were determined, relying on experts' judgment through semi-structured interviews. A total of 17 expert interviews were undertaken with engineers from different Canadian ministries of transportation having extensive bridge experience and knowledge. The experts were asked to provide the degree of relative importance among the considered defects based on the 9-point Saaty's linguistic scale of absolute values, developed by Saaty (1980), representing the strength of judgements. Comparing surface defects was done at first; the experts were asked to provide the degree of importance of surface scaling if compared with spalling, pop-outs, and cracking on the health of RC bridge decks. Then the experts were asked to provide the degree of importance with regards to the health of a RC

bridge deck of delamination defects if compared with corrosion, and surface defects. The degree of relative importance gathered from the experts was utilized to construct pairwise comparison matrices.

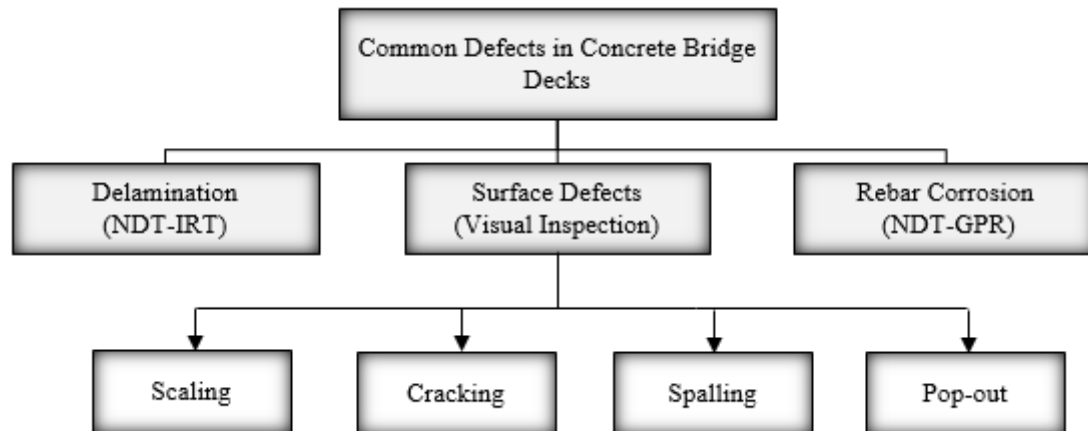


**Figure 6-4: Common bridge deck defects and related investigation techniques utilized in this study.**

Due to uncertainties associated with experts' judgments, the linear triangular fuzzy scale, presented in Chapter 3 (**Table 3-4**), was applied to all the constructed pairwise comparison matrices. The difference between most probable (actual response received) with the upper and lower values is equal to one. Thus, for a  $(n \times n)$  comparison matrix, there are  $(n + 1)$  variables representing  $n$  weights  $(x_1, x_2, \dots, x_n)$  and a consistency index  $(\lambda = x_{(n+1)})$ . **Table 6-1** illustrates a fuzzified pairwise comparison sample of one respondent for the relative importance of the considered surface defects on the health of a bridge deck. Each cell in the matrix has three values obtained from the fuzzification process. The matrix has 5 variables in linear equality constraint (4 local weights and a consistency index). The FPP method presented in Chapter 3 was employed to acquire the consistency values and calculate weights from the triangular fuzzy pairwise comparison matrices using the Matlab fuzzy optimization algorithm "*fmincon*", generally referred to as constrained nonlinear optimization function. It is a medium-scale algorithm that attempts to find a constrained minimum of a scalar function of several variables. **Table 6-2** summarizes the achieved average weights of the various defects considered in this study.

**Table 6-1: Example for a fuzzy pairwise comparison matrix of a participated expert**

<b>Pairwise Comparison of Common Surface Defects in Concrete Bridge Decks</b>				
Defect Type	Scaling	Cracking	Spalling	Pop-out
Scaling	1,1,1	3/10,3/7,3/4	1/8,1/7,1/6	5/12,5/7,5/2
Cracking	4/3,7/3,10/3	1,1,1	1/4,1/3,1/2	2/3,5/3,8/3
Spalling	6,7,8	2,3,4	1,1,1	4,5,6
Pop-out	2/5,7/5,12/5	3/8,3/5,3/2	1/6,1/5,1/4	1,1,1

**Table 6-2: Final weights of bridge deck defects investigated in this study**

<b>Relative Weights of Common Defects in Concrete Bridge Decks</b>			
Main Defect	Weight	Sub-Defect	Sub-Weight
Sub-surface Delamination (IRT)	0.382	N/A	N/A
		Scaling	0.185
Surface Defects (Visual Inspection)	0.354	Cracking	0.237
		Spalling	0.363
		Pop-out	0.215
Sub-surface Rebar Corrosion (GPR)	0.264	N/A	N/A

### 6.3.1.3 Translation of Fuzzy Defects into Condition Categories

Each fuzzy measured defect using both NDT and visual inspection (e.g. delamination, scaling, cracking, spalling, pop-out, and corrosion) was translated into the bridge deck's four condition categories. Consequently, the percentage of extent of each defect was converted to a percentage of the defect in the four condition categories. **Equation 6-1** represents the implemented translation formula.

$$C_i = [P_{il} \quad P_{im} \quad P_{is} \quad P_{ivs}] \cdot \begin{bmatrix} \lambda_{E(P_{il})} & \lambda_{G(P_{il})} & \lambda_{F(P_{il})} & \lambda_{P(P_{il})} \\ \vdots & \vdots & \vdots & \vdots \\ \lambda_{E(P_{nvs})} & \lambda_{G(P_{nvs})} & \lambda_{F(P_{nvs})} & \lambda_{P(P_{nvs})} \end{bmatrix} \quad \text{Eq. 6 - 1}$$

Where:

$C_i$ : % of defect  $i$  in each condition category [ $E, G, F, P$ ]

$i \in (1, 2, \dots, n)$                        $n = \text{number of defects.}$

$P_i$ : % of defect  $i$  in the four severity degrees (Light, Medium, Severe, Very Severe).

$\lambda_{F(P_{iL})}$ : Membership function for the light severity of defect  $i$  to the condition category (e.g. Fair).

#### 6.3.1.4 *Integration of Condition Categories Belonging to Different Defects*

To obtain overall condition categories for a bridge deck, the condition categories translated from various defects were integrated using the identified relative importance weight of each defect. Initially, the condition categories of surface defects (e.g. scaling, cracking, spalling, and pop-out) were aggregated and then integrated with the condition categories of the delamination and corrosion defects, identified by IRT and GPR testing. **Equation 6-2** represents the implemented integration formula.

$$D_c = [w_1 \quad w_2 \quad \dots \quad w_i \quad \dots \quad w_n] \cdot \begin{bmatrix} C_{E(1)} & C_{G(1)} & C_{F(1)} & C_{P(1)} \\ \vdots & \vdots & \vdots & \vdots \\ \vdots & \vdots & \vdots & \vdots \\ C_{E(i)} & C_{G(i)} & C_{F(i)} & C_{P(i)} \\ \vdots & \vdots & \vdots & \vdots \\ \vdots & \vdots & \vdots & \vdots \\ C_{E(n)} & C_{G(n)} & C_{F(n)} & C_{P(n)} \end{bmatrix} \quad \text{Eq. 6 - 2}$$

Where:

$D_c$ : % of overall bridge deck area in each condition category.

$i \in (1, 2, \dots, n)$                        $n = \text{number of defects.}$

$w_i$ : weight of defect  $i$ .

$C_{E(i)}$ : % of defect  $i$  in the condition category (e.g. Excellent).

### 6.3.2 Weighted Fuzzy Union (WFU) Operation

The proposed condition rating model utilizes a numerical scale from 0 to 100 to represent the overall bridge deck condition index (BDCI); 0 being failure condition and 100 being excellent condition. The scale is divided into the four condition categories previously mentioned: excellent (*E*), good (*G*), fair (*F*), and poor (*P*). The application of the FSE process explained above resulted in area percentages of various condition categories of a bridge deck that need to be converted into a numerical BDCI value. Therefore, during interviews with the bridge experts, the principle of the proposed condition rating model was introduced and the experts were asked to identify the values regarding the boundaries of each condition category in the BDCI scale in order to provide specific percentages for  $k_1$ ,  $k_2$ , and  $k_3$  illustrated in **Fig. 6-5**.

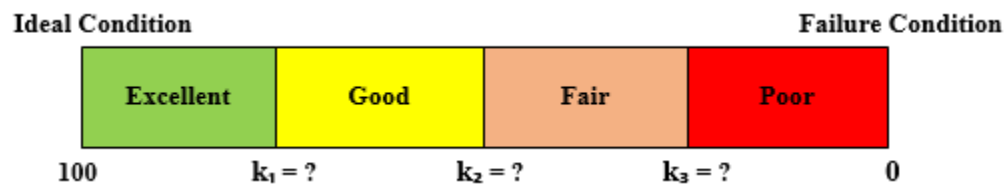


**Figure 6-5: Conception of the proposed bridge deck condition index (BDCI).**

Due to the uncertainty associated with experts' judgments, fuzzy modelling was necessary to represent these boundaries and solve the aggregation process. The weighted Fuzzy Union (WFU) operation is a basic operation for aggregating fuzzy sets. It provides an "optimistic" aggregate by assuming credibility in opinions expressed in the two fuzzy sets to be aggregated. WFU was utilized to aggregate the membership functions of the condition categories, which was then defuzzified to determine the BDCI. The fuzzification, aggregation and defuzzification processes are described below.

#### 6.3.2.1 Construction of Condition Categories Fuzzy Membership Functions

The fuzzification process requires the construction of a fuzzy membership function for the zone of each of the four condition categories. As previously discussed, several techniques for generating membership functions have been proposed in the literature based on the

nature of the related application. The values of  $k_1$ ,  $k_2$  and  $k_3$  proposed by the bridge experts are presented in **Table 6-3** and were utilized to construct the membership functions of the four condition categories. Primarily, it was necessary to verify the consistency of the experts' opinions. **Figure 6-6** illustrates a histogram and assumed normal distribution fitting, which confirms that no individual expert provided inconsistent judgment.

**Table 6-3: Experts' replies for boundaries identification of the condition categories**

Response No.	$k_1$	$k_2$	$k_3$
1	85	70	50
2	75	60	35
3	80	65	50
4	85	65	50
5	80	60	45
6	75	55	35
7	85	60	45
8	80	65	40
9	85	70	45
10	90	60	40
11	85	65	35
12	90	70	50
13	85	55	35
14	85	65	35
15	80	60	40
16	75	55	35
17	85	65	45

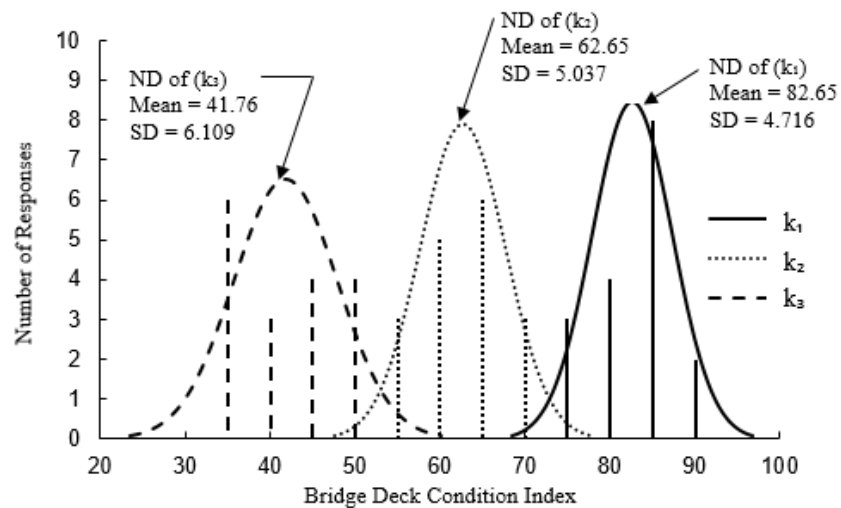


**Figure 6-6: Histogram and normal distribution curve of  $k_1$ ,  $k_2$ , and  $k_3$ .**

Subsequently, the membership functions were assumed to be piecewise linear. Linear regression analysis was conducted and the boundaries of each condition category were determined as illustrated in Fig. 6-7. The final constructed membership functions of the four condition categories are shown in Fig. 6-8 where the area percentage in each condition category would be utilized to aggregate these functions towards a numerical BDCI value.

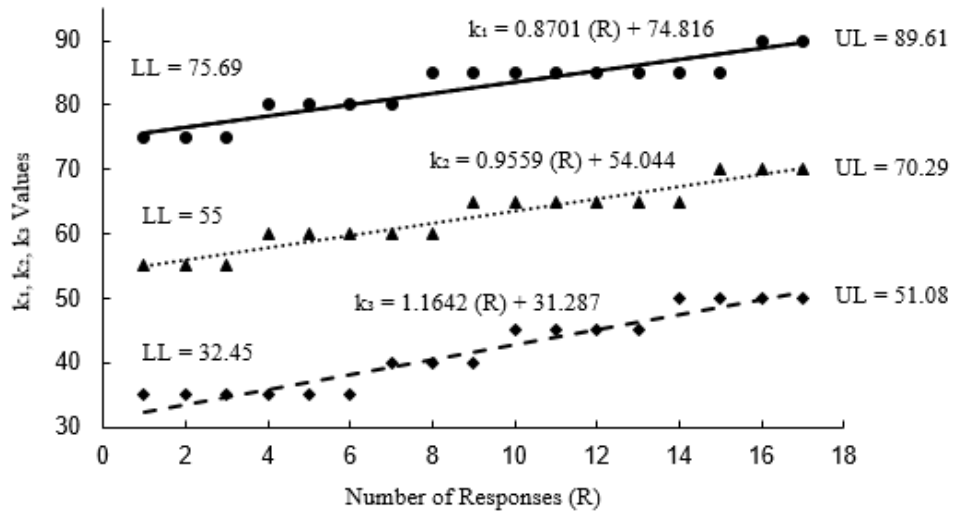


Figure 6-7: Boundaries of condition categories membership functions using linear regression method.

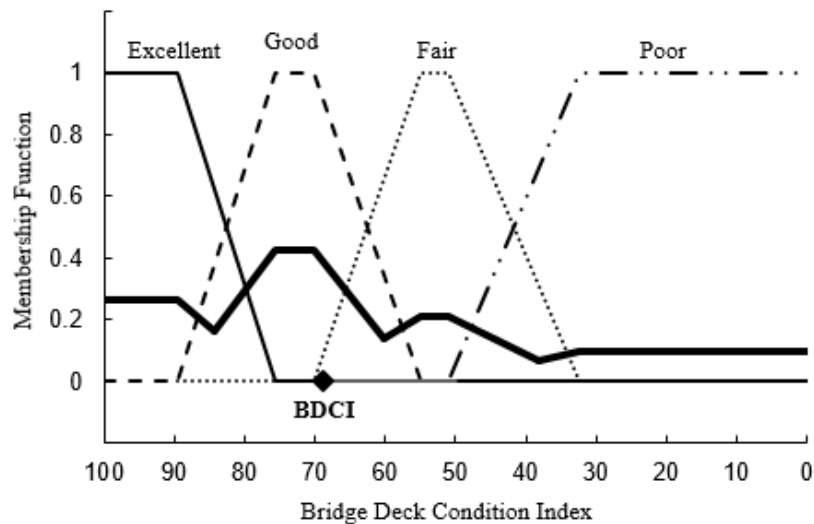


Figure 6-8: Condition categories membership functions based on k1, k2, and k3.

### 6.3.2.2 *Weighted Aggregation of Fuzzy Condition Categories*

The WFU method is an appropriate operation when the importance coefficients are considered as fuzzy modifiers. The fuzzy modifier is a fuzzy logic operator which may be used to change the characteristic function by spreading out the transition between full membership and nonmembership, by sharpening the transition, or by moving the position of the transition region. **Equation 6-3** represents the mathematical formula of the WFU operation.

$$\bar{A} = U \left[ \sum_{i=1}^{i=n} F_i \quad X_i \right] \quad \text{Eq. 6 - 3}$$

Where:

$\bar{A}$  = output fuzzy set

$U$  = fuzzy union operator

$F_i$  = nonfuzzy weighting factors

$X_i$  = fuzzy set #  $i$        $i \in (1, 2, \dots, n)$        $n$  = number of fuzzy sets

To demonstrate how the WFU works, assume a bridge deck has area percentages of the four condition categories as: [ $E$  (26.7%),  $G$  (42.5%),  $F$  (21.3%),  $P$  (9.5%)], then the aggregated fuzzy membership functions of the four condition categories was represented by a thick line as illustrated in **Fig. 6-8**.

### 6.3.2.3 *Bisector Defuzzification to Identify Bridge Deck Condition Index (BDCI)*

The output obtained from the WFU operation is a fuzzy set that needs to be defuzzified to have a crisp value representing the BDCI. There are several defuzzification methods supported in the Matlab fuzzy logic toolbox such as the middle, smallest, and largest of maximum value assumed by the aggregate membership function, the bisector and centroid

defuzzification methods. The most commonly used methods are the centroid and bisector defuzzification methods. The centroid defuzzification returns the center of area under the shape, while bisector is the vertical line that divides the possibility distribution of the output fuzzy set into two sub-regions of equal area. The bisector defuzzification method was utilized in this study where the intersection of the bisector line with the condition rating scale axis is the numerical output represents the BDCI value as illustrated in **Fig. 6-8** for the above example.

## 6.4 Bridge Deck Condition Rating Model Implementation

### 6.4.1 Data Collection and Analysis

As explained in the research methodology, field deployment is required to build the proposed model. The field deployment includes IRT testing, GPR scanning, and visual inspection to identify both surface and subsurface defects, gain a broader insight into the overall bridge deck condition and assign a reliable rating value. Guidelines for visual inspection of existing bridges have been developed in many countries and the use of bridge inspection reporting software has been explored by several asset management software developers and adopted for element-level inspection. Thus, surface defects can be extracted from the inspection reports where the extent and severity degrees are registered.

In this section, the proposed condition rating model was implemented as a proof of concept on an in-service RC bridge deck located in Montreal, Canada. Visual inspection was carried out by an experienced bridge inspector from the Ministry of Transportation, Quebec and the surface defects were quantified and recorded along with their severity degrees. Field testing was conducted using IRT and GPR. The IRT data collection and analysis were presented in Chapter 4, while the GPR data collection on the same bridge deck and its analysis were presented in Chapter 5. The IRT and GPR analyses located the delamination and the potential of rebar corrosion sub-surface defects as previously presented in **Fig 5-4** and **Fig. 5-5**, respectively. These quantified subsurface defects were then integrated with the surface defects to identify the BDCI. **Table 6-4** summarizes the area percentages of the different detected defects in each severity degree (light, medium, severe, very severe) resulting from visual inspection, IRT survey, and GPR scan.

**Table 6-4: Summary of severity and extent of defects in the inspected Montreal's bridge deck**

Defect	Inspection Technique	Severity and Extent
Delamination	IRT	Light 108m <sup>2</sup> (30%), Medium 61.2m <sup>2</sup> (17%), Severe 90m <sup>2</sup> (25%)
Scaling		Light 158m <sup>2</sup> (44%), Medium 108m <sup>2</sup> (30%), Severe 36m <sup>2</sup> (10%)
Cracking	Visual	Light 158m <sup>2</sup> (44%), Medium 90m <sup>2</sup> (25%), Severe 54m <sup>2</sup> (15%)
Spalling	Inspection	Light 115m <sup>2</sup> (32%), Medium 30.6m <sup>2</sup> (8.5%), Severe 25m <sup>2</sup> (7%)
Pop-out		Light 144m <sup>2</sup> (40%), Medium 28.8m <sup>2</sup> (8%), Severe 21.6 m <sup>2</sup> (6%)
Corrosion	GPR	Light 144m <sup>2</sup> (40%), Medium 54m <sup>2</sup> (15%), Severe 75.6m <sup>2</sup> (21%)

#### 6.4.2 Developing BDCI of Bridge Deck

The BDCI of the surveyed bridge deck was identified as follows: (i) each defect type in the four severity degrees was fuzzified using the constructed defects' fuzzy membership functions in **Fig. 6-3**; (ii) the extent of each fuzzy defect was then translated to an area percentage in the four condition categories (excellent, good, fair, poor) using **Eq. 6-1**; (iii) the area percentages in the four condition categories resulting from the surface defects were combined using **Eq. 6-2** to represent the overall deck condition based solely on the visual inspection technique; (iv) the area percentages in the four condition categories resulting from both IRT and GPR testing, respectively, were integrated with the area percentages in the four condition categories resulting from the visual inspection using **Eq. 6-2** to have an overall integrated area percentage of the bridge deck in the four condition categories. **Figure 6-9** illustrates the condition of the surveyed bridge deck in the four categories as indicated by the IRT, GPR, and visual inspection, as well as the overall integrated condition of the deck; (v) the area percentages in the four condition categories were utilized to aggregate the constructed fuzzy membership functions using WFU operation. For comparison purposes, the thick colored lines in **Fig. 6-10** represent the aggregated fuzzy membership functions of the deck condition as determined by the IRT, GPR, and visual inspection techniques, along with the overall integrated condition of the deck; (vi) bisector defuzzification was applied and the BDCI was determined for each inspection technique as well as for the overall integrated condition of the deck as illustrated in **Fig. 6-10**.

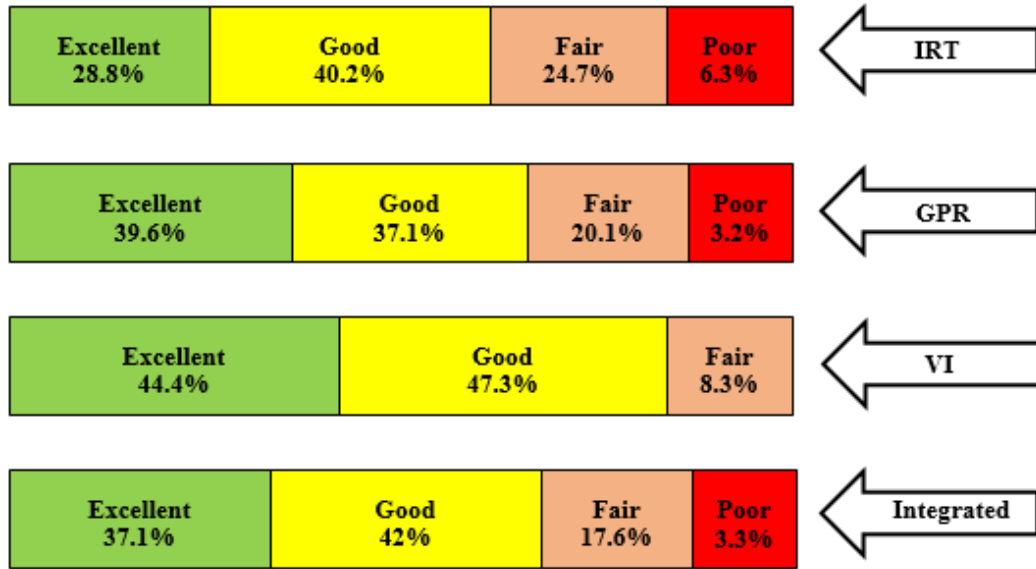


Figure 6-9: Aggregated condition categories of Montreal’s bridge deck based on defects measured using different techniques.

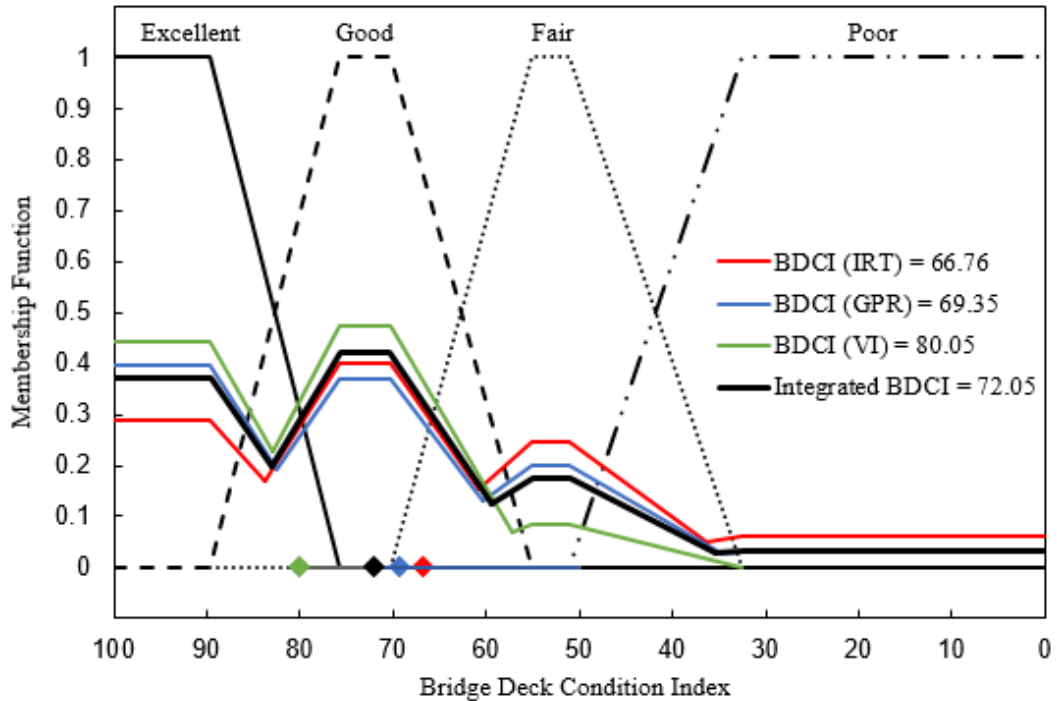


Figure 6-10: Condition rating index of Montreal’s bridge deck based on the proposed model in this study.

## 6.5 Evaluation of the Proposed BDCI Model

Integrating the deficiency areas identified by visual inspection and NDT technologies would yield both surface and subsurface indicators of condition for a variety of bridge decks in the network and thus, provides meaningful information for maintenance decision makers. As previously discussed, the differences between the IRT and GPR area percentages in the different condition categories shown in **Fig. 4-9** could be due to the fact that not all delaminations can be observed in GPR images and only highly advanced corrosion areas were identified by the GPR scanning. In addition, corrosion is among the primary reasons that could lead to delaminations in RC bridge decks. It should be noted that the delaminated and corroded area percentages identified by analyzing the IRT and GPR survey data have been validated by other NDT techniques and chloride ion concentration analyses in some cores taken from the deck as presented in Chapter 5. However, the main concern of this study is to apply a management aspect by utilizing the NDT results in the proposed condition rating procedure.

**Figure 6-9** demonstrates the importance of the integration concept in having a reliable condition rating of a bridge deck. For instance, the visual inspection does not consider any area of the deck in a poor condition and indicated that only 8.3% of the deck's area is in a fair condition, while the IRT and GPR considered that 31% and 23.3% of the deck's area, respectively, are in fair and poor conditions. In addition, the deck's area in good condition was evaluated as 47.3% by visual inspection, while the IRT and GPR evaluations were 40.2% and 37.1%, respectively. Similarly, visual inspection indicated that 44.4% of the deck's area is in excellent condition, while the IRT and GPR evaluated the deck's area in the same condition category as 28.8% and 39.6%, respectively. Consequently, visual inspection indicated a BDCI value of 80.05, while the IRT and GPR indicated values of 66.76 and 69.35, respectively as shown in **Fig. 6-10**. The condition rating index based on the IRT and GPR results was about 16.6% and 13.4%, respectively, lower than the condition rating index indicated by visual inspection results. The overall integrated area percentages in the four condition categories from the three inspection technologies identified a final BDCI value of 72.05 for the surveyed deck, about 10% less than the value if the deck were evaluated based solely on visual inspection.

These results could significantly affect maintenance actions to be taken and should draw attention to the importance of integrating the results of different technologies. With respect to how the proposed index can be used by maintenance decision makers, this study does not enforce strict actions. In fact, the conducted interviews with bridge experts indicated various opinions regarding the action needed for a bridge deck with a specific BDCI. For instance, some experts proposed repair or partial deck replacement, while others proposed full replacement of a deck with the same BDCI value. Thus, each transportation agency can apply its maintenance strategy in rating the achieved BDCI and select the appropriate action. However, based on discussions with the bridge experts and the maintenance strategies of the Ontario Bridge Condition Index (OBCI) and other preservation guides in the literature, ratings and recommended actions for the proposed BDCI in this study were summarized in **Table 6-5**. The proposed actions aim at having reliable and safe bridge conditions. It should be noted that the maintenance actions in the majority of existing BMSs are based on optimization models to determine the most cost-effective maintenance strategies.

**Table 6-5: Recommended actions for the proposed BDCI in this study**

<b>BDCI Range</b>	<b>Deck Rating</b>	<b>Recommended Action</b>
80 - 100	Excellent	Maintenance is not required within the next five years.
70 - 80	Good	Frequent monitoring and repair defects within the next five to ten years.
60 - 70	Fair	Major repairs should take place within the next five years. NDT using IRT and GPR should be conducted after five years.
50 - 60	Poor	Immediate maintenance is required. Total deck replacement to take place within the next five to ten years.
Less than 50	Very Poor	Immediate rehabilitation is required. Total deck replacement to take place within the next five years but if the BDCI < 30, immediate closure to traffic.

Considering the relative importance of defects on the health of a bridge deck, applying NDT techniques and addressing the fuzzyness of the detected defects were paramount in developing the proposed procedure, which can be used for evaluating an individual or a

network of bridge decks. It should be noted that the main idea here is to propose a methodology rather than apply the exact numbers achieved in this study. The model data can be retrieved from in-depth bridge inspection reports, where visual inspection could be supplemented by NDT methods. Indeed, employing several NDT techniques will reduce the uncertainty inherent in the defect measurements and provide more reliable condition rating indices. For instance, it would be objective to detect possible defects using the results of multi-model NDT, such as the recently developed “RABIT” system. RABIT (Robotics Assisted Bridge Inspection Tool) is a fully autonomous robotic system for the condition assessment of concrete bridge decks using multiple NDT technologies (Gucunski *et al.*, 2015). However, because not all transportation agencies employ NDT evaluation due to the associated costs, the model proposed herein integrates visual inspection, being the commonly used inspection method, with only two NDT techniques.

The selection of IRT and GPR in this study was based on their ability to rapidly survey large with minimum traffic disruption, lane closures, and exposure of personnel to traffic, thus saving significant time and labor costs. However, the proposed procedure provides a platform for continuous updates on a bridge deck’s condition as more related data become available. The model could also be amended by increasing the hierarchy layers through involving more defects, other deck elements, such as the drainage system and wearing surface or other bridge components, such as the superstructure and substructure. Consequently, the proposed rating procedure is flexible and can accommodate future upgrading.

## 6.6 Conclusions

An attempt has been made in the present research to develop a novel condition rating methodology for existing RC bridge decks by integrating the results of NDT and visual inspection. Fuzzy set theory has been utilized to account for uncertainties and imprecision in the measurements of common subsurface and surface bridge deck defects detected by NDT such as IRT and GPR along with bridge inspector observations recorded through visual inspection. Using fuzzy membership-based defect measurement in combination with the importance relative weighting approach, the proposed procedure translated uncertain measurements of surface and subsurface defects into fuzzy bridge condition categories.

The Fuzzy Preference Programme (FPP) based nonlinear method was adopted to calculate the relative defects' weights using the Matlab software. Considering the uncertainty inherent in determining the zone of each condition category, a fuzzy condition category scheme was built where the weighted fuzzy union (WFU) technique was employed to aggregate the fuzzy membership functions of the condition categories towards a bridge deck condition index (BDCI). A case study was provided to illustrate the process of implementing the proposed approach. The advantages of the developed system include the utilization of various inspection technologies, employment of the knowledge provided by bridge engineers with extensive experience and intuition, and conducting the analysis in a fuzzy domain. The proposed model could be upgraded to include other bridge elements and components, consider more possible defects, and employ other NDT techniques. Thus, it would be an effective tool for transportation agencies to prioritize repair and rehabilitation efforts and focus limited funding on most deserving bridge decks.

## 6.7 References

- ASTM Standard D4788-03 (2013). "Standard Test Method for Detecting Delaminations in Bridge Decks Using Infrared Thermography." *ASTM International*, West Conshohocken, PA.
- ASTM D6087-08 (2010). "Standard Test Method for Evaluating Asphalt-Covered Concrete Bridge Decks Using Ground Penetrating Radar," *ASTM International*, West Conshohocken, PA.
- Bektas, B., Carriquiry, A., and Smadi, O. (2013). "Using Classification Trees for Predicting National Bridge Inventory Condition Ratings." *Infrastructure Systems*, Vol. 19 (4), 425-433.
- Dinh, K., and Zayed, T. (2015). "GPR-Based Fuzzy Model for Bridge Deck Corrosiveness Index." *Performance of Constructed Facilities*, Vol. 30 (4), 1-14.
- FHWA (1995). "Recording and Coding Guide for the Structure Inventory and Appraisal of the Nation's Bridges." *FHWA-PD-96-001*, Federal Highway Administration, U.S Department of Transportation.
- Gucunski, N., Kee, S., La, H., Basily, B., Maher, A., and Ghasemi, H. (2015). "Implementation of a Fully Autonomous Platform for Assessment of Concrete Bridge Decks RABIT." *Proc., Structure Congress*, ASCE, Portland, Oregon, 367-378.
- Gucunski, N., Imani, A., Romero, F., Nazarian, S., Yuan, D., Wiggenhauser, H., Shokouhi, P., Taffe, A., and Kutrubes, D. (2013). "Non-destructive testing to identify concrete bridge deck deterioration." *Proc., 92<sup>nd</sup> Annual Meeting, TRB*, Washington, DC, SHRP 2 Report, 96 p.

- Maser, K. (2009). "Integration of Ground Penetrating Radar and Infrared Thermography for Bridge Deck Condition Testing." *Materials Evaluation*. Vol. 66 (11), 1130-1136.
- Matsumoto, M., Mitani, K. and Catbas, F. (2013): Bridge Assessment Methods Using Image Processing and Infrared Thermography Technology." *Proc., 92<sup>nd</sup> Annual Meeting, TRB*, Washington, DC, 1-9.
- Nasrollahi, M., and Washer, G. (2014). "Estimating Inspection Intervals for Bridges Based on Statistical Analysis of National Bridge Inventory Data." *Bridge Engineering*, Vol. 11, 1-11.
- Ontario Structure Inspection Manual-OSIM, (2008), *Ontario Ministry of Transportation*, the Queen's Printer for Ontario, 394 p.
- Omar, T., Nehdi, M., and Zayed, T. "Integrated Condition Rating Model for Reinforced Concrete Bridge Decks." *J. of Performance of Constructed Facilities*. DOI: 10.1061/(ASCE)CF.1943-5509.0001084.
- Reardon, M. F., and Chase, S. (2016). "Migration of Element-Level Inspection Data for Bridge Management System." *Proc., 95<sup>th</sup> Annual Meeting, TRB*, Washington, DC, 1-15.
- Reed, M., Thompson, M., and Gagnon, R. (2008). "Design and Implementation of a New Bridge Management System for the Québec Ministry of Transport." *Proc., 10<sup>th</sup> International Conference on Bridge and Structure Management*, Buffalo, New York, 77-86.
- Saaty. (1980). "*The analytic hierarchy process: Planning, Priority Setting and Resource Allocation*." Book, Publisher: McGraw-Hill, New York, 237 p.
- Thompson, P., and Shepard, R. (2000). "AASHTO commonly recognized bridge elements, successful applications and lessons learned." *Prepared for the national Workshop on Commonly Recognized Measures for Maintenance*. Paul D. Thompson Consultant, 1-13.
- Wang, Y. and Elhag, T., (2008). "Evidential reasoning approach for bridge condition assessment." *Expert Systems with Applications*, Vol. 34 (1), 689–699.
- Yehia. S., Abudayyeh, O., Nabulsi, S., and Abdel-Qader, I. (2007). "Detection of Common Defects in Concrete Bridge Decks Using NDE Techniques." *Bridge Engineering*, Vol. 12, 215-225.

## Chapter 7

### 7. Remote Sensing of Reinforced Concrete Bridge Decks Using Unmanned Aerial Vehicle Infrared Thermography

#### 7.1 Introduction

There is a need to develop cost-effective and innovative solutions to evaluate bridge deck conditions on regular time intervals, without interrupting traffic. This makes remote sensing technologies viable options in the field of bridge inspection. As previously discussed, IRT as a remote sensing technology does not require direct access to the surface under inspection since the images can be captured from distance using appropriate optical lenses. However, conducting ground IRT testing in-situ on full-scale bridge decks requires mounting the IR camera on a vehicle. The ideal option for data collection is to scan one traffic lane on each pass. Obtaining such horizontal field of view is not always achievable in the field as it may require to mount the camera at a high level. Thus a number of survey passes should be adopted to cover the entire bridge deck area. In addition, the requirements of ASTM D4788-03 (2013), ground IRT testing in-situ on full-scale RC bridges should be conducted at low driving speeds of no greater than 20 km/h. Thus, the arrangements of traffic control is necessary to conduct IRT survey on the field.

The generic definition of remote sensing technologies allows for a variety of deployment platforms including satellites, aerial inspection using fixed wing aircrafts, or vehicle mounted systems, making remote sensing potentially valuable in the field of inspection and monitoring (Harris *et al.*, 2016). The main limitation to perform a manned aircraft scanning is to maintain a fixed distance from the structure, which can be mitigated using an unmanned aerial vehicle (UAV) equipped with a GPS system (Chen *et al.*, 2011). In recent years, UAV technology has increasingly been used in various application areas such as monitoring construction and operation of buildings and other types of engineering systems. The improvements in navigation and sensor technology have made UAVs more reliable in terms of flight control. In addition, the advanced telecommunication technologies permit their flying at different altitudes over considerable distances (Chen *et al.*, 2011). Operating UAVs at lower altitudes than piloted aircrafts, result in a higher spatial resolution.

Compared with satellite remote sensing and aerial photogrammetry, UAV has several merits, which makes it a reliable and cost-effective technology for data acquisition. Therefore, remote sensing UAV equipped with high definition photo and video cameras can facilitate the inspection tasks of bridge infrastructure. The limitations of applying ground IRT could motivate the pursuit of this technology for bridge inspection. A UAV-borne imaging system with a high resolution digital and thermal cameras can be deployed frequently to provide rapid condition assessment and enable monitoring of deterioration progression through periodical surveys and thus, allow the surveys of hundreds of RC bridge decks to become feasible. Consequently, considerable reductions in costs associated with the inspection processes of bridge decks and in the frequency and duration of traffic interruptions can be achieved. However, the ability to extract quantitative information of subsurface anomalies from images captured by a UAV-IRT system is still needed to fully realize its potential in detecting these defects.

In this Chapter, the potential application of a UAV-borne thermal imaging system for the condition assessment of full-scale RC bridge decks is investigated and the reliability of the achieved results is evaluated. To achieve this goal, the following objectives are pursued throughout the chapter sections: (1) studying the working principles of aerial UAV remote sensing technology; and (2) utilizing a UAV thermal imaging system for the detection of subsurface delaminations in RC bridge decks. **Figure 7-1** illustrates the adopted systematic methodology to achieve the above-mentioned objectives. It can be summarized as follows: (1) conducting UAV-borne thermal imaging in-situ on two deteriorated full-scale RC bridge decks; (2) collecting thermal images via low altitude flights using a high resolution thermal camera; (3) producing a mosaicked thermogram for the entire bridge decks from the IRT data using especially developed Matlab codes; (3) segmenting the mosaic to determine objective thresholds using the k-means clustering algorithm in the Matlab software; (4) creating a condition map delineating different categories of the delamination severity using a commercial mapping software; and (5) validating the detected delaminated areas using the results provided by other testing technologies on the same bridge decks. A brief description of the UAV remote sensing technology and its current practices of bridge condition inspection as well as its main drawbacks will be presented first.

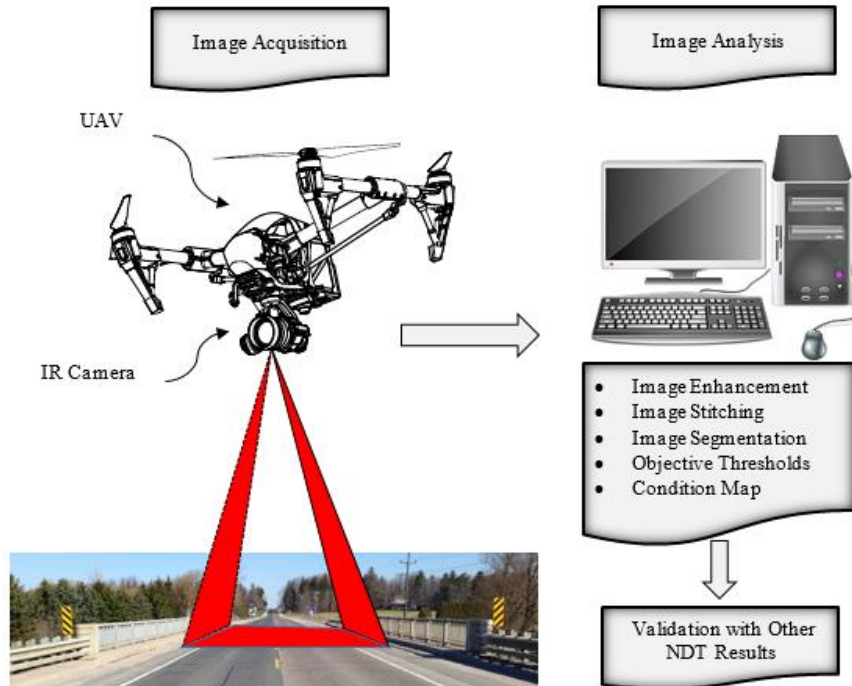


**Figure 7-1:** UAV-borne thermal survey methodology adopted in this study.

## 7.2 Unmanned Aerial Vehicle (UAV)

### 7.2.1 Basic Principle of UAV

A general definition of remote sensing can be summarized as the collection and measurement of spatial information at a distance from the data source, without direct contact. UAVs are a remote sensing technology that have been referred to as drones, robot planes, pilotless aircraft, remotely pilot vehicles, remotely pilot aircrafts, and other terms which describe aircraft that fly under the control of an operator with no person aboard. It can be controlled by a computer and fly autonomously, remotely controlled by a navigator on the ground, or semi-autonomously as a combination of both capabilities. A UAV remote sensing system consists of four main components: aircraft with sensor(s) for data acquisition; remote control for the entire craft; GPS for navigation; and inertial measurement unit (IMU) for altitude measurement. Recently, ground station software releases on mobile device platforms have allowed operators to use tablets and smartphones to control aircrafts. Flight permissions are often required to ensure that the regulations of civil and security authorities are followed.

UAVs can be equipped with different high definition cameras to offer several mapping applications in the field of photography, geology, geography, meteorology or in agriculture and forestry (Hallermann and Morgenthal, 2013). The most critical factor in the UAV imaging applications is the movement of the camera directly caused by the movement of the flight system, which reacts to changes in wind conditions due to its low weight (Hallermann and Morgenthal, 2013). All flight parameters (e.g. longitude, latitude, time, GPS altitude, position etc.) are usually stored in a log-file together with the aircraft status parameters (e.g. battery status, flight modus and GPS signal quality). Additionally, the camera parameters (position, image number, altitude relative to launching area etc.) are also stored in the log-file, and thus are available for processing the individual images (Vasterling and Meyer, 2013). During the UAV operations, the acquired images are commonly stored on the SD card of the camera. The flight time of a UAV depends on its payload and is also strongly influenced by wind conditions (Vasterling and Meyer, 2013).

### **7.2.2 UAV Applications in Civil Engineering**

UAVs have potential applications in a variety of civil engineering tasks owing to its ability of pre-programmed flight paths and collecting data at low altitudes. In construction engineering, a large variety of commercial, small and very light UAVs have been recently developed and used in surveying construction sites, monitoring work-in-progress, and inspecting existing structures, especially inaccessible areas. These UAVs are able to take off and land vertically, requiring less area to operate, and can hover over fixed areas. During flight, operators can view live video from the camera on a monitor. The gathered data can be geo-referenced so as to offer the possibility of 3D-modelling of structures. Vaghefi *et al.* (2012) argued that many aspects of bridge inspection could be aided by UAV remote sensing, including remote inspection and producing close up and high-resolution still and video imagery of bridges from multiple viewing angles. The inspection results can be related to locations on the bridge in relation to a direct visualisation of the detected damage. Thus, UAVs can greatly change how bridge infrastructures are assessed and how their maintenance can be prioritized (Ellenberg *et al.*, 2016).

A UAV-borne thermal imaging system utilizes an infrared thermal camera to provide information of the ground surface temperature, without the need to access the ground.

Thermal imaging with a UAV has several advantages compared to satellite and ground-based measurements. It generates spatial data with good geometric resolution without the need to interpolate the data which might cause errors. Satellite imaging, in contrast, requires very high resolution data in order to obtain a high geometric accuracy. Hence, it could play a major role in bridge condition assessment. Several researchers have investigated the use of UAV in inspecting bridge decks. For example, Khan *et al.* (2015) collected thermal images of a mock up bridge to demonstrate the types of data that can be collected with a UAV and were able to detect possible delaminations in the concrete bridge deck. Brooks *et al.* (2015) investigated several applications of UAV technology, including bridge inspection. They used the UAV to capture imagery, both digital and thermal, of the bridge deck and applied some algorithms to detect surface defects on the deck.

### **7.2.3 Successful Application of UAV-IRT System**

Vasterling and Meyer (2013) addressed some critical parameters that should be considered to successfully apply a UAV-borne thermal imaging to bridge inspection. For instance, the camera should be sufficiently lightweight due to the limited payload of the UAV. It also must be robust (e.g. insensitivity towards vibrations and dust). Although thermal cameras for the (8-14)  $\mu\text{m}$  bandwidth generally do not have a cooled sensor, resulting in low signal to noise ratio, they are relatively lightweight, which is an essential advantage for use in UAV. It should also be noted that some lightweight infrared cameras do not have an autofocus. Thus, before mounting the camera onto the UVA the focus has to be adjusted manually by focusing at an object at the same distance as the planned flight altitude. Additionally, visual images or video recorded at the same time as the thermal image allow mapping thermal subsurface anomalies and differentiating the surface defects.

The flight altitude is another parameter that has to be selected via a compromise between resolution and efficiency. In addition, satisfactory mosaicking a set of thermal images is not fully resolved to date. Therefore, if the data are not recorded continuously (video), then the overlap of individual images should be at least 50%. Thus, only the central part of the images is used, which improves the quality of the composite image. Setting ground control points for further processing is another consideration. These points should preferably be visible in both the thermal and visual bandwidths. Therefore, a material with an emissivity

as well as visual contrast to the survey area has to be chosen (e.g. aluminum foil). These marker points have to be positioned in the field accurately. The images can then be stitched to fit with the markers at the respective coordinates (Gillins *et al.*, 2016).

### 7.3 UAV/IRT Model Development

To investigate the feasibility of using UAV technology for inspecting bridge decks, two full-scale in-service RC bridge decks (named herein bridge (A) and bridge (B)), located on the same highway in north London, Ontario, Canada were surveyed using a UAV-born thermal imaging system. The bridges were scheduled, by the Ministry of Transportation Ontario (MTO) for rehabilitation because delaminations were recently identified by a condition survey. Thus, they were considered as good candidates and selected for the UAV thermal survey. Both bridges were constructed in 1965. Either bridge is a single span RC frame passing over a watercourse, supported directly on abutments, and paved with about 100 mm asphalt wearing surface. The bridge structures have a north-south orientation and their external limits have concrete curbs and steel handrails. The structural drawings of both bridges indicate a deck slab thickness varying from 900 mm at the abutments to 480 mm at the mid-span of the deck with a parabolic soffit. The span of each bridge is 15.24 m with a roadway width of 12.18 m carrying one lane of traffic (3.65 m) and a shoulder (2.44 m) in each direction. Both bridges were rehabilitated in 1985 and 2007, including repair of the spalled and delaminated areas. The bridge decks exhibited the presence of numerous transverse, longitudinal and diagonal cracks. A west elevation of bridge (A) and a view of the condition of its deck are displayed in **Fig. 7-2**.



**Figure 7-2: Illustration of the surveyed concrete bridge (A) and an overview of the deck surface condition.**

### 7.3.1 Planning and Preparation Phase

#### 7.3.1.1 Selection of IR Thermal Camera

The testing involves collecting thermal images from the concrete surface using an IRT camera. As previously discussed, the key parameters in choosing an IR camera include the spectral range, spatial resolution, temperature range and frame rate. For observing objects at ambient temperature, a long wave length band (8–14  $\mu\text{m}$ ) is preferable to detect small thermal contrasts and reduce the effects of direct solar radiation during daytime testing. The spatial resolution of an IRT camera decreases with increasing object-to-camera distance, while lens systems with a small field of view have higher spatial resolution. An advanced thermal camera (FLIR Vue Pro) was utilized in this survey with its settings optimized for airborne operation. The camera is compatible with the flight system and has an uncooled micro-bolometer detector. It displays thermal images with a resolution of 640 x 512 pixels. The camera weighs 113 grams, which makes it ideal for UAV applications. When connected to the flight control system, it automatically considers the aircraft geo-location. Thus, it facilitates further stitching of the captured still images and recorded thermal videos. The IRT camera records the surface temperature using automatic gain control and saves the image data on a micro CD card in JPEG, TIFF or FFF format, so that it could be further processed using the FLIR software. Each image contains a maximum of 256 gray shades, each representing a different temperature range in the same scene. The features and specifications of the thermal camera are summarized in **Table 7-1**.

**Table 7-1: Features and specifications of the utilized camera (FLIR Vue Pro)**

Characteristic	Specification
Size	62.7 mm x 44.5 mm
Weight	101 g to 122 g
Detector Type	Uncooled Micro-bolometer
Spectral Band	7.5 $\mu\text{m}$ – 13.5 $\mu\text{m}$
Thermal Resolution	640 x 512
Full Frame Rate	30 Hz
Field of View	9-mm lens (69° x 56°)
Input Supply Voltage	4-6 VDC
On-board Storage	MicroSD
Operating Temperature Range	-20°C to 50°C
Operational Altitude	+40,000 feet
Polarity Control	Yes

### 7.3.1.2 *Selection of UAV*

The (Inspire 1 Pro) UAV from DJI was utilized in this study. The features and specifications of the utilized aircraft are summarized in **Table 7-2**. The components of the utilized flight system as well as the thermal camera are illustrated in **Fig. 7-3**. The aircraft is equipped with retractable landing gear and its camera has an integrated 3-axis stabilized gimbal to provide a steady platform and maximize stability and weight efficiency during flight. The aircraft boasts a maximum flight speed of 18 m/s and a maximum flight time of 20 minutes using a fully charged battery. It uses a global positioning system (GPS) and a vision positioning system (VPS) to fly as per predefined paths, pinpoint its position and stabilize each flight. The GPS is capable of correcting for altitude and coordinate positions to allow systematic image acquisition, as well as aiding in producing 3D models, if required, from the imagery. The flight remote controller has three flight modes, which could be automatically selected based on the strength of the GPS signal and the sensors of the VPS. The GPS has the capability to control the aircraft orientation and to assist in holding its position, while maintaining the desired altitude. It allows the system to hold position with  $\pm 2.5$  m horizontal and  $\pm 0.5$  m vertical accuracy. The remote controller also has three safe modes to ensure safe return and landing of the aircraft to the last recorded home point if the control signal is lost or if low battery warning is triggered. The flight system has a flight recorder which stores data for each flight (e.g. duration, orientation, speed, etc.).

**Table 7-2: Features and specifications of the utilized UAV (Inspire 1 Pro)**

<b>Characteristic</b>	<b>Specification</b>
Aircraft/Motor Model	T600/DJI 3510 H
Propeller Model	DJI 1345 T
Maximum Take-off Weight	3500 g
Vertical Hovering Accuracy	0.5 m
Horizontal Hovering Accuracy	2.5 m
Maximum Aircraft Speed	18 m/s
Maximum Altitude	120 m (from take-off point)
Maximum Flight Time	18-22 Minutes
Maximum Wind Speed Resistance	10 m/s
Operating Temperature Range	-10°C to +40°C
Maximum transmitting Distance	3.5 km
Mobile Device Holder	Tablet or Smart Phone



**Figure 7-3: Illustration of the UAV-borne thermal system utilized to scan two RC bridge decks.**

### 7.3.1.3 *Setting up UAV-borne Thermal System*

It is required to have a registered UAV and a certificate describing the operation of a particular UAV for a particular purpose and in a specific area. In addition, the Canadian Aviation Regulations (CAR) require training of UAV pilots to comply with safety requirements and hold a special flight operation certificate (SFOC) for Transport Canada to ensure UAV reliable and safe operation. Therefore, the UAV-borne thermal imaging in the present research was conducted by a consultant specializing in aerial photography, videography and thermography who has completed UAV training, IRT training, pilot licensing, and acquired special risk aviation insurance and gained a SFOC. The pre-flight preparation includes the setup of both the drone and thermal camera. The four propellers were installed and fixed firmly to the drone (a quadcopter). The DJI Go app and FLIR Vue Pro app were downloaded to link the drone and the camera to the flight controller. The DGI Go App controls the drone and allows the user to see a live video stream on a supported mobile device, which further allows the pilot to determine when images can be taken. The FLIR Vue Pro app allows the setup of the image format, orientation, shutter speed, camera focus adjustment, shooting mode, and color palette and communication options with the mobile device. An iPad Mini 4 device was utilized to display the live streaming video of the flight information on its LED screen. All batteries and iPad were fully charged and the camera was mounted on the drone and oriented facing straight-down to be perpendicular to the concrete deck surface being surveyed. Fixing the camera at the bottom of the drone

assists flight stability. The operator controlled the drone to maintain altitude and position. GPS positioning was activated and the compass was recalibrated before every flight.

### 7.3.2 Data Acquisition Phase

The flights were initiated on May 24<sup>th</sup>, 2016 at 1 PM, six hours after sunrise. During the survey, the ambient temperature was 79° F, relative humidity was 22%, and wind speed was 8 km/hr. Bridge deck dryness was considered during data collection since surface moisture can reduce the thermal contrast on thermal IR images. Sun direction was also considered to avoid shadows on images. It is important to note that traffic on the bridge was not interrupted during data collection. The total flight time was about three minutes for each bridge deck. The total time taken to complete a bridge deck inspection from setup to tear-down was approximately 20 minutes. A calibrated 9 mm focal lens (69° x 56°) was utilized. This allowed a large Field-of-View (FOV) of 13.74 m (horizontally) x 10.62 m (vertically) for each image to be taken at 10 m altitude. Hence, a total of only four thermal images, at spacing of 5 m, were collected with an overlap of 50% to cover the entire deck length. Each image covers the entire deck width and shoulders, in addition to 0.78 m side walk at both sides. It should be noted that the flight altitude could be increased to survey longer bridge decks utilizing an ultra-wide angle lens which will result in larger FOV.

The utilized drone can hover in place and is capable of vertical take-offs and landings. Its platform was placed closely to the bridge deck being investigated, while ensuring sufficient stand-off distance of about 5 m from the outside kerb line. The flight paths were predefined for the two bridge decks as two straight line passes in opposite directions at the center of each deck. The drone was stable and controlled by the pilot during tests. The survey was started by hovering the drone from its platform after recording the home point and then pointing it to the top of the bridge deck at a maintained altitude of 10 m using the remote controller. The flight path was displayed in real-time on the LED. The still images were captured at the center of the bridge deck with several snapshots at each position. The images were taken perpendicular to the bridge deck to minimize the effects of possible lens distortion. Since it was not possible to measure the angle while flying, an estimation of the drone's perpendicular position to the deck surface was made from the view displayed on the screen. The drone was landed after each flight and all equipment was turned off.

In addition to thermal images, various digital images of the bridge decks were taken as snapshots from the ground using a high resolution (16.1 megapixel) digital camera. These images allowed providing preliminary assessment of the surface deck condition. Consequently, visual interpretation of the captured thermal images could highlight and separate patches and surface defects from actual subsurface anomalies in order to provide accurate estimation of the detected subsurface defects.

### 7.3.3 Data Analysis Phase

As discussed in Chapter 4, data on thermal cameras appears as a color-coded image in which a color palette is assigned to temperatures at a certain “level” and across a certain “span” determined by the user. The span of the image is the difference between the minimum and maximum temperature in the image, and the “level” is the center of the span. **Figure 7-4** shows a snapshot of the UAV and a typical thermal image taken during the conducted survey. Based on visual interpretation, which is inherently subjective, the potential of delaminated areas can be identified as displayed in the figure. The image shows a delamination being much warmer than the surrounding sound concrete after several hours of exposure to sunlight. However, it should be noted that the transverse, longitudinal and diagonal lines displayed with a lighter color could be misinterpreted as a delamination area, whereas the digital images indicate that they are sealed surface cracks. Thus, taking optical images of the bridge deck is key for IR data collection and analysis.

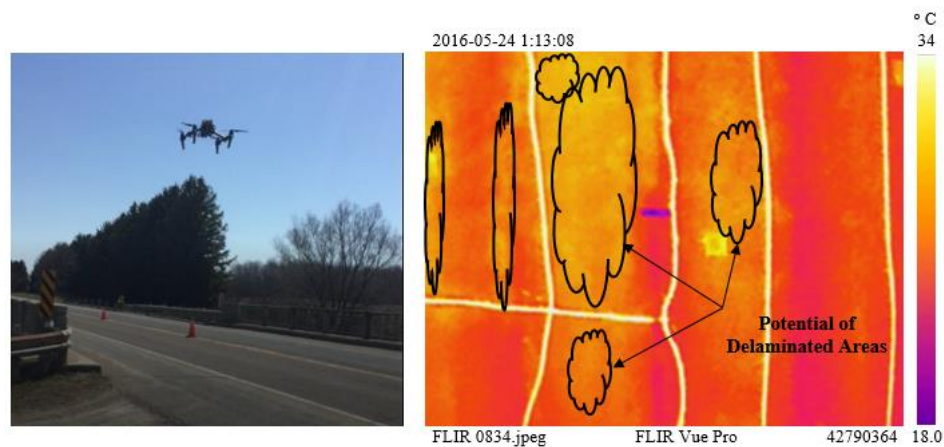


**Figure 7-4: Snapshot of the UAV during the flight to scan bridge (A) and a captured thermal image indicating potential delaminated areas.**

### 7.3.3.1 *UAV/IRT Delamination Maps*

The captured raw images could be post-processed using a variety of commercial image processing software, such as *Pix4D*, *ImageJ*, and Matlab image processing toolbox. For example, importing the thermal images onto the *Pix4D mapper* software can provide highly precise georeferenced 2D maps and 3D models. This requires to use the *Pix4D* app to automatically capture the images in predetermined routes in order to create the model. However, this option was not available, and hence the captured IR images of each bridge deck were first enhanced using several functions in the *ImageJ* software to improve its quality. The thermal data was then analyzed similar to the developed procedure for ground IRT presented in Chapter 4 as follows: (i) the scaled temperature data of each image was first saved as .csv in a separate Excel file; (ii) a selected window was extracted from each image and stitched with the extracted window from the next image. The dimension of the final mosaic, for each of the entire two lane decks, was  $640 \times 780 = 499,200$  pixels; (iii) the data dimension was scaled-down and resulted in a reduced file with  $128 \times 156 = 19,968$  pixels; (iv); the co-ordinates of each pixel were identified and then arranged in a column order with ( $x$ ,  $y$ , scaled temperature) values of each pixel. The final output was an excel file containing pixel information (coordinates and scaled temperature) with no change in thermal contrast values over the entire deck; (v) the k-means clustering algorithm in Matlab was applied to identify objective thresholds. The number of clusters ( $k$ ) for both surveyed bridge decks was considered as four to represent the level of severity of potential deterioration identified by the UAV-borne thermal testing.

For the bridge decks being considered and based on the identified thresholds, the temperature values in each severity level were grouped and uploaded in a commercial mapping software to construct high contrast composite condition maps accurately delineating the severity levels of potential subsurface delaminations, as illustrated in **Figs. 7-5** and **7-6**. The area of very severe delamination was very small and hence, has been combined with the areas of severe delaminations in order to ensure identical degree of attention with respect to the maintenance actions to be taken for these areas. Sound concrete areas were represented by a green color, concrete areas that require close monitoring were represented by a yellow color, and warning concrete areas that require repair were

represented by a red color. The sound concrete areas had the lowest scaled temperature values, while the warning concrete areas had the highest scaled temperature values since the surveys were conducted during daytime. During the day, a warming trend existed such that the targets had positive thermal contrasts, which meant that the delaminated regions were at a temperature higher than that of the sound concrete. As previously discussed, this is the anticipated behavior based on fundamental heat transfer theories and complies with previous results reported for instance by Washer *et al.* (2013).

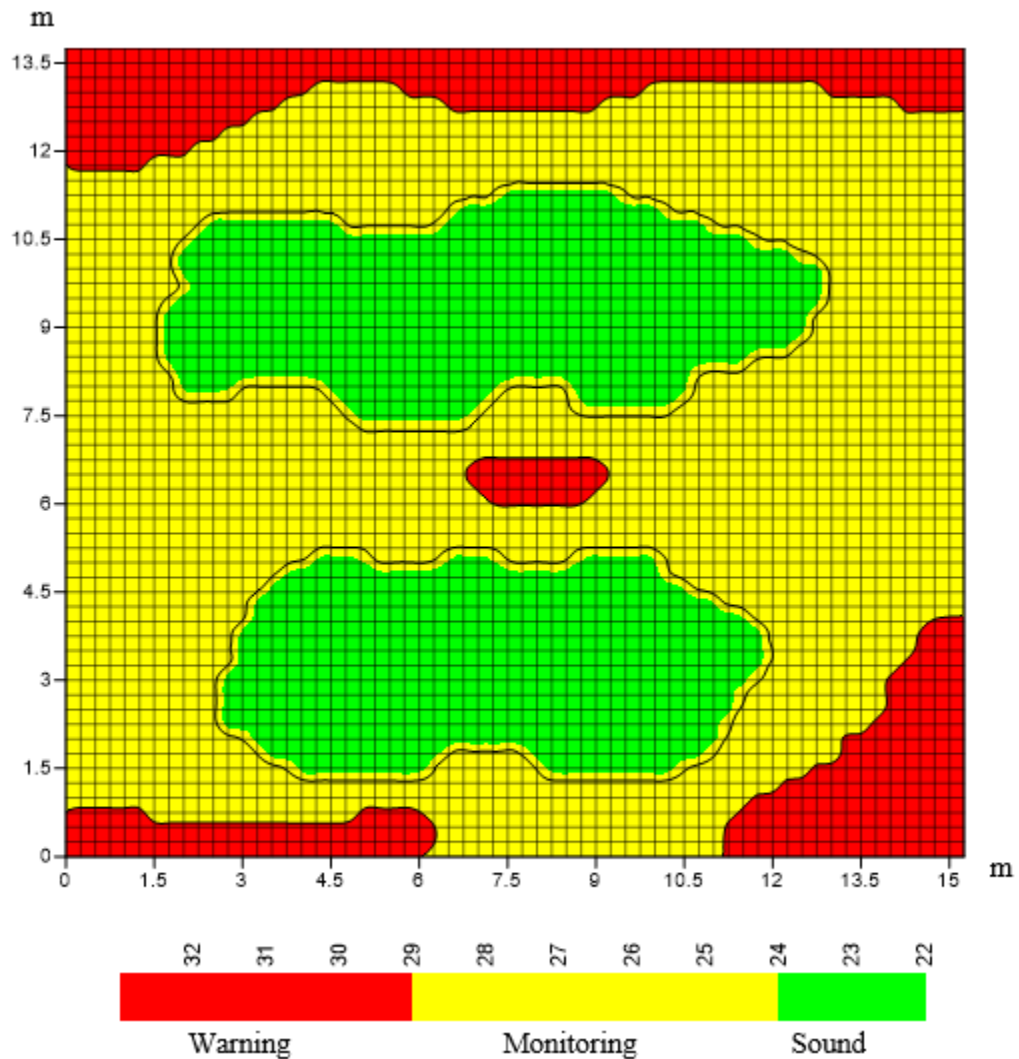


**Figure 7-5: Condition map of bridge (A) indicating the severity of the identified delaminated areas for the bridge deck and curbs using UAV-borne thermal imagery system.**

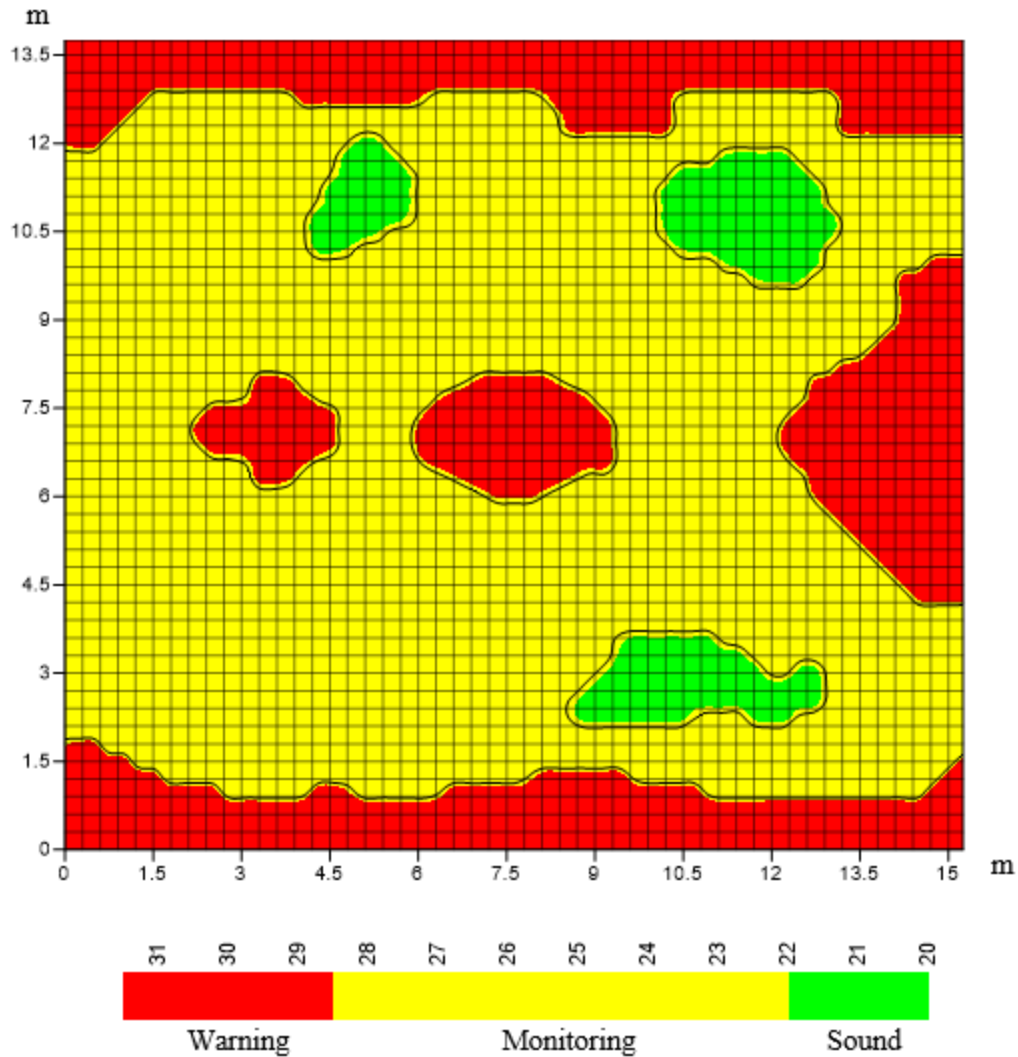


**Figure 7-6: Condition map of bridge (B) indicating the severity of the identified delaminated areas for the bridge deck and curbs using UAV-borne thermal imagery system.**

### 7.3.3.2 *Quantification of Defects*

Calculating total delaminated areas in different categories from the mosaicked thermogram can provide a quantified basis for powerful decision making. It would hence be useful in prioritizing alternatives for bridge deck repair. The percentage of bridge deck area in each condition category was calculated by computing the total pixels in the same category over the total pixels in the entire deck area. Since k-means clustering neglects the stochastic

nature of the threshold values, the calculated area percentage in each condition category was considered as a variable. Generally, a probability distribution describes the probabilities associated with all values of a random variable. For example, if the random variable is a threshold value, then the probabilities associated with all of its values are described by a probability distribution function rather than a deterministic value. There is a wide range of possible statistical techniques that can be used to perform this task. However, to highlight the influence of the identified threshold values on the calculated delaminated areas, a statistical analysis was conducted considering a consistent  $\pm 5\%$  change in the threshold values and computing the corresponding area percentage in each condition category. Then, the two primary parameters (mean and standard deviation) of the obtained values were calculated. **Table 7-3** shows the results of the statistical analysis for the two surveyed bridge decks. The basic assumption is that the data has a normal probability or Gaussian distribution. The obtained low standard deviation, which indicates the average spread around the mean, implies that the percentages of defective areas do not change significantly with the change in the identified thresholds. Consequently, the mean values were considered as final percentages of bridge deck areas in each condition category and were employed to compare the results of the UAV-thermal image analysis with that of other NDT techniques conducted on the same bridge decks.

**Table 7-3: Statistical analysis for the influence of IR threshold on the identified defective areas**

Change in Threshold (%)	Bridge (A)			Bridge (B)		
	Bridge Deck Condition (%)			Bridge Deck Condition (%)		
	Sound	Monitoring	Warning	Sound	Monitoring	Warning
-20	31	52.4	16.6	4.5	64.9	30.6
-15	31.5	52.4	16.1	4.9	65	30.1
-10	32.1	52.1	15.8	5.2	65.1	29.7
-5	32.4	52	15.6	5.4	65.1	29.5
+5	32.9	51.8	15.3	5.7	65.2	29.1
+10	33.2	51.7	15.1	5.9	65.3	28.8
+15	33.6	51.7	14.7	6.4	65.3	28.3
+20	34.1	51.8	14.1	7.2	65.2	27.6
<b>Mean</b>	32.6	52.0	15.4	5.7	65.1	29.2
<b>Standard Deviation</b>	1.05	0.29	0.79	0.86	0.14	0.97

## 7.4 Validation of UAV/IRT Model Results

UAV-borne thermal imaging can be used to delineate surface temperature of concrete structures from thermal infrared measurements. The present research aimed to rationalize the use of this technology for bridge deck inspection. The resulting detection of subsurface delaminations in RC bridge decks using remote sensing and data collection without physical contact can be a substantial advantage of this system. When testing full-scale bridge decks, quantifying subsurface defective areas at different severity levels remains a challenge. The defective areas in UAV-borne thermal imaging are commonly identified based on a visual interpretation of the captured IR images. Therefore, the thermal contrast developed from the concrete subsurface provided numerical values for the color contrasts that were used in the present research to process data more effectively than simply comparing multiple images. The created 2D mosaic of the entire bridge deck facilitated the application of a thresholding classification technique to identify objective thresholds and distinguish the severity of subsurface delaminated areas without interference of the analyst. However, to validate the reliability of the achieved results, the produced delamination condition maps and the subsequent quantified defects were verified through the results of other NDT methods, as discussed below.

### 7.4.1 Hammer Sounding Test Results

Hammer sounding was conducted on the bridge decks by a bridge inspector from the Ontario Ministry of Transportation (MTO). Delaminations in the bridge decks were detected by striking the surface with a heavy hammer and noting the type of sound being emitted. The areas and locations of patches, spalls, delaminations, honey-combing, wet areas, scaling and other observed defects were recorded. The created IR delamination maps of the two surveyed bridge decks in **Figs. 7-5** and **7-6** were compared with the hammer sounding results. It was found that the location and geometry of severely delaminated subsurface regions identified by the two methods were considerably similar. However, hammer sounding results did not indicate the warning regions that were identified by IRT. The quantified delaminated areas as identified by the UAV-borne thermal imaging system are presented in **Table 7-4**. The total percentage of delaminated areas resulting from hammer sounding tests were also indicated. For bridge (A), the analysis of the thermal data

indicated that 15.4% of the total deck area had subsurface severe delamination defects that require repair and 52% of the total deck area requiring close monitoring, while the hammer sounding results unveiled 17% total delaminated areas. For bridge (B), the analysis of the thermal data indicated that 29.2% of the total deck area had subsurface severe delamination defects that require repair and 65.1% of the total deck area requiring close monitoring, whereas the total delaminated areas identified by hammer sounding was 32%. Thus, the analysis procedure proposed herein could precisely define the location and extent of delaminations in bridge decks. It was also necessary to validate the identified warning regions using the results of a different technique as presented subsequently.

**Table 7-4: Percentage of defective areas in the analyzed two bridge decks**

Bridge Deck	NDT Survey Type	Survey Result	Concrete Condition		
			Sound	Monitoring	Warning
Bridge (A)	UAV-borne Thermal	Present Research	32.6%	52%	15.4%
	Hammer Sounding	MTO Record	17% Total Delaminated Areas		
	HCP		29.7%	56.2%	14.1%
Bridge (B)	UAV-Borne Thermal	Present Research	5.7%	65.1%	29.2%
	Hammer Sounding	MTO Record	32% Total Delaminated Areas		
	HCP		8.9%	63.7%	27.4%

#### 7.4.2 Half-Cell Potential Test Results

A corrosion survey was carried out on both bridge decks by a consulting firm specializing in NDT of concrete structures, as part of a condition survey program with MTO. This survey was conducted one month before the UAV thermal imaging. The principle of HCP testing was presented in Chapter 2. HCP Testing is usually performed at points arranged in a grid. HCP testing was performed on the surveyed bridge decks including the concrete curbs, in accordance with the requirements of ASTM C876 and the MTO structure rehabilitation manual. A positive ground connection was made directly to the reinforcing steel at predefined locations and the quantified results are presented in **Table 7-4**. For bridge (A), the tests indicated that 29.7% of the deck area likely had no corrosion activity, with corrosion potential values between 0.000 V and -0.199 V. The survey identified

uncertain low corrosion activity for 56.2% of the deck area, with values ranging from -0.200 V to -0.349 V. Probable active corrosion was detected for 14.1% of the deck area, with corrosion potential values more negative than -0.350 V. These results confirm the presence of the warning areas identified by IRT results. It should be noted that HCP results vary with moisture conditions, temperature and ion concentration.

**Figure 7-7** illustrates the corrosion potential readings for the bridge deck and curbs. The high corrosion potential areas were mostly found along the curbs. Three drilled concrete core specimens for chloride ion concentration analysis were retrieved from each bridge deck. Two cores were taken at corrosion areas and one core was taken at a sound concrete area. Evidence of corrosion was not observed on the reinforcement encountered in the cores extracted from the deck. The chloride content at the level of the reinforcing steel was below the chloride threshold level of 0.025% in all tested cores. The average compressive strength of the hardened concrete for these cores was 27.1 MPa. The design drawings specified a minimum 28-day strength of 20.7 MPa (3000 Psi) for the concrete deck. The core samples also indicated actual overlay thickness of about 50-60 mm, while the delamination layers were observed at about 45-50 mm depth from the concrete surface.

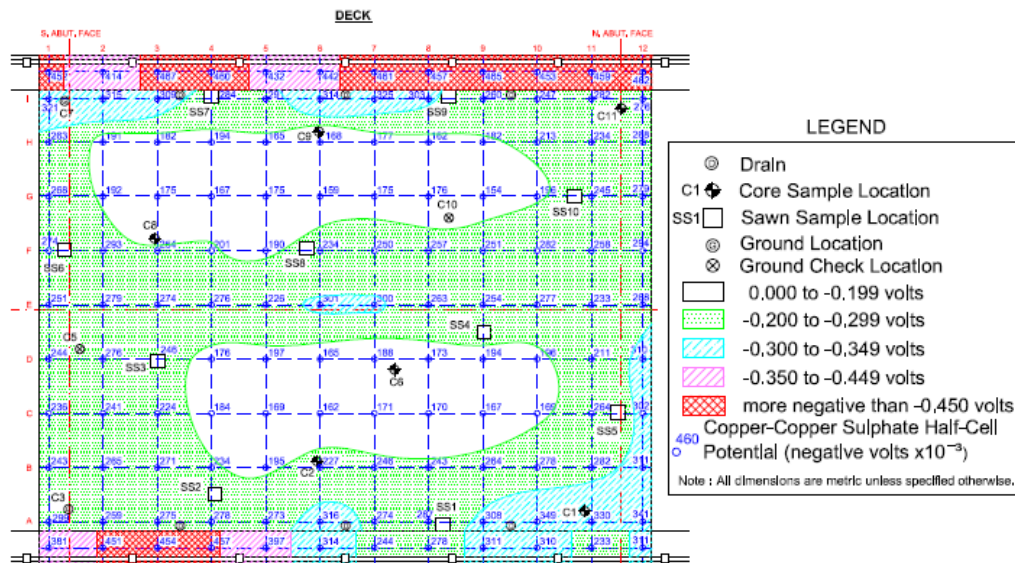


**Figure 7-7: Condition map of bridge deck (A) indicating the potential corrosion readings for the bridge deck and curbs using HCP testing (Omar and Nehdi, 2017).**

For bridge (B), the results indicated that 8.9% of the deck area likely had no corrosion activity, with corrosion potential values between 0.000 V and -0.199 V. The survey identified uncertain low corrosion activity for 63.7% of the deck area, with potential values ranging from -0.200 V to -0.349 V. Probable active corrosion was detected for 27.4% of the deck area with corrosion potential values of more negative than -0.350 V. The high corrosion potential areas were mostly found along the center line of the bridge deck and for all curb areas. It was also observed that 13% of the deck and curb areas showed corrosion potential values more negative than -0.450 V, and thus would require immediate attention. These results confirm the presence of the warning areas identified by IRT results.

The areas of potential active corrosion, as indicated by the HCP testing, have been validated by chloride ion concentration analysis. The core samples extracted from this bridge were located at areas prone to salt exposure (e.g. high corrosion potential areas, construction joints, low points of the deck near the curbs). For the two cores located at corrosion areas, the chloride ion concentrations were detrimental reaching 0.033% by concrete mass. Visual inspection results of the core samples indicated that chloride contamination has extended to the upper layer of reinforcing in some areas of the deck, particularly in areas with higher exposure to salt contamination. The average compressive strength of the hardened concrete for these cores was 29.4 MPa. **Figure 7-8** illustrates the corrosion potential readings for the bridge deck and curbs. The core samples also indicated actual overlay thickness and delamination depth similar to those indicated in Bridge (A).

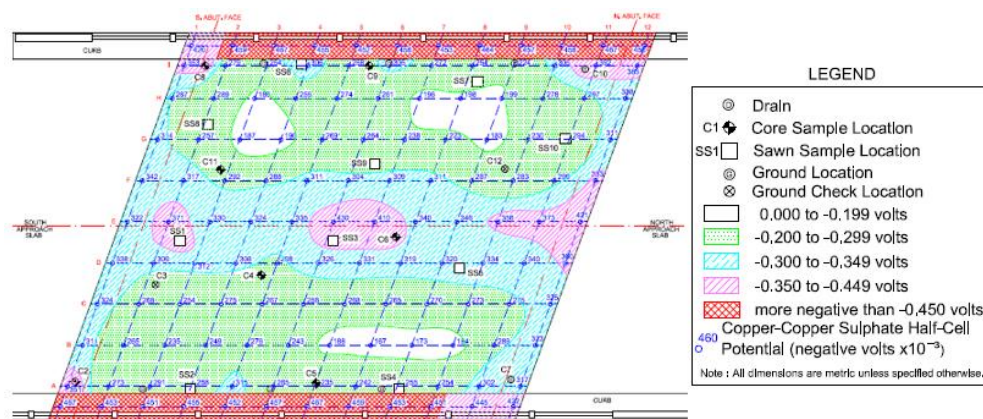


**Figure 7-8: Condition map of bridge deck (B) indicating the potential corrosion readings for the bridge deck and curbs using HCP testing (Omar and Nehdi, 2017).**

## 7.5 Evaluation of the Proposed UAV/IRT Model

The delamination maps achieved from the thermal analysis in **Figs. 7-5** and **7-6** were compared with the corrosion maps provided by the HCP testing results in **Figs. 7-7** and **7-8**. It should be noted that IRT and HCP have different working mechanisms, and thus are associated with capability of detecting different deterioration defects. In addition, corrosion is among several reasons that could lead to delaminations in RC bridge decks. Despite such differences, their condition maps were comparable. Though the locations and shapes (geometry) of the defects do not match exactly, the areas in which potential delaminations/corrosion activity were identified had reasonable correlation. Comparing the area percentages as indicated by both techniques, it can be observed from **Table 7-4** that all areas which had potential active corrosion as identified by the HCP testing were also indicated by IRT results. Conversely, not all the identified delaminated areas were indicated by the HCP results. This indicates that only areas with high probability of advanced corrosion activity were identified by the HCP testing. Such results comply with that of previous studies, which indicated that in most bridge structures, areas of corrosion are usually associated with delamination even if cracks are not detected directly. Thus, the analysis procedure proposed in the present research could define the potential location and extent of delaminations in concrete bridge decks with acceptable accuracy.

Despite the accuracy of the developed analysis procedure in detecting and quantifying delaminated areas in the surveyed bridge decks, the results could be affected by the precision of the UAV-thermal system orientation during flying. Therefore, a more rigorous analysis could be achieved based on a photogrammetric 3D reconstruction and generation of orthophotos, in which the internal and external orientation, triangulation and bundle adjustment could be considered. There are several commercial software capable of producing accurate 3D stereomodels, orthophotos and orthomosaics from data collected by various sensor systems. These orthophotos and mosaics are geographically referenced and commonly created using automated tools for tie-point matching, orthorectification, relative orientation, and color-balancing. However, it should be noted that inaccuracies in input control values could cause problems in the photogrammetric modeling process, and thus it is preferable to employ the capture app belonging to the utilized software in the data

acquisition process to ensure adequate quality imagery and accurate geospatial control in order to facilitate the creation of such orthomosaics.

## 7.6 Further Research to Improve the Proposed System

Wireless connectivity and maneuverability are two key parameters that can facilitate using UAV systems in inspections of bridge components thus enhancing bridge inventory management. For instance, using a UAV equipped with different sensors (e.g. LiDAR, thermal and optical cameras, etc.) should allow the collection of imagery that highlights surface (e.g. spalls and patches) and sub-surface (delamination) defects in bridge decks and soffits. Using such UAV multi-sensors along with inertial and spatial sensors could assist in producing geo-registered 3D data for bridges. UAVs can also be effectively utilized for determining stream or river bank conditions at bridge ends. They can serve for monitoring specific geotechnical assets related to bridges, including slope stability assessment, dynamic bank erosion and lateral scour conditions (Otero *et al.*, 2015). Despite these benefits, UAV systems have some limitations. For example, due to their small payload, only small and light digital and thermal cameras can be used for photo or video documentation. The limited payload allows only small battery packs, which causes a relatively short flight time. Furthermore, due to the low weight, the flight system is very sensitive to changes in weather conditions, especially during high wind speeds, which can compromise image quality or impose a change from automatic to manual flight mode, which requires especially well-trained operators (Hallermann and Morgenthal, 2013).

Such considerations mandate concerted research efforts for instance to: (1) enhance UAV performance in various wind conditions that can be experienced during bridge inspections; (2) investigate the relation between the flight altitude and the accuracy of detecting subsurface anomalies; (3) study the effects of vibration which camera gimbals could be exposed to during flights; (4) explore the effects of using different propeller types on the UAV stability; (5) conduct cost estimation studies that consider parameters associated with operating UAVs during bridge inspection, such as data collection and operator's time costs, equipment costs including batteries, and the maintenance or repair costs; (6) develop several effective image post-processing algorithms for defect detection and classification; and (7) establish a guide for practical implementation in order to incorporate the UAV

technology in bridge inspection manuals. It should also be noted that to utilize UAVs as an effective tool in bridge inspection, qualified bridge inspectors should be trained to operate such UAV systems in order to ensure high flight performance and objective inspection processes. Other options that may be desirable by bridge owners include conducting inspections through partnerships with private companies that offer UAV-based data collection services.

## 7.7 Conclusions

The UAV technology is evolving at a rapid pace, becoming more reliable and efficient. UAVs allow remote imaging, which can be useful in infrastructure condition evaluation. The present research demonstrates the applicability of UAV and associated thermal imaging for quantitative measurements of delaminations in RC bridge decks. Two bridge deck case studies demonstrated the potential of using UAV-borne thermal imaging in fast and safe data acquisition for the condition assessment of RC bridge decks. The subsurface defect regions identified by the proposed system were confirmed through the results of other NDT techniques including hammer sounding and HCP testing. Thus, UAVs could provide reliable, rapid and cost-effective bridge deck evaluation compared with conventional methods, which involve laborious inspections of bridge decks, especially at the network-level. The remote sensing feature of UAV avoids traffic disturbance and mitigates risk associated with bridge inspections.

The proposed methodology allows post-flight data processing. A robust analysis procedure was developed herein to detect and classify the severity of subsurface delaminations in RC bridge decks. Thus, UAV could become a preferred method for IR imaging of bridge decks. This would enable monitoring the progression of deterioration through regular surveys and facilitate surveying hundreds of bridges. Consequently, this could yield sizeable reductions in costs associated with the application of NDT technologies and in the frequency and duration of traffic interruptions. Periodic UAV-borne thermal imaging surveys can help bridge owners assess bridge condition at all service life stages, thus making repair decisions based on actual condition data by tracking areas of anomalies and prioritizing maintenance needs. While the attention herein has been mainly devoted to the condition evaluation of RC bridge decks, UAV-borne thermal imaging can be advantageously exploited on other

bridge components. In future work, the authors plan to explore the applicability of the deployed system to bridge soffit areas. In addition, the application of further developed image processing tools on the infrared thermal data, along with artificial intelligence-based approaches, can result in full automation of the analysis and augmentation of the decision-making process to make it more effective.

## 7.8 References

- ASTM. *D4788-03* (2013). “Standard Test Method for Detecting Delaminations in Bridge Decks Using Infrared Thermography.” ASTM International, West Conshohocken, PA. [www.astm.org](http://www.astm.org).
- ASTM. *C876-09* (2009). “Standard Test Method for Corrosion Potentials of Uncoated Reinforcing Steel in Concrete.” ASTM International, West Conshohocken, PA. [www.astm.org](http://www.astm.org).
- Brooks, C., Dobson, R., Banach, D., Dean, D., Oommen, T., Wolf, R., Havens, T., Ahlborn, T., and Hart, B. (2015). “*Evaluating the Use of Unmanned Aerial Vehicles for Transportation Purposes.*” Michigan Tech Research Institute, Report, 201 p.
- Chen, E., Rice, C., Boyle, C., and Hauser, E. (2011). “Small-format aerial photography for highway-bridge monitoring.” *Performance of Constructed Facilities*, Vol. 25 (2), 105-112.
- Ellenberg, A., Kotsos, A., Moon, F., and Bartoli, I. (2016). “Bridge related damage quantification using unmanned aerial vehicle imagery.” *Structure Control Health Monitoring*, Vol. 23 (9), 1168 – 1179.
- Gillins, M., Gillins, D., and Parrish, C. (2016). “Cost-Effective Bridge Safety Inspections Using Unmanned Aircraft Systems (UAS).” *Proc., Geotechnical and Structural Engineering Congress*, Phoenix, Arizona, United States, 165-177.
- Harris, D., Brooks, C., and Ahlborn, T. (2016). “Synthesis of Field Performance of Remote Sensing Strategies for Condition Assessment of In-Service Bridges in Michigan.” *Performance of Constructed Facilities*, Vol. 30 (5), 1-19.
- Hallermann, N., and Morgenthal, G. (2013). “Unmanned Aerial Vehicles (UAV) for the Assessment of Existing Structures.” *Proc., IABSE Conference*, Rotterdam, Netherlands, Vol. 101(14), 1-8.
- Khan, F., Ellenberg, A., Mazzotti, M., Kotsos, A., Moon, F., Pradhan, A., and Bartoli, I. (2015). “Investigation on Bridge Assessment Using Unmanned Aerial Systems.” *Proc., Structures Congress*, ASCE, Portland Oregon, United States, 404-413.
- Omar, T., and Nehdi, M. (2017). “Unmanned Aerial Vehicle Infrared Thermography Remote Sensing for Condition Assessment of Concrete Bridge Decks.” *J. of Automation in Construction*. DOI: 10.1016/j.autcon.2017.06.024.

- Vaghefi, K., Oats, R., Harris, D., Ahlborn, T., Brooks, C., Endsley, K., Roussi, C., and Shuchman, R. (2012). "Evaluation of Commercially Available Remote Sensors for Highway Bridge Condition Assessment." *Bridge Engineering*, Vol. 17 (6), 886-895.
- Vasterling, M., and Meyer, U. (2013). "*Challenges and Opportunities for UAV-Borne Thermal Imaging.*" In book: *Thermal Infrared Remote Sensing*, Chapter 4, Publisher: Springer, Editors: Claudia Kuenzer and Stefan Dech, 69-93.
- Washer, G., Fenwick, R., and Nelson, S. (2013). "Guidelines for the Thermographic Inspection of Concrete Bridge Components in Shaded Conditions." *Proc., 92<sup>nd</sup> Annual Meeting, TRB*, Washington, DC, 1-14.

## Chapter 8

### 8. Summary, Conclusions and Recommendations

#### 8.1 Summary and Conclusions

Subsurface delamination, which is primarily caused by the corrosion of steel reinforcement, is the most common damage mechanism that can compromise the service life of RC bridge decks. Visual inspection is still the most used method for bridge condition assessment. Research results have shown that assessing the condition of a bridge deck by visual inspection is unreliable, as it often does not reveal real conditions, nor does it point to correct priorities when decisions about repair works are made. IRT has gradually gained wider acceptance as a NDT and evaluation tool in the civil engineering field. Therefore, the main goal of this dissertation is to develop an automated condition assessment procedure for RC bridge decks based on the IRT technology. The research also aimed to develop a combination process between the IRT and the GPR survey results to provide more precise assessments of RC bridge deck conditions. In addition, the research aimed to develop a new bridge deck rating index as a health indicator of the overall bridge deck condition based on the integration of IRT, GPR, and visual inspection defects' measurement. Another focus of the research program was to explore the feasibility of using UAVs for detecting hidden defects in RC bridge decks.

In Chapter 2, state-of-the-art of bridge condition assessment was appraised. To proceed with this task, a comprehensive review was undertaken aiming to gain a perspective on technical issues associated with bridge condition assessment techniques and deterioration prediction tools that have been used successfully. Current practices and other advanced evaluation methodologies, which employ artificial intelligence techniques, were examined. The review indicated a clear need to upgrade existing BMSs to incorporate recent research in the bridge condition assessment domain. Also, the review demonstrated that reliable bridge condition assessment can be effectively achieved using several complementary NDT technologies. Thus, this dissertation pursued such approach.

In Chapter 3, an evaluation of the capabilities and limitations of the most common NDT techniques used to detect and characterize typical deterioration mechanisms in concrete

bridge decks was carried out. A fuzzy hierarchical decision-making model was developed to evaluate the techniques from the perspectives of capability, speed, simplicity, accuracy, and cost. The results revealed that no single technology is capable of recognizing all deterioration types. IRT was identified as the most rapid technology capable of detecting delaminations in RC bridge decks accurately. Yet, it is the NDT technology of choice by transportation agencies due to the difficulty of establishing a rule-based criterion by which to evaluate its raw data. Thus, automation of the analysis process of the IRT survey was one of the main objectives of this dissertation.

In Chapter 4, a robust automated analysis procedure for detecting and classifying delaminations in RC bridge decks using IRT technology was developed. The developed approach resulted in effective identification of delaminated areas within the bridge decks of several full-scale case studies. It allows for the detection of subsurface delaminations at different survey times and environmental conditions, and hence, solves a major concern that has been of interest to many researchers in the NDT community for a long time. The developed system could stimulate wider acceptance of IRT as a rapid, systematic and cost-effective evaluation technique for critical bridge deck subsurface deficiencies. Consequently, adding this invaluable technique to the bridge inspector's tool box encourages a focus on the maintenance and repair budgets of the most deserving bridge decks.

In Chapter 5, IRT and GPR testing were employed to survey full-scale RC bridge decks and their results were combined to maximize the capabilities of each method and compensate for the limitations. The developed integration analysis aimed to rationalize their combined use as reliable NDT tools for bridge deck inspection. The developed integration methodology produced condition maps that delineate the different severity levels of subsurface delaminated and potential active corroded areas. The achieved results provided a great degree of confidence in the overall identified deterioration quantities. Consequently, employing the developed approach could provide rapid and reliable analysis, and an excellent harvest of information for maintenance decision makers.

In Chapter 6, an integrated bridge deck condition rating system based on the results of visual inspection, IRT, and GPR techniques was developed. The developed computational algorithms link technology-based (NDT) and inspector findings in an objective manner, while preserving the uncertain properties of the deterioration processes of bridge decks. The relative importance of the deterioration mechanisms and the gradual transition from one condition category to another were considered in the rating process. The developed model accounts for both surface and hidden quantified defects. The accuracy of the model was improved by combining NDT and visual inspection results in an uncertainty fuzzy-based mathematical methodology. Thus, a unique and useful integration process was developed, which should be emulated by other researchers in the bridge infrastructure field.

In Chapter 7, the potential for using thermal imaging with remote sensing unmanned aerial vehicles as carrying devices to evaluate the sub-surface conditions of RC bridge decks was demonstrated. Thus, UAV equipped with high definition photo and thermal cameras can facilitate the inspection tasks of bridge infrastructure. The proposed UAV-IRT system is capable of frequent bridge deck inspection at low cost, rapid and safe data collection, and provides reliable quantitative results. The proposed system could help transportation agencies in identifying critical deficiencies at various service life stages, and thus, apply proactive maintenance actions. In addition, considerable reductions in costs associated with the inspection processes of bridge decks and in the frequency and duration of traffic interruptions can be achieved.

## **8.2 Recommendations for Future Research**

The current thesis discusses several topics related to bridge condition assessment and highlights some challenges that require further concerted research efforts as follows:

1. Exploring the applicability of the automated IRT analysis procedure developed in this research to bridge soffit areas; correlating the findings of daytime and nighttime survey results; and studying the reliability of the developed system in detecting defects in the presence of asphalt overlays.

2. Investigating the capability of applying an IRT continuous monitoring system for detecting the depth and thickness of delaminations in full-scale RC bridge decks.
3. Studying the characterization of IRT data using several feature vectors of the recorded pixel readings in the thermal images. For example, using the pixel shape and texture instead of relying only on the pixel numerical values.
4. Advancing the application of other IRT image processing techniques, along with artificial intelligence-based approaches, to provide more objective classification of the detected delamination categories and augment a faster decision-making process.
5. Conducting extensive NDT comparative studies on full-scale deteriorated bridges and quantifying the achieved results to motivate practical evaluation of the employed methods and their wider implementation in bridge inspection.
6. Developing various fully automated data acquisition and analysis processes using several complementary NDT techniques to improve the efficiency, reliability and repeatability of NDT data collection and interpretation.
7. Developing computational algorithms for integrating various NDT accomplished results in order to have fully objective condition assessment systems.
8. Improving the bridge condition rating model developed in this research by utilizing various NDT techniques, including other bridge elements and components, and considering more possible deterioration mechanisms.
9. Developing correlations between the bridge element damage and internal deterioration processes and investigating the structural robustness and redundancy concepts in the assessment process in order to determine bridge elements' or components' conditions based on their resilience.
10. Studying the rebar spacing variation, surface properties, and structural variation and construction quality on the efficiency of analyzing GPR reflection amplitudes.

11. Utilizing UAV multi-sensors along with inertial and spatial sensors for producing geo-registered 3D data for bridges and detecting surface and subsurface defects in bridge decks as well as inaccessible areas, such as bridge soffits.
12. Exploring the use of UAV multi-sensor systems for determining stream or river bank conditions at bridge ends and for monitoring specific geotechnical assets related to bridges, including slope stability assessment, dynamic bank erosion and lateral scour conditions.
13. Establishing a guide for practical implementation of UAV multi-sensor systems in order to incorporate this emerging technology in bridge inspection manuals.

## Appendix A (Questionnaire Survey)

 <b>Western Engineering</b>	
<b>Expert Opinion on NDT Techniques for Detection of Subsurface Defects in Concrete Bridge Decks</b>	
UNIVERSITY OF WESTERN ONTARIO DEPARTMENT OF CIVIL AND ENVIRONMENTAL ENGINEERING	
1 / 13	8%
<p>Dear Sir/Madam,</p> <p>The extensive number of prematurely deteriorated concrete bridge decks drew the attention of many transportation agencies towards the importance of using non-destructive testing technologies (NDT) as potential assessment tools for the condition of such bridges. This questionnaire aims at identifying the significance of the factors affecting the selection of NDT methods for detecting subsurface defects in concrete bridge decks. Your opinion and expertise in bridge condition assessment at large and the NDT field in particular are paramount in the completion of this study. The information provided will be exclusively used for academic research purposes, with our full commitment for absolute confidentiality. We are grateful for your valuable time and feedback in completing this questionnaire.</p> <p>Best Regards,</p> <p>Tarek Omar PhD Candidate, Western University</p> <p>Dr. Tarek Zayed, P. Eng. Professor, Concordia University</p> <p>Dr. Moncef Nehdi, P. Eng. Professor, Western University</p>	



## Expert Opinion on NDT Techniques for Detection of Subsurface Defects in Concrete Bridge Decks

### Section 1. General Information

2/13

20%

#### 1. Expert's Contact Information (Optional):

Name

Company

City/Town

Country

Email Address

Phone Number

#### 2. Which of the following options describes your expertise?

- A bridge management engineer (Transportation agency)
- A bridge management engineer (Municipal)
- A bridge management engineer (Consultant/Contractor)
- A bridge NDT management engineer
- A bridge inspector/NDT technician
- A bridge researcher
- Other (please specify):

#### 3. How many years of experience do you have in the bridge community?

- 0-5 years
- 5-10 years
- 10-15 years
- 15-20 years
- More than 20 years

[Prev](#) [Next](#)



## Expert Opinion on NDT Techniques for Detection of Subsurface Defects in Concrete Bridge Decks

### Section 2. Inspection of Concrete Bridge Decks

4 / 12

21%

1. How the NDT evaluation of concrete bridge deck condition is being used in your organization's bridge assessment scheme?

- Frequently used
- As recommended by our bridge inspection manual
- When recommended by the Inspector
- Never used

Please specify if you select the first or the second option:

2. What NDT method(s) do you often use/recommend for bridge deck evaluation?

- Impact Echo
- Pulse Velocity
- Ground Penetrating Radar
- Infrared Thermography
- Half-Cell Potential and/or Resistivity
- Other (please specify)

3. Please rate your choices in question 2 above, from the most used/recommended to the least used/recommended:

Prev Next

Expert Opinion on NDT Techniques for Detection of Subsurface Defects in Concrete Bridge Decks

Section 3. Pair-Wise Comparison Between Factors

5/19 20%

In an attempt to determine the significance of factors affecting the selection of NDT methods in bridge deck assessment, the following scale is adopted in this study.

Saaty's Scale					
Scale of Importance	Equal Important	Moderate Important	Strong Important	Very Strong Important	Absolute Important
Intensity of Importance (Ranking)	1	3	5	7	9

Kindly fill in the tables below by selecting the appropriate box from your point of view as per the below example.

**Example:**

In the table below, consider comparing "Speed of the method" (Criterion X) with "Capability of the method to detect the subsurface defects" (Criterion Y) with respect to "Selection of the appropriate NDT method".

Criterion (X)	Degree of Importance									Criterion (Y)	
	(9) Absolute	(7) Very Strong	(5) Strong	(3) Moderate	(1) Equal	(3) Moderate	(5) Strong	(7) Very Strong	(9) Absolute		
Selection of NDT Method											
Speed											Capability
Simplicity											
Accuracy											
Cost											

If you consider that the Speed of the NDT method is more important than its Capability to detect the subsurface defects, and the degree of importance is "Strong".

If you consider that both Speed and Capability Criteria of the NDT method have equal importance when you use or recommend a method.

If you consider that the Capability of the NDT method to detect the subsurface defects is more important than its Speed, and the degree of importance is "Absolute".

1/20 Next

Expert Opinion on NDT Techniques for Detection of Subsurface Defects in Concrete Bridge Decks

Section 3. Pair-Wise Comparisons

A)- Between the main-criterion with respect to the objective

8 / 12  48%

Criterion (X)	Degree of Importance									Criterion (Y)
	(9) Absolute	(7) Very Strong	(5) Strong	(3) Moderate	(1) Equal	(3) Moderate	(5) Strong	(7) Very Strong	(9) Absolute	
Selection of NDT Method										
Speed										Capability
Simplicity										
Accuracy										
Cost										

1. What is the degree of importance of the following factors (Criterion X) if compared with capability of the method to detect the subsurface defects (Criterion Y) when you use/recommend any of the NDT methods?

	Absolute Importance (9)	Very Strong Importance (7)	Strong Importance (5)	Moderate Importance (3)	Equal Importance (1)	Moderate Importance (3)	Strong Importance (5)	Very Strong Importance (7)	Absolute Importance (9)
Speed of the method.	<input type="radio"/>	<input type="radio"/>	<input type="radio"/>	<input type="radio"/>	<input type="radio"/>	<input type="radio"/>	<input type="radio"/>	<input type="radio"/>	<input type="radio"/>
Simplicity of using the method.	<input type="radio"/>	<input type="radio"/>	<input type="radio"/>	<input type="radio"/>	<input type="radio"/>	<input type="radio"/>	<input type="radio"/>	<input type="radio"/>	<input type="radio"/>
Accuracy of the results obtained by the method.	<input type="radio"/>	<input type="radio"/>	<input type="radio"/>	<input type="radio"/>	<input type="radio"/>	<input type="radio"/>	<input type="radio"/>	<input type="radio"/>	<input type="radio"/>
Cost of using the method.	<input type="radio"/>	<input type="radio"/>	<input type="radio"/>	<input type="radio"/>	<input type="radio"/>	<input type="radio"/>	<input type="radio"/>	<input type="radio"/>	<input type="radio"/>

Prev Next







**Expert Opinion on NDT Techniques for Detection of Subsurface Defects in Concrete Bridge Decks**

**Section 4. Pair-Wise Comparison Between NDT Alternatives**

Impact echo, pulse velocity, half-cell potential, ground penetrating radar and infrared thermography are the most commonly implemented NDT methods for onsite assessment of concrete structures. They specifically suit the purpose of evaluating reinforced concrete bridges. These different technologies selected for this comparative study are based on various indicators (acoustic, electromagnetic, electrochemical and thermal principals). In order to obtain the degree of importance of these methods with respect to each of the sub-criteria, kindly fill in the forthcoming Tables by selecting the appropriate box based on your expertise. The example below attempts to clarify the approach:

**Example:**

In the table below, consider comparing the “Infrared Thermography method” (Criterion X) with the “Impact Echo method” (Criterion Y) with respect to “the capability of detecting subsurface delamination”.

Criterion (X)	Degree of Importance									Criterion (Y)	
	(9) Absolute	(7) Very Strong	(5) Strong	(3) Moderate	(1) Equal	(3) Moderate	(5) Strong	(7) Very Strong	(9) Absolute		
<b>Detection of Subsurface Delamination</b>											
Pulse Velocity											Impact Echo
Ground Penetrating Radar											
Infrared Thermography			✓		✓					✓	
Half-Cell Potential											

If you consider that the **Infrared Thermography** method is more important than the **Impact Echo** method in detecting the subsurface delamination, and the degree of importance is “**Strong**”.

If you consider that both **Impact Echo** and **Infrared Thermography** methods have **Equal** importance in detecting the subsurface delamination.

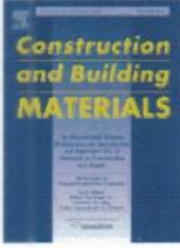
If you consider that the **Impact Echo** method is more important than the **Infrared Thermography** method in detecting the subsurface delamination, and the degree of importance is “**Absolute**”.

## Appendix B (Copyright Permissions)



# RightsLink®

[Home](#)
[Create Account](#)
[Help](#)

**Title:** Infrared thermography model for automated detection of delamination in RC bridge decks

**Author:** Tarek Omar, Moncef L. Nehdi, Tarek Zayed

**Publication:** Construction and Building Materials

**Publisher:** Elsevier

**Date:** 20 April 2018

© 2018 Elsevier Ltd. All rights reserved.

**LOGIN**

**If you're a copyright.com user,** you can login to RightsLink using your copyright.com credentials.

Already a **RightsLink user** or want to [learn more?](#)

Please note that, as the author of this Elsevier article, you retain the right to include it in a thesis or dissertation, provided it is not published commercially. Permission is not required, but please ensure that you reference the journal as the original source. For more information on this and on your other retained rights, please visit: <https://www.elsevier.com/about/our-business/policies/copyright#Author-rights>

[BACK](#)
[CLOSE WINDOW](#)

Copyright © 2018 [Copyright Clearance Center, Inc.](#) All Rights Reserved. [Privacy statement](#). [Terms and Conditions](#). Comments? We would like to hear from you. E-mail us at [customercare@copyright.com](mailto:customercare@copyright.com)

**From:** Nenad Gucunski  
**Sent:** March 5, 2018 10:34:42 PM  
**To:** Tarek Omar  
**Subject:** RE: Permission to Use Images in my Doctoral Thesis

Dear Tarek,

Thanks. Yes, please feel free to use the images in your thesis, since I am the author of both.

Best, NG

---

**From:** Tarek Omar  
**Sent:** Monday, March 5, 2018 7:51 PM  
**To:** Nenad Gucunski  
**Subject:** Re: Permission to Use Images in my Doctoral Thesis

Thanks Dr. Nenad.

The two figures are from SHRP 2 Report S2-R06A-RR-1 as follows:

- 1- Figure 2.2. Corrosion process.
- 2- Figure 2.3 (top): "Corroded rebar in an excavated deck".

Sincerely

Tarek Omar

**From:** PERMISSIONS <permissions@asce.org>  
**Sent:** March 5, 2018 9:00:14 AM  
**To:** Tarek Omar; ASCE Library  
**Subject:** RE: Permission to Use A Figure in my Doctroal Thesis

Dear Tarek Omar,

Thank you for your inquiry. You have permission to reuse the following figure in your thesis provided the figure in total does not account for more than **25% of the new work**.

- Figure 1 from [Fuzzy-Based Model for Predicting Failure of Oil Pipelines](#) in J. of Infrastructure Systems, 12/2014, Volume 20, Issue 4

A full credit line must be added to the material being reprinted. For reuse in non-ASCE publications, add the words "With permission from ASCE" to your source citation. For Intranet posting, add the following additional notice: "This material may be downloaded for personal use only. Any other use requires prior permission of the American Society of Civil Engineers. This material may be found at [URL/link of abstract in the ASCE Library or Civil Engineering Database]."

Each license is unique, covering only the terms and conditions specified in it. Even if you have obtained a license for certain ASCE copyrighted content, you will need to obtain another license if you plan to reuse that content outside the terms of the existing license. For example: If you already have a license to reuse a figure in a journal, you still need a new license to use the same figure in a magazine. You need separate license for each edition.

Sincerely,

Leslie Connelly  
Senior Marketing Coordinator  
American Society of Civil Engineers  
1801 Alexander Bell Drive  
Reston, VA 20191

[PERMISSIONS@asce.org](mailto:PERMISSIONS@asce.org)

**From:** Milner, Rob  
**Sent:** March 5, 2018 8:19 AM  
**To:** Tarek Omar  
**Subject:** RE: Permission to Use Two Figures in my Doctroal Thesis

Yes, that would be fine.

Rob

**Rob Milner, MSc, P.Eng.**  
National Science, Automation, Optical Gas Imaging & sUAS Manager

**FLIR Systems**

---

**From:** Tarek Omar  
**Sent:** Sunday, March 4, 2018 6:08 PM  
**To:** Milner, Rob  
**Subject:** Permission to Use Two Figures in my Doctroal Thesis

Dear Mr. Rob,

I hope everything is going well at your end. I am completing my Doctoral 's thesis entitled "Condition Assessment of Concrete Bridge Decks Using Ground and Airborne Infrared Thermography". My thesis will be available in full-text on the internet for reference, study and / or copy. I will also be granting Library and Archives Canada and ProQuest/UMI a non-exclusive license to reproduce, loan, or distribute copies of my thesis.

I would like permission to allow inclusion two figures from "FLIR Guidebook" in my thesis. In particular, "the infrared region in the electromagnetic spectrum, and configuration of a typical IR camera". The material will be attributed through a proper citation.

Kindly advise your acceptance.

Sincerely

## CURRICULUM VITAE

**Name:** Tarek Omar, P.Eng.

**Post-secondary Education and Degrees:** Ain Shams University  
Cairo, Egypt  
1979-1984 B.Sc.

The University of Western Ontario  
London, Ontario, Canada  
2012-2013 M.Sc.

The University of Western Ontario  
London, Ontario, Canada  
2014-2017 Ph.D.

**Honours and Awards:** Alexander Graham Bell Canada Graduate Scholarships (NSERC)  
2016-2017, 2017-2018

Doctoral Excellence Research Award (UWO)  
2016-2017

Province of Ontario Graduate Scholarship (OGS)  
2015-2016

Transportation Association of Canada Scholarship (TAC)  
2015-2016

Academic Achievement Scholarships (UWO)  
2014-2015, 2015-2016, 2016-2017

**Related Work Experience** Research and Teaching Assistant  
University of Western Ontario  
2012-2017

Project Director / Independent Reviewer  
Hyder International Consulting, UK  
1998-2011

Project Manager  
Dorsch International Consultant, Germany  
1990-1998

Executive Engineer  
Arab Contracting “Osman Ahmed Osman”, Egypt  
1984-1990

## Publications:

### Articles Published in Refereed Journals:

**Omar, T.**, Nehdi, M., and Zayed, T. (2018). “Infrared Thermography Model for Automated Detection of Delamination in RC Concrete Bridge Decks.” *J. Construction and Building Materials*. Vol. 168, pp: 313-327. DOI: [10.1016/j.conbuildmat.2018.02.126](https://doi.org/10.1016/j.conbuildmat.2018.02.126) (Ph.D. work).

**Omar, T.**, and Nehdi, M., (2017). “Unmanned Aerial Vehicle Infrared Thermography Remote Sensing for Condition Assessment of Concrete Bridge Decks.” *J. Automation in Construction*. Vol. 83, pp: 360-371. DOI: [10.1016/j.autcon.2017.06.024](https://doi.org/10.1016/j.autcon.2017.06.024) (Ph.D. work).

**Omar, T.**, Nehdi, M., and Zayed, T. (2017). “Integrated Condition Rating Model for Reinforced Concrete Bridge Decks.” *J. Performance of Constructed Facilities*. Vol. 31 (5), pp: 04017090 (1-14). DOI: [10.1061/\(ASCE\)CF.1943-5509.0001084](https://doi.org/10.1061/(ASCE)CF.1943-5509.0001084) (Ph.D. work).

**Omar, T.**, Nehdi, M., Zayed, T. (2017). “Rational Condition Assessment of Reinforced Concrete Bridge Decks Subjected to Corrosion-Induced Delamination.” *J. Materials in Civil Engineering*. DOI: [10.1061/\(ASCE\)MT.1943-5533.0002114](https://doi.org/10.1061/(ASCE)MT.1943-5533.0002114) (Ph.D. work).

**Omar, T.**, Nehdi, M., and Zayed, T. (2017). “Performance of NDT Techniques in Appraising Condition of Reinforced Concrete Bridge Decks.” *J. Performance of Constructed Facilities*. Vol. 31 (6), 04017104 (1-16). DOI: [10.1061/\(ASCE\)CF.1943-5509.0001098](https://doi.org/10.1061/(ASCE)CF.1943-5509.0001098) (Ph.D. work).

**Omar, T.**, and Nehdi, M. (2017). “Thermal Detection of Sub-Surface Defects in Concrete Bridge Decks Using Unmanned Ariel Vehicle.” *In Press, American Concrete Institute (ACI) Special Publication*. (Ph.D. work).

**Omar, T.**, and Nehdi, M. (2016). “Data Acquisition Technologies for Construction Progress Tracking.” *J. Automation in Construction*. Vol. 70, pp: 143-155. DOI: [10.1016/j.autcon.2016.06.016](https://doi.org/10.1016/j.autcon.2016.06.016) (Ph.D. work).

**Omar, T.**, and Sadrekarimi, A. (2015). “Effect of Triaxial Specimen Size on Engineering Design and Analysis.” *International J. of Geo-Engineering*, Vol. 6 (1); pp: 1-17. DOI: [10.1186/s40703-015-0006-3](https://doi.org/10.1186/s40703-015-0006-3) (M.E.Sc. work).

**Omar, T.**, and Sadrekarimi, A. (2015). “Specimen Size Effects on the Behaviour of Loose Sand in Triaxial Compression Tests.” *Canadian Geotechnical Journal*, Vol. 52 (6), pp: 732-746. DOI: [10.1139/cgj-2014-0234](https://doi.org/10.1139/cgj-2014-0234) (M.E.Sc. work).

**Omar, T.**, and Sadrekarimi, A. (2014). “Effects of Multiple Corrections on Triaxial Compression Testing of Sands.” *J. of GeoEngineering*, Vol. 9 (2), pp: 33-40. DOI: [10.6310/jog.2014.9\(2\).3](https://doi.org/10.6310/jog.2014.9(2).3) (M.E.Sc. work).

### Articles Submitted to Refereed Journals:

**Omar, T.**, Nehdi, M., Zayed, T. (2017). “Condition Assessment of Reinforced Concrete Bridges: Current Practice and Research Challenges.” *Canadian Journal of Civil Engineering*. Submission ID #: [cjce-2017-0339](https://doi.org/10.1139/cjce-2017-0339) (Ph.D. work).

**Papers Published in Peer-Reviewed Conference Proceedings:**

**Omar, T.**, and Nehdi, M. (2017). “Clustering-Based Threshold Model for Condition Assessment of Concrete Bridge Decks Using Infrared Thermography.” Chapter. In book: “*Facing the Challenges in Structural Engineering, Sustainable Civil Infrastructures*”, pp: 242-253. H. Rodrigues et al. (eds.), Springer International Publishing AG. Switzerland. DOI: [10.1007/978-3-319-61914-9\\_19](https://doi.org/10.1007/978-3-319-61914-9_19)

**Omar, T.**, and Nehdi, M. (2017). “Automated Data Collection for Progress Tracking Purposes: A Review of Related Techniques.” Chapter. In book: “*Facing the Challenges in Structural Engineering, Sustainable Civil Infrastructures*”, pp: 391-405. H. Rodrigues et al. (eds.), Springer International Publishing AG. Switzerland. DOI: [10.1007/978-3-319-61914-9\\_30](https://doi.org/10.1007/978-3-319-61914-9_30)

**Omar, T.**, and Nehdi, M. (2016) “Non-Destructive Testing of Bridge Deck Using Passive Infrared Thermography & Ground Penetrating Radar.” *In Proceedings, Annual Conference of the Transportation Association of Canada (TAC)*, Toronto, Canada, Sep 25-28.

**Omar, T.**, and Nehdi, M. (2016) “Application of Passive Infrared Thermography for the Detection of Defects in Concrete Bridge Elements.” *In Proceedings, Annual Conference of the Transportation Association of Canada (TAC)*, Toronto, Canada, Sep 25–28.

**Omar, T.**, and Nehdi, M. (2016) “Condition Assessment and Deterioration Prediction Tools for Concrete Bridges: A New Look.” *In Proceedings, Annual Conference of the Canadian Society of Civil Engineering (CSCE)*, London, Ontario, Canada, June 1-4.

**Omar, T.**, and Nehdi, M. (2016) “Evaluation of NDT Techniques for Concrete Bridge Decks Using Fuzzy Analytical Hierarchy.” *In Proceedings, Annual Conference of the Canadian Society of Civil Engineering (CSCE)*, London, Ontario, Canada, June 1-4.

**Omar, T.**, and Nehdi, M. (2015) “Learned Lessons from Adelaide Desalination Project.” *In Proceedings, Annual Conference of the Canadian Society of Civil Engineering (CSCE)*, Regina, Saskatchewan, Canada, May 27–30.

**Omar, T.**, and Sadrekarimi, A. (2015). “Corrections Effect on Shear Strength Parameters of Loose Ottawa Sands.” *In Proceedings, Annual Conference of the Canadian Society of Civil Engineering (CSCE)*, Regina, Saskatchewan, Canada, May 27–30.

**Omar, T.**, and Sadrekarimi, A. (2014) “Specimen Size Effect on Shear Behaviour of Loose Sand in Triaxial Testing and its Implication in Engineering Design and Analysis.” *In Proceedings, Annual Conference of the Canadian Geotechnical Society (CGS), GeoRegina*, Regina, Saskatchewan, Canada. September 27-30.

**Omar, T.**, Osouli, A., and Sadrekarimi, A. (2014). “Influence of Specimen Size in Engineering Practice.” *In Proceedings, Geotechnical Special Publication, Geo-Congress (ASCE)*, Atlanta, Georgia, USA. February 23-26. DOI: [10.1061/9780784413272.287](https://doi.org/10.1061/9780784413272.287)